Lappeenranta
University of Technology

Ville Sihvo

INSULATION SYSTEM IN AN INTEGRATED MOTOR COMPRESSOR

Thesis for the degree of Doctor of Science (Technology) to be presented with due permission for public examination and criticism in the Auditorium 1382 at Lappeenranta University of Technology, Lappeenranta, Finland on the 16th of December, 2010, at noon.

Acta Universitatis
Lappeenrantaensis 411

Supervisor	Prof. Juha Pyrhönen LUT Energy Lappeenranta University of Technology Finland
Reviewers and opponents	Dr. Eero Keskinen Kone Oyj Hyvinkää Finland
	Dr. Li Ming ABB Corporate Research Västerås Sweden

ISBN 978-952-265-011-5
ISBN 978-952-265-012-2 (PDF)
ISSN 1456-4491

Lappeenrannan teknillinen yliopisto
Digipaino 2010

Abstract

Ville Sihvo

Insulation System in an Integrated Motor Compressor

Lappeenranta 2010

201 p.

Acta Universitatis Lappeenrantaensis 411

Diss. Lappeenranta University of Technology

ISBN 978-952-265-011-5
ISBN 978-952-265-012-2 (PDF)
ISSN 1456-4491

A high-speed and high-voltage solid-rotor induction machine provides beneficial features for natural gas compressor technology. The mechanical robustness of the machine enables its use in an integrated motor-compressor. The technology uses a centrifugal compressor, which is mounted on the same shaft with the high-speed electrical machine driving it. No gearbox is needed as the speed is determined by the frequency converter. The cooling is provided by the process gas, which flows through the motor and is capable of transferring the heat away from the motor. The technology has been used in the compressors in the natural gas supply chain in the central Europe. New areas of application include natural gas compressors working at the wellheads of the subsea gas reservoir. A key challenge for the design of such a motor is the resistance of the stator insulation to the raw natural gas from the well. The gas contains water and heavy hydrocarbon compounds and it is far harsher than the sales gas in the natural gas supply network. The objective of this doctoral thesis is to discuss the resistance of the insulation to the raw natural gas and the phenomena degrading the insulation.

The presence of partial discharges is analyzed in this doctoral dissertation. The breakdown

voltage of the gas is measured as a function of pressure and gap distance. The partial discharge activity is measured on small samples representing the windings of the machine. The electrical field behavior is also modeled by finite element methods. Based on the measurements it has been concluded that the discharges are expected to disappear at gas pressures above 4 – 5 bar. The disappearance of discharges is caused by the breakdown strength of the gas, which increases as the pressure increases. Based on the finite element analysis, the physical length of a discharge seen in the PD measurements at atmospheric pressure was approximated to be 40 – 120 μm.

The chemical aging of the insulation when exposed to raw natural gas is discussed based on a vast set of experimental tests with the gas mixture representing the real gas mixture at the wellhead. The mixture was created by mixing dry hydrocarbon gas, heavy hydrocarbon compounds, monoethylene glycol, and water. The mixture was chosen to be more aggressive by increasing the amount of liquid substances. Furthermore, the temperature and pressure were increased, which resulted in accelerated test conditions. The time required to detect severe degradation was thus decreased. The test program included a comparison of materials, an analysis of the effects of different compounds in the gas mixture, namely water and heavy hydrocarbons, on the aging, an analysis of the effects of temperature and exposure duration, and also an analysis on the effect of sudden pressure changes on the degradation of the insulating materials.

It was found in the tests that an insulation consisting of mica, glass, and epoxy resin can tolerate the raw natural gas, but it experiences some degradation. The key material in the composite insulation is the resin, which largely defines the performance of the insulation system. The degradation of the insulation is mostly determined by the amount of gas mixture diffused into it. The diffusion was seen to follow Fick's second law, but the coefficients were not accurately defined. The diffusion was not sensitive to temperature, but it was dependent upon the thermodynamic state of the gas mixture, in other words, the amounts of liquid components in the gas. The weight increase observed was mostly related to heavy hydrocarbon compounds, which act as plasticizers in the epoxy resin. The diffusion of these compounds is determined by the crosslink density of the resin. Water causes slight changes in the chemical structure, but these changes do not significantly contribute to the aging phenomena. Sudden changes in pressure can lead to severe damages in the insulation, because the motion of the diffused gas is able to create internal cracks in the insulation. Therefore, the diffusion only reduces the mechanical strength of the insulation, but the ultimate breakdown can potentially be caused by a sudden drop in the pressure of the process gas.

Keywords: epoxy, high voltage, induction motor, insulation, life estimation, mica, natural gas compressor
UDC 621.51 : 537.226

Acknowledgements

The research documented in this book was carried out between the years 2007 and 2010 at Lappeenranta University of Technology (LUT) and at Statoil research center in Trondheim. Some of the measurements have been carried out at the laboratories of Sintef Energiforskning in Trondheim. The project has been funded by Statoil ASA.

This research work has been rather an unusual one. It has included various kinds of tests and measurements covering many branches of science and engineering. Hence, the researcher has needed a lot of assistance in analysis, and especially, in practical work.

First, I would like to thank professor Juha Pyrhönen for giving me the opportunity for the research work with such an interesting and unique topic, and associate professor Janne Nerg for encouragement and guidance with finite element methods. I wish to thank Dr. Hanna Niemelä for assistance in writing the thesis. Also, I would like to thank Dr. Arto Pihlajamäki for giving me the perspective of a chemist in interpreting the results.

The pre-examination process made the thesis many times better. Not only did it fix the mistakes, but it also made the text more thoughtful. The comments by reviewers Dr. Eero Keskinen and Dr. Li Ming are the most gratefully appreciated.

The practical work was carried out at Statoil research center. Unfortunately, it is possible to name only a few who have helped me during the years. I wish to express my gratitude to Dr. Lars Brenne for keeping me on right track with the work, and for providing me the computational tools and equipment for experimental tests. I also wish to thank Dr. Tor Bjørge for teaching me some thermodynamics. With practical work, the researcher every now and then found himself stuck, because the equipment did not simply work. According to Mr. Kjell Tiller ”there is always something going wrong.” I am deeply grateful for him for fixing the thousands of practical problems in the Statoil laboratory, hence making it possible for me to perform the aging experiments. I would also like to thank Ms. Marit Larsen for instructing me to use the FTIR and DSC instruments, Mr. Inge Morten Kulbotten for teaching me to perform the three-point bending tests, and everyone else in the Statoil laboratory and workshop, who provided assistance, when I needed it.

The research work included fruitful cooperation with Sintef Energiforskning and their role is acknowledged. I would like to thank Mr. Oddgeir Kvien for performing the dielectric

response and insulation resistance measurements, and for arranging the practical issues at Sintef. I wish to thank Dr. Dag Linhjell for performing the breakdown strength measurements for gases and Ms. Mildrid Selsjord for taking the SEM images. Also, I want to express my gratitude to Dr. Sverre Hvidsten for his valuable and critical comments on the work.

Financial support provided by Emil Aaltonen foundation, Ulla Tuominen foundation, and Walter Ahlström foundation is highly appreciated.

Finally, I wish to express my utmost appreciation to my wife Inga and my son Onni for their understanding, support, and love. Without you, any accomplishment is simply beyond reach.

Lappeenranta, November 30th, 2010

Ville Sihvo

Contents

List of Symbols and Abbreviations

Roman Letters

A	area
c	concentration
C	capacitance
C_0	capacitance of free space
d	insulation thickness
d	distance between electrodes
D	diffusivity
e	electron charge
E	electrical field strength
E_a	activation energy
E_BD	breakdown field strength
f	frequency
F	force
G	Gibbs free energy
h	Planck's constant
h	height
H	enthalpy
I	current
I_C	capacitive current (imaginary part of I)
I_R	resistive current (real part of I)
J	current density
k	Boltzmann's constant
K	reaction rate constant
l	length
L	lifetime of insulation
m	weight
m_∞	weight at saturation in the diffusion process
n	rotational speed

N	size of the data set
Q	partial discharge level, apparent charge
Q_{IEC}	partial discharge level according to the IEC standard
Q_{max}	maximum partial discharge level
p	pressure
P	polarization
r	radius
R	universal gas constant
R	resistance
s	span, distance
S	entropy
t	time
T	temperature
T_{g}	glass transition temperature
U	voltage
U_{BD}	breakdown voltage
$U_{\mathrm{L\text{-}L}}$	line-to-line voltage
U_{E}	E-modulus
U_{T}	toughness
V	volume
V	potential
w	width
x	position
x	displacement
Z	impedance

Greek Letters

α	angle
α	shape parameter of the Weibull distribution
β	scale parameter of the Weibull distribution
δ	argument (angle) of complex permittivity
ϵ	permittivity
$\epsilon*$	complex permittivity
ϵ'	real part of complex permittivity
ϵ''	imaginary part of complex permittivity
ϵ_0	permittivity of free space
ϵ_{s}	constant real permittivity at low frequency
ϵ_∞	constant real permittivity at high frequency
ϵ_{r}	relative permittivity, dielectric constant
ε	strain
ε_{f}	elongation at break
Θ	absolute temperature

λ	activation length
μ	chemical potential
$\hat{\mu}$	statistical estimate
ρ	resistivity
ρ	density
σ	flexural stress
σ_{f}	tensile strength
σ	conductivity
σ^2	statistical variance
τ	time constant
ω	angular frequency

Acronyms

AC	alternating current
atm	atomspheric pressure
BCl_3	boron trichloride
DC	direct current
DSC	differential scanning calorimetry
FEM	finite element methods
FTIR	Fourier transform infrared
IR	infrared
MEG	monoethylene glycol
PD	partial discharge
PET	polyethylene terephtalate
PWM	pulse-width modulation
RR	resin rich
rt	room temperature
SEM	scanning electron microscope
SiC	silicon carbide
VPI	vacuum pressure impregnation
XLPE	cross-linked polyethylene

Chapter 1

Introduction

The topic and scope of the doctoral thesis are related to the harvesting of natural gas resources. It is, therefore, a very sensitive subject nowadays. The introductory chapter is written in a rather conservative manner regarding the general attitudes towards the global warming and energy policy. A realistic approach is taken to renewable energy sources (i.e., renewables are addressed in their actual scope and significance among global energy sources), while the role of fossil fuels is highlighted. Nevertheless, the need for less polluting energy sources is emphasized.

The world's energy market is facing winds of change; in practice, this is actualized in two ways. On the one hand and almost literally, it means major efforts to exploit renewable energy sources, particularly wind, solar, and biofuels, instead of traditional fossil fuels, coal, oil, and natural gas, in order to fight the climate change. On the other hand and relating to the topic of this doctoral thesis, it means that the world's resources for oil and natural gas are diminishing. The resources are no longer easy to exploit as the reserves lie in very challenging places, such as in the bottom of the Arctic Sea. Oil and gas are getting more expensive to drill, and meanwhile, their use is taxed more heavily in Europe.

The world's energy usage as of 2007 is illustrated in Fig. 1.1. It can be seen that the combined share of fossil fuels is over 80%. The world is accustomed to using these energy sources, and their prices are far lower than the prices of renewable energy sources. They are thus essential to modern lifestyle and their replacement – even to some degree – requires significant efforts and takes many years.

The political leaders of the world have still to set their objectives to replace notable parts of fossil fuels by renewable energy sources. Fossil fuels do not participate in the carbon cycle, since they have been lying beneath the earth's surface for millions of years. The burning of them creates additional carbon to the carbon cycle, which the natural processes cannot handle. The surface temperature of the earth has increased significantly within the past 150 years essentially as a result of human activity, which basically refers to the burning of fossil

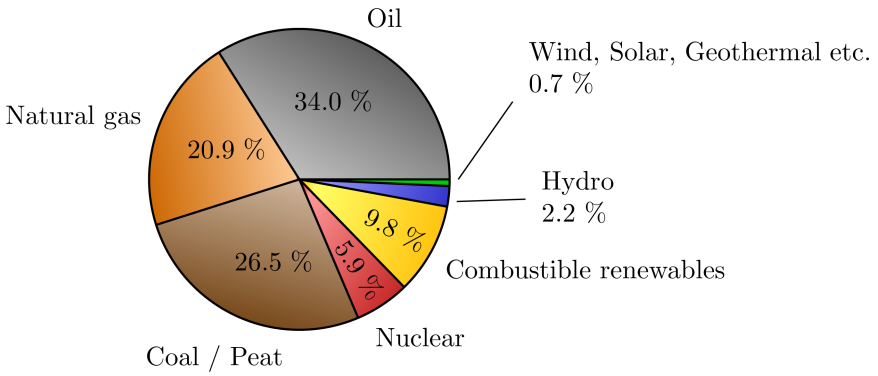

Fig. 1.1. World's energy consumption in 2007. Combustible renewables include biofuels, biomass, municipal waste, and wood. The total usage is 12 029 Mtoe, which corresponds to a total power of 15.97 TW. Data collected from IEA (2009).

fuels. The fossil fuels were the prerequisite of the industrial revolution in the 19$^{\text{th}}$ century. The global warming itself was already going on before the industrial revolution, and such warm periods have taken place earlier in the earth's history also. However, the human activity has accelerated the climate change.

One of the key reasons for the global warming has been the increasing amount of carbon dioxide (CO_2) in the atmosphere. CO_2 is released in the burning process of any organic fuel. The natural processes can convert the carbon dioxide into sugar and oxygen. Therefore, another reason for global warming has been the deforestation of tropical rain forests, which reduces the effectiveness of natural processes.

The environmental effects of fossil fuels, namely coal, oil, and natural gas, can be summarized according to EIA (1999) as follows. When burning, coal releases ash containing small metallic particles, sulfur dioxide (SO_2), carbon monoxide (CO), and carbon dioxide, and nitrous oxides, which form corresponding acids when they react with water in the atmosphere. The burning process of petroleum releases practically the same hazardous substances as the burning of coal, excluding the ash. Some amount of particles is released because of the incomplete burning process, but it is much less than that with coal. Natural gas, on the other hand, produces no sulphur dioxide, because the source of sulphur, hydrogen sulphide (H_2S), is removed from the gas in the processing stage. Natural gas produces very small amounts of particles and essentially less nitrous oxides than oil and coal. The carbon dioxide emissions from the burning process of coal, oil, and natural gas, are 178, 140, and 100 units of CO_2, respectively, per produced amount of energy (adapted from EIA, 1999). The above comparison on the environmental effects only takes the burning process into account. The harvesting and processing of such resources also create notable pollution. Nevertheless, natural gas is significantly less dangerous to the environment than oil and coal. Therefore, the politicians have been encouraging the use of natural gas for instance in domestic heating applications as a replacement for coal and oil.

The climate change cannot fully be prevented by renewable energy sources. Furthermore,

some of their desired effects on global warming can be argued. Large hydroelectric plants are not favored, because they change the local ecosystems so drastically. In addition, in many developed countries, such as in Finland, most of the rivers have already been harnessed for hydroelectric energy conversion. Wind energy has its limitations in many areas. It is usable in coastlines, where the wind is steady and constant, but the technology is sophisticated and expensive. Furthermore, it is too rarely realized by the politicians that a wind power plant can only convert energy when the wind blows, which strongly limits its use as a primary energy source. In the short term, the biofuels cannot solve the global warming problems, because they keep releasing carbon dioxide into the air, even though the fuel itself has been harvested from living plants. Furthermore, in many occasions the exploitation of biofuels means deforestation of rain forests into fields, thus reducing the earth's capability to handle carbon dioxide. Consequently, the climate change gets actually worse, which has been pointed out by Fargione et al. (2008), Searchinger et al. (2008), and Melillo et al. (2009).

The western world seems to agree now that it has to change its lifestyle by replacing at least some of the fossil fuels with renewable energy sources or with fuels generating less CO_2 emissions. The latter category contains nuclear power, towards which there has been increasing enthusiasm. Also the fuels with less CO_2 emissions include natural gas. However, there are not too many alternatives to combustion processes, and in many occasions the old habits still apply; airplanes need kerosene, ships need diesel and cars need fuel. Industries in all these forms of transportation have been searching for and investigating for replacing energy sources, such as biofuels for airplanes and cars and liquefied natural gas for ships, but on a global scale, significant changes take a very long time. Furthermore, there have been attempts to reduce traffic emissions by cars powered with electrical engines, but in many cases the philosophy is not very comprehensive. For instance, if the traditional cars in the city of Helsinki were replaced with electrically powered ones, the city would have to build another coal power plant to recharge them. Electricity itself is not a renewable energy source, but it has to be generated somehow.

Despite the encouragement to utilize renewable energy sources, and despite their most obvious needs, the world will be dependent upon fossil fuels for years to come. From an economic point of view, they are the most attractive choice. The use of renewable energy can generally be cost-effective only if the pollution caused by fossil fuels is charged with an additional fee. Such fees have been set in Europe, but globally this has a negligible effect, since European companies can move their factories to the Third World and provide them with energy generated from coal. Furthermore, changes needed to replace the old applications that use coal or oil will take a long time. For instance, the airplanes and ships built today for the use of kerosene or diesel will be replaced after 20 years or so. Moreover, the actual amount of energy that needs to be replaced is colossal. For instance, if all the oil (i.e. 34% of the total power of approximately 16 TW) were replaced with wind energy, it would require more than 5.4 million wind power plants to be built assuming that one plant can deliver 3 MW of power to the grid with the utilization period of a maximum load of 2900 h (121 days) per year. Therefore, it may well be assumed that the world will replace oil no sooner than its price climbs above a certain economic limit not because of pollution fees, but because the resources get too expensive to harvest, that is, the world runs out of cheap oil. The same applies also to natural gas.

Natural gas is more environmentally friendly than oil or coal, and in many applications, for instance in domestic heating, it is even an encouraged energy source. However, the world's resources for natural gas are diminishing. The natural gas fields that are relatively easy to exploit have been largely taken into use already. Many of such fields are located in the Persian Gulf area and Russia. A great number of fields providing high potential for the future are located underneath ocean floors. Such include the Snøhvit field located at approximately 200 km from the coast of Northern Norway and the Shtokman field located in the Barents Sea 600 km north of Kola Peninsula. Hence, the gas vendors have to go further away to the sea to find their resources, which means increased costs and need for more sophisticated technology.

1.1 Natural gas production from subsea wells

The role of subsea reserves in natural gas production is getting more important. It has been estimated (Lecarpentier, 2009) that 27% of the world's natural gas resources lie in offshore gas fields, and the share is expected to rise to 35% by 2020. Harvesting of such resources is more challenging and requires more sophisticated technology than the exploitation of onshore fields.

The natural gas, which is used in power stations or for other purposes, consists essentially of methane. For example, a gas mixture distributed to the end user from Kårstø gas processing plant in Norway contains roughly 90% of methane (CH_3), 6% of ethane (C_2H_6), 1% of nitrogen (N_2), 2% of carbon dioxide (CO_2), and fractions of a percent of propane (C_3H_8), butane (C_4H_{10}), and pentane (C_5H_{12}). The sales gas undergoes a complex processing scheme before transportation to the end user.

Raw natural gas existing in the well is a far more complex and hazardous mixture of different elements. Most of the processing steps take place in gas processing plants, but prior to transporting the raw natural gas to such a plant, the condensate and produced water are removed from the mixture. This process takes place near the gas wells; at subsea fields it takes place in the platforms.

The raw natural gas in the well consists mainly of methane, but also of many other compounds, the amounts of which depend essentially upon the reservoir. The raw natural gas contains the components in the sales gas mixture mentioned above but also hydrocarbon condensate, water, monoethylene glycol (MEG), hydrogen sulfide (H_2S), and mercury. The hydrocarbon condensate contains pentanes and hydrocarbons of higher molecular weight, that is, hydrocarbon compounds containing five or more carbon atoms. The condensate is liquid at room temperature, and it is typically sent to an oil refinery for further processing. The water produced from the well can include various salts and ions; this is highly dependent on the well, though. It is very corrosive and requires additional care with the design of pipelines and processing equipment. Some gas fields are not allowed to produce any water, and they are shut down immediately, if such occurs. Monoethylene glycol is added to the gas mixture at the wellhead to prevent hydrate formation in the pipelines.

The natural gas reserves usually lie far, say 2000 meters, below the surface. The water depths at Åsgard field in the North Sea are approximately 250 m, at Shtokman field 350 m, and at Snøhvit field 310 – 340 m. The gas inside the reservoir needs high pressure to be even able to flow to the surface. The pressure loss from the reservoir to the platform can be 20 – 50 bar, depending on the gas flow rate and design of the pipelines.

At the initial stage of production, the gas is able to flow from the reservoir to the surface by its own pressure, which naturally decreases as the production goes on. When the pressure is too low to aid the gas flow up to the surface at a rate economically worth producing, the field is forced to shut down. At this point, roughly 35 – 40% of the gas is still left into the reservoir. The exploitation of the field in the tail production stage can be improved by an artificial lift. The lift can be provided by a compressor installed near the wellhead on the sea floor. The subsea compressor must be driven by an electrical motor.

Subsea installations have potential of offering several advantages over the old platform-based production techniques. The gas flow is directed from the wellhead to the pipeline leading to the gas processing plant located on the continent. The gas flow is increased with the aid of a compressor installed near the wellhead at the sea floor. Therefore, the platform or any other topside installation is not required. Cost savings are achieved, but also the exploitation of fields in challenging locations is made possible. Such challenging fields include the ones located in arctic areas, where the weather conditions cause continuous difficulties to topside installations, and the fields located in environmentally vulnerable areas containing diverse fish population and nesting areas for birds.

The advantages of subsea compression technology are considerable, but so are also the challenges. Obviously, a technological breakthrough of this kind requires new innovations in many areas of engineering. The electrical motor driving the compressor and in particular its insulation system, which is in the focus of this doctoral thesis, is only one of them. But it is, like other innovations required, vital for the whole technology. The thesis focuses on a certain integrated motor-compressor concept, which is proposed as an alternative to subsea compression.

1.2 Integrated motor compressor

The compressor concept consists essentially of the centrifugal compressor and a high-speed electrical motor mounted on the very same shaft and supported by active magnetic bearings. Owing to the high and adjustable speed of the electrical motor, the concept does not need a gearbox, which is a very critical component in this kind of an application, because the maintenance costs of the subsea compressor are considerable. The subsea compressor is designed to operate for approximately five years without any maintenance. The simplicity of the compressor is therefore a clear advantage. Traditional compressor and motor concepts do not generally meet this requirement. In an integrated structure, the gas from the compressor flows also through the motor. The flow of process gas provides motor cooling, since the gas has a high pressure and a high flow rate. On the other hand, the gas mixture is rather

aggressive and the insulation system of the motor has to tolerate it at all times.

There are a few alternatives for the integrated motor-compressor technology, which are currently under consideration. The benefits and drawbacks of different technologies are at least to some extent industrial secrets, and not within the scope of this thesis. Therefore, they are not compared or discussed any further here, and the reader is referred to (Brenne et al., 2008) for more information. This thesis discusses the technology that relies on the use of a high-speed induction motor. The investigations for the uses of other motor types are currently ongoing, but they are not discussed in this thesis. The output power of the compressor motor is relatively high, 9 MW. Basically, with sophisticated design features, it is possible to build a motor of such output power with low-voltage technology. However, the current in a low-voltage machine is very high and the cable penetrators of subsea installations cannot handle high currents. It is, therefore, less risky to use high-voltage motor technology and the operating voltage of 6.6 kV.

The electrical motor is a high-speed, solid-rotor induction motor. It is a close relative to the axially slitted solid rotor construction, which has been used in the natural gas distribution network (Pyrhönen et al., 2010). The motor with a typical high-voltage insulation system can operate in the sales gas quality, but does not tolerate raw natural gas containing heavy hydrocarbons and water.

This is the first attempt to operate a high-voltage electrical motor subsea and in direct contact with raw natural gas. It was found early in the reasearch that there are no commercially available insulation systems that have been shown to tolerate such conditions. Therefore, the insulation system used in the sales gas compressor presented in (Pyrhönen et al., 2010) was taken as a starting point. It consists of glass-backed mica tape and polyesterimide impregnating resin. The insulation system also contains a stress grading layer and protective tapes made of a polyester or polyethylene terephtalate (PET) film. The insulation system and its components are illustrated later in Fig. 2.1. The polyesterimide impregnating resin and materials based on polyester and PET have been found not to withstand raw natural gas. The problematic component in the insulation system in this respect is the stress grading layer, because all commercial stress grading materials are based on a polyester or PET film. The insulation system to withstand raw natural gas requires further evaluation, which is the objective of this thesis.

The motor is driven by a frequency converter located onshore. It is connected to the motor by a high-voltage subsea cable. The transformers are located at both ends of the high-voltage link, that is, onshore and in the bottom of the sea at the wellhead. They act as filters and smooth the fast transient components potentially caused by the inverter. Fast transients in the windings are known (Stone et al., 2004) to cause partial discharges and thereby degradation of the insulation. However, the transformers cause the voltage waveform to be closer to a sinusoidal. Therefore, the motor insulation is not expected to suffer from degrading effects caused by the variable speed drive.

1.3 Objectives of the work

The primary objective of the work was to find an insulation system that works in an electrical motor operating in direct contact with raw natural gas. Furthermore, the goal was to define the required changes to the fundamental machine design including insulating materials. The most reliable way to achieve the primary objective is to go through a complicated set of experimental tests in actual conditions and with a full-scale test apparatus, which is far too complicated and time-consuming for a single thesis. Thus, the approach was taken and the objective achieved by investigating the physical phenomena related to the materials and the environment.

The role of partial discharges, which are perhaps the most common reason for an insulation system in an electrical machine of such size and operating voltage to fail, was approached by measuring them as a function of pressure. The results indicated that no discharges are present at the gas pressures at which the motor operates. This conclusion rules out the given failure cause. Additional design features were discussed with theoretical methods, but practical tests indicated that there is no need for such features. Another purpose for the theoretical study was to create a tool for the electrical field analysis of an insulation system in a high-voltage electrical machine. It provided a viewpoint on the insulation of high-voltage machines in general, not only regarding the application at hand.

The chemical effect of the raw natural gas on the insulation is also an apparent failure cause of the machine. The objective was to detect these effects. The materials were investigated and it was discovered that certain epoxy resin and glass-backed mica tape can provide adequate chemical resistance. It was observed that the insulation system is facing the diffusion process under the influence of the raw natural gas. The diffusion reduces the properties of the insulation, but not severely if the system can protect the machine from additional stress factors. The role of rapid pressure changes was emphasized. Moreover, it was seen that diffusion is the dominating influence, and the performance of the insulation system is dependent upon it.

The investigation for aging effects in hydrocarbon gas mixture under high temperature and pressure is difficult to carry out. In order to meet the objectives above, the test procedures had to be designed and tested. The objective of the practical work was to define a test method that can distinquish the effects caused by the aging phenomena, and minimize the effects caused by the test arrangements.

1.4 Outline of the thesis

This doctoral thesis consists essentially of two parts: partial discharge measurements and chemical aging tests. The performance of an electrical motor in a natural gas environment and the aspects that need to be taken into account are discussed based on the results of these two investigations.

Chapter 2 provides the background study on the high-voltage electrical motor technology over the past 100 years. The materials that can be used in the insulation systems of modern high-voltage electrical motors are described. The main philosophy of the aging phenomena in an electrical insulation is depicted with a few relevant aging models. The theory behind the physical phenomena (namely diffusion and dielectric relaxation) related to the study are provided.

Chapter 3 describes the methods of analysis. First, the test matrix is presented and the stress factors and their significance discussed. The test arrangements for gas properties and partial discharge measurements are described. Finite element modeling is also briefly enlightened. The preparation of the test specimens is described. The chapter also describes how the natural gas mixtures are prepared for chemical aging tests and how the tests are carried out. The methods used to discern what has happened to the materials, including measurements on mechanical and electrical parameters, chemical composition, and certain physical properties are presented together with a statistical analysis.

Chapter 4 presents the results on partial discharge and surface tracking investigations. First, the measurements on breakdown strengths of the gas mixtures are illustrated. Second, the measurements on partial discharges at different pressures are presented and discussed. Such measurements have also been analyzed with finite element methods. Finally, an investigation on ways to prevent surface tracking is shown. Such a study is fully theoretical and carried out with the model based on the measurements of partial discharges. A comparative analysis on different methods is shown, and the applicability of each method for the use in a subsea compressor discussed.

Chapter 5 covers the chemical aging experiments. Comparative studies on the suitability of different materials are shown. More detailed aging tests focusing on the analysis on the effects of individual components in the raw natural gas on the insulating materials, the effect of temperature on the aging phenomena, long-term performance of insulating materials, and the influence of rapid decompression are evaluated. The results are presented in Sections 5.1 – 5.6 with the focus on the observations. The discussion on the chemical aging phenomena and on the implications of the observations is presented in Section 5.7. The discussion aims to interpret the results in the whole context and to discern the physical meaning of them. Finally, the validity of the test matrix used is critically discussed.

Chapter 6 summarizes the primary conclusions of the work and discusses the topics of future research.

1.5 Scientific contribution

The scientific contributions of this doctoral thesis can be listed as follows:

- Definition of the linear sections of Paschen curves for nitrogen, methane, a mixture of hydrocarbon gases, and wet methane.

- Determination of a pressure limit above which the partial discharges disappear in an electrical system similar to the winding of an electrical motor.
- Development of a two-dimensional calculation model for dielectric problems and in particular for the behavior of electrical field in an electrical system similar to the winding of an electrical motor.
- Evaluation of the suitability of the insulating materials when exposed to raw natural gas. The materials suitable for the environment were identified, and materials that cannot withstand the conditions were also discerned.
- Analysis of the effects that the individual components in raw natural gas, such as heavy hydrocarbon compounds and water, have on the insulating materials.
- Identification of the effects that rapid pressure changes have on the insulation system.
- Observation that degradation is related to the amount of gas mixture that the materials have absorbed.

Chapter 2

Insulation system of a high-voltage electrical machine

This chapter contains the theory on which the research is based. In order to understand the functions and purposes of the insulating materials and to tailor them as parts of an insulation system of an electrical motor, it is useful to review the evolution of the technology starting from the first high-voltage machines ever built. The modern insulation systems aim to be essentially cost-effective, and their performance is 'adequate' instead of being 'maximized'. Many decades ago the philosophy was, explicitly, to introduce a new insulation system, because the old system simply did not work.

An insulation system is a key factor in the reliability of an electrical machine. Thorsen and Dalva (1995) investigated failures of electrical motors used in oil and gas applications in Norway. According to them, the stator winding failures account for 13% of all failures of high-voltage electrical motors. However, the most dominating cause they observed was the bearing faults with the share of 42%. It was mentioned earlier that the subsea compressor is supported by active magnetic bearings. Therefore, the contribution of the stator insulation is expected to be higher in a subsea compressor. The reliability is emphasized in special applications that do not include spare equipment in parallel with the operating one. In a subsea compressor, a broken motor causes a long outage, because the whole compressor has to be lifted from the bottom of the ocean, a new motor installed, and the compressor reassembled to the bottom of the ocean. Therefore, the price of a failed insulation is extremely high.

The basic structure of an insulation system in a high-voltage motor is illustrated in Fig. 2.1. Such an insulation system is used in common motors operating in industrial applications. The turn insulation is typically laid on the copper in the manufacturing process of the coils. It is provided by the vendor of the conductors. The mainwall insulation and all the protective and field grading tapes are wrapped on the coils, and finally, the insulation is impregnated with resin.

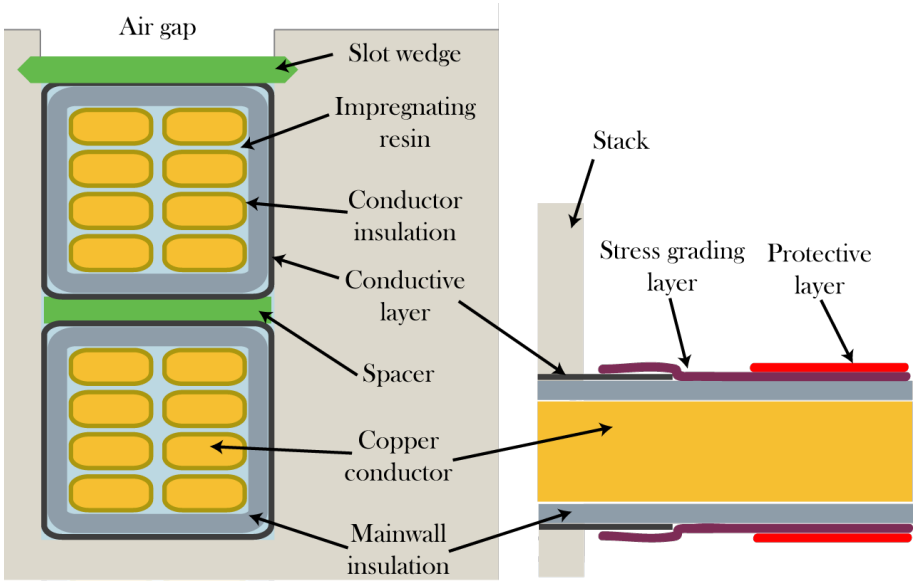

Fig. 2.1. Basic structure of the insulation system in a high-voltage induction machine stator. Cross-section of the slot area on the left and end-winding area on the right.

In the resin rich (RR) technology, the resin is provided within the mainwall insulation tape. The mainwall insulation is pressed into a desired shape and heated so that the resin inside the tape cures and a solid composite insulation is formed. The RR process has been used in large motors and generators for decades. An alternative to resin rich is vacuum pressure impregnation (VPI), in which the mainwall insulation tape does not contain impregnating resin – although it does contain a small amount of resin to bind the mica flakes and glass together. The winding is submerged into impregnating resin under vacuum and then under pressure allowing the impregnating resin to fill all the voids inside the insulation. Then, the insulation is cured. The VPI process has many advantages over the RR process; for instance, the whole stator is impregnated and also the voids outside of the mainwall insulation tape are filled with resin. However, the VPI process requires more sophisticated properties from the resin, such as low viscosity.

The functions of different parts in the insulation system change when the machine is operating in harsh environments. The protective layer is not capable of protecting the insulation system from gases and liquids present in the surrounding environment. It has been observed (Sihvo et al., 2008) that water can penetrate through the polymeric materials and it can cause damage to materials that are covered by other materials, which can withstand water. Hence, all materials in the insulation system must be resistant to the surrounding environment. Considering Fig. 2.1, the protective layer is not able to protect the materials underneath it from the natural gas mixture, but the gas can penetrate through the protective layer. Thus, there is no distinct purpose for the whole protective layer. It is used in industrial motors to protect the winding from dirt, contaminants, and moisture.

The purpose of and need for the stress grading layer in Fig. 2.1 are discussed in Chapter 4. The chemical aging tests have been performed on the mainwall insulation and impregnating resin.

2.1 Partial discharges and electrical breakdown in gases

High-voltage electrical motors must typically deal with partial discharges, which are small discharges taking place in the stator slot or in the end-winding region. They occur as a result of a high local electrical field strength. When the field strength exceeds the breakdown field strength of the medium between the electrodes, a discharge takes place. If the discharge takes place along the insulation surface, it is called a surface discharge, and the phenomenon causing degradation to the insulating materials is referred to as surface tracking. It has slightly different symptoms in the windings, but it originates from the same reason as partial discharges located inside the internal voids in the insulation.

There are some ways to reduce partial discharges and surface tracking, but normally, high-voltage electrical machines can tolerate them to some extent. They do not instantly cause a failure, but gradually weaken the insulating materials, which ultimately leads to a breakdown of the machine. In high-voltage motors and generators, a great deal of breakdowns and faults are, in one way or another, linked to partial discharges.

The role of partial discharges is essential in air-cooled motors having a voltage rating above 4 kV. The breakdown strength of air is approximately 3 kV/mm at atmospheric pressure. The breakdown strength of air increases as the pressure increases, which holds also for other gases. This was first observed by Paschen (1889). Therefore, with respect to partial discharges, a motor operating with a higher pressure in the air-gap would be a less vulnerable one. This is a known issue in hydrogen-cooled large generators. Emery (2005) reported that the partial discharge inception voltage, that is, the voltage above which the discharges appear, is approximately doubled if the pressure is increased to 4 bar. This happens even though the dielectric strength of hydrogen is lower than that of air (Meek and Craggs, 1953).

The dielectric breakdown of a gas medium is caused by the ionization of the gas molecules, as described by Townsend (1915). When exposed to a high electric field, gas molecules produce ions, which, having either positive or negative sign, are attracted to the electrode of opposite sign. Thus, they acquire a velocity and frequently collide with other gas molecules that happen to be in their way. Collisions produce new ions, which also begin to move. The energy needed to ionize the gas molecule is obtained from the kinetic energy of the colliding ion. The kinetic energy itself has been obtained from the external electrical field. As the activity goes on, the motion of ions will reach from electrode to electrode giving the gas a constant conductivity. In practice, the result of ionization, or the conductive state of the gas, is seen as an arc or a lightning, in which a very large amount of energy is released. This is also called a Townsend avalanche referring to the ionization process, which, when initiated, progresses uncontrollably like an avalanche. The voltage needed to maintain the constant current does not need to be very high, if enough current is provided. However, the

voltage required to initiate the ionization process, which then more or less feeds itself, is rather high. As the pressure of the gas increases, the gas medium between the electrodes contains more molecules and more energy is needed to ionize them. Furthermore, the ions are located more densely and provided less space to acquire the velocity. This is seen as a higher voltage needed to cause a breakdown, in other words, as the pressure increases, the breakdown strength of gas increases.

2.2 Mainwall insulation

An overview of trade-marked insulation systems for high-voltage electrical motors by Stone et al. (2004) shows that all primary motor vendors use glass-backed mica tape and epoxy resin. Still, the majority of the insulation systems for 6.6 kV electrical machines use either polyester or polyesterimide resins nowadays. With respect to performance, they are both worse than epoxies, but they can significantly lower the costs of the machines, and their properties are still adequate for normal operation. However, polyesterimide and polyester resins do not have good chemical resistance. It has been reported (Sihvo et al., 2008) that neither of them is able to tolerate water at a high temperature. Apart from glass fabric, the backing material for mica tape can also be a PET film (polyethylene terephthalate), Kapton® polyimide, or Nomex® aramid fabric. Also glass fabric can be modified. These solutions are discussed in more detail later in this section.

2.2.1 The first high-voltage machines

In the early days, there was no distinct way to build the insulation system. Nowadays, there lies a rather clear division between low-voltage and high-voltage machine insulations, that is, mica-based and fully organic insulators, but it was not so in the dawn of the 20th century. Large low-speed machines had mica-based insulation. As an example, the first generators (3750 kVA, 2200 V) of the Niagara Falls hydro power plant built in 1894 used mica splittings applied on a cambric (Newbury, 1915). However, turbo-generators favored cellulose, because mica was difficult to apply on long stators (Lamme, 1913).

Soon after such turbo-generators with cellulose insulation began to prematurely break down, laboratory tests for alternative insulation systems showed that mica does not suffer any damage because of partial discharges even if the wrapper material surrounding it has been ”eaten away” as described by Lamme (1913). Earlier findings had shown that mica possessed the best thermal properties of the materials then considered as insulators in electrical machinery. Considering its properties and performance, mica was put in the position of a superior material. Lamme (1913) seized the opportunity and stated: ”This is one of the rare cases in large turbo-generators where two desirable conditions do not conflict with each other.” Almost 100 years later it still seems that this kind of a statement cannot be expressed too often.

2.2.2 Mica and asphalt varnish

In the early days, a common way to build a mica-based mainwall insulation was to apply mica flakes on a cambric or some strong paper (e.g. fish paper or kraft paper) and to use shellac or copal resin as a binder (Stone et al., 2004; Flight, 1923; Fleming and Johnson, 1913; Flynn et al., 1958). To improve the mechanical properties, varnish-treated cotton cloth or tape was applied as outermost layer in the end-winding region (Laffoon, 1930; Miner, 1941; Fleming and Johnson, 1913). However, shellac or copal resins became very hard and brittle especially when they were heat-aged (Flynn et al., 1958). They were replaced by asphalt varnish in the early 1920s. Asphalt varnish provided better flexibility, thermal stability, and a longer service life than the shellac-bonded insulation (Hill, 1928; Flynn et al., 1958). Insulation systems consisting of mica paper and asphalt varnish were used widely for approximately three decades. Such an insulation was used for instance in Queenston plant generators built in 1922 by Westinghouse (McCarty and Hart, 1922) and in Niagara Falls generators built in 1923 by General Electric (Foster and Glass, 1924). Both generators were designed for 12 kV operation. During the 1920s and 1930s there was a trend to go for higher voltages, which led to voltage levels such as 13,8 kV, 22 kV, and 33 kV. Concurrently with the increasing voltage, the output power was increased. As a consequence, more stress was put on the insulation requiring better materials.

With the increasing power, the problems related to machine cooling were stressed even further. Machines were seen to heat easily and the thermal stability of insulating materials was not very good, especially asphalt was performing poorly at high temperatures (Laffoon et al., 1951). The insulation – its thickness and heat conductivity – was probably one of the reasons for poor cooling. Almost all the heat from the conductors flows through the insulation, and engineers in the 1920s were aware of this (e.g. Steinmetz and Lamme, 1913). The engineers did not, obviously, want to increase the thickness of the insulation any further. It was already taking notable space inside the stator slot.

Mica-asphalt insulation had its benefits and drawbacks. Such an insulation system was able to provide a very long service life. It was mostly inorganic and able to tolerate partial discharges. Timperley and Michalek (1994) defined the remaining service life for an insulation system of a machine put into service 37 years ago, and David et al. (2004) investigated windings of a machine put into service 52 years ago. Mica-asphalt insulation was subjected to vacuum and pressure treatments (Miner, 1941). Basically, the manufacturing procedure was similar to that of the resin rich method used today. However, mica-asphalt insulation was rather difficult and time-consuming to manufacture, since the viscosity of the varnish was very high and the insulation had to be varnished after each layer of mica tape applied and even multiple times (Laffoon et al., 1951). Furthermore, it produced high dielectric losses and was mechanically weak at a high temperature. The asphalt varnish is a thermoplastic material. At a high temperature, it does not behave like a solid, but rather like a fluid with a high viscosity. According to Laffoon et al. (1951), the temperature limit is approximately 100 °C. At a high temperature the asphalt bonding is not able to keep the mica splittings in place, which leads to delamination of the mica tape layers and further to mechanical damage. In fact, this was called a ”thermal damage” at that time, while ”mechanical damage” referred to the flaws and errors originating from the manufacturing process, (Flynn et al., 1958). The

poor performance of mica asphalt insulation at high temperatures was emphasized in stators with long coils, which are used for instance in turbo-generators. The asphalt bonding was modified to improve thermal stability and strength (Hill, 1928; Laffoon and Calvert, 1935; Flynn et al., 1958) and, finally, it was replaced by synthetic resins in the 1950s.

Synthetic resins, both epoxy and polyester, were developed during the 1940s. They were instantly being investigated for electrical machine insulation purposes and soon replaced asphalt varnishes in many machine applications. However, the resins were not the only innovations of the insulation systems of the new generation. Perhaps one of the prerequisites for their use in high-voltage machines was the introduction of semi-conductive paints for stress grading materials. Previously, mica-asphalt insulations used asbestos in the slot portion of the coil, but mostly the partial discharge problems were escaped, because the insulation system simply tolerated them. It was mentioned by Alger (1928) that his company had 22 kV machines without any protection that had been operating without problems for five years. But then he adds: "These machines have so much corona on the end-windings that the lines between the terminal coils of each phase and the adjacent end-windings of the next phase are continually illuminated by a line of light during operation."

2.2.3 Mica, glass fabric, and synthetic resin

Laffoon et al. (1951) published an insulation system containing mica tape impregnated with a solventless polyester resin. The coils were reinforced with a glass fiber tape in the end-winding regions. Such an insulation system was used by Westinghouse in 1949. Laffoon et al. (1951) reported the new insulation system to have superior performance in a high temperature when compared with mica-asphalt insulation: they reported the tensile strength to be over 30 times as high and the loss tangent to be less than one fourth at 100 degrees centigrade. However, they did not discuss whether the changes were caused only by the new resin, or by the modified, more porous backing of mica tape. A few years later, a new generation insulation concept by General Electric was introduced (Flynn et al., 1958). It utilized a modified epoxy resin as a binder and glass fabric as the backing material of the mica tape. Flynn et al. (1958) reported similar improvements in the insulation performance as Laffoon et al. (1951).

Andersson and Örbeck (1967) presented the insulation system of the Swedish motor manufacturer ASEA (now ABB), which contained no binder resin inside the mica tape. The binding between mica and glass was produced by a film, which was melted. The insulation was then impregnated with epoxy resin under vacuum. Also Siemens used the VPI method in the 1960s (Wichmann, 1972). At present, the VPI method is preferred in many occasions, but RR still remains in use.

Since the 1950s, the construction of mica-based mainwall insulation in high-voltage machines has been essentially similar: mica, glass fiber, and epoxy impregnating resin. Although the last component is nowadays more frequently polyester or polyesterimide, it is still epoxy, if excellent chemical resistance is required. The development has been mostly pointed to reduce the number of internal voids and to improve the thermal conductivity of the insulation. There have been advantages in mica tape manufacturing and taping methods leading to a better

quality of tapes and the whole insulation, and thereby to a lower partial discharge level. Yet, improvements may not have been that significant, that is, the insulation systems built in the 1960s can be considered competitive also from today's point of view. The tensile strength reported by Andersson and Örbeck (1967) is close to that reported by Emery and Williams (2007). Also the discharge levels reported by Andersson and Örbeck (1967) and by Wichmann (1972) are not essentially higher than the ones reported for modern insulation (Emery and Smith, 2001).

2.2.4 Insulation systems used in the present-day high-voltage machines

Regarding normal operating conditions and the voltage level of 6.6 kV, there are several alternatives today. PET films can decrease the costs of the insulation system (Brütsch et al., 1999) without reducing its performance (McNaughton, 1993). Also Kapton® polyimide films can be used as a more corona-resistant Kapton CR® quality (e.g. Emery and Smith, 2001). The film provides a thinner backing than the glass fabric, which allows more space to be filled with mica or reduction of the thickness of the whole mainwall insulation. Applying more mica inside the insulation improves both the dielectric strength and thermal conductivity of the insulation. Even though the film increases the dielectric strength of the tape, mica is still considered the primary dielectric barrier. The film is only a reinforcement. This philosophy is based on the poor PD resistance of the film materials. The dielectric barrier is not allowed to be damaged by the partial discharges.

A disadvantage of the film backing is that the impregnating resin is not, obviously, capable of flowing through the film. Therefore, the resin is only allowed to flow along channels parallel with the conductors. This may lead to imperfect impregnation of the insulation, and thus, to a higher number of voids inside the insulation, and further, to a higher partial discharge level. However, the penetration through different layers is not very good with the glass backing either. During the impregnation of the glass-backed tape the resin is able to flow easily along the tape layers, but cannot pass through them. The resin gets between the different layers at the end-winding where the taping is less dense, and then flows along the layers into the slots. Inside the stator slots, only little resin can pass through the tape layer.

Aramid fibers (Nomex®) can also be used as a backing material. Such a mica tape is more flexible and it can be more easily impregnated than the common glass-backed tape. To improve the impregnability, the amounts of glass and mica can be optimized. Further optimization can be done on the particle size and distribution of mica flakes. The backing glass fabric can also be modified into a thinner shape (Grubelnik et al., 2005). A thinner glass fabric reduces the thickness of the tape, thus allowing to apply more layers or to reduce the thickness of the insulation. In both cases, the heat transfer through the insulation is improved, because the insulation contains more mica and less resin, which has a lower thermal conductivity than glass or mica. It has been reported that a thinner glass fabric can provide a lower partial discharge level and a higher tensile strength (Grubelnik et al., 2005; Emery and Williams, 2007), but it was noted by Emery and Williams (2007) that such a tape is difficult to fully impregnate. Yet another method to increase thermal conductivity is to apply fillers inside the mica tape (Tari et al., 2002).

The epoxy resins used for high-voltage machine insulation today are mainly bisphenol A epoxy resins and epoxy novolac resins. A common chemical structure of the base epoxy component of the former is illustrated in Fig. 2.2 and of the latter in Fig. 2.3. The complex polymer matrix of an epoxy resin is produced with a curing agent, which attaches to the epoxide groups (a ring C-O-C at both ends of the polymer chain in Fig. 2.2). The curing agent combines the base epoxy groups into a complex polymer matrix by producing crosslinks between the epoxy groups of adjacent bisphenol A molecules. The curing reaction with an anhydride curing agent is illustrated in Fig. 2.4. The illustration covers only the reacting part of the anhydride. The rest of the chemical structure depends on the type of the anhydride curing agent used. The presence of the crosslinks is determined by the base epoxy resin. The crosslink density is determined based on how large a chemical structure there is between the epoxy groups. If the crosslinks are allowed to form close to each other, the crosslink density of the cured resin is high.

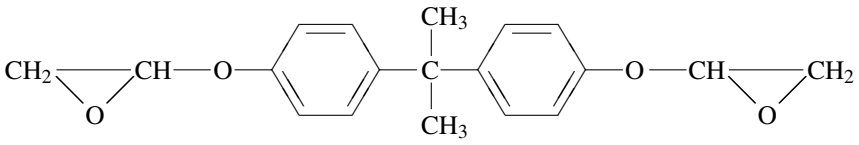

Fig. 2.2. Chemical structure of a bisphenol A epoxy resin (Sperling, 2006).

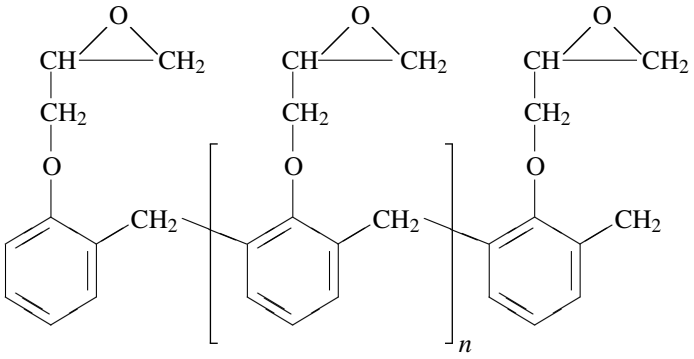

Fig. 2.3. Chemical structure of an epoxy novolac resin (Petrie, 2006).

In addition to bisphenol A and epoxy novolac resins, also bisphenol F resins can be used. They are very similar to bisphenol A and cure in the same way. As compared with bisphenol A epoxies, bisphenol F resins have a lower viscosity and a greater flexibility. The resin is more flexible, because its glass transition temperature is lower. Epoxy novolac resins differ significantly from bisphenol A epoxy resins regarding their chemistry. The epoxy groups appear densely in the chemical structure, which provides a high crosslink density when the epoxy groups react during the curing process. They typically have a better high-temperature performance, a better chemical resistance, and a higher adhesion strength than bisphenol A

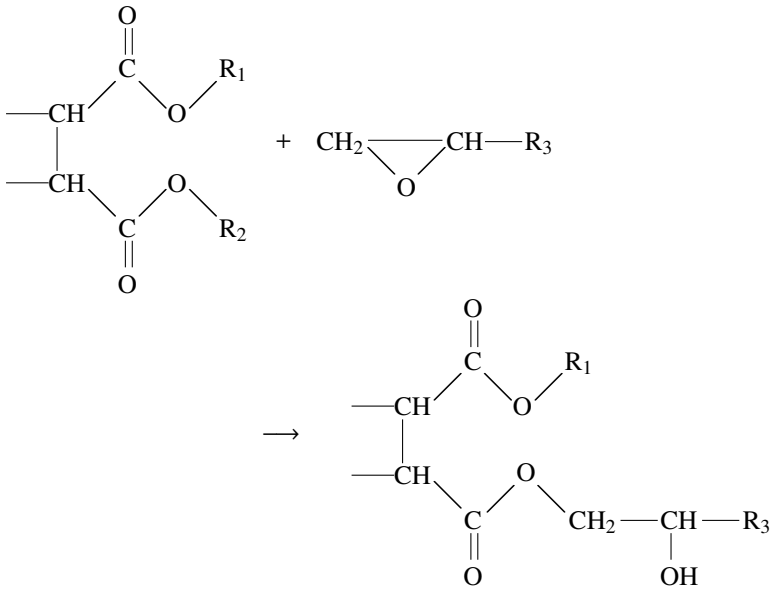

Fig. 2.4. Typical curing reaction of the bisphenol A epoxy resin and the anhydride curing agent (Petrie, 2006). The CO groups in the anhydride component are initially connected with an -O- linkage. Prior to the curing reaction, this linkage is opened.

resins. The high crosslink density of epoxy novolac resins is responsible for their rigid and brittle nature. The properties of different resins were collected from Petrie (2006).

One of the key properties of polymers is their glass transition temperature T_g. It is the temperature at which the polymer undergoes a second-order phase transition from stiff and rigid "glassy" state into more flexible "rubbery" state. The terms in quotation marks are used widely to describe the phenomenon, even though they are rather arbitrary and not precise. Yet, they illustrate the phenomenon quite well, because it is a statistical one. The glass transition is related to the motion of molecules inside the polymers. At T_g, the internal energy of a certain polymer chain exceeds the energy barrier that prevents its motion, and the molecule can slide past the other molecule that stands on its way. Glass transition is a statistical phenomenon, because all the molecules are not allowed to move at the exact same temperature, and the changes observed in the measurements of heat flow (the measurement is described briefly in Section 3.6.4) can be seen in a wide temperature range of 20 °C for instance. The T_g is located in the middle of this region. The T_g is dependent upon many properties of the polymers, such as the crosslink density and molecular weight, but the researchers still have difficulties to fully and thoroughly explain the phenomenon and all of its implications (Sperling, 2006).

There are many possible curing agents for epoxy resins, such as bisphenol A. The curing agent depends on the application and its requirements, because the curing agent also affects the properties of the finished resin system. Anhydrides and aromatic amines are commonly used in electrical machine insulation, because they provide good heat resistance. Both cur-

ing agents require a long curing time, and anhydrides are rather sensitive to the mixing ratio (Petrie, 2006). The curing reaction as described in Fig. 2.4 can be activated with an additional accelerator component, which opens the ring structure in the epoxide groups. Boron trichloride (BCl_3), tertiary amines and metallic salts can be used for the purpose.

The accelerators used in high-voltage electrical machine insulation include mainly BCl_3 and zinc naphthenate. The advantage of zinc naphthenate is that it can be applied inside the mica tape, and it does not need to be premixed with the resin. The resin mixture does not contain any accelerator and its pot life is thereby increased. In addition, the amount of BCl_3 accelerator needed is precise and very small, roughly 1/1000 parts by weight versus resin and curing agent, and it has to be thoroughly mixed with the base component and the curing agent. Furthermore, the curing time of the resin with zinc naphthenate (e.g. 8 hours) is lower than that with BCl_3 (usually in two steps, e.g. 12 hours + 16 hours). The faster gel time, that is the time until the resin begins to turn into solid, of the resin with zinc naphethenate accelerator also leads to a reduced amount of resin flow-out in the winding. The viscosity of the resin is very low before it reaches the gel point and begins to turn into solid. It has been reported (Emery and Smith, 2001) that mica tape with zinc naphthenate accelerator provides lower dielectric losses, higher breakdown strength, and higher tensile strength than a similar tape with the BCl_3 accelerator. However, zinc naphthenate is generally not able to provide very good thermal stability. The technical reasons listed above reduce the costs of the zinc naphthenate-accelerated insulation without significant compromises on the performance.

2.3 Stress grading

The stress grading or field grading is related to the reduction of the local electrical field strength at the end of the conductive layer in the end-winding region, as seen in Fig. 2.1. High local field strengths are caused by the sharp edge of a ground electrode, which is virtually formed by the conductive layer and the stator stack. High fields cause partial discharges in the insulation and surface tracking on the surface. Materials with a high and nonlinearly field-dependent resistivity are used for stress grading nowadays.

2.3.1 Early implementations and introduction of nonlinear materials

The machines built with mica and asphalt varnish were not as vulnerable to partial discharges and surface tracking as the modern machines. The old insulation construction with a larger thickness and a lower relative permittivity did not generate as much discharges as the modern insulation. Furthermore, the insulation systems used in the early high-voltage machines were completely inorganic and experienced very little degradation caused by partial discharges even at very high voltages. Nowadays, 6.6 kV is considered a dangerous voltage level, if the issue has not been solved in the machine design. The dielectric constant of the mainwall insulation built of mica and asphalt varnish is approximately 3 (Alger, 1928), whereas that of a present-day mainwall insulation is in the range between 5.5 and 6 (e.g. Hong et al.,

2009b). The insulation system used in the experimental program had a dielectric constant of approximately 5. Furthermore, the old insulation needed more space than the modern insulation. The thickness of 2 mm is more than enough with modern materials, but according to Miner (1941) the recommended thickness was 3.2 mm for the 6.6 kV insulation. The difference between old and modern constructions is linked to the materials used then and now.

One of the earliest approaches to stress grading was presented by Hill (1928). He introduced a stress grading method having a resistive layer at the end of the conductive film installed inside the slot. He said that in the ideal case the resistance would have to change as a function of voltage – like the present-day stress grading materials work. Hill proposed a highly resistive "damping layer" made of asbestos that contained no organic fillers. Some time later in his book Miner (1941), who together with Hill worked with Westinghouse, instructed to implement the stress grading in a similar way, basically by terminating the conductive layer with well-varnished mica tape and covering the whole insulation with asbestos tape. The purpose of varnish in this case is to fill all the voids. Before vacuum impregnation processes were introduced, the insulation system, even if very carefully constructed, contained a large amount of internal voids.

The Parsons generator (25 MVA, 33 kV, 3000 rpm) built in 1929 applied a special winding construction (Parsons and Rosen, 1929). Its winding consisted of concentric conductors assembled in partially closed slots. The machine had thus to be wound by sewing. The coils contained an inner conductor and two conductors inside the insulation. These conductors formed different groups, which were connected in series. The insulation system only saw the voltage of 11 kV, instead of 33 kV. The potential gradients were practically absent, because there were no sharp edges. Inspired by the Parsons generator, Laffoon (1930) proposed a stress grading method having three conductive films assembled inside the insulation everywhere in the winding. He thought that the stress grading is most urgently needed at the corners of the conductors, and therefore did not discuss the slot exit region.

Laffoon and Calvert (1935) proposed three methods of stress grading. The first one contained semi-conductive foils inside the mainwall insulation in slot exit areas. This method was used for a certain degree still in the 1960s (Manni and Schneider, 1960). The second method contained a resistive stress grading region consisting of four different layers, all having different resistivity. The need for nonlinear behavior of resistivity was tackled by changing the whole material, not just its resistivity. They did not consider that the resistivity of the material could change. The third method was a combination of the first two methods. The foils were considered semiconductive, because the authors suspected that conductive foils might cause high eddy current losses.

Manni and Schneider (1960) proposed their method of stress grading with conductive foils inside the insulation. They also defined the desired places for foils. Such a method was mentioned earlier by Fleming and Johnson (1913). There are some practical limitations to the use of foils. The space the foils take cannot be occupied by the insulation and the breakdown strength of the insulation is thus weakened. Furthermore, the foils are difficult to assemble (Roberts, 1995). Considering the former difficulty, Laffoon and Calvert (1935) mentioned

that the maximum number of foils (in their proposal the foils were semi-conductive) can be three. If increased, the thickness of insulation would become insufficient.

In the 1950s and 60s, semi-conductive paints were introduced. Soon they became widely used as stress grading materials (Moses, 1951; Wichmann, 1983). They were later replaced by nonlinear materials (Kelen and Virsberg, 1964; Thienpont and Sie, 1964). Today, silicon carbide, SiC, is almost universally used for stress grading because of its simplicity and efficiency (Roberts, 1995).

2.3.2 Recent studies

Rivenc and Lebey (1999) studied resistive and capacitive stress grading methods in a theoretical manner. They concluded that a capacitive stress grading layer cannot provide adequate performance, even if the permittivity is 10. Resistive stress grading, on the other hand, is said to provide sufficient protection when the resistivity of the material is 0.1 MΩm. If the resistivity is increased from that, the stress grading properties are weakened. Rivenc and Lebey conclude that the resistivity of a proper stress grading material does not need to be nonlinearly dependent on the electrical field but it can also be constant.

It has been found that SiC stress grading materials face severe difficulties in the motors fed by a high-voltage PWM drive (Espino-Cortez et al., 2005; Sharifi et al., 2008; Wheeler et al., 2007). It was earlier reported by Kadotani et al. (1980) that SiC-based materials do not perform well with high frequencies. Based on calculations, Espino-Cortez et al. (2005) concluded that the stress grading material must have some conductivity in addition to its nonlinear resistance behavior. Sharifi et al. (2008) have proposed conductive foils to be used inside the mainwall insulation together with stress grading SiC tapes on top. Previously, Kimura and Hirabayashi (1985) had reported that an embedded semi-conductive sheet inside insulation improves the heat suppression in that area. Wheeler et al. (2007) proposed a more complex stress grading structure having a layer of mainwall insulation between two layers of stress grading tape.

For the cases for which the most commonly used stress grading materials are not suitable, the cable industry has provided inspiration for a long time. High-voltage cables operate with a voltage significantly higher than what could even be considered in electrical machines, although higher voltage levels can be used with cable windings (Nestli et al., 2003). High-voltage cable terminations and joints are to a certain degree similar spots as the terminations of conductive layers in high-voltage electrical machine windings. However, all the methods suitable for cable terminations cannot be applied to electrical machines, because the space available for terminations is very limited. The distance between adjacent coils is usually less than a few centimeters and the termination of both coils should fit in there. Roberts (1995) mentions two possible ways for stress grading both adapted from cable industry; termination with a high-permittivity layer, which is actually a straightforward derivation from the laws of physics, and a stress cone. The latter was already mentioned by Short (1949), and perhaps this was not the first time such a solution was employed.

Termination of a high-permittivity material is a very simple solution. It requires only a layer of material applied on the termination spot. Basically, it works, if the permittivity is high enough. However, the permittivity needed for this is another matter. Roberts (1995) defines that it has to be over 30. As mentioned above, Rivenc and Lebey (1999) studied materials with a permittivity of 10 at highest and concluded that such materials do not provide notable improvement. For the requirements of cable industry, there are materials capable of providing the permittivity values in the desired range (Nelson and Hervig, 1984), but such materials cannot be used in an electrical machine insulation system. Their geometry and mechanical strength do not meet the requirements.

2.4 Insulation systems for harsh environments

One of the future trends in the field of electrical machines is to operate them in harsh operating conditions. The frequency converters and adjustable speed drives provide significant advantages for the control of the application and energy efficiency. Such benefits drive the engineers to beat the traditional obstacles related to heat or chemical resistance of the materials, namely motor insulation. The processes containing aggressive chemicals, water, or some other degrading components are powered by electrical motors exposed directly to the process conditions.

Water is one example of harsh environments. For many years, submersible water pumps have been exposed to water at the temperature of 90 °C at highest. These machines have windings made of special polyethylene-insulated wire, which looks like cable. The insulation can tolerate water up to 90 °C, above which temperature the water begins to react with polyethylene. Another approach to hot water resistant insulation has been taken with a biofuel-powered combined heat and power (CHP) plant (Sihvo et al., 2007). The plant was basically a common steam power plant, but the adjustable-speed generator was mounted on the same shaft with the steam turbine. The gearbox and axle seal, which both require a lot of maintenance, were not needed in this case, because the generator was able to operate in the same speed range with the turbine, but the insulation system in the generator stator had to withstand steam. The experiments with the insulation system, although the machine was a low-voltage one, suggested that Nomex® aramid paper and epoxy resins of bisphenol A and F can tolerate the environment. By contrast, polyester and polyesterimide resins and Kapton® polyimide film were found to react with water.

There has also been attempts to use cable windings in electrical machines. The benefit of such technology is that the transformer can be omitted, because the stator voltage can be increased to the level of the distribution network. The lack of the transformer offers cost savings, but the motor itself is very complex, large, and expensive. Such technology can be considered for the motors of very high output power. Cable windings are used in a 40 MW synchronous motor in Troll A gas production platform in the North Sea (Nestli et al., 2003). Basically, the cable windings can be built of materials that tolerate very aggressive environments. However, the cable winding takes a lot of space and drastically increases the length and outer diameter of the stator.

There are no commercially available insulation systems that have been proven to withstand raw natural gas. Yet, the historical development of the insulation systems provide some starting points for the quest for such an insulation system. At first, it appears beneficial to go back in time and change the cost-effective polyesterimide impregnating resin back to the more chemically-resistant epoxy resin. Furthermore, the stress grading materials based either on polyester or PET films that are used in modern high-voltage insulation systems must be replaced. However, there are no replacements, because all the stress grading materials widely available use a backing material that does not tolerate the environment. It is therefore important to look for other means to implement the stress grading than the resistive stress grading tape, which is, according to Roberts (1995), used almost universally today. Yet, the need for stress grading is not imminent under high pressure. The old development provides some ideas for the design of an insulation system that withstands raw natural gas. However, the suitability of an insulation system for a completely new application can only be verified by experimental tests.

2.5 Aging of insulating materials

When exposed to different stressing environments, insulating materials deteriorate and their key properties such as dielectric or mechanical strength decrease. This is called aging and in normal applications it is a relatively slow process taking for instance 20 years. IEC (2004) states that aging contains irreversible changes to the materials, and leads to the degradation of the insulation system. But the standard also points out that some changes can be partly reversible, if the ambient conditions change.

The aging can be caused by several stressing factors, which are normally categorized as **t**hermal, **e**lectrical, **a**mbient, and **m**echanical. This is well known order of the stresses, because their first letters form the word 'team', which illustrates that the stress factors usually interact. Yet, almost in every case when the machine insulation suffers a service failure and despite the root cause, the failure is indicated by an electrical breakdown, which triggers the safety equipment and shuts down the process.

The first two factors in the 'team' refer to the temperature and electrical field, respectively. Mechanical stresses are related to the vibration of coils, which is caused by the AC stator current and also influenced by transient components caused by power electronics or some other part of the drive system. Also continuous changes in the operating temperature cause mechanical stresses. Ambient stresses are caused by the surrounding environment, and in common applications they include for instance moisture, oil from bearings, chemicals, abrasive particles, dirt, and debris (Stone et al., 2004). IEC (2004) states that these stresses include "all ambient physical, radiative, chemical, and biological processes."

The message of the listings by Stone et al. (2004) and IEC (2004) is that the possible causes of aging have to be thoroughly contemplated for any new application. To some extent all the stress factors are usually present and they also interact. The lifetime is therefore determined by the combined effect of all the stresses. However, one stress factor may still be the dom-

inating one and cause initial forms of degradation. After the initiation of degradation, other stress factors step into the picture and accelerate the aging process. Furthermore, the physical phenomena causing the degradation tend to interact.

For instance electrical stress is caused by partial discharges, which degrade the insulating materials. When a discharge takes place in an internal void in the insulation, an amount of electrons are accelerated towards the walls of the void. If the wall consists of organic material, this causes chemical reactions, which decompose the insulating material. The influence of partial discharges is more severe at a high temperature, because chemical reactions tend to occur at an increased rate at higher temperatures. However, the partial discharge activity typically reduces slightly over time, because as a result of the chemical reactions the walls of the internal voids become slightly conductive. The interaction of thermal and electrical stresses has been investigated widely both from the perspectives of high-voltage cables and high-voltage electrical machines. Also, the thermal stress factor easily interacts with the ambient stress factor by accelerating the rate of chemical reactions caused by contamination or water.

From the subsea compressor's point of view, the classification of stress factors differs considerably from the common industrial applications. The raw natural gas and the components within it constitute the most severe stress factor. The insulating materials suffer from degradation as the gas penetrates into them. The penetration is enhanced by high temperature and high pressure. Furthermore, the gas mixture may contain components, which cause chemical changes in the materials. From the stress factors mentioned, the ambient factor is the dominating one and it is likely to interact with the thermal stress factor. By contrast, the electrical stress is more or less canceled out by the pressure, which reduces the amount of partial discharges. Yet, the electrical field can possibly accelerate the phenomena causing the aging, but the issue is not discussed in this thesis; it has been left for a future research topic. The effect of the electrical field is not likely to be dominating, because the voltage in the electrical machine is still rather low and certain high-voltage phenomena, such as space charges, are not dominantly present.

The prevailing temperature of the machine is not very high. The materials used in the experiments belong to thermal class 180 or higher while the operating temperature of the motor is approximately 100 °C. If the surrounding environment were air, the temperature would probably cause no aging at all, in other words, it would take very long time to observe any changes. However, temperature is an accelerating factor for diffusion and for chemical reactions. When polymer materials are heated close to their glass transition temperature T_{g}, they begin to soften. The glass transition temperature of epoxy resins used in electrical machines is typically over 140 °C, but the diffusion process causes a reduction in their glass transition temperature.

The lifetime of the winding of an electrical machine is a measure of its weakest point. An electrical flashover or a mechanical crack, which are typical reasons for the breakdown of the insulation, take place at the weakest point of the system. At this point, the insulation is poor, but elsewhere it might still be in acceptable condition. In other words, when a breakdown takes place in one of the coils in the electrical machine, the other coils may still have several

years of operation left.

When the degradation of insulation progresses, it is typically indicated by the increased partial discharge intensity. Therefore, the measurement on partial discharges is a good indication that some degradation has taken place, and in some cases it can even give predictions on the remaining lifetime. However, partial discharges take place, because there are voids filled with air or some other gas inside the insulation. Partial discharge activity may expand these voids, but initially they need some other form of stress or a manufacturing flaw to appear. The measurement on partial discharges is therefore only an indicator of the void content, but it cannot give information on the aging processes causing the voids. In the pressurized subsea compressor, the voids are filled with pressurized raw natural gas. The pressurized gas mixture inside the insulation does not increase the partial discharge activity similarly as the air does in air-cooled machines. Obviously, the measurements carried out during an outage for a dried stator would reveal the voids, but during operation the partial discharges are not expected to accelerate the formation or expansion of the voids.

The service lifetime of the insulation system in an industrial electrical machine is at least 20 years. The tests in the laboratory are performed by accelerating the aging stresses, which causes the specimens to break down much faster than they would in service. The test conditions and the level of acceleration of the stresses are difficult to determine. One of the most common disadvantages of insulation testing and evaluation is that the laboratory test results do not correlate with the experience. There are several reasons for this, one of them being the wrong design of the aging test matrix. Too harsh acceleration of stresses may create aging phenomena that are not present in reality. For example, if the electrical stress is too harshly accelerated by increasing the voltage too excessively, space charges may form in the insulation and distort the field. This causes higher peaks in the field than expected based on the voltage level. The aging is then accelerated more than anticipated. Correspondingly, too high a temperature can cause chemical reactions, which would not happen at all during service.

The problem of correct stress levels was approached by Paloniemi (1982) by equally accelerating all the components affecting the aging process. The stresses he considered were thermal stress as oxidation on the insulation surface, electrical stress as AC voltage, and mechanical stress as a number of starts. He defined the acceleration of thermal stress by other tests on the amount of oxidation. He then used the temperature calculated to produce correspondingly accelerated oxidation rate. He accelerated the electrical stress by increasing the frequency. The approach led to similar aging curvatures to what had been obtained for service conditions.

The lifetime of the insulation is generally determined with the aid of some test procedure. The evaluation of the procedure is done based on the stress factors present in the application. A general principle is to determine the end-point criterion at which the insulation is considered no longer usable. This can be an electrical breakdown, loss of mechanical strength, or some other criterion, or a combination of the criteria (IEEE, 2007). The time to meet the end-point criterion is recorded and analyzed statistically over a number of samples. The estimate is then taken as expected lifetime. The selection of end-point criterion is related to the stresses causing the aging, but it can also be dependent upon the test procedure used. For instance, the guide for evaluation by IEEE (2007) recommends using electrical breakdown as an end-

point for the thermal cycling test, but points out the validity of mechanical strength after the thermal endurance test. The thermal endurance test exposes the specimens to a high temperature without applied voltage or any other stress factor. The specimens are exposed to a high temperature for a certain amount of time, and their properties are evaluated to see how much they have deteriorated. The exposure is repeated for different durations and at least three different temperatures. The guide by IEEE (2007) points out that the evaluation should be done by investigating the rate at which the properties decline as functions of time and temperature (the guide advices to carry out measurements for several properties). The decline in properties is expected to follow the Arrhenius relationship (inverse power law, Eq. (2.1) later in this section). According to Stone et al. (2004), the end-point criterion is typically defined as the point at which either the mechanical or dielectric strength is reduced by 50%. Therefore, the thermal endurance test does not aim at determining the end of life, as for example the voltage endurance test does. In such a test, the specimens are exposed to high voltages until they break down, and the time for that is recorded. IEEE (2007) advices to use a large scale of voltages so that the time to failure ranges from 1 min to 10 000 h.

In this study, the recommended test procedures cannot be followed step-by-step, because the test environment is so complicated, and furthermore, because the expected aging mechanism is chemical aging by nature. As can be seen from the descriptions above, the evaluation according to IEEE (2007) requires a large number of repeated tests. The repetition of tests by varying the stress only little is very difficult, if the insulation degradation is caused by the presence of rich hydrocarbon gas under high temperature and pressure. The variation of temperature changes the thermodynamical state of the gas mixture, which is discussed in more detail in Section 3.5. As a result, also the liquid content in the gas mixture is changed, which then changes the chemical stress factor, not only the thermal stress factor. Correspondingly, the equal acceleration approach defined by Paloniemi (1982) is not as such applicable, because the increase in stresses is determined by the thermodynamics of the gas mixture, and only certain combinations of acceleration can be obtained. Furthermore, in an equal acceleration method all the stress factors and their influences should be known in advance to be able to accelerate them equally. The test matrix had, therefore, to be designed differently. Nevertheless, the evaluation followed the general philosophy and recommendations by IEEE (2007) that several measurements have to be performed and the degradation of properties analyzed. Also, the acceleration of stresses follows in a way the logic of Paloniemi (1982) as the acceleration is applied to several stresses. The test matrix is shown in Chapter 3.

In addition to the challenges of the complicated test environment, the application of voltage was not possible with the chemical aging experiments carried out. With hydrocarbon gas mixtures and high pressures, the arrangements for applying voltage become very complicated. Thus, the effect of electrical stress, particularly in the form of partial discharges, was investigated by other means. It was only detected that partial discharges are not present under high pressures. This was approached by investigating the electrical breakdown in hydrocarbon gases and measuring the discharge level as a function of pressure. Therefore, the evaluation of electrical aging relied on detecting whether or not such stress is present, not on how much it actually degrades the insulation.

2.5.1 Considerations on the philosophy of aging

Over the years, the investigation on the degradation of insulating materials has been motivated by the detected failures that were due to poor insulation. The key to the symptoms like this one was the reason for more thorough search for materials that withstand the conditions. Another motivation was provided by the measurements on the insulation resistance. The engineers at the beginning of the 20^{th} century could only measure the insulation resistance and the breakdown voltage. It was discovered that these measurements were influenced by weather conditions. The insulation resistance was higher on a dry than on a rainy day.

Motivated by the observation on weather conditions, Evershed (1913) discussed insulation resistance and pointed out the role of moisture the insulation absorbs. He stated that "the insulation resistance of any electrical system in which they are used is governed almost entirely by the moisture they absorb." Evershed's materials included porous materials such as cotton and paper, but also a varnished winding of an electrical machine. Steinmetz and Lamme (1913) discussed the effect of temperature on the properties of insulating materials. They pointed out that the lifetime of insulation depends on many variables, only one of which is the temperature.

Steinmetz and Lamme (1913) further stated that the insulation suffers mechanically when exposed to high temperatures, but the mechanical properties may "recover" (quotation marks by the original authors) when the temperature is decreased. This is somewhat strange, as they also said that the insulation becomes brittle, which may then cause cracking and delamination. From a modern viewpoint, the degrading changes in insulation are often irreversible and the insulation cannot "recover." This kind of aging is related to partial discharges, whose effects on the insulation are always permanent as they erode the insulation. However, if the properties of the insulating material are reduced as a result of diffusion of for instance water, the insulation as a whole system does "recover" at least to some extent, when it is dried, as pointed out by Evershed (1913).

Steinmetz and Lamme (1913) also proposed that there is a threshold value for the stress, and no aging takes place below the threshold value. For instance, the lifetime of insulation at room temperature is infinity. The threshold has also been approached by Montanari and Mazzanti (1994), although their report also discusses a situation when no threshold can be evidenced.

Montsinger (1930) studied the thermal aging of transformers and claimed that the insulation suffers from degradation and ultimately cracks mechanically, instantly after which an electrical breakdown takes place along the crack. Steinmetz and Lamme (1913) also hinted at this theory. Thus, he claimed that the insulation breaks down, because its mechanical strength is weakened too much and the electrical breakdown is merely a consequence. Nowadays and regarding the materials of modern insulation system either in transformers or in electrical machines, the claim by Montsinger feels somewhat bizarre. High-voltage electrical machines tend to suffer from degradation caused by partial discharges, which erode the insulation until the dielectric strength is too low to resist the field. At that point, the electrical breakdown takes place, but the material may still have adequate mechanical strength.

Montsinger (1930) studied insulation systems built of mica and asphalt varnish, and he used high temperatures to stress the insulation. At high temperatures, the mechanical properties of mica-asphalt insulation were very low, which was pointed out by Laffoon et al. (1951). Asphalt varnish is a thermosetting material, which is not actually solid, but liquid with a high viscosity. When the temperature is increased, the viscosity decreases, resulting in poor performance from the insulation point of view. Modern insulating materials, namely the impregnating resins, are thermoplastic and do not experience so severe degradation of mechanical properties when their temperature is increased.

Revolutionary consideration of insulation lifetime was introduced by Dakin (1948). He discussed the reduction of insulation properties as functions of chemical changes. By that time, the effect of temperature on the insulation was merely described by the 10 degree rule, which simply states that the lifetime decreases to half, if the temperature is increased by 10 °C. It was known that the 10 °C rule does not hold for all materials, and different temperature rules were defined experimentally for materials. For instance, Montsinger (1930) used 8 degree, 10 degree, and 12 degree rules. Dakin (1948) assumed that the physical property of an insulating material is dependent upon the concentration of a compound in the insulating material, which is changed by the thermal aging. He then considered the Arrhenius law for the chemical rate constant K, at which rate the chemical reactions occur:

$$K = A \exp\left\{-\frac{B}{T}\right\} \tag{2.1}$$

where A and B are constants. The constant B in Eq. (2.1) was later defined as the activation energy E_a divided by the universal gas constant R, but Dakin (1948) used a constant B without deriving it. Dakin assumed that the degradation is dependent upon the constant rate K and time, which resulted in

$$\frac{f_0'(P)}{t} = K = A \exp\left\{-\frac{B}{T}\right\} \tag{2.2}$$

where $f_0'(P)$ is the magnitude of a physical property. Although the equation is nowadays assigned to him, Dakin did not actually discuss the lifetime, but the physical properties, which decline at a given rate. Furthermore, the Arrhenius relationship as in Eq. (2.1) was also used by Montsinger (1930), when he defined his temperature rules. But he did not consider that the aging could be caused by chemical reactions. It was stated by Lewis (2001) that the changes in the chemical structure are related to all aging processes. He applied the rate theory also to mechanical stresses. The Arrhenius relationship had previously been linked to mechanical aging by Zhurkov (1984). He defined an equation for the lifetime of a solid under mechanical stress as

$$L = L_0 \exp\left\{-\frac{E_\mathrm{a} - \gamma\sigma}{k\Theta}\right\} \tag{2.3}$$

where σ is the stress, Θ the absolute temperature, E_a "magnitude of the energy barrier determining the probability of breakage of the bonds responsible for strength" (Zhurkov, 1984), γ is a coefficient proportional to the disorientation of the molecular structure, and L_0 is a coefficient related to the natural oscillation frequency of atoms in the solid. Zhurkov used his vast experimental data and graphical methods to define the coefficients.

There have been plenty of approaches to the modeling of lifetime, but the different models are not compared or criticized here. The models are mainly empirical and do not apply universally. The most undeniable conclusion on what has been reported is that the aging phenomena are extremely complex and highly dependent on the materials and the applications. Furthermore, the subsea compressor is significantly different from the typical industrial motors, for which the most of the aging models related to electrical machines have been defined. Furthermore, the majority of the aging modeling have been carried out with respect to high-voltage cable insulation. The aging models by Montanari and Mazzanti (1994) and Crine (1991) are only mentioned. They are derived from the rate theory and also contain thermodynamic quantities. Moreover, they can be discussed, although merely suggestively, in the light of the results of this doctoral thesis, which is done in Section 5.7.

The model by Montanari and Mazzanti (1994) is essentially analogous with Eq. (2.2). The only difference is the reaction rate constant, which takes the electrical field into account. According to Montanari and Mazzanti (1994), the lifetime of insulation L can be written as

$$L = \frac{h}{k\Theta} \exp\left\{-\frac{\Delta S}{k}\right\} \exp\left\{\frac{\Delta H}{k\Theta} - \frac{e\Gamma_1 E}{k} - \frac{e\Gamma_0 E}{k\Theta}\right\} \tag{2.4}$$

where e is the electron charge, h Planck's constant, k Boltzmann's constant, ΔS the entropy of the material in correspondence with the end of life criterion, and ΔH the enthalpy, while Γ_1 and Γ_0 define the scattering distance as

$$\Gamma = \Gamma_0 + \Theta\Gamma_1 \tag{2.5}$$

Equation (2.4) contains many quantities, which seem arbitrary. Montanari and Mazzanti (1994) did not even themselves seem to be fully aware of what their parameters physically mean. Yet, their model could interpret their experimental data. The model in Eq. (2.4) originates from the earlier model by Simoni (1973), which was strictly empirical, but was reported to fit rather well to the aging data. Montanari and Mazzanti dressed Simoni's model into a physical outfit. The model by Crine (1991) is essentially similar and can be written as follows

$$L = \frac{h}{k\Theta} \exp\left\{\frac{\Delta G}{k\Theta}\right\} \operatorname{csch}\left(\frac{e\lambda E}{k\Theta}\right) \tag{2.6}$$

where ΔG is the Gibbs free energy, λ the activation length, and the product $e\lambda E$ is the work of deformation under the electrical field E. Neither did Crine explain the activation length any

further. It is only considered to be a constant, which can be determined based on experimental data. The models by Montanari and Mazzanti (1994) and Crine (1991) are essentially similar, because $\Gamma = \lambda$, and they are also similar with the model by Zhurkov. The most significant difference is that Montanari and Mazzanti consider the activation length to be a function of temperature. The models (2.4) and (2.6) can be further united by expressing the Gibbs free energy with enthalpy and entropy as

$$\Delta G = \Delta H - \Theta \Delta S \tag{2.7}$$

All the models are derived from the same basic assumption that there are two possible thermodynamic states for insulating material: original and failure. They can be illustrated as potential wells A and B, respectively, like in Fig. 2.5. The distance between the wells is the activation length λ, and there is an energy barrier ΔG between the wells. If the potential in well A exceeds the energy barrier, the ball, which represents the state of the insulation, can freely roll into well B, and the insulation breaks down.

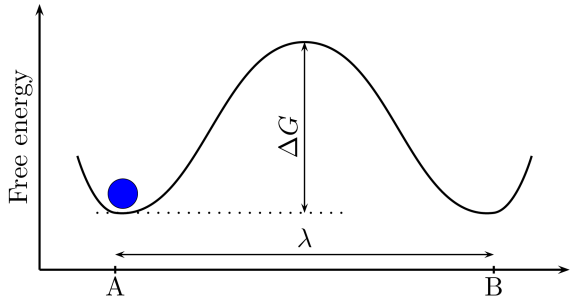

Fig. 2.5. Thermodynamic states of the original and failed insulation.

It has always been considered that an insulation ages until it breaks, and the breaking point is the end of its life. Up to that point everyone seems to agree (even though the estimates for lifetime are not necessarily derived based on breakdowns, which was mentioned earlier in this section), but there are still no clear and undeniable explanations on what aging is like and on what causes the actual breakdown. Obviously, the environment, materials used, and the applications all have enormous effects on both phenomena. The aging is not a simple phenomenon, but a complex combination of different activities going on in the insulation system.

The models in Eqs. (2.4) and (2.6) have been defined for a high-voltage cable insulation. Such cables are exposed to very high voltages; the thermal rating of XLPE (cross-linked polyethylene) insulation, which is widely used in such cables, is only 90 °C and the insulating materials are very vulnerable to partial discharges. The insulation systems in high-voltage machines face a different kind of an application: they are exposed to less voltage, they tolerate some amount of partial discharges, and the insulation is a combination of three different materials: mica, glass, and epoxy.

In a complex insulation the aging takes place both in the bulk materials and in the interfaces. The latter effect has been emphasized by Park (1987), Jia et al. (2006), and Hong et al. (2009a). Park (1987) studied mainwall insulation samples made of mica, glass, and epoxy and he concluded that the dielectric losses of the insulation increase and the breakdown strength reduces when mechanical stress is applied to the insulation. He discovered that the binding of glass and epoxy was weakened as a result of the applied mechanical stress. Jia et al. (2006) performed aging tests on a mainwall insulation consisting of mica, glass, and epoxy. They observed with a scanning electron microscope that the attachment of epoxy and glass is significantly reduced after a long period of aging. Hong et al. (2009a) studied the diffusion of water into mainwall insulation consisting of mica, glass, and epoxy. They observed that the permittivity and losses increased considerably because of water absorption. They concluded that the diffusion process is closely related to the interfaces of epoxy, mica, and glass.

2.5.2 Diffusion

Diffusion is a process by which matter is transported from one part of a system to another as a result of molecular motions, as described by Crank (1975). Here, it means the penetration of raw natural gas into insulating materials. When polymers are submerged to water, their properties weaken as a result of water absorption, which is rather rapid in the initial stage, but then levels off when the saturation value is reached. After saturation, the material cannot absorb more water. Diffusion of water into epoxy resins have been widely investigated (e.g. Banks and Ellis, 1979; Fernández-García and Chiang, 2002; Fukuda et al., 1997; Hong et al., 2009a; Kumazawa et al., 1994; Kärner and Ieda, 1991; Liu et al., 2002; Musto et al., 2000; Nogueira et al., 2001; Wu and Siesler, 2003; Xiao and Shanahan, 1998).

The internal structure of epoxy resin contains molecular chains and crosslinks, which attach them to each other. However, between the molecular chains and crosslinks, there is empty space called free volume. Such space is initially empty, but it can be filled with the diffusing substance in the diffusion process. Water, for instance, fills the free volume inside the chemical structure of epoxy resin. The diffusion into the free volume causes no volume change of the material. This is typically an initial stage of the diffusion process. After all the free volume is filled, the molecular chains are getting reorganized and the volume increases.

The properties of the insulating material are first reduced rather heavily, but after some time the aging appears to stop. The degradation of physical properties is proportional to the water absorption. The diffusion is, therefore, causing as if the opposite kind of a threshold than mentioned by Montanari and Mazzanti (1994). The nature of diffusion usually follows Fick's second law (Fick, 1855)

$$\frac{\partial c}{\partial t} = D\frac{\partial^2 c}{\partial x^2} \tag{2.8}$$

where c is the concentration, D the diffusion coefficient, and x the direction. Fick studied the concentrations and fluxes by putting salt into water. Nowadays, his research constitutes the

basis for diffusion of liquids into solids, but his experiments actually discussed the opposite phenomenon. Fick's law can be observed by the increase in weight in polymer materials when they are exposed to some diffusive substance, such as water. The weight increase is rapid in the initial stages of the diffusion process and approaches a saturation value. With epoxy resins that contain fillers, the diffusion process is a sum of two individual diffusion processes: diffusion into epoxy and diffusion into fillers. The weight increase approaches the saturation value in a slower rate than with plain epoxy. It is more difficult for water to penetrate into the filler, because it has to go through the resin first. Composite insulation containing mica, glass, and epoxy is expected to behave in a similar way as epoxy with fillers. The diffusion process is illustrated in Fig. 2.6. Crank (1975) defined an equation for the weight increase at time t by solving Eq. (2.8) as

$$\frac{m_t}{m_\infty} = 1 - \sum_{n=0}^{\infty}\left(\frac{8}{(2n+1)^2\pi^2}\exp\left\{-\frac{D(2n+1)^2\pi^2 t}{4l^2}\right\}\right) \tag{2.9}$$

where m_t and m_∞ are weights at time t and infinity, respectively, and the region discussed is defined by $-l < x < l$. According to ISO (2008) the sufficient number of summands is generally 20. An analytical approximation for Eq. (2.9) is given by (Jacobs and Jones, 1989)

$$\frac{m_t}{m_\infty} = 1 - \exp\left\{-7.3\left(\frac{Dt}{d^2}\right)^{0.75}\right\} \tag{2.10}$$

where d is the thickness of the sample. It has been reported by Maggana and Pissis (1999) that the approximation fits the data concerning bisphenol A epoxy resin that contains plasticizers, and by Hong et al. (2009a) that it fits the data of a mainwall insulation of a high-voltage electrical machine. The authors of the latter study pointed out that the slower diffusion process

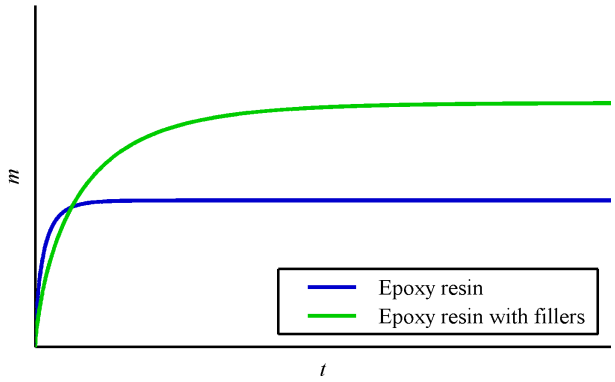

Fig. 2.6. General behavior of diffusion of water into epoxy resin with and without fillers. The curve of plain resin is based on (Nogueira et al., 2001; Xiao and Shanahan, 1998; Fukuda et al., 1997) and the curve of resin with fillers on (Fukuda et al., 1997; Fernández-García and Chiang, 2002; Maggana and Pissis, 1999).

involves diffusion into the interfaces of epoxy and glass or mica. The mica and glass do not absorb anything.

Nogueira et al. (2001) reported that tensile strength, elongation, and toughness are reduced as a result of diffusion. E-modulus was ultimately decreased, but in the early stages of diffusion it increased slightly. Reduction of tensile strength was also reported by Kumazawa et al. (1994). An early study by Banks and Ellis (1979) concluded that the glass transition temperature of Bisphenol A epoxy resin decreases because of water absorption. Corresponding results were also reported by Nogueira et al. (2001) and Xiao and Shanahan (1998), who both reported in addition that the glass transition temperature correlates with the volume increase.

Hong et al. (2009a) investigated water absorption of a mainwall insulation constructed of glass-backed mica tape and epoxy resin. They reported that the loss tangent and the permittivity increase as a result of water absorption. Similar observations have also been reported by Kärner and Ieda (1991) and Fukuda et al. (1997).

The diffusion is only one cause of changes in insulating materials. Diffusion, which is (regarding the lifetime of an electrical motor) a relatively fast phenomenon, may trigger other aging phenomena or interact with them. If such takes place, the physical properties continue to decline after the diffusion has set to the saturation value, which means that diffusion is not the only aging mechanism. The decline in properties at this point can be caused by chemical reactions between the insulation and the diffusing substance.

2.6 Dielectric material in an electrical field

The behavior of a dielectric in an electrical field is briefly described here. The description in this section has been written roughly according to Solymar and Walsh (2004), Blythe and Bloor (2005), and Jonscher (1983).

A dielectric material (an insulator) forms a capacitor, the capacitance of which, assuming that it is a parallel plate capacitor, can be defined by the universal equation

$$C = \frac{\epsilon A}{d} = \epsilon_0 \epsilon_\mathrm{r} \frac{A}{d} \tag{2.11}$$

where A is the area of the electrodes and d is the distance between them. The permittivity ϵ is a complex quantity and depends on frequency. Its real part is related to the energy stored in the material, and its imaginary part to the energy loss. The complex permittivity can be expressed as

$$\epsilon^* = \epsilon_0(\epsilon' - i\epsilon'') \tag{2.12}$$

Equation (2.11) holds only when the loss part in Eq. (2.11) is neglected, that is, $\epsilon'' = 0$. The real part of complex permittivity ϵ' refers to the dielectric constant or relative permittivity of the insulation ϵ_r. The imaginary part ϵ'' is related to the losses defined by conductivity divided by frequency, σ/ω. The dissipation factor or loss tangent tan δ defines the angle of complex permittivity.

$$\tan\delta = \frac{\epsilon''}{\epsilon'} \tag{2.13}$$

Accordingly to Eq. (2.12), also the capacitance in Eq. (2.11) is a complex variable. When an AC voltage $U(\omega)$ is applied over the capacitor, it produces a current $I(\omega)$:

$$I(\omega) = \frac{U(\omega)}{Z(\omega)} = \frac{U(\omega)}{\frac{1}{i\omega C}} = U(\omega) i\omega\epsilon^* \frac{A}{d} = \omega C_0 (i\epsilon' + \epsilon'') U(\omega) \tag{2.14}$$

where C_0 is the capacitance of free space. The current, obviously, has resistive (real) I_R and capacitive (imaginary) I_C components, which can be expressed separately as

$$I_C = i\omega C_0 \epsilon' U \tag{2.15}$$

$$I_R = \omega C_0 \epsilon'' U \tag{2.16}$$

The imaginary part of the permittivity ϵ'' is producing a resistive component to the current, in other words, a component that produces losses in the whole electrical system. Correspondingly, ϵ' is producing the capacitive component of the current.

2.6.1 Dielectric relaxation

The dielectric response is used to discern the polarization of the insulating materials. When an insulator is exposed to an electrical field, "the material will respond to the applied electric field by redistributing its component charges to some extent, positive charges being attracted towards the negative electrode and vice versa," according to Blythe and Bloor (2005). In a similar way, the polarization can involve whole molecules, the bonds between atoms in the molecule, or electrodes. These three types of polarization have their characteristic frequencies, which are roughly according to Blythe and Bloor (2005) 10^6 Hz, 10^{12} Hz, and 10^{15} Hz, respectively. In addition to these phenomena, materials that consist of several components experience an additional polarization phenomenon, which is related to the interfaces of different components and takes place at low frequencies, that is, it is a very slow process. A distinct example of this kind of a material is a composite insulation consisting of mica, glass

fiber, and epoxy resin, which has been studied in this thesis. The interfacial polarization is the only type of polarization that can be observed within the frequency frame and diagnostic method used. However, in dielectrics it is often the most informative one, as the dielectric spectroscopy aims at discerning the anomalies or impurities (e.g. voids filled by a foreign diffusing substance) that the insulation contains.

The electronic and atomic polarizations are very fast and indiscernible with the common measuring methods used. Thus, there are roughly two polarization processes: "fast" processes, which cannot be observed and "slow" processes, which can be observed. In the frequencies close to the "slow" region, the "fast" processes do not lag behind the applied field and their permittivity appears constant, ϵ_∞. The permittivity can be expressed as

$$\epsilon(\omega) = \epsilon_\infty + f(\omega) \tag{2.17}$$

At very low frequencies, $\omega \to 0$, nothing lags behind the field and the permittivity is static ϵ_s. Therefore,

$$f(0) = \epsilon_s - \epsilon_\infty \tag{2.18}$$

When the field is applied and sufficient time allowed, the molecules get aligned with the field. When the field at this point is switched off, the molecules begin to turn back to their original states and the polarization and internal field gradually diminish. The decay process is following the Arrhenius relation, and the polarization at this point can be written as

$$P(t) = P_0 \exp\left\{-\frac{t}{\tau}\right\} \tag{2.19}$$

where τ is the relaxation time. Blythe and Bloor (2005) pointed out that this is an inconsistent description for τ, because the process is more like "retardation" than "relaxation." The solution of Eq. (2.17) can be written as

$$\epsilon(\omega) = \epsilon_\infty + \frac{\epsilon_s - \epsilon_\infty}{1 + i\omega\tau} \tag{2.20}$$

Equation (2.20) is called Debye dispersion equation. It was derived by Debye (1929), and its real and imaginary parts can be separated as

$$\epsilon'(\omega) = \epsilon_\infty + \frac{\epsilon_s - \epsilon_\infty}{1 + \omega^2\tau^2} \tag{2.21}$$

$$\epsilon''(\omega) = \epsilon_\infty + \frac{\epsilon_s - \epsilon_\infty}{1 + \omega^2\tau^2}\omega\tau \tag{2.22}$$

Equations (2.21) and (2.22) are commonly used to interpret the data obtained. At a polarization frequency, the ϵ' experiences a sudden drop and ϵ" a somewhat flat peak, as shown in Fig. 2.7. At this point $\omega = 1/\tau$. The model by Debye does not, however, work with composite insulation structures. As such, the Debye model can only describe the molecular polarization phenomena, but not the interfacial phenomena.

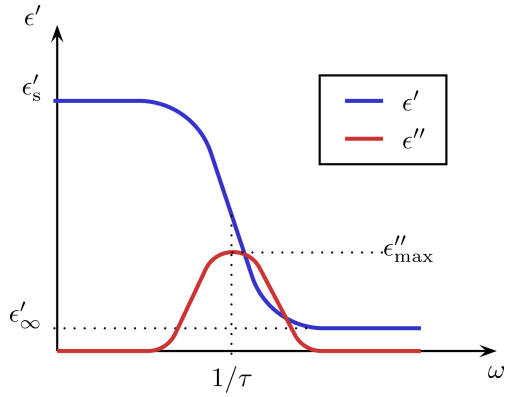

Fig. 2.7. Dielectric relaxation with a solid dielectric. The figure represents an ideal case defined by Debye. Common polymers normally depart somewhat from this form.

For composite structures, the dominating phenomena are called the Maxwell-Wagner effects. Maxwell (1892) studied theoretically a system containing layers of materials of different permittivities (ϵ'_1, ϵ'_2) and conductivities (σ_1, σ_2). Maxwell's objective was only to introduce the 'electric absorption' phenomenon, and he noted that the approach of layer-shaped materials was adopted to keep the calculation at a simple level. Wagner (1914) studied a system containing a material (ϵ'_1, σ_1), which has impurities (ϵ'_2, σ_2) in the form of spheres.

The model by Debye (1929) is capable of describing the behavior of an ideal dielectric. Experimental results have been seen to depart from Debye's model, and many improvements have been made to better match the experimental data. One of the well-known models is the Cole-Cole equation, which was derived based on vast experimental data on different kinds of dielectrics, solids, and liquids, by Cole and Cole (1941). It can be written as:

$$\epsilon(\omega) = \epsilon_\infty + \frac{\epsilon_s - \epsilon_\infty}{1 + (i\omega\tau)^{1-\alpha}} \tag{2.23}$$

The exponential parameter α ($0 < \alpha < 1$) represents the statistical nature of dielectric relaxation. In the case of an ideal dielectric, $\alpha = 1$, and Eq. (2.23) becomes Eq. (2.20). The parameter α states that the polarization process does not take place in exactly the same way everywhere in the material. All the molecules do not get perfectly aligned with the applied field. This applies to the materials that contain defects or consist of several materials. The mainwall insulation is an example of the latter, since it is built of mica, glass, and epoxy. Yet, the Cole-Cole equation does not take the conductivity into account. The conductivity can be expressed in the complex form $\sigma = \sigma' + i\sigma''$ and it is inversely proportional to the frequency.

Its real part σ' is the DC conductivity and contributes to the dielectric loss, and the imaginary part σ'' is the conductivity caused by localized charges. By taking the conductivity into account, the Cole-Cole equation can be written as (Thongbai et al., 2008):

$$\epsilon(\omega) = \epsilon_\infty + \frac{\epsilon_s - \epsilon_\infty}{1 + (i\omega\tau)^{1-\alpha}} - i\frac{\sigma}{\epsilon_0\omega^s} \tag{2.24}$$

The exponent s ($0 < s < 1$) takes the statistical effect of conductivity into account, similarly as the parameter α on permittivity. In the case of ideal conductivity $s = 1$, which has been used for instance with oil-filled cellulose insulation in transformers (Linhjell et al., 2007). Fractional s has been used with ceramic materials, examples of which are some ferroelectric oxides (e.g. nickel oxide, NiO) doped with metallic particles (e.g. aluminum or titanium), by Thongbai et al. (2008). For such materials, the permittivity is very high (e.g. 1000), and the material also has notable conductivity (approximately 10^{-4} S/m). These properties emphasize the changes in the dielectric response so that the complex conductivity and fractional exponent s have to be taken into account. The real and imaginary parts of Eq. (2.24) can be written as

$$\epsilon(\omega)' = \epsilon_\infty + (\epsilon_s - \epsilon_\infty)\frac{1 + (\omega\tau)^{1-\alpha}\sin\left(\alpha\frac{\pi}{2}\right)}{1 + 2(\omega\tau)^{1-\alpha}\sin\left(\alpha\frac{\pi}{2}\right) + (\omega\tau)^{2-2\alpha}} + \frac{\sigma''}{\epsilon_0\omega^s} \tag{2.25}$$

$$\epsilon(\omega)'' = (\epsilon_s - \epsilon_\infty)\frac{(\omega\tau)^{1-\alpha}\cos\left(\alpha\frac{\pi}{2}\right)}{1 + 2(\omega\tau)^{1-\alpha}\sin\left(\alpha\frac{\pi}{2}\right) + (\omega\tau)^{2-2\alpha}} + \frac{\sigma'}{\epsilon_0\omega^s} \tag{2.26}$$

Derivations for Eqs. (2.25) and (2.26) can be found in Appendix A.

2.6.2 Insulation resistance

The concept of insulation resistance is a time-domain phenomenon. It cannot be generally derived from the equations for frequency domain. When a dielectric is exposed to a DC field, it behaves seemingly as a resistor with a high resistance. However, when the voltage is switched on, the insulator experiences the polarization phenomena as described above, because its structure is organizing itself aligned with the field. The transient is very fast, which basically also causes fast polarization phenomena to occur during the first few moments after switching. Because of these phenomena, the current is relatively high instantly after switching, but then slowly decreases and eventually levels off to a saturation value. During the steady-state condition, the insulation resistance can be calculated according to Ohm's law

$$R = \frac{U}{I} \tag{2.27}$$

The current through an insulation in the insulation resistance measurement (DC voltage applied) can be divided into several components. The guide by IEEE (2006) states that the total observable current contains four components: leakage, capacitance, conductance, and absorption currents. The saturation value of the current is the leakage current and represents the steady-state leakage. The insulation resistance is determined based on the leakage current. Conductance current is caused by the natural conductivity of the insulation and is essentially zero for modern insulation systems. The capacitance current is said to be caused by the geometric capacitance of the winding and by the disturbances from the measuring instrument. Such current is said to reduce shortly after switching. The absorption current contains all the polarization phenomena and it also reduces after some time, but, depending on the materials and their polarization phenomena, it may take several minutes to reduce. In other words, it takes some time for Maxwell-Wagner effects to level off. For a modern insulation, the insulation resistance can be measured 1 minute after the application of voltage, but for an old mica-asphalt winding, this value is said to be 10 – 15 minutes (IEEE, 2006).

Chapter 3

Experimental methods

This chapter describes the test methods and manufacturing and preparation of the test specimens. The procedure of testing with hydrocarbon gases is described. The work contains plenty of tests and additional measurements. Measurements for electrical properties have been carried out externally, and are described only briefly here.

3.1 Test matrix

As mentioned in the previous chapter, there are four stress factors: thermal, electrical, ambient, and mechanical, which form a ”team”. The influences of each of these during the service conditions of a subsea compressor are illustrated in Fig. 3.1. The majority of the stresses the insulation experiences are related to the normal operation of a high-voltage electrical machine: operating temperature, voltage, mechanical vibration, and fault conditions. The vibration is created by the stator current and its frequency is twice the frequency of the current (Calvert, 1931). The fault conditions include short-circuit conditions, which generate high transient forces, but they are mostly absorbed by the support structures and the winding itself, and not by the insulation system. The hypothesis is that the insulation system can tolerate these stress factors and their interaction, because a similar machine can operate safely in a dry natural gas compressor. This hypothesis is expected to be valid even, if the insulating materials are changed into more chemically resistant ones. A re-evaluation is needed on the role of partial discharges, because the stress grading layer used in the dry natural gas compressor cannot tolerate the raw natural gas and hence must be replaced or removed.

Therefore, the dominating stress factor is expected to be the ambient stress, which is created by the presence of raw natural gas under high temperature and pressure. The ambient stress factor is in close interaction with the thermal stress factor, because the thermodynamic state of the gas mixture, including the amount of liquid components the gas contains, is dependent

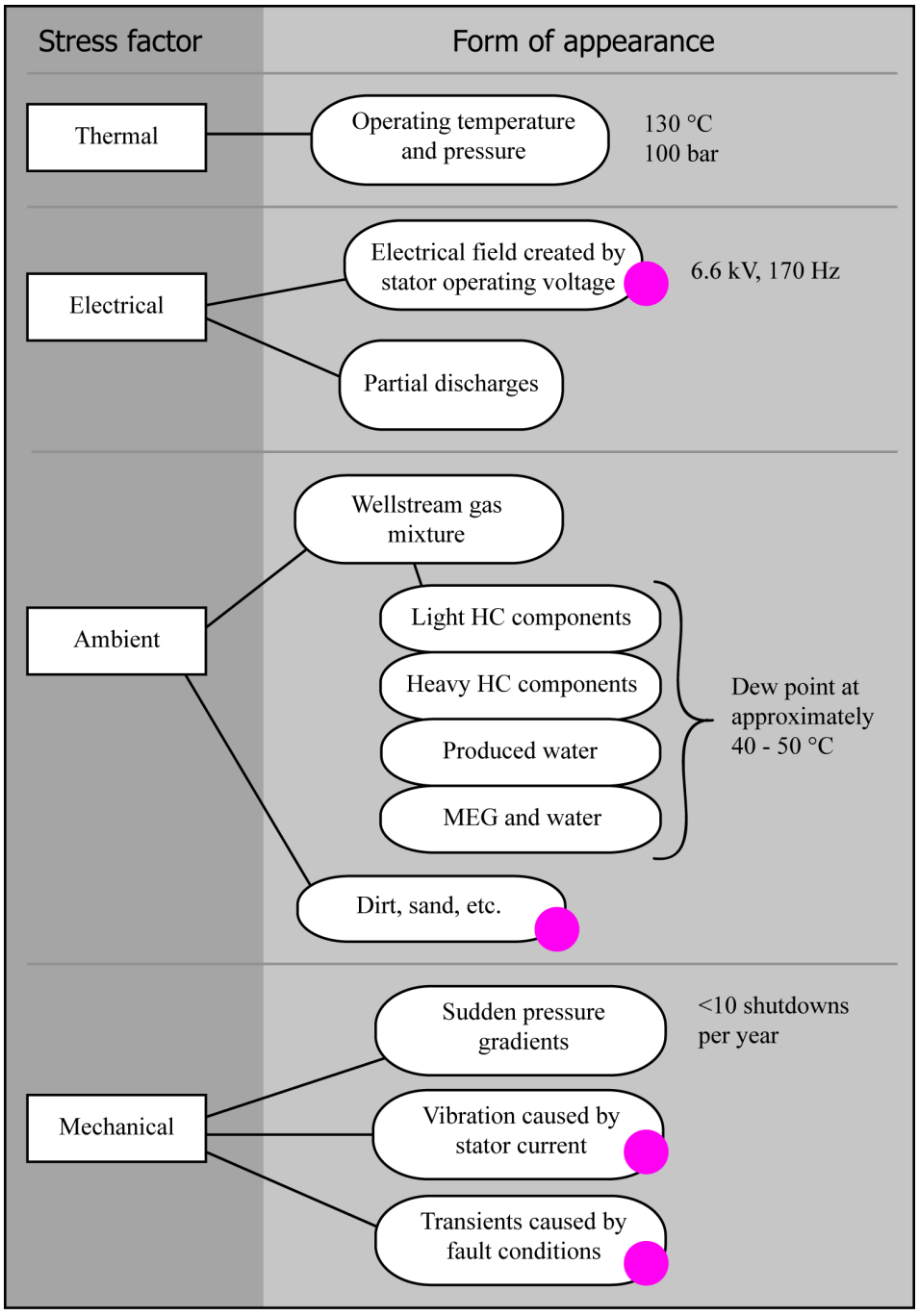

Fig. 3.1. Block diagram of the stress levels in operating conditions. Circles indicate forms of stress factors, which have not been discussed in the experimental program.

on temperature and pressure. Therefore, pressure has been addressed to the thermal stress in Fig. 3.1.

Depressurization is also an issue in the natural gas compressor. During steady-state operation, the pressure fluctuates only a little, but sudden fault conditions, such as a leak, in the entire production system may trigger a steep decrease in the pressure. This takes place at the operating temperature of the machine. Based on earlier experience on the gas production and on the design aims for new technology, up to ten shutdowns can be experienced in a subsea compressor during a year. Each shutdown may involve a rapid decompression, if the system does not include proper safety and control equipment. Although rapid decompression is a rather infrequent and unpredictable occurrence, the stress level has to be considered as part of the normal operation of the machine.

The experimental test program tackled the effects of the stress factors listed in Fig. 3.1, and the experiments carried out to discuss each stress factor are shown in Fig. 3.2. The test matrix is divided into two main sections: investigation on the presence of partial discharges and study on the effects of the raw natural gas. The former contains measurements on the breakdown strength of gases and on the partial and surface discharges as functions of pressure. The latter contains several exposures in different environments related to the raw natural gas.

The presence of partial discharges was investigated by measurements on the breakdown strength of gases, partial discharges, and by a theoretical study with finite element methods (FEM). These are not actually diagnostic methods, because they were all aiming at an explanation of the physical phenomenon, not at determining the state of the insulating materials. No aging was included in the investigation on the PD activity.

The test matrix for hydrocarbon gases is based on the environment referred to as ”wellstream gas,” which contains dry hydrocarbon gas, hydrocarbon condensate, and the mixture of MEG and water at 130 °C and 150 bar. This environment acts as a kind of a reference case of raw natural gas. It is, however, an accelerated aging environment, as explained below in Section 3.5. This environment was modified in the tests to emphasize individual effects of the entire gas mixture.

To gather up information on the aging, various diagnostic methods were used. An overview is shown in Fig. 3.3. The measurements with each method are described later in this chapter. The backbone of the analysis of the insulation samples was based on measurements on weight and volume, mechanical three-point bending test, infrared spectroscopy, differential scanning calorimetry (DSC), and dielectric response. These measurements can give information on diffusion, mechanical and dielectric properties, and possible chemical changes. Also, insulation resistance was measured, but for one sample set only. The purpose of the microscopic examination was to investigate the delamination of the mainwall insulation samples. SEM provided a closer image on the mainwall insulation and also on resin samples. In the aging experiments, it was not possible to record the parameters during the test. They were measured only before and after the tests, and the analysis focused on the relative change.

The destructive nature of the mechanical properties measurements and DSC (to prepare a

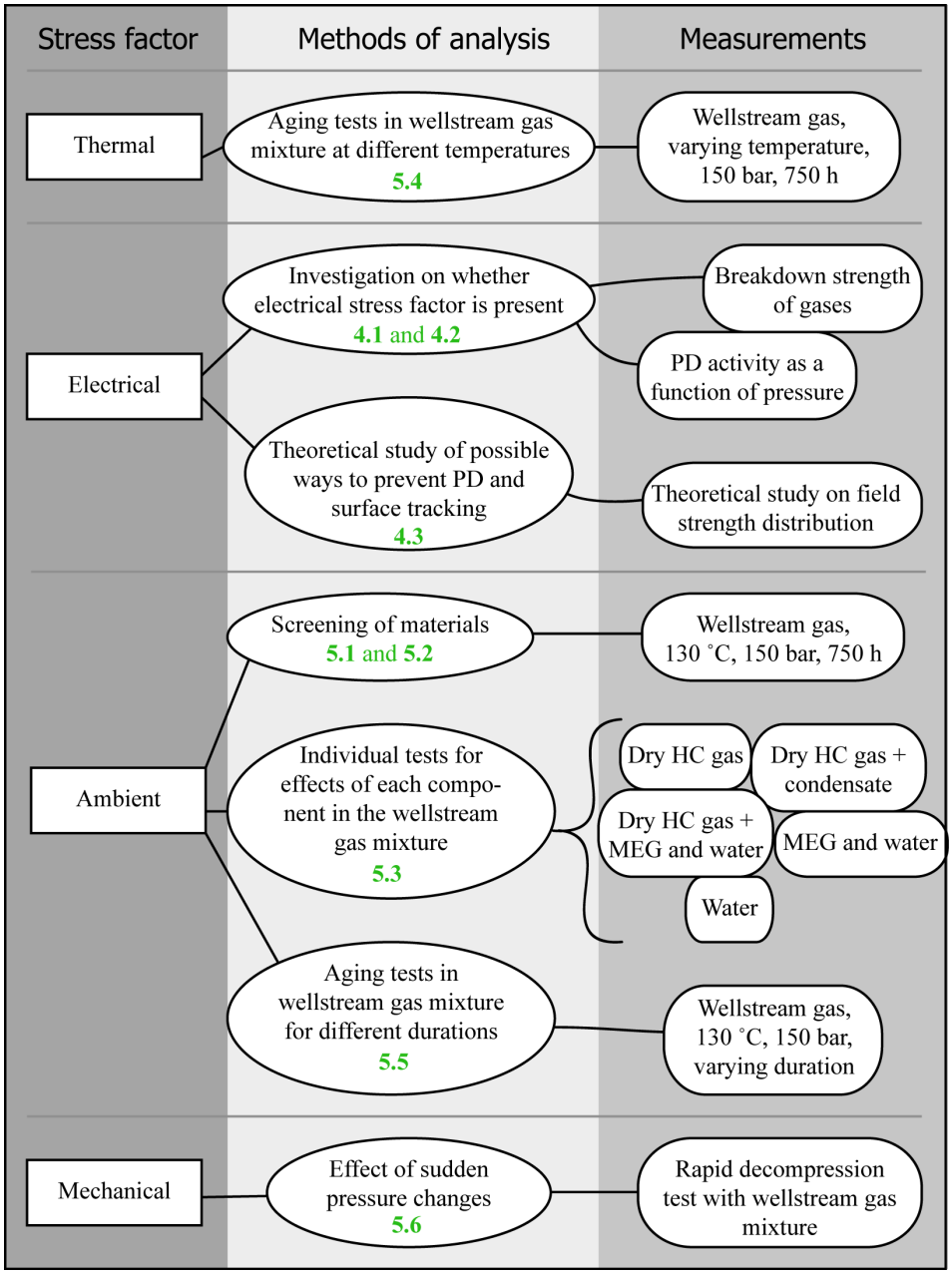

Fig. 3.2. Block diagram of the stress factors and tests to determine their significance.

sample for this measurement, the original material sample is destroyed) required another set of samples for measurements on each time marker. This increased the importance of the statistical treatment. Weight, volume, and FTIR were measured on the exact same samples before and after the exposures.

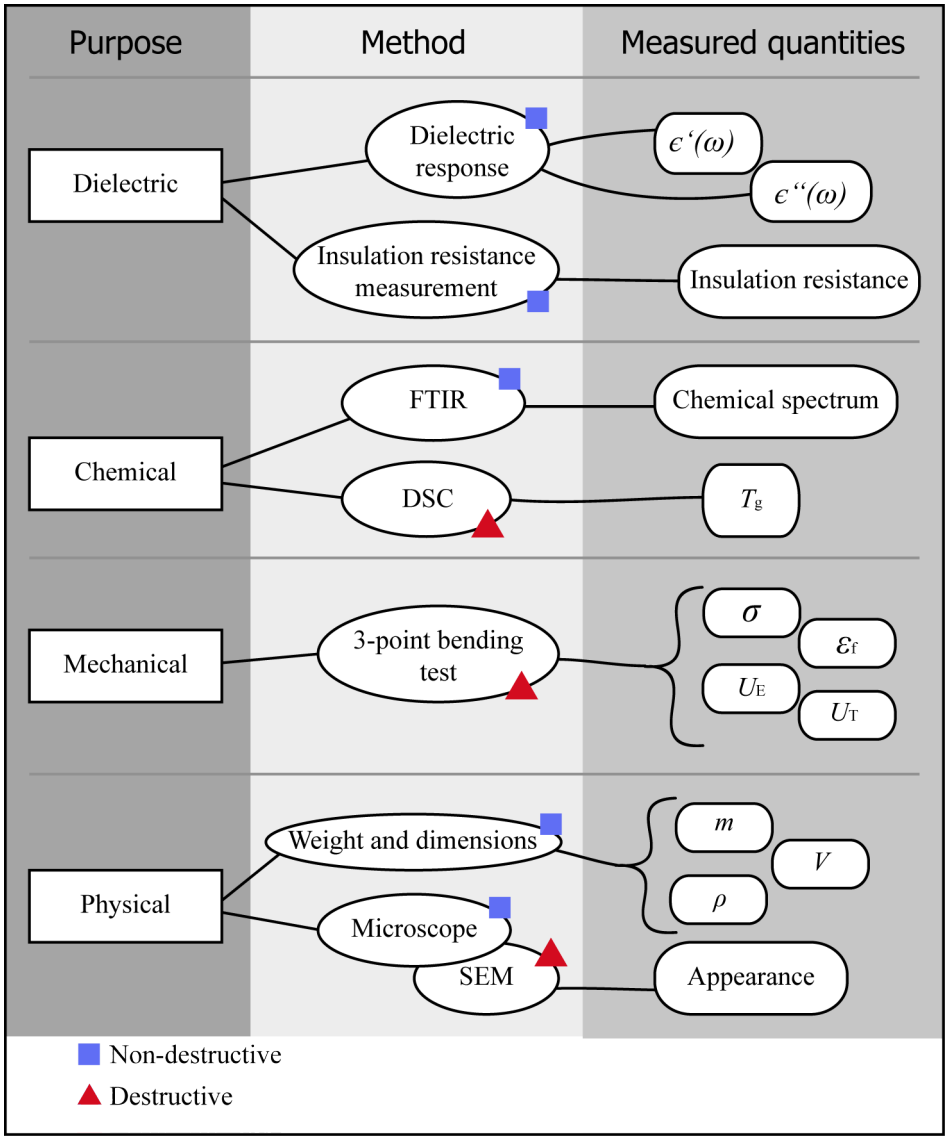

Fig. 3.3. Block diagram of the diagnostic methods applied. The methods to investigate the PD activity are also included, even though they are not used to define the state of the materials.

3.2 Measurements on breakdown strengths of gases

The measurements were carried out in a small chamber designed for the purpose. The chamber contained two plane-parallel electrodes, the positions of which could be adjusted. The chamber and the dimensions of the electrodes are given in Fig. 3.4. The measurements were performed on gap distances of 0.25 mm, 0.5 mm, 1.0 mm, and 2.0 mm. With nitrogen gas, also a distance of 1.5 mm was used. One of the electrodes was connected to ground and the other one to a high resistance and an adjustable high-voltage DC source capable of providing 80 kV. The breakdown was detected by measuring the current with an oscilloscope. The voltage was increased slowly until breakdown occurred, and then recorded. The measurements were repeated five times for each pressure and gap length. After the measurements on each

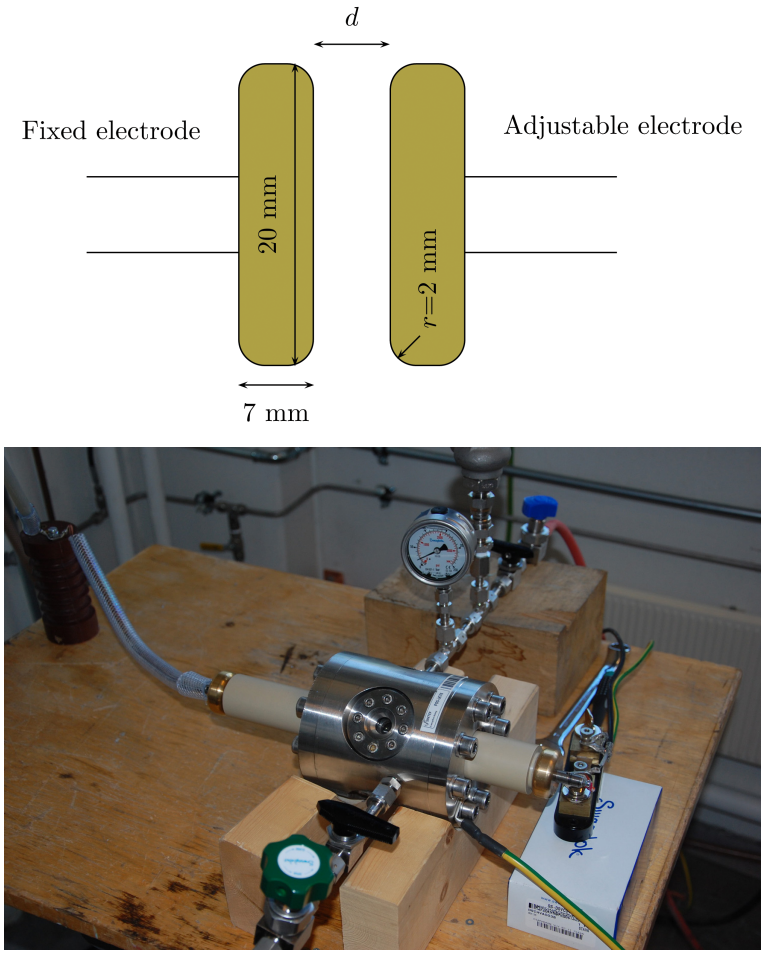

Fig. 3.4. Chamber for the breakdown strength measurements on gases (bottom) and a schematic of the electrodes inside the chamber (top) including the dimensions.

gap length, the electrode surfaces were cleaned.

Table 3.1. Composition of the hydrocarbon gas mixture used in the breakdown measurements and in the chemical aging tests.

Component	Amount [mol %]
Carbon dioxide	1.0
Nitrogen	1.0
Methane	85
Ethane	9.0
Propane	3.5
n-Butane	0.5

The gases investigated include nitrogen, methane, hydrocarbon gas mixture, and wet methane. The composition of the hydrocarbon gas mixture is shown in Table 3.1. The wet methane mixture was prepared in another chamber and then pumped into the test chamber. No liquid water was added into the test chamber. It was seen to condense on the electrodes and cause false results. Wet methane refers to the mixture of methane and water at the dew point at room temperature and 120 bars, which was the pressure in the storage chamber. At this pressure, the relative humidity of the mixture was 100%. At lower pressures, some of the water from the gas condensed as the pressure decreased, but the relative humidity was still 100%. The relative humidity was not altered during the test. The control of relative humidity is very difficult in the chamber of this size. In other words, only a single drop of water would yield a relative humidity of 100%, because the volume of the chamber is so small.

3.3 Partial discharge measurements

The test samples were installed horizontally inside a pressure vessel. The measuring setup inside a safety cell and the measuring circuit are illustrated in Fig. 3.5. The ground electrode of a sample was connected directly to the chamber lid. The high-voltage electrode was connected to a voltage supply via PD-free cable penetrator. The voltage was supplied by a variac and a high-voltage transformer. A coupling capacitor and the measuring instrument (Omicron MPD 600) were connected between the high voltage feed and ground. The measuring instrument was connected to a PC, which used software provided by Omicron in the data analysis. The data analysis defined the standardized discharge level Q_{IEC}, which is the apparent charge of a PD pulse. Q_{IEC} represents the charge of a PD current pulse within a certain integration time, but according to IEC (2000) it ”is not equal to the amount of charge locally involved at the site of the discharge.” The maximum discharge level Q_{max} was manually traced from the discharge plots.

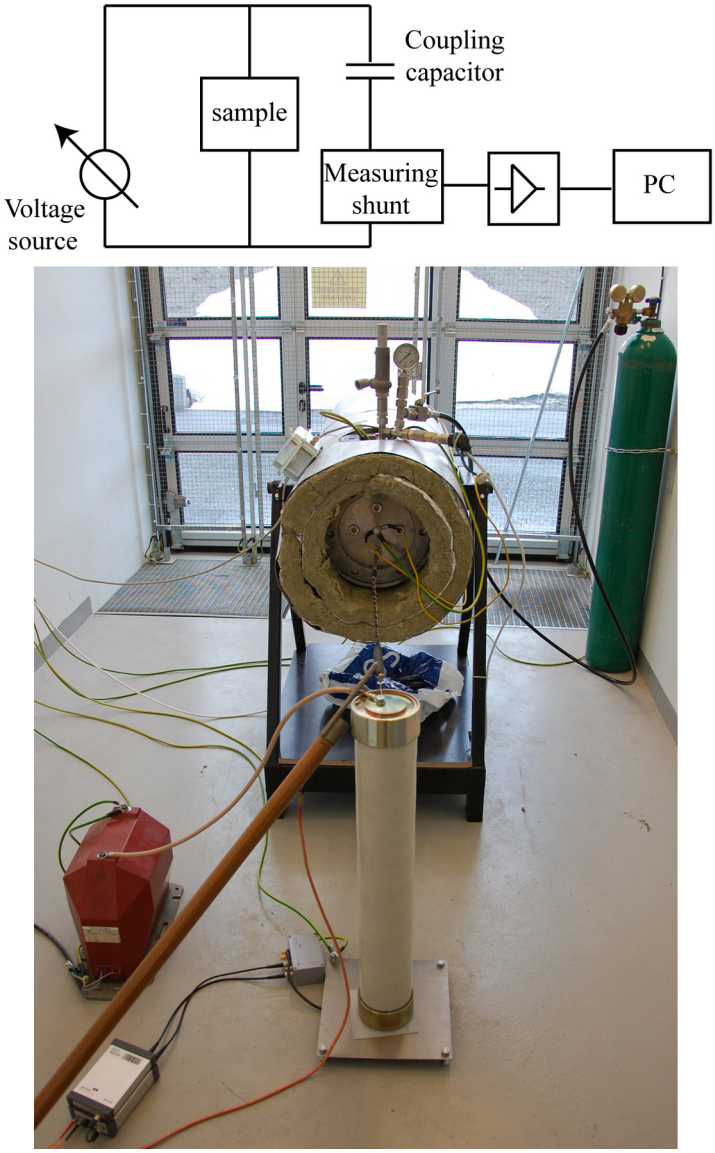

Fig. 3.5. Measuring circuit for PD measurements (top) and the setup located in a safety cell (bottom). The voltage source in the circuit contains a variac placed outside of the safety cell and a high-voltage transformer seen in the lower left corner of the setup. The pressure vessel is in the middle of the safety cell and the nitrogen gas bottle on the right. Heat insulation on the chamber was used for other purposes. The measurements were performed at ambient temperature, 20 °C. The coupling capacitor can be seen in front with the measuring instrument and its power supply placed on the floor. The brown rod touching the high-voltage end of the capacitor is part of the safety equipment, and it was removed prior to the measurements.

The measuring setup itself did not produce partial discharges. The PD level measured on the equipment itself is illustrated in Fig. 3.6. Only a few discharges can be seen and they cannot cause notable disturbances in the measurements. The discharge levels on the samples were very high, which is illustrated later in Section 4.2. The sinusoidal curve in partial discharge figures (Fig. 3.6 and the figures in Section 4.2) illustrates the voltage applied to the system and the small dots indicate the partial discharges. The level of discharges in picocoulombs is seen on the left. The intensity of the discharges, in other words, how frequently they appear, can be determined according to the color scheme on the right.

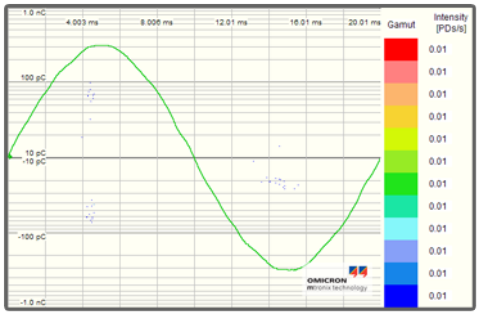

Fig. 3.6. Partial discharge level of the measuring equipment.

The samples included two kinds of bar samples, which were manufactured in a VPI process (described in Section 3.4.1), and a cable sample. A bar sample is illustrated in Fig. 3.7 and the cable sample in Fig. 3.8. The purpose of the measurements was to analyze the discharges located on the surface of the insulation in the vicinity of the termination of the ground electrode (conductive layer in Fig. 2.1) Usually, the insulation is protected from these discharges by the stress grading layer. Based on the poor chemical resistance of the materials used for such a purpose, the aim of the study was to replace or remove the stress grading layer. Each sample contained a similar ground electrode, which was implemented as semiconductive silicone-based paint (black section in Fig. 3.7) laid on top of the insulation. The edge of the ground electrode is sharp, and the maximum field strength of the sample is expected to be located in the vicinity of the edge. Even though the highest field strength is in the vicinity of the edge of the ground electrode and on top of the insulation, there were also plenty of partial discharges inside the insulation in both bar samples. These discharges caused interference in the results.

To detect the effect of the discharges inside the insulation, the insulation section of the bar sample was covered with field grading paint. The paint covered the whole area of the insulation visible in Fig. 3.7 by extending from the black semiconductive paint to the copper on the right-hand side of the figure. The field grading prevents the discharges on the surface of the mica-based insulation. Therefore, all the discharges seen in this kind of a sample are located inside the insulation. Consequently, their pattern can be recognized and then omitted from the discharge pattern of the bar sample without any field grading. Hence, what remains in such results is the discharge pattern caused by surface discharges on top of the insulation. The sample with field grading did not produce surface discharges.

Fig. 3.7. Bar sample used in the partial discharge measurements. The black section is the ground electrode. The sample does not contain field grading.

Fig. 3.8. Cable sample used in the partial discharge measurements. The white section is the insulation and the black cord is the ground conductor. The thick assembly on the right end contains cable termination. Conductive ring electrodes were added to reduce corona discharges. The thickness of insulation was 4.35 mm.

The functionality of field grading layer is based on its high resistivity, which gradually reduces the electrical field. Its effect is demonstrated later in Figs. 4.20 and 4.21. Basically, field grading of this kind is implemented in common high-voltage electrical machines by applying it as a tape, which can be seen in Fig. 2.1, but as mentioned above, such materials cannot withstand raw natural gas.

The purpose of the cable sample was as if the opposite to that of the field grading. It intended to highlight the discharges on the surface. The cable consisted of an XLPE (cross-linked polyethylene) insulation, which is virtually void-free experiencing only small amount of internal discharges. Thus, the discharges it experiences must exist on top of the insulation surface near the end of the ground electrode. Another reason for the use of the cable sample was its compatibility with the 2D FEM model. The radial cross-section of the cable sample is round, which causes the field to be evenly distributed along the cross-section. By contrast, the modeling of the bar sample is not accurate, because the field is stronger near the corners of the bar. Also the insulation is highly homogeneous and contains very little defects or voids. Hence, the cable sample can be more accurately modeled with a 2D FEM than the bar sample. The semiconductive layer on top of the cable construction was removed and the insulation was partly covered with the semiconductive paint, which acted as a ground electrode

similarly as in the bar sample. The corona rings visible in Fig. 3.8 were used also in the bar sample.

In the test procedure, the pressure was adjusted and the voltage was slowly increased until the first discharges appeared. The PD inception voltage was written down at this point. After the PD inception voltage was found, the voltage was increased to desired level and the PD activity was recorded for a 2 minute time period. Then the voltage was decreased, and the level at which the discharges disappeared was marked. The same procedure was carried out for all pressure levels. With the bar sample, the constant voltage level was 4 kV, which corresponds to a 6.928 kV line-to-line voltage in an electrical machine. The constant voltage level with a cable sample was 8 kV, because the insulation thickness was larger.

3.3.1 Finite element modeling

Two different investigations were carried out with two-dimensional finite element methods (FEM). The calculations were performed using FLUX2D® software by Cedrat. The cable sample was modeled with the 2D FEM and the theoretical results were compared with the measured ones. Theoretically, the cable sample is equivalent to the 2D FEM model, because its radial cross-section does not contain sharp edges. The bar sample was also modeled. Furthermore, a theoretical examination on different stress grading methods in an electrical machine was performed. The results of the former are presented in Section 4.2.3 and the latter in Section 4.3.

The FEM model used in cable calculations is illustrated in Fig. 3.9. The model imitates the actual geometry of the cable having the same thickness and properties (permittivity and loss tangent) of insulation. The operating voltage was applied to the ”conductor” region, while 0 V potential was imposed to the ”ground electrode” region. The model was used also for the bar sample without field grading. The thickness and properties of the insulation were changed and a different voltage applied. The voltage level with the cable model was 8 kV and with the bar model 4 kV according to the ones used in the measurements. The purpose of the ”termination region” in the model was to modify the calculation mesh; by using such a region it was possible to create a dense mesh (the distance between nodes 2 μm) in the desired place and a sparse mesh in the air region, where high accuracy was not needed.

The aim of the FEM model is to investigate the behavior of electrical field strength in the vicinity of the edge of the ground electrode. This region involving a sharp edge of an electrode is the most electrically stressed region in a corresponding electrical system and the most obvious setting for partial discharge and surface tracking phenomena. The occurrence of discharges is more frequent when the field strength in this vicinity is higher. However, it is not known where the discharges exactly take place. One end of the discharge is obviously the ground electrode, but it is not known how far they reach from it, in other words, the physical length of the discharges is not known. Furthermore, the FEM model does not exactly match the physical condition, which difference and its influence to the results is discussed further in Section 4.2.3. Therefore, it is necessary to record the field strength along a certain path in parallel with the conductor as seen in Fig. 3.9. It should be noted that the calculation path in

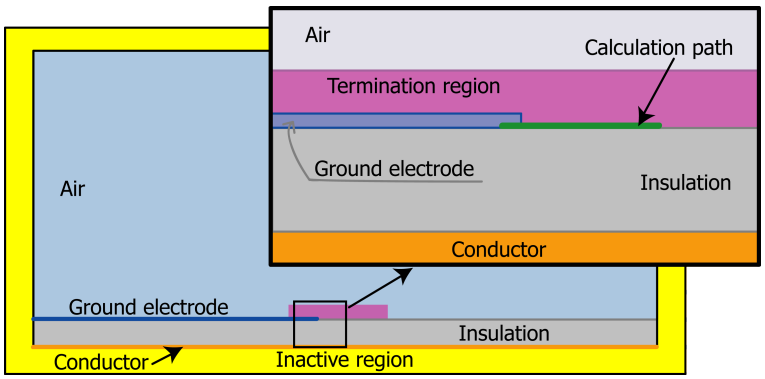

Fig. 3.9. Model used in the 2D FEM calculations of the cable sample.

Fig. 3.9 extends to the right from the end of the conductive layer. In the cable sample used in the measurements and illustrated in Fig. 3.8, a similar path would extend to the left from the end of the conductive layer.

The FEM model for stress grading investigation (Section 4.3) was tailored from the model seen in Fig. 3.9. The stress grading model was further modified for different geometries used in the study. In such an investigation, the validity of the model and its error sources were also discussed more closely. The model is presented in Section 4.3.

3.4 Preparation of the specimens

Essentially, the experimental tests contained samples of pure impregnating resins and of the whole mainwall insulation structures. The shapes of the specimens were determined mainly by methods of analysis, which is discussed below in Section 3.6.

Usually, the samples used in laboratory tests are manufactured with extreme care, and hence they do not correspond to actual products. This is beneficial when the target is to carefully study the physical phenomena related to the degradation of insulation. However, it is also one of the reasons, why laboratory tests on insulating materials do not fully correlate with the field tests of the same materials. The stochastic flaws caused by the automatized industrial manufacturing process are not that frequently present in the laboratory tests. In this study, the focus has been rather to meet the actual performance than to illustrate the physical phenomena affecting it, although the physical phenomena are discussed. Therefore, the samples used in the experimental test program were built according to the procedure designed for the manufacturing of the entire motor winding.

3.4.1 Mainwall insulation samples

The samples of mainwall insulation were manufactured with a vacuum pressure impregnation (VPI) method. The method reduces the amount of air inside the insulation leading to a better performance and longer lifetime of the insulation. The issue is emphasized with high-voltage motors and generators, which experience PD activity.

The samples used in the chemical aging tests were cut from large bars. The copper bars were covered with a Kapton® polyimide film, and a layer of mold release agent and taped over with a 2 mm layer of mica tape. Finally, they were impregnated with epoxy resin using a VPI method. Similar bars were used also in the partial discharge measurements. Prior to the VPI procedure, the bars were put into a mold, which is also called ”a dummy stator.” The mold was made of stainless steel and covered with a thin layer of Teflon. A layer of mold release agent was applied on top of Teflon to ensure that the samples do not get stuck to the mold when the resin cures. It was found that the Teflon itself was not a sufficient release method.

As the name vacuum pressure impregnation implies, the VPI procedure contains two steps: a vacuum phase and a pressure phase. In the vacuum phase the air is sucked out and the resin poured in. Some time after the resin had been inserted, the pressure is applied to further improve the resin penetration. After the VPI scheme, the mold was cured in an oven. The vacuum level used was approximately 5 – 10 mbar and the pressure level was 100 bar. The latter value is significantly higher than what is used in manufacturing of electrical machines (e.g. 5 bar or less). The chamber used in the impregnation was planned for experiments with gases at high pressures, and therefore, the use of a high pressure during the VPI scheme did not require additional care. The VPI equipment is illustrated in Fig. 3.10. The detailed procedure for the VPI manufacturing method used in the study is presented in Appendix B. Such a manufacturing method including a high pressure treatment has been proposed for the subsea compressor, which can be impregnated inside its own casing. The increase in pressure can improve the quality of the VPI process, because more air can be pushed out from the internal voids. Yet, despite quality improvements, the insulation of this kind is never totally void-free.

After curing, the mainwall insulation structures were removed from the bars and cakes (50 mm x 25 mm) were cut from them. The dimensions of the cakes were defined with respect to three-point bending test (Section 3.6.2) used to determine the mechanical properties. The bars were 95 mm wide. This was due to the dielectric response measurement, which required large samples as described in Section 3.6.5. For such measurements, square samples with an edge of approximately 90 mm were cut from the mainwall insulation structures.

3.4.2 Resin samples

The resin samples were made with a traditional dip and bake method. The resin was poured into a mold and cured in an oven. The curing depended upon the resin used. There were two kinds of molds with thicknesses of 2 mm and 4 mm. The former was used to build large

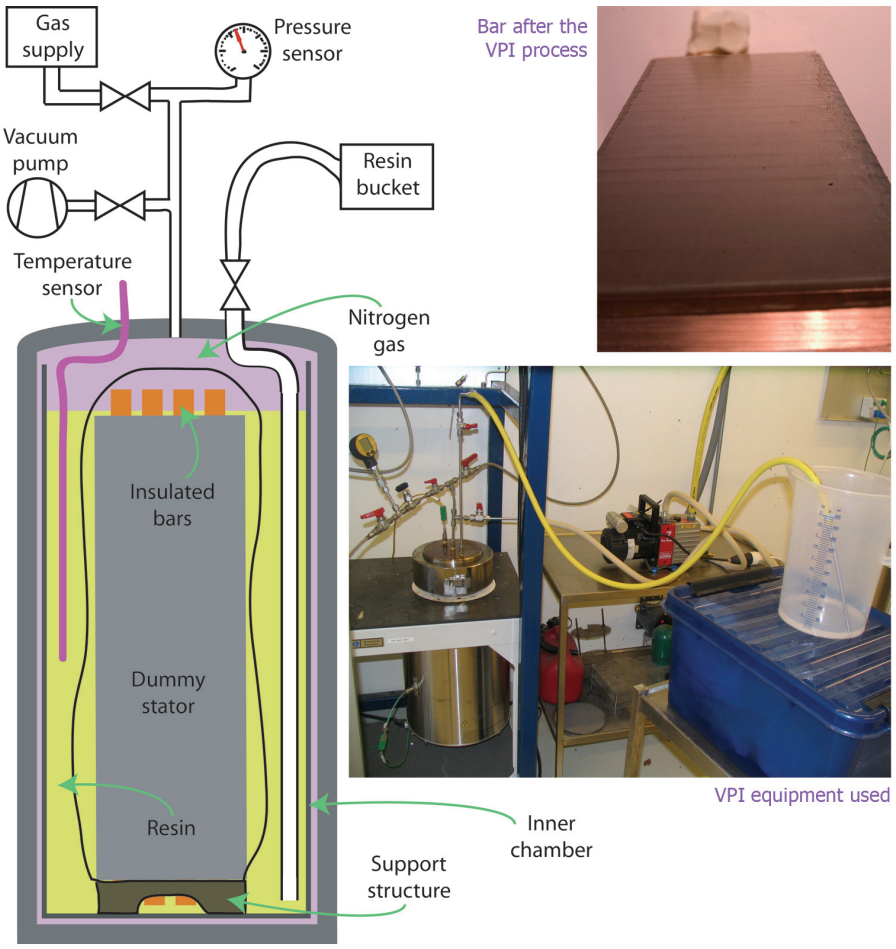

Fig. 3.10. Vacuum pressure impregnation test chamber.

samples for dielectric response measurements and the latter to build pins for the measurement of mechanical properties. Weights and dimensions were measured from the pins. The molds were made of stainless steel and covered with mold release agent.

The curing times and temperatures were dependent on the resins used. For epoxy anhydride resins with BCl_3 accelerator, the curing procedure was carried out in two steps: roughly 12 h at 90 °C and 16 h at 140 °C. The first step was considered final when the resin had turned into solid. The time required for this was dependent on the amount of accelerator used in the resin. The second step was carried out to finalize the chemical reaction. With zinc naphthenate accelerator, the curing was carried out in one step: 12 h at 150 °C. Epoxy novolac resin and bisphenol F epoxy resin were cured for 12 h at 165 °C. The curing schedules are included in Table 5.1, in which the resins are listed.

3.5 Experiments with hydrocarbon gas mixtures

Hydrocarbon gas is able to absorb moisture. When saturated, the gas mixture cannot absorb any more liquids. If there are more liquids in the test chamber, they will just stay on the bottom. The phase envelope of the wellstream gas mixture used in the test program is illustrated in Fig. 3.11. Different lines refer to formations of either a liquid phase (HC) or an aqueous phase (Aq) when the phase transformation is experienced. These phases refer to condensation of hydrocarbon compounds and water, respectively.

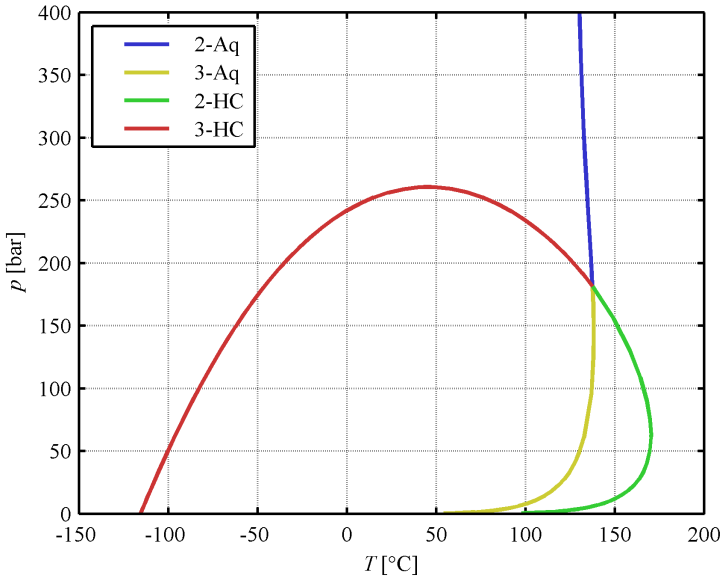

Fig. 3.11. Phase envelope of the wellstream gas mixture used in the experimental program. 2-Aq indicates a new aqueous phase and 2-HC, respectively, a new liquid phase when entering the two-phase region from the gaseous phase. 3-Aq refers to appearing of an aqueous phase and 3-HC, respectively, a liquid phase when entering the three-phase region from the two-phase area.

Raw natural gas in the wellstream is a complex mixture containing several substances, and it is difficult to reproduce exactly the same mixture. The raw natural gas mixture considered here refers to the mixture in the Åsgard B field in the North Sea. The hydrocarbon condensate and produced water were both collected from the Åsgard B field. The dry hydrocarbon gas mixture was prepared at the gas treatment laboratory. Its composition as described in Table 3.1 was chosen to be as close as possible to the mixture in the Åsgard B field. The mixture is essentially designed for the compressor, which operates at the Åsgard B field, but the hydrocarbon compounds it contains are present also in other gas/condensate fields. The selected environment can represent the general behavior of raw natural gas with respect to heavy hydrocarbons, water, and monoethylene glycol (MEG). For other gas fields, a re-evaluation is needed to define the composition of the mixture (i.e. the amounts of condensate and water) and the dew point. Further evaluation is needed regarding the additional compounds in the

gas mixture, such as hydrogen sulfide and corrosive particles in the produced water.

The hydrocarbon condensate contains heavy hydrocarbon compounds, which are liquid at room temperature. The weight fractions of hydrocarbon compounds of different molecular weights (i.e. the amounts of hexanes C6, heptanes C7, octanes C8, nonanes C9, and decanes or heavier C10+) are quite similar. Unlike the dry hydrocarbon gas mixture, the condensate does not consist mainly of the lightest component in the mixture. The produced water contains ions of many elements with highest portions of chlorine (Cl), sodium (Na), calcium (Ca), and potassium (K). It also contains ions such as carbonate (HCO_3^-) and sulphate (SO_4^{2-}), which are able to form acid components. The resistivity of produced water is approximately 0.1 Ωm and the pH value approximately 6.6. It is a somewhat conductive and slightly acidic mixture.

The actual wellstream mixture from the Åsgard B gas field will be water saturated at approximately 30 – 50 °C. In the operating conditions, the gas mixture is heated above its water saturation line having the potential of absorbing more water, if such was available. In the experimental program, the gas mixture was modified to be water saturated at 130 °C. This was done by putting in more water and more hydrocarbon condensate. From the insulating material's point of view, such an action causes accelerated chemical aging conditions as the gas contains more water and more condensate than the real gas mixture would. Also the pressure was slightly higher than in the operating conditions.

If the aging under these conditions is related to chemical reactions, which was one of the hypotheses, the reactions with water occur more frequently, if more water molecules are available. Hence, the higher fraction of water the gas mixture contains, the more aging it causes in the insulating materials. The hypothesis applies also to the hydrocarbon condensate.

The optimal duration of the test was defined to be 750 hours, which is approximately one month. Experimental tests carried out earlier with different materials and gas mixtures suggested to use such a test duration. The experiments listed in the test matrix were carried out with only one exposure. In the initial aging test, the results of which are not included in this thesis, some of the specimens were removed from the chamber after one week and the exposure was restarted with the rest of the specimens. It was found that such a method created too much uncertainty, because the specimens, which are tested for a longer duration, experience more depressurization steps. Therefore, the results for different durations are not fully comparable. It was concluded that aging tests under high pressure should be carried out with a single exposure only. The disadvantage of such a test procedure is that it limits the possibility to study the degradation as a function of time, because each time marker requires a new experiment.

3.5.1 Preparation of the gas mixtures

In the experimental program, the essential substances inside the raw natural gas (light and heavy hydrocarbon compounds, water, and MEG) were used together in a mixture, which is hereafter referred to as the wellstream gas mixture. The amounts of each component were

calculated so that the mixture will have the desired properties as seen in the phase envelope in Fig. 3.11. The mixture is water saturated at 130 °C and 150 bar. Its dew point, that is, the cross-section of the saturation lines, is approximately at this temperature but at a higher pressure. The gas mixture is, however, not very sensitive to pressure in this part of the p versus T plane, which can be seen in the phase envelope as the 2-Aq line is in parallel with the y-axis in this region. The wellstream gas mixture was used also in other conditions (Section 5.4), but in such experiments the mixtures were in different thermodynamical states. The purpose of such experiments was to investigate the effect of temperature.

The wellstream gas mixture was constructed by applying a hydrocarbon condensate and a mixture of produced water and MEG in the chamber and pressurizing the chamber with dry hydrocarbon gas, the composition of which is presented in Table 3.1. The amounts of condensate and MEG/water were determined by iterative simulation methods so that the gas mixture has the desired properties at 130 °C and 150 bar. PVTSim® software by Calsep was used in the simulation of the gas mixture. The software uses thermodynamic and chemical equations to determine the desired thermodynamic states of the given gas or liquid mixture.

3.5.2 Test equipment

The test chamber is illustrated in Fig. 3.12. The chamber contained the samples and liquids in the bottom of the chamber. The number of samples depended upon the test used. In the screening tests for epoxy resins and mica tape samples (Sections 5.1 and 5.2, respectively), there were many samples and the chamber was practically almost full. On the other hand, tests for the wellstream gas content analysis (Section 5.3), tests for different temperatures (Section 5.4) and tests of longer duration (Section 5.5) contained only the samples of relevant materials while most of the space inside the chamber was unoccupied. Therefore, the effective volume of the chamber was different in all the tests, and correspondingly, the amounts of liquid substances added were different. The procedure for the experiments with hydrocarbon gases is shown in Appendix C.

3.5.3 Depressurization

The depressurization of the test chamber after each chemical aging test was carried out in room temperature conditions. The test equipment contained no valves that could provide slow depressurization. The procedure was done in steps and it was repeated in a similar way after each exposure. Therefore, the samples must have experienced some mechanical stress during the depressurization, but the stress has been similar in all experiments. The first test, which considered different epoxy resins, involved more rapid depressurization. This was also seen in the results, which are presented in Section 5.1.

A rapid decompression test was carried out to investigate the effects of unscheduled and uncontrolled shutdowns. In this test, the specimens were exposed to steep pressure gradients while the temperature was high. For this experiment, a needle valve was assembled in the

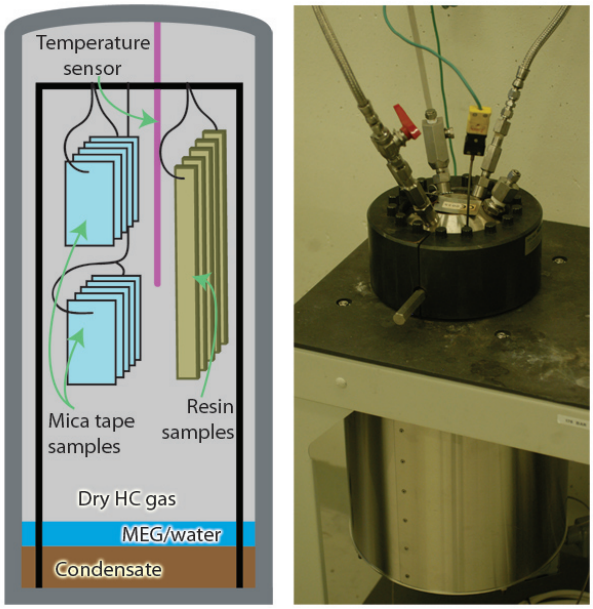

Fig. 3.12. Test chamber and the specimens in wellstream gas exposure.

gas outlet of the chamber. This allowed the desired depressurization rate. The test procedure contained nine cycles of depressurization and pressurization. The method is described in more detail and the results shown in Section 5.6. In the rapid decompression test, the chamber was pressurized when it was hot allowing no option to insert the liquids after each cycle. Hence, all the liquids for nine cycles were inserted before the test began.

3.6 Diagnostic methods

The test specimens are shown in Fig. 3.13. The materials used in the tests are described in the corresponding sections in Tables 5.1 and 5.2. The samples illustrated in Fig. 3.13 were used for all diagnostic methods, except for dielectric response measurements. No dielectric measurement or inspection was carried out for these samples. Together with such specimens, larger plate-shaped samples were used for dielectric response measurements. The analysis of the effects that the test environments caused leaned on a number of measurements on different quantities. Apart from the actual measurements, the physical appearance was investigated. Microscopic examination was also carried out; the cracks that had appeared during the tests were examined with a microscope. Similarly, the cracks caused by a three-point bending test (Section 3.6.2) were subjected to microscopic analysis. Typically, no treatment was carried out for the test specimens, but occasionally for photographing purposes the specimens were submerged into water before microscopic examination. The water highlighted the cracks. This was done with the rapid decompression test (Section 5.6). Closer photos on some sam-

ples were taken with a scanning electron microscope (SEM). The SEM investigation was carried out for samples of the long-term aging test.

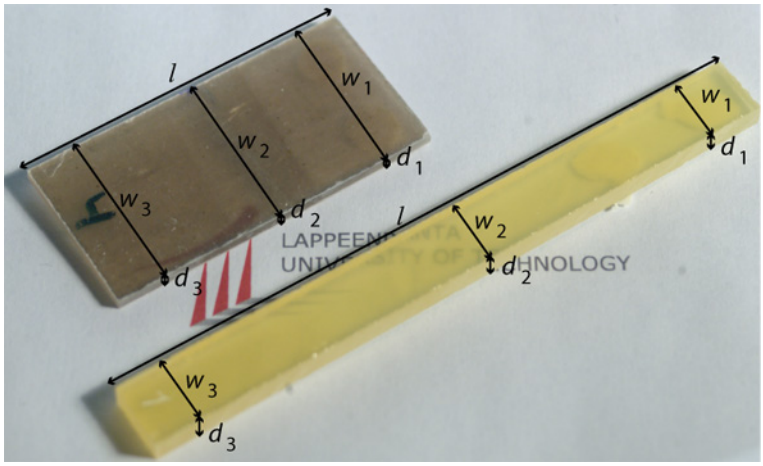

Fig. 3.13. Mainwall insulation and resin test specimens. The figure contains reference samples. The aged samples had a hole at which the width w_1 was measured.

The physical and mechanical properties were measured on both types of samples illustrated in Fig. 3.13. The samples for dielectric properties measurements were large square-shaped plates. The resin samples were used first to compare the different resins, but later on for the measurements on the chemical changes of the insulation. The resin samples were used in the measurements for chemical spectrum (FTIR) and glass transition temperature (DSC), and their purpose was to highlight the changes in the material structure. The mainwall insulation samples imitated the actual insulation of the motor.

Samples of the entire bar were used in the rapid decompression experiment (Section 5.6). The purpose of the bar samples was merely to illustrate the behavior of the insulation on the entire bar. No diagnostic tests were carried out for the bars. The bars used in the test were similar to the one used in the PD measurements (Fig. 3.7). However, no PD measurements were carried out for the bar samples exposed in hydrocarbon gas mixtures, because the conductive paint used as a ground electrode in the PD measurements could not tolerate the test environment. The partial disintegration of the conductive layer from the bar surface would have produced additional discharge in between the conductive layer and the insulation.

3.6.1 Weights and physical dimensions

Weights and dimensions (length, width, and thickness) were measured both before and after the tests. Volumes of the samples were calculated from the physical dimensions. For determination of volume, the thicknesses and widths of the samples were measured from three spots of the samples, Fig. 3.13, and the length in the middle of the sample. The volume was calculated according to the following equation:

$$V = \frac{w_1 + w_2 + w_3}{3} \cdot \frac{d_1 + d_2 + d_3}{3} \cdot l - \pi \cdot \left(\frac{D_{\text{hole}}}{2}\right)^2 \cdot d_1 \tag{3.1}$$

There was some scatter in the volume values. This was due to varying widths. The cutting process caused some variation. Clearly inaccurate volumes were removed from the statistical group. The differences in weight, volume, and density were defined by the following equations.

$$\Delta m = \frac{m_1 - m_0}{m_0} = \frac{m_1}{m_0} - 1 \tag{3.2}$$

$$\Delta V = \frac{V_1 - V_0}{V_0} = \frac{V_1}{V_0} - 1 \tag{3.3}$$

$$\Delta \rho = \frac{\rho_1 - \rho_0}{\rho_0} = \frac{\frac{m_1}{V_1} - \frac{m_0}{V_0}}{\frac{m_0}{V_0}} = \frac{\Delta m - \Delta V}{\Delta V + 1} \tag{3.4}$$

3.6.2 Mechanical properties

Mechanical properties were measured with a three-point bending test by following the ISO (2001) standard. The test method applies a downward force in the middle of the test specimen, which rests on two supports located at a distance s away from each other. The force is causing the test specimen to bend and ultimately crack. The measurements include force F and displacement x. According to them, the stress σ and strain ε can be calculated as follows:

$$\sigma = \frac{3Fs}{2wd^2} \tag{3.5}$$

$$\varepsilon = 100\frac{6dx}{s^2} \tag{3.6}$$

The distance s between the supports was set to 60 mm with resin pins and to 35 mm with mainwall insulation cakes. The mechanical properties (tensile strength σ_{f}, elongation at break ε_{f}, E-modulus U_{E}, and toughness U_{T}) are determined based on stress versus strain curves. An example curve with the parameters is illustrated in Fig. 3.14. The toughness of a sample is the area underneath the stress versus strain curve. It was calculated with a discrete integral by using each measurement point i as

$$U_{\mathrm{T}} = \int_0^{\varepsilon_{\mathrm{f}}} \sigma \mathrm{d}\varepsilon = \sum_i (\varepsilon_i - \varepsilon_{i-1}) \frac{\sigma_i + \sigma_{i-1}}{2} \tag{3.7}$$

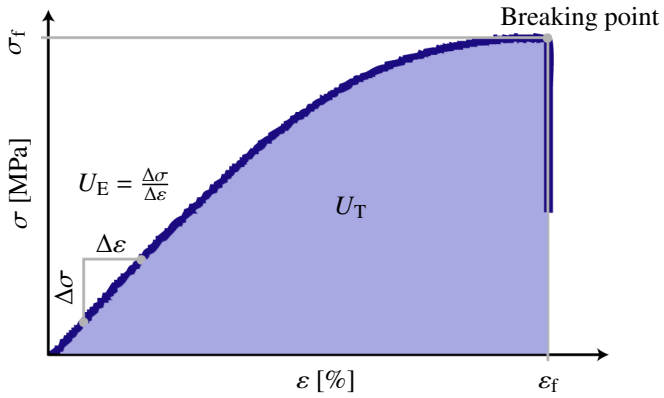

Fig. 3.14. Mechanical properties based on the stress versus strain curve obtained from the three-point bending test.

The resin samples were very brittle and they usually broke down before the expected breaking point in Fig. 3.14. Thus, the measurements indicated too low values for tensile strength, elongation at break, and toughness. The E-modulus could still be defined, because the premature breaking points were above the yielding point of the curve, that is, where the curve bends and is no longer linear. Therefore, the resin samples were analyzed based on the E-modulus values and their tensile strength, elongation at break, and toughness were not used. For the mainwall insulation cakes all the parameters were valid, since the materials did not suffer from premature breakdowns. The whole stress versus strain curves were also used in the analysis to illustrate the nature of the materials.

3.6.3 FTIR spectroscopy

FTIR (Fourier Transform Infrared) spectroscopy was carried out in the range of 4000 cm^{-1} to 600 cm^{-1}. The method exposes the specimens to electromagnetic radiation in the range of infrared frequencies (in this study 18 – 120 THz) causing the molecules of the measured specimens to vibrate. Such a method reveals information of the chemical structure as chemical bonds tend to have their own specific frequency. IR spectra were measured from randomly selected samples of each material before and after the exposure. The measurements were taken from five spots of each samples. The measurements after the test were carried out on exactly the same individual samples as the ones measured before the test.

FTIR spectra were roughly analyzed with the methods provided by the instrumentation software (PerkinElmer). The curves were smoothed and their baseline was corrected. The mea-

surements with small wave numbers tended to be distorted so that the spots that had no absorption were seen at some absorption level. This distortion can be corrected with the baseline correction feature of the software. Finally, the curves were normalized. Depending on the sample quality, the rate of absorption is changed in the measurements. Therefore, the magnitudes of the absorption peaks depend upon the sample quality. Normalization sets the highest peaks to maximum absorbance and scales the rest of the spectrum accordingly. With the normalization feature, it is possible to compare samples of different absorptions, for example, samples of different materials. The analysis of the results relied on the reference material provided by the manufacturer, (PerkinElmer; Hannah).

3.6.4 Glass transition temperature

A Differential Scanning Calorimeter (DSC) study was carried out to determine the glass transition temperature T_g of the specimens. The glass transition temperature refers to the temperature at which the material experiences a phase change from glassy to rubbery. In the DSC method, the temperature is increased steadily (20 °C per minute) and the heat flow is measured. The temperature at which the heating was stopped ranges between 120 – 180 °C depending on the T_g of the materials. The glass transition can be seen as a smooth step in heat flow versus temperature curve. The glass transition temperature was calculated by the algorithm integrated in the PerkinElmer measuring instrument used.

A DSC measurement is rather sensitive to the thermal history of the sample. The first heating run always contains additional information caused by the previous handling of the specimens, and the first measurement thus gives erroneous results. The measurement was performed three times and the value obtained from the third measurement was used as the glass transition temperature. With samples that have absorbed water, the measurements may not be correct as some water may evaporate during the heating and the T_g measured is then too high. This is discussed in Section 5.3. Nevertheless, the evaporation of water could not be discerned in the heat flow versus temperature curve.

3.6.5 Dielectric measurements

The dielectric response measurements were used in the wellstream gas content study in Section 5.3 and also with long term test in Section 5.5. The measurements for dielectric response were carried out at room temperature using IDA 200® instrument manufactured by Programma Electric (now part of Megger) and designed for such measurements. The measurements were performed in a frequency range 10 mHz – 1 kHz. The electrodes were connected to both sides of the sample creating a parallel-plate capacitor with round electrodes. The samples were initially square-shaped plates with 90 mm edges. The area of the capacitor (i.e. the area of the electrodes) was that of a circle with 50 mm diameter. A layer of conductive silver-filled epoxy paint was laid between the sample and the electrodes to ensure good connection. A guard ring was used around the ground electrode to prevent interference caused by twisted electrical field. The guarding was implemented according to ASTM

(2004). The electrodes were connected to the terminals of the instrument and the measuring run was carried out according to the automatic procedure of the measurement. The IDA 200 instrument recorded the real and imaginary parts of the complex permittivity according to IEC (1969). The peak voltage was 200 V.

The insulation resistance was measured with the aid of an electrometer. The samples were modified into parallel-plate capacitors in the same way as in dielectric response measurements. The sample was connected in series with a resistor (2 MΩ) and the electrometer, and then into a high-voltage DC source (1 kV). The Keithley 6517 electrometer measured the current once in every second. The data was then processed with a computer and Labview software. The measurement was started approximately one minute after the voltage had been applied to prevent interferences caused by the polarization. An average was taken on measurements during each minute to reduce the amount of data. The resistance was calculated according to Eq. (2.27) for each one-minute average. Finally, mean values and standard deviation were calculated based on the data. The method did not strictly follow the IEEE standard (IEEE, 2006), but the fundamental idea was the same. The measured current values were very low, only a few pA, which corresponds to high insulation resistance. Hence, the measurements were very sensitive to noise, which was seen as a high standard deviation, particularly with reference materials, the resistance of which was the highest. Because of the interference and small current, the measuring procedure defined in IEEE (2006) could not be used. Such a procedure includes only one or few measurements at a given time. It works with complete motors and generators, the insulation resistance of which is lower and the current significantly higher.

3.6.6 Statistical analysis

The statistical methods are explained at a macroscopic level. The choice of a proper statistical tool for each data type was made between normal, lognormal, and Weibull distributions.

The estimate of the normal distribution is an arithmetic mean of the samples. The values of variables are evenly distributed around the mean value. Normal distribution can be applied to physical measurements of linear scale, such as heights, weights, and diameters (Nelson et al., 2003). Lognormal distribution defines a random variable, the logarithm of which is normally distributed. Lognormal distribution is applied to lifetime distributions on some occasions (Nelson et al., 2003) and to thermal aging data (Stone et al., 2004). The Weibull distribution is a special case of exponential distribution. It is commonly used with the lifetime estimates of electrical insulation, when the insulation is aged by electrical stress, for instance (Stone and Lawless, 1979) and (Mitsui and Inoue, 1977). The specimens suffer a breakdown when the weakest point in their structure fails, in other words, the flashover is most likely to take place at the point of the shortest thickness of insulation. The probability density functions and estimates for the distributions are shown in Appendix D.

The three-point bending test, which was used to define the mechanical properties of the samples, is basically a test for the weakest point. When the specimen is bent to the breaking point, it cuts at the weakest point, where the strength is the lowest. At this point there is usually a

small micro crack at the edge of the sample, which initiates the breakdown process. A micro crack involves a sharp edge, where the force accumulates during the bending test. Also the thickness of the material is reduced by the thickness of the micro crack.

Yet, in the three-point bending test the mechanical stress is applied only to the short section on the specimen, where the bending head is located. The breakdown can only take place in the vicinity of the bending head. Thus, the breakdown is not fully determined by the weakest point, because such a point would have to be located in the vicinity of the bending head. The nature of the test for reference samples is more of a lognormal than the weakest point (Weibull), but the relevance of the weakest point was found to increase during the aging experiments.

There were some differences between the distributions, when they were fit into the data. The sets contained 30 samples at highest. However, the differences were very small (below 1%), and each of the three distributions would have produced the same conclusions. The normal and lognormal distribution seemed to fit better the weight and volume data than the Weibull. The lognormal distribution provided the best fit for the data on the mechanical properties of the reference samples, but the Weibull distribution fitted best to the aged samples. The data on the mechanical properties of the epoxy anhydride resin samples followed generally the lognormal distribution. For the epoxy novolac resin, on the other hand, the Weibull distribution provided the best fit. This was due to the hard and brittle nature of the materials. The comparison of the distributions regarding the data on the E-modulus of the resins is presented in Appendix D.

The sample sizes used in the resin screening test were as high as 30. The value was based on the maximum number of samples from a single manufacturing scheme. The screening tests indicated that the required sample size for the resin samples is approximately 10 – 15. It was seen that the mainwall insulation samples deviated less from the estimate values. The number of mainwall insulation samples used in the tests was 10, but in some cases with resin rich samples the number was reduced to 5, which was still considered adequate.

Normal distribution was used to interpret weight and volume data and thereby to calculate the density according to Eq. (3.4). It provided an equally good fit with the lognormal distribution and was notably simpler to use. Both the lognormal and Weibull distributions would have needed additional data treatment. Weibull distribution was used in the analysis of the mechanical properties of both the aged and unaged samples, because it appeared to be the best overall fit to all samples. It provided a slightly larger error with anhydride resins, but was found to better fit to the data on epoxy novolac resin after the exposures, as explained in Appendix D. Nevertheless, the differences between the distributions were negligibly small.

Chapter 4

PD and surface tracking

This chapter contains measurements on breakdown strengths of different gases; nitrogen, methane, mixture containing light hydrocarbon gases, and wet methane. One of the objectives is to compare the hydrocarbon gases and nitrogen, because hydrocarbon gases are very expensive to use in laboratory tests. Nitrogen, on the other hand, is an inert gas, which is not dangerous to people and environment. Furthermore, its use does not require so many additional instruments.

Measurements on partial discharges (PD) are included in this chapter. The measurements were performed on a bar sample and on a cable sample. The objective was to detect how the discharges behave as a function of pressure. The purpose of the bar sample is to imitate electrical machine windings, while the cable sample is convergent with the two-dimensional theoretical model.

This chapter also contains theoretical study on different stress grading methods and how they could replace the standard field grading materials in applications related to operation in harsh environments. The study is strictly theoretical and carried out in a comparative manner applying finite element methods (FEM). The FEM model created has been compared with the results on PD and breakdown strength measurements.

4.1 Breakdown strengths of gas mixtures

The measurements on the breakdown strengths of gases were carried out as explained in Section 3.2. The breakdown strengths of nitrogen, dry methane, hydrocarbon gas mixture, and wet methane were measured with different gap distances and pressures. Breakdown voltages with respect to pressure times distance are illustrated in Fig. 4.1.

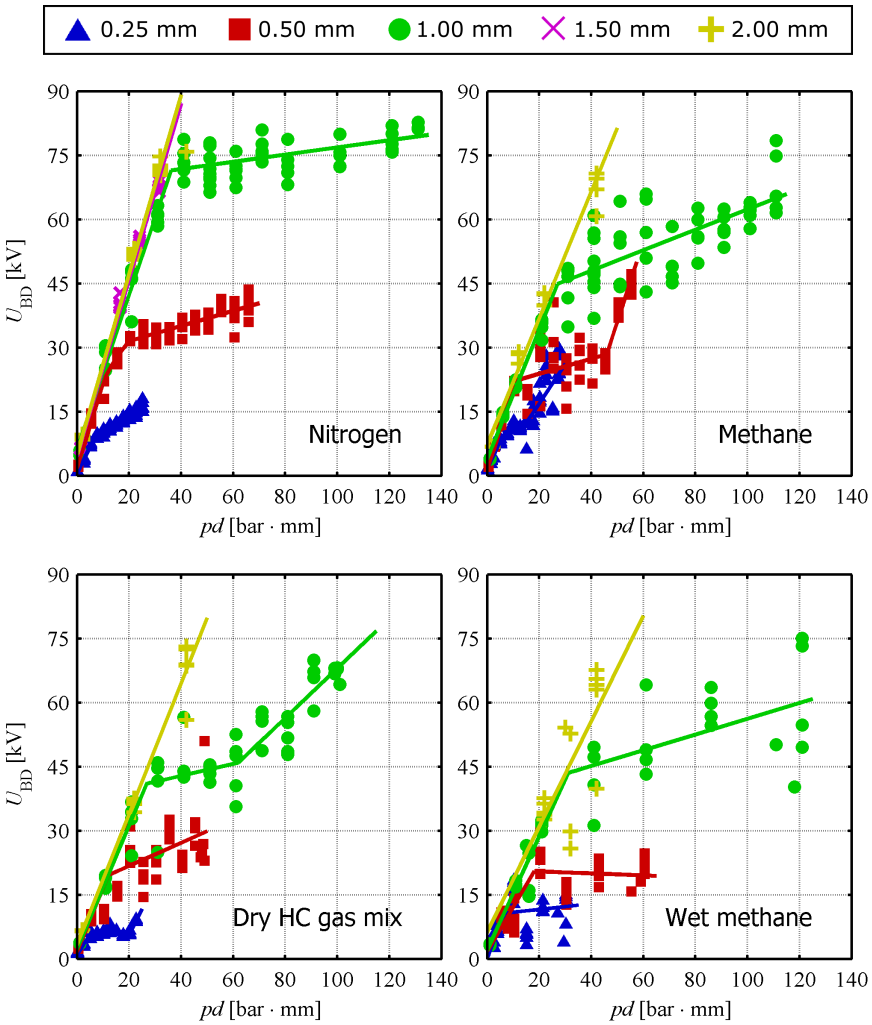

Fig. 4.1. Breakdown strengths of different gases with different gap distances as functions of pressure times gap distance. Linear curve fitting method is applied to determine the estimate curves.

In Fig. 4.1, knee-points can be observed with all gases with gap distances of 1 mm or less. The linear section below the knee-point participates in the Paschen curve and is convergent with all the gap distances. Leveling of the breakdown strength has been reported in other studies, (Meek and Craggs, 1953), and is ascribed to the field emission of electrode from the cathode. The approximated Paschen curves are illustrated in Fig. 4.2. The approximations are simply linear curve fits for sections below the knee-points as follows:

$$N_2: \quad U_{BD} = 2.20Pd + 1.18 \tag{4.1}$$
$$CH_3: \quad U_{BD} = 1.61Pd + 3.14 \tag{4.2}$$
$$\text{HC gas mixture}: \quad U_{BD} = 1.57Pd + 1.67 \tag{4.3}$$
$$\text{wet } CH_3: \quad U_{BD} = 1.39Pd + 0.54 \tag{4.4}$$

According to Fig. 4.1, the breakdown strength of methane and hydrocarbon gas mixture appears to be similar. Furthermore, the breakdown phenomenon in these two gases is more unpredictable than in nitrogen. This is seen as higher deviation. The breakdown in wet methane is of even more unpredictable form. The breakdown is much more chaotic than in dry gases.

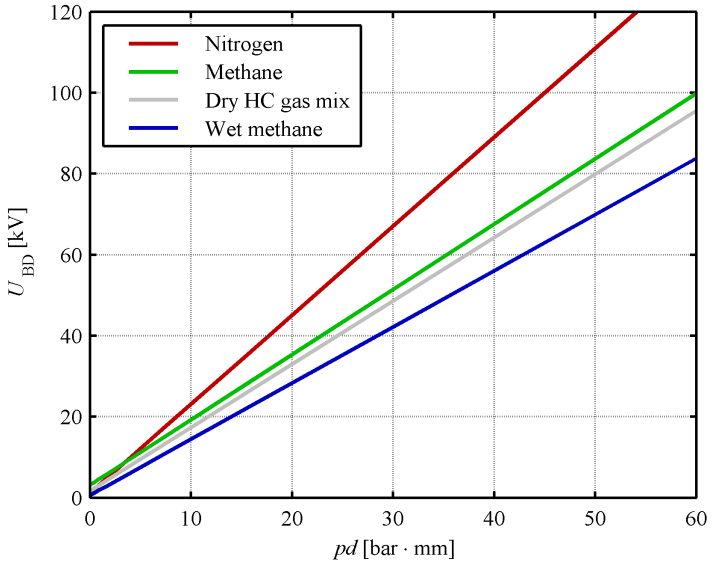

Fig. 4.2. Approximated Paschen curves for different gases. The curves are presented as breakdown voltage as a function of pressure times distance $U_{BD}(pd)$. They are also applicable as breakdown field strength as a function of pressure $E_{BD}(p)$.

It can be observed in Figs. 4.1 and 4.2 that the breakdown voltage of nitrogen is higher than that of methane and hydrocarbon gas mixture. Both methane and the hydrocarbon gas mixture behave in a similar way, the breakdown voltage of methane being slightly higher. This was the basis for using methane instead of a hydrocarbon gas mixture in the moist gas experiment. The breakdown strength of a moist hydrocarbon gas is lower than that of a dry gas, but the difference is not significant.

Measurements indicate that the breakdown strength of nitrogen gas is higher than that of hydrocarbon gases. Yet, the trend is similar and the use of nitrogen gas in partial discharge measurements can be justified. Nevertheless, the difference in breakdown strength has to be

taken into account. The differences in the breakdown strengths are related to the ionization energies of the corresponding gas mixtures. The energy needed to ionize the nitrogen gas molecules and initiate the Townsend avalanche, which leads to the breakdown, is higher than the energy needed to ionize the hydrocarbon gas molecules.

According to Paschen's curve, the breakdown strength is dependent on the pressure and distance. The dependence is linear as in Fig. 4.2 with the *pd* products used in the measurements. At very low *pd* product values, which correlates practically to low pressures, the curve begins to level off and the change in the *pd* product does not change the breakdown voltage as significantly. When the *pd* product is further decreased and the pressure level is extended more towards vacuum, the breakdown strength suddenly increases. At this point, the pressure is so low and the vacuum is so deep that there are simply no ions to ionize and cause the Townsend avalanche. At low values of the *pd* product, the Paschen's curve is nonlinear. However, in the range discussed in this dissertation, the curve is linear as in Fig. 4.2. However, the breakdown voltage U_{BD} as a function of *pd* cannot be directly changed into breakdown field strength E_{BD} as a function of pressure p (Kuffel et al., 2000). Yet, by considering the range of pressures and the gap distance $d = 1$ mm, which was actually used, the transformation can be made with reasonable accuracy.

4.2 Partial discharges and surface tracking

The partial discharge measurements have been carried out for bar and cable samples as described in Section 3.3. The reader has to bear in mind that the pressure is shown in absolute values, 1 bar referring to atmospheric pressure.

4.2.1 PD measurements on a bar sample

Partial discharges of the bar sample at 1 bar and 1.5 bar are illustrated in Fig. 4.3. The measurements on a plain bar sample at 3.5 – 6 bar and on a bar sample with field grading paint at 4 – 6 bar are shown in Fig. 4.4. The discharge level and the PD inception voltage as functions of pressure are illustrated in Fig. 4.5.

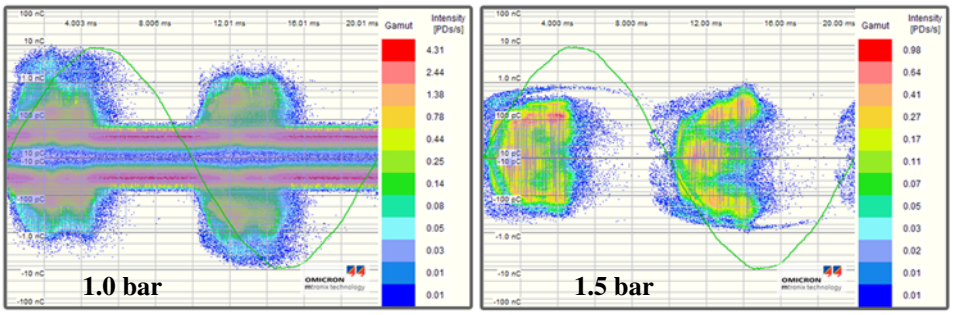

Fig. 4.3. Partial discharges of the bar sample without field grading in nitrogen gas at atmospheric pressure and at a 1.5 bar absolute pressure. The voltage was 4 kV. The color scheme on the left extends to much higher intensities than the one on the right.

It can be seen in Fig. 4.3 that there are plenty of discharges at atmospheric pressure, and the partial discharge activity is significantly reduced when the pressure is increased only to 1.5 bar. The difference is undeniable despite different color schemes. The same observation is clear also in Fig. 4.5 below.

It can be seen in Figs. 4.3 and 4.4 that as the pressure was increased, the surface discharges disappeared, but the discharges from internal voids remained and they were not affected by the pressure. The measurements were carried out with nitrogen gas at room temperature; these conditions regardless of the pressure did not cause the internal voids to get pressurized. The pressure of 50 bar was maintained for a week, and still the internal voids were not pressurized. This was an unfortunate outcome and it is mostly misleading in this case. It was clear based on chemical aging tests (Chapter 5) that rich hydrocarbon gas under high pressure and high temperature is able to penetrate everywhere in the mainwall insulation. When the temperature increases the insulating materials soften even below the glass transition temperature. When the insulation system (namely the resin) approaches the glass transition temperature, its molecular structure becomes more flexible allowing the gas to flow through

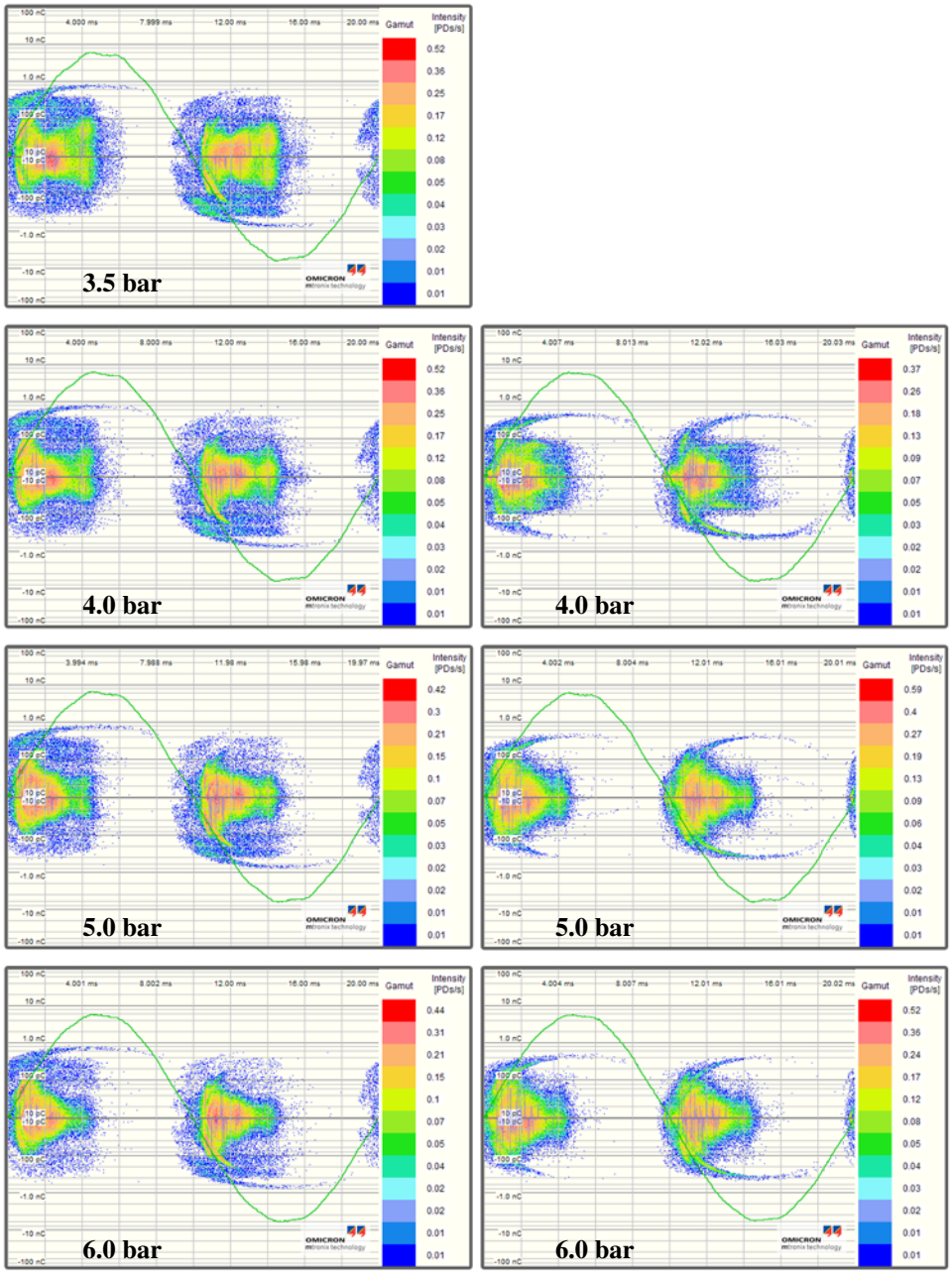

Fig. 4.4. Partial discharge activity of the bar sample in nitrogen gas at different pressures. Results on the bar sample without field grading (illustrations on the left column) and with field grading (illustrations on the right column). The voltage was 4 kV. The intensity color scheme is not constant for all measurements, but the differences are very small in practice.

the insulation at least to some extent. It should be noted here that the operating pressure of the machine is very high. Therefore, the internal voids in a full-scale motor insulation will get pressurized.

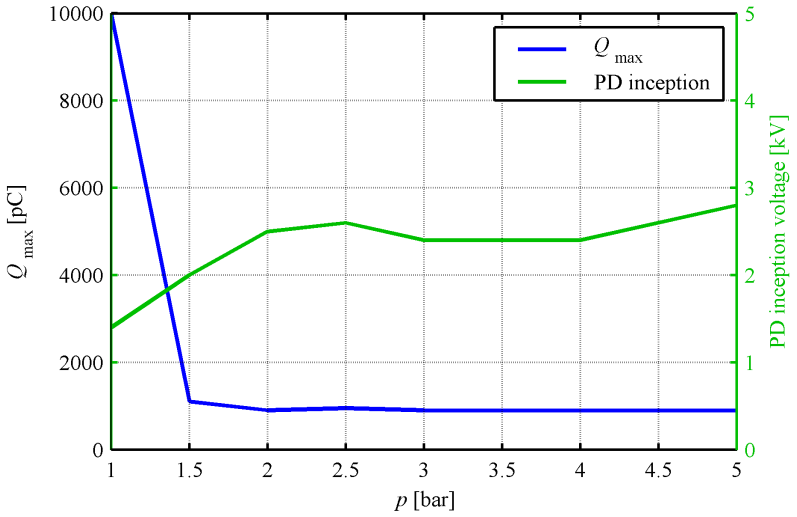

Fig. 4.5. Maximum partial discharge level and PD inception voltage as functions of absolute pressure. The voltage in the Q_{max} measurement was 4 kV (RMS).

It can be seen in Fig. 4.5 that the PD inception voltage is not increased after 2 bar despite the increasing pressure. The discharges first observed above 2 bar are located in the internal voids. According to the discharge level curve, the internal discharges begin to dominate when the pressure is above approximately 1.5 bar. Therefore, the intensity of the surface discharges is high only at pressure levels near atmospheric; It reduces significantly instantly when the pressure is increased. Yet, the discharge level caused by internal discharges is rather high and it obscures at least some of the surface discharges. It cannot be said that the surface tracking disappears when the pressure is 2 bar or above. This estimate would be too low, as can be seen in Fig. 4.4.

The measuring of a bar sample was very challenging. The sample contained plenty of internal voids, which had a major contribution to the measured discharge level, especially with higher pressures. In addition, the copper bar contained sharp edges, which caused high local field strengths around them. This is seen as emphasized PD activity at atmospheric pressure. The internal voids were mainly due to poor sample quality. The bar was taped by hand and some tape layers were slightly tangled near the bar corners. The voids between the layers had obviously been too large for the impregnating resin to fill. The chemical aging tests, for which purpose the mainwall insulation samples were designed, were carried out with smaller samples cut out from the bar. These samples can be cut from sections of good quality, and the internal voids in certain areas of the bar have no effect. From the full-scale machine point of view, this issue is irrelevant, because the manufacturing process is automatic and its quality is assured by additional measurements of internal void content (dielectric

response). Therefore, the number of internal voids is significantly smaller in the full-scale machine, and the majority of discharges the machine experiences are located in the end-winding region where the conductive layer is terminated. In fact, most of the PD activity in atmospheric pressure was caused by the surface discharges also in this measurement, which can be seen in Fig. 4.5. The surface discharges play an important role in the study on the given insulation system, because the method to protect the insulation from them (stress grading layer) is considered to be removed or replaced. However, the purpose of the investigation is also to replace the impregnating resin with an epoxy resin. Mica-based insulation with epoxy resin can usually tolerate surface discharges much better than a similar insulation with polyesterimide resin.

The discharges located in the internal voids can, at least to some extent, be detected from the partial discharge pattern. They tend to have distinct shapes. For instance, the pattern that looks like rabbit ears typically indicates discharges in internal voids. In this case, the discharge pattern produced by internal discharges can be seen in the right column of Fig. 4.4. The rabbit ears have bent as if the rabbit was running very fast. The sample in such a measurement was covered with field grading paint allowing the discharges to take place inside the insulation only, while the discharges on the surface cause no interference. As the pressure was increased, the left column in Fig. 4.4 began to look more like the right column in the figure.

Based on Fig. 4.4, it was not possible to define the exact pressure above which the surface discharges disappear. Furthermore, it was not possible to measure the PD inception voltage, that is, the voltage above which partial discharges appear. Neither was it possible to define the PD level. Both quantities were dominated by the discharges in internal voids. Yet, it is possible to estimate roughly that the pressure level is in the range of 4 – 5 bar. In the left column of Fig. 4.4, a reduction can be seen in the tail section of the discharge pattern (approximately at 14 ms) when the pressure is increased from 4 bar to 5 bar. This observation is still rather indefinite, and further investigation was needed with a cable sample.

4.2.2 PD measurements on a cable sample

The results of the PD measurements on a cable sample are illustrated in Fig. 4.6. The discharge level as a function of pressure is illustrated in Fig. 4.7 and the PD inception voltage as a function of pressure is Fig. 4.8. It can be seen in Fig. 4.6 that the discharge level gradually reduces as the pressure is increased. The discharge activity was seen to cease completely at approximately 11 bar, although this is not visible in the figure. The definite pressure above which the discharges disappear is still difficult to define.

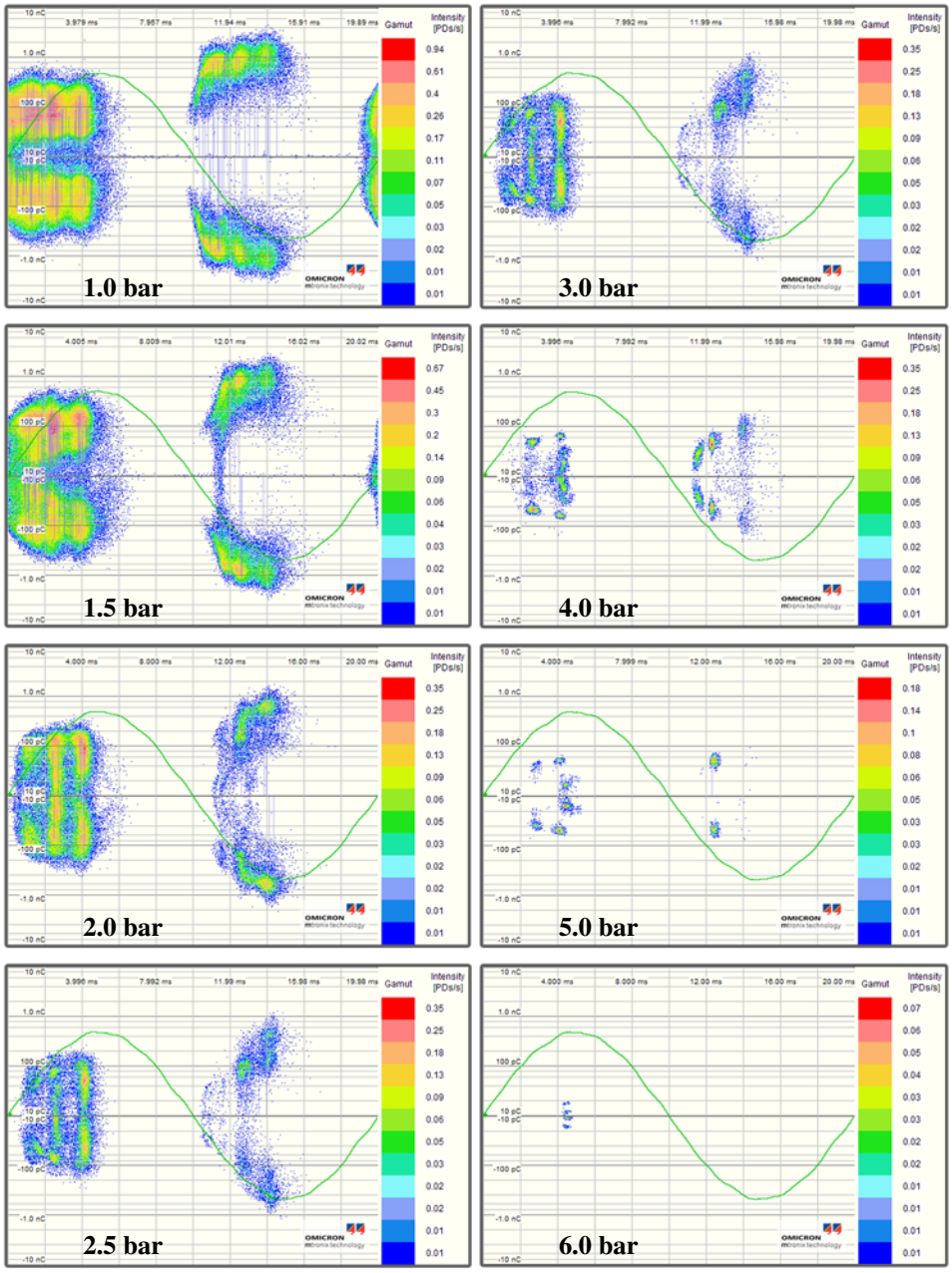

Fig. 4.6. PD of the cable sample with different pressures of nitrogen gas. Pressures are presented in absolute values. The voltage was 8 kV. Small illustrations are produced by the measuring software. The intensity color scheme is not fixed, but it is constant for the pressure range 2 – 4 bar.

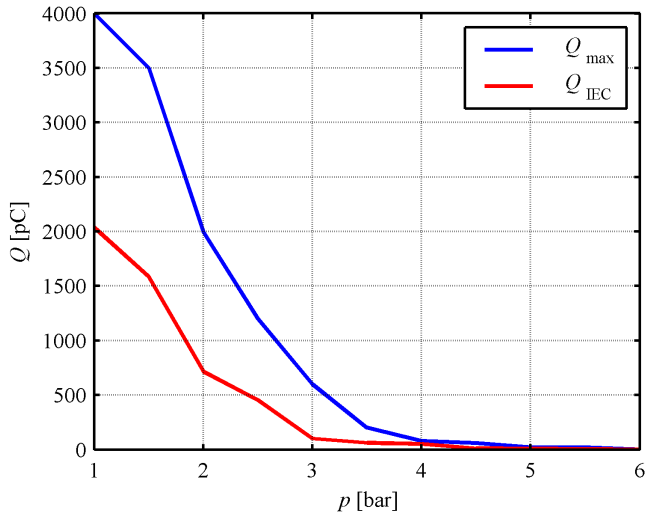

Fig. 4.7. Partial discharge level as a function of absolute pressure. Q_{max} refers to the maximum discharge value and Q_{IEC} to the standardized estimate value. The voltage was 8 kV (RMS).

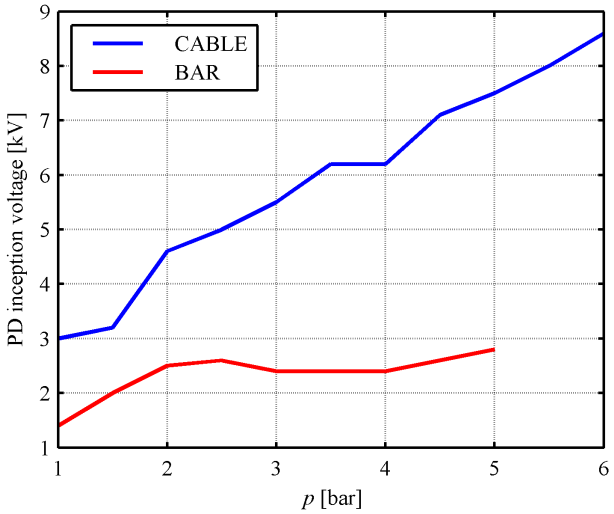

Fig. 4.8. PD inception voltage as a function of absolute pressure. The curve for the bar sample illustrated above in Fig. 4.5 is repeated for comparison.

It can be seen in Fig. 4.7 that the discharges disappear at approximately 4 bar. The reduction in Q is much smoother than with a bar sample in Fig. 4.5. The maximum discharge level Q_{max} is more reliable than the standardized estimate, Q_{IEC}. The latter quantity can basically refer to any discharge, and in these kinds of measurements the value is not very reliable, although it appears to behave in a similar way as Q_{max}. It can be seen in Fig. 4.8 that the

voltage required to cause partial discharges increases when the pressure is increased. Based on the measurements on breakdown strengths of gases (Section 4.1), this was an expected outcome. It is not convergent with the bar sample, Fig. 4.5, which is due to the internal discharges in the bar sample.

Typically, the PD inception voltage is affected by the roughness of the insulation surface. It can be approximated that the surface roughness has been lower in the bar sample than in the cable sample, because the bar sample has been manufactured in a mold. However, the surface roughness was not discussed in this study.

The cable sample was virtually free of internal discharges. It consisted of extruded XLPE, which is practically not allowed to have any internal discharges. The PD level in the XLPE material is considered dangerous, if it is 10 pC or more. With electrical machines the level is not accurately defined and PD testing is advised to be carried out in a comparative manner (Stone et al., 2004), which means that the aging of insulation can be detected by an increased PD level when it is compared with the measurements performed when the motor winding was new. Still, the winding can tolerate at least 1000 pC, but this refers to the entire winding and the value is not comparable with the values shown in the figures of this chapter. The fundamental difference between a mica-based mainwall insulation and XLPE is that the former is built to tolerate partial discharges to some extent, while the latter does not tolerate them at all.

It has to be kept in mind that the breakdown strength of nitrogen is slightly higher than that of hydrocarbon gases, as pointed out in Fig. 4.2. At the pressure of 4 bar the breakdown strength of nitrogen gas is according to Eq. (4.1) 9.96 kV/mm. The same breakdown strength in wet methane requires a pressure of 6.79 bar, according to Eq. (4.4), which is over 30% more. However, the pressure limit sought here is the limit above which there is virtually no discharge activity. The electrical machine windings, if consisting of mica, glass, and epoxy, can tolerate some discharge activity. Furthermore, the most significant reduction in partial discharge activity is seen at the initial increases in pressure, in other words, in the first fractions of a bar above atmospheric pressure. Therefore, above the region from 4 to 5 bar, it is not expected that the motor winding will experience any problems caused by partial discharges. Considering that the pressure at operating conditions is around 100 bar, the PD and surface tracking cannot cause aging of insulating materials. This conclusion is based on the assumption that the internal voids will have the same pressure as the surroundings. It is concluded in Chapter 5 that the gas mixture is able to penetrate into the insulation and pressurize the internal voids at operating conditions. It is assumed that this takes place also at lower pressures as long as the temperature is near the operating temperature.

4.2.3 Theoretical modeling

The modeling was carried out with all the PD inception voltages in Fig. 4.8. The PD inception voltages, corresponding pressure levels, breakdown voltages, and breakdown field strengths are listed in Table 4.1.

Table 4.1. PD inception voltage measured for each pressure (see Fig. 4.8), the corresponding breakdown voltages of nitrogen calculated according to Eq. (4.1), and the corresponding breakdown field strengths with a 1 mm gap distance.

p [bar]	PD inception voltage [kV]	U_{BD} in nitrogen [kV]	E_{BD} [kV/mm]
1.0	3.0	3.37	3.37
1.5	3.2	4.47	4.47
2.0	4.6	5.57	5.57
2.5	5.0	6.67	6.67
3.0	5.5	7.77	7.77
3.5	6.2	8.86	8.86
4.0	6.2	9.96	9.96
4.5	7.1	11.06	11.06
5.0	7.5	12.16	12.16
5.5	8.0	13.26	13.26
6.0	8.6	14.35	14.35

For each measured PD inception voltage, the field strength was recorded along the calculation path shown in Fig. 3.9. The distance x as a function of voltage is illustrated in Fig. 4.9. The distance x is the distance from the edge of the conductor to the spot, where the field strength is equal to the breakdown field strength for a given voltage and the corresponding pressure. Meanwhile, x refers to the length of the discharges, which can first be detected at the PD inception voltage.

According to Fig. 4.9, the distance x is in the range of 0.04 – 0.12 mm with all voltages. Also the modeling of the bar sample results in the distances within this range. Fig. 4.9 is indicating that a single discharge requires a certain finite length, which cannot be lower than x. The discharges that are detected at the PD inception voltage are the ones extending from the end of the ground electrode ($x = 0$) to the distance x. When the voltage is increased to nominal, there will also be discharges of higher length. It has to be emphasized that along with voltage also the pressure is increased in Fig. 4.9.

Another approach was taken to define the distance x more accurately. The field strength was recorded from the model with the voltage of 8 kV, corresponding to the voltage used in the PD measurements for all pressures, see Fig. 4.7. The distance x was defined individually for each pressure using corresponding breakdown field strength values in Table 4.1. The distance x as a function of pressure is shown in Fig. 4.10 with a reprint of Fig. 4.7.

In Fig. 4.10, it can be seen that the distance x reduces as the pressure is increasing. This

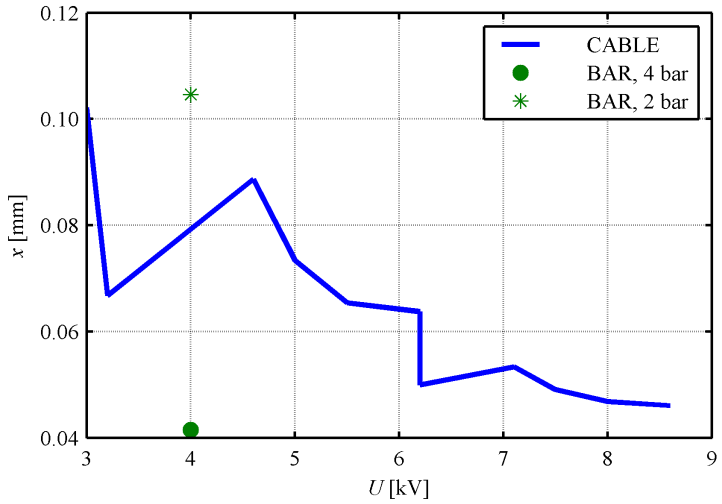

Fig. 4.9. Distance x as a function of voltage. The distance x is also defined for the bar sample with two different pressures. The voltages on the x-axis refer to the measured PD inception voltages. It should be noted that also the pressure varies along with the voltage on the x-axis.

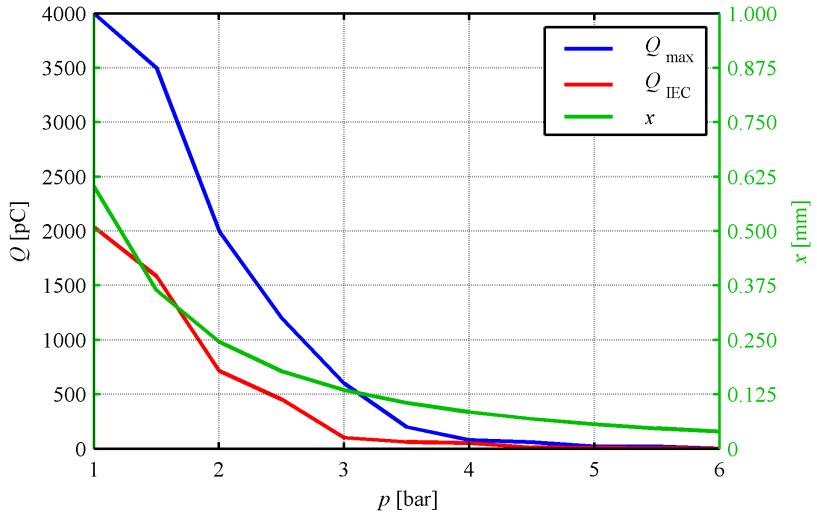

Fig. 4.10. Measured partial discharge levels Q_{max} and Q_{IEC} and the calculated critical distance x as a function of absolute pressure. The voltage was 8 kV.

is straightforward, since the higher pressure refers to a higher breakdown strength, which is located nearer to the ground electrode as the voltage remains constant in Fig. 4.10. At some pressure the discharge activity ceases, because the distance x becomes too short for discharges to form. At 4 bar, where the PD activity is assumed to stop, the distance $x = 0.084$

mm. The value is not fully convergent with Fig. 4.9, according to which $x = 0.045$ mm, but it is still in the same range (0.04 mm – 0.12 mm).

The main conclusion based on finite element modeling is that the critical distance within which discharges take place is around 40 – 120 μm. Keeping this in mind, the modeling can be done also for other dielectric problems. If the model contains a sharp edge, the field values should not be investigated close to the edge, but at approximately 40 – 120 μm away from it. This distance x refers to two things. On the one hand, it points to that partial discharges need a finite distance to take place. Otherwise, the electrodes would touch each other. Furthermore, there has to be a certain finite distance for a single discharge to progress into a Townsend avalanche. Practically, the distance depends on the electrode system, but fundamentally the decisive quantity is the field strength. On the other hand, it indicates the difference between the theoretical model and the reality. At least some part of the distance is caused by too high field strength near the sharp edge.

In reality, the cable is an axisymmetric object, which is modeled accurately with cylindrical coordinates. Here the cable has been modeled as a two-dimensional object with cartesian coordinates. The method is therefore an approximation. It holds if the radius of the conductor is very large, because then the surface of the cable approaches a plane. Also, if the electrical field is very high, the uncertainties caused by the axisymmetricity are emphasized. The radius of the conductor of the cable object used in the measurements was approximately 5 mm and the thickness of insulation 4.35 mm. In the nominal case, the voltage was 8 kV in the FEM model, yielding to an electrical field of 1.84 kV/mm in the straight portion between the electrodes. The field strength is lower than the breakdown strength of air (3.108 kV/mm as calculated in the following section). Therefore, it is assumed that the 2D approximation is reasonable for the dimensions and voltage levels used.

The edge of the ground electrode has been considered sharp in the FEM model, but in an actual cable sample, it was not like that. The ground electrode in the cable sample was a conductive paint consisting of silicone and carbon black. Silicone is an insulator and the conductivity of the paint material is provided by conductive carbon black particles scattered around in the paint. The very edge of the paint layer ($x = 0$) could be either conductive carbon black or insulating silicone, but certainly not of a material the conductivity of which matches the overall conductivity of this very paint. This applies also to the corresponding material in an electrical machine.

A theoretical model is rarely capable of taking every possible aspects into account. In addition, the measurements for PD inception voltage contained uncertainties (e.g. not the strictly linear trend in Fig. 4.8), which have been adopted in the FEM model also (see similar anomalies in Fig. 4.9). In addition, the approximation of the length of a discharge has been defined based on the measurements carried out with a 1 mm gap distance. The approximated value of 40 μm is essentially less than that, and the breakdown field strength at such a gap should be theoretically higher. However, no difference was observed in the measurements between the gap distances of 0.25 mm and 1 mm. Nevertheless, there are always some uncertainties and the researcher has to find a way to minimize them. In this case, absolute values may – and in many cases will – be wrong, but the general trend is reliable.

4.3 Theoretical considerations on stress grading

Over the 1990s, many researchers have tackled the modeling by lumped parameters. With respect to silicon carbide, SiC, and its gradually changing resistivity, this is quite a flexible approach. However, FEM is more accurate than a lumped parameter model. It is noteworthy that the recent research has, more or less, leaned on the use of SiC-based materials. Therefore, the main issue has been the distribution of voltage along the material while the magnitude of the field strength at certain spots is mainly a consequence. In addition, resistive stress grading methods have been modeled with conformal mapping. Andersen (1977) and Rivenc et al. (1998) have determined equations for potential, but such equations are relatively complex and they cannot be applied to other stress grading methods.

The occurrence of partial discharges is related to the breakdown strength of the gas, as pointed out in the previous section. In typical machines the gas is air, but the gas inside the voids in the insulation can also contain gas from the curing reaction, such as hydrogen, boron, or chlorine. Also, the forced air cooling may cause the air right next to the windings to be slightly pressurized and to have a higher breakdown strength. Yet, air at atmospheric pressure and room temperature was considered to be the gas medium in the investigation presented in this section. The breakdown strength of air can be calculated as follows (Kuffel et al., 2000)

$$\frac{U_{\mathrm{BD}}}{pd} = \frac{E_{\mathrm{BD}}}{p} = \frac{6.72}{\sqrt{pd}} + 24.36 \qquad \frac{\mathrm{kV}}{\mathrm{cm\ bar}} \tag{4.5}$$

With p = 1 bar and d = 1 mm, Eq. (4.5) produces 3.108 kV/mm. This value was used in the analysis. The breakdown strengths of nitrogen and hydrocarbon gases were also discussed.

4.3.1 Description of the FEM model

The FEM model and material parameters are illustrated in Fig. 4.11. The model is essentially similar to the model in the previous section, which was presented in Fig. 3.9. The stator stack acts as a ground electrode with an imposed potential of 0 V. The lower edge of the mainwall region acts as a high-voltage electrode (labeled ”Copper” in Fig. 4.11) having a potential of 4 kV. This corresponds to the line-to-line voltage of 6.928 kV. The choice of voltage was affected by the PD measurements described in the previous section, which were performed with the 4 kV voltage. The mesh is constructed by triangular elements, the sizes of which are carefully determined. The mesh is very dense (distance between nodes 2 μm) around the end of conductive layer region and relatively sparse elsewhere. The path along which the electrical field strength is recorded is placed at 1 μm above the surface of the mainwall insulation to ensure that the field strength is in the air (or termination) region and not in the mainwall insulation.

The end plate is considered as a highly corrosion-resistant stainless steel. The conductive layer is a material that contains both conducting and insulating regions. Practically, it is

made of some insulating base (e.g. polyester) on which conductive particles (e.g. carbon black) are attached. Therefore, the material has to be given both resistivity and relative permittivity. It was found that the parameters of the end plate and the conductive layer have no influence on the field strength along the calculation path in Fig. 4.11 as long as they refer to conductive materials. The mainwall insulation was modeled with loss tangent and resistivity. The termination region was set to air (relative permittivity, $\epsilon_r = 1$) in the reference model, Fig. 4.11. Relative permittivity refers to the real part of complex permittivity, as explained in Chapter 2.

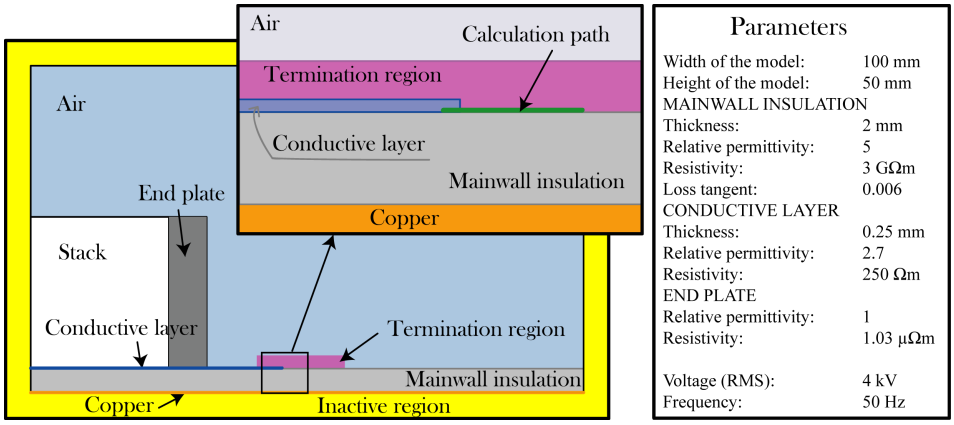

Fig. 4.11. FEM model and calculation path to record the field strength.

The study has been carried out keeping early design methods and future trends in mind. The machine windings constructed in the first half of the 20th century experienced less partial discharges than the machines with a modern mainwall insulation. This was due to the geometries and materials used. For comparison, the study was performed also for two old winding constructions. The mainwall insulation consisted of mica tape and asphalt varnish with a relative permittivity $\epsilon_r = 3$. The thickness of the mainwall insulation used was 3.2 mm, which according to Miner (1941), refers to the recommended thickness for line-to-line voltage level of 6.6 kV. The thickness was used in the model with a 4 kV phase voltage corresponding to the reference case. In the future, the thickness of the mainwall insulation of high-voltage machines is expected to reduce even further. This is made possible by mica tapes of better quality and smaller thickness and by more thorough impregnation, which is linked to the development of impregnating resins. The future machine is considered to have a 1 mm thick mainwall insulation with a relative permittivity $\epsilon_r = 5$. The permittivity of a future insulation is not likely to change significantly, because the materials will most probably not change. The industry does not have a replacement for mica as a PD resistant material.

4.3.2 Geometries

The reference model, illustrated in Fig. 4.11, has no stress grading. Actually, it is not a very good reference, since this kind of a solution is virtually never used in high-voltage

applications. In this case, however, it is considered the worst-case solution; in other words, it is not likely, no matter the methods used, to get the field behavior worse than that. The stress grading methods considered in the study are illustrated in Fig. 4.12.

Capacitive stress grading with a termination layer is illustrated in Fig. 4.12a. Termination with a high-permittivity material is a very simple solution. It requires only a layer of material applied on the termination spot. The termination with a high-permittivity material produces an interface of materials with permittivities ϵ_1 and ϵ_2 causing refraction in the electric flux:

$$\frac{\tan\alpha_1}{\tan\alpha_2} = \frac{E_2}{E_1} = \frac{\epsilon_1}{\epsilon_2} \tag{4.6}$$

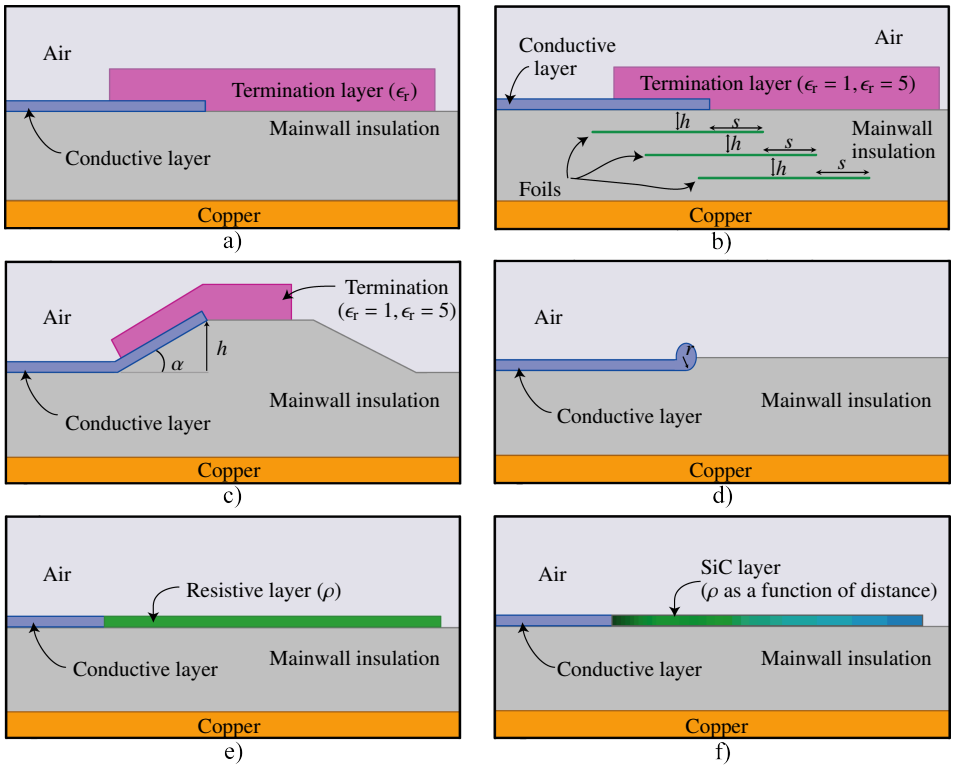

Fig. 4.12. Stress grading methods considered.
a) Capacitive stress grading with a termination layer of different relative permittivity
b) Capacitive stress grading with conductive foils
c) Capacitive stress grading with a stress cone
d) Capacitive stress grading by modifying the end of the conductive layer
e) Resistive stress grading with a material of different resistivity
f) Resistive stress grading with a material of nonlinearly changing resistivity

where α_1 and α_2 are the angles of the flux with respect to the normal of the interface and E_2 and E_1 the electrical field strengths in the materials, respectively. Equation (4.6) is also present in the reference model with no stress grading. In such a model, the ratio of permittivities is 1/5, resulting in a field strength of five times as high in the air as in the mainwall insulation at the interface. The ratio is higher, if the permittivity of the mainwall insulation is increased.

Basically, the capacitive stress grading with termination works well, if the ratio of permittivities is high, that is, the permittivity of the stress grading layer is high as the permittivity of the mainwall insulation cannot be altered. For the requirements of the cable industry, there are materials capable of providing a very high permittivity (Nelson and Hervig, 1984). High relative permittivity materials can be made by doping some base polymer with high-permittivity particles, such as carbon black or ferroelectric oxides. An example of the latter group is barium titanate ($BaTiO_3$), for which $\epsilon_r = 1000$.

Nelson and Hervig (1984) used carbon black and EPDM (ethylene propylene diene monomer) rubber, and they reported that it is theoretically possible to achieve high permittivity values, but accordingly the tensile strength and breakdown strength of the material are reduced. They constructed a material with $\epsilon_r = 25 - 35$, which were adequate for cable industry use. Nikolajevic et al. (1998) studied a similar high-permittivity material with $\epsilon_r = 40.4$. High-permittivity materials are, however, not mechanically strong, and their shape, namely the thickness, is not desirable from an electrical machine point of view. The high-permittivity materials available for cable termination are used in the model together with some fictitious materials, even though they cannot be considered to be used in practical applications. The mainwall insulation itself is considered a suitable termination material in applications including harsh operating environments.

Capacitive stress grading with conductive foils inside the mainwall insulation can be seen in Fig. 4.12b. The placement of foils is varied and the effect of termination with the mainwall insulation investigated. Also the effect of the number of foils is investigated in the range from no foils to seven foils, where the model containing no foils is the reference model. The foils in each model divide the mainwall insulation into sections of equal thickness. The models for different numbers of foils do not consider the placement of foils.

The key in controlling the maximum values of field strength is to control the shapes of the electrodes. As a rule of a thumb one might advise to avoid sharp edges. The model in Fig. 4.11 seems to break this rule as the conductive layer ends with two sharp 90-degree angles. In the cable industry, there are various possible ways to modify the geometries of conductors. Some considerations were presented by Mårtensson (2003) and previously by Short (1949). The cable terminations can take much space, whereas there is virtually no room for terminations in the electrical machine windings. The stress cone (Fig. 4.12c) and a rounded end of the conductive layer (Fig. 4.12d) are considered the only possible ways to implement the stress grading with geometrical modifications. In the case of the cone, the angle and height are both varied and the limitations of space were easily observed.

The resistive method contains a layer of material with either high resistivity or such resistivity

that depends on the field strength. Considering the case of a simple stress grading layer, which covers the end section of the conductive layer (such as in Figs. 4.12a, 4.12e, and 4.12f), the surface current density in the stress grading layer can be written as:

$$\boldsymbol{J} = (\sigma + \omega\epsilon_0\epsilon'')\boldsymbol{E} + j\omega\epsilon_0\epsilon')\boldsymbol{E} \tag{4.7}$$

where σ, is the conductivity, ω the angular frequency with ϵ' and ϵ'' referring to real and imaginary parts of the relative permittivity. The real part of $\boldsymbol{J}$ refers to the resistive and the imaginary part to the capacitive stress grading. In the frequency range used in electrical machines, the magnitude of the real part of relative permittivity, ϵ', is notably, say 50 – 100 times, larger than the imaginary part, ϵ''. Hence, the real part of $\boldsymbol{J}$ is dominant, if the conductivity is higher than the product $\omega\epsilon_0\epsilon'$. Thus, we may write that the stress grading applies the resistive method, if

$$\rho < \frac{1}{\omega\epsilon_0\epsilon_\mathrm{r}} \tag{4.8}$$

where ρ is the resistivity and ϵ_r the relative permittivity, or dielectric constant, of the stress grading material. With the parameters used in the model (listed in Fig. 4.11), the critical value of resistivity is approximately 70 MΩm.

The resistive stress grading method is illustrated in Fig. 4.12e. In this model, only the bulk resistivity of the material is discussed. The resistivity values used in the calculation basically cover the whole range from conductors to insulators. The field strength is recorded at the ends of both the conductive and stress grading layer.

The model in Fig. 4.12f considers the nonlinear stress grading materials. The model imitates the behavior of silicon carbide stress grading. However, the implementation of a material, the resistivity of which depends on a quantity calculated in the model (electrical field strength in this case) is not easy. Instead, the material was modeled with multiple fragments, each of which having individual resistivity. The resistivity of the stress grading material as a whole is thus discrete and dependent upon the distance from the end of the conductive layer. The resistivity of the stress grading is illustrated later with the electrical field strength behavior in Fig. 4.22. The color gradient in Fig. 4.12f illustrates the changing resistivity.

4.3.3 Definition of the field strength

The correct value of the field strength is difficult to determine. It approaches infinity, if we approach the edge of an electrode. In the vicinity of a sharp edge, the field and surface charge density become singular, if the distance from the edge $x \to 0$. If we consider a finite charge density and a finite field at the finite distance from the edge, the field strength becomes very

large when we let the distance $x \to 0$ (Johnson, 1998). This is emphasized with numerical methods as the computational errors accumulate in sharp edges.

On the other hand, the end of the conductive layer contains sharp edges, which is not the case in the actual electrical machine windings. The conductive layer is formed by conductive particles inside insulating material, such as Nomex® or PET film. Such a material is virtually impossible to implement in the FEM model without consuming most of the computer memory available. Sharp edges cause electric field to behave in a more aggressive way, and higher values of field strength are expected to appear in the FEM model than in reality, which was pointed out in the previous section.

Nevertheless, the determination of a reasonable field strength value is problematic. This has also been emphasized by Makuc et al. (2005). The approach for a reasonable field strength value has been taken by comparing the geometry that contains sharp edges with the one that contains rounded edges. The field strength along different paths starting from the edge with a sharp corner and rounded corners is illustrated in Fig. 4.13.

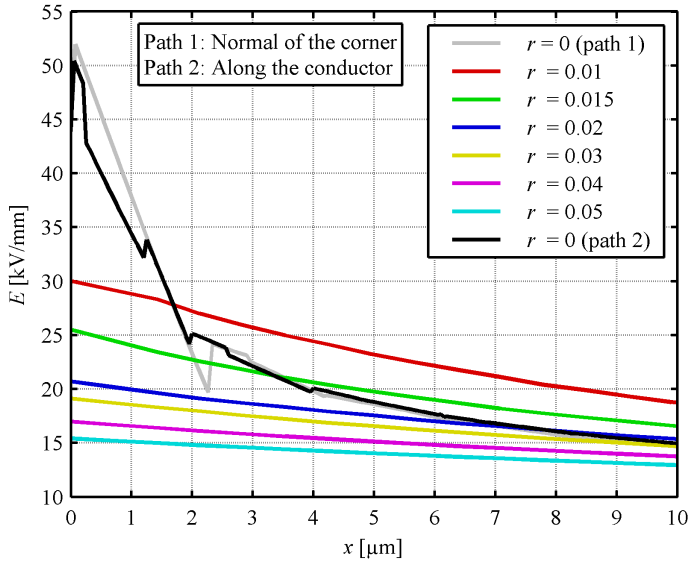

Fig. 4.13. Field strength along paths starting at the edge. Path 1 goes along the normal of the corner and path 2 travels along the copper conductor.

It is evident in Fig. 4.13 that the model is erroneous near the sharp edge. Furthermore, the model with a 0.01 mm radius rounded corner is slightly irregularly shaped near the edge. The errors are due to calculation routines, which contain some erroneous factors. The error is then accumulated on the sharp edge, which results in the discontinuous values seen in Fig. 4.13. The discontinuation spots refer to the nodes in the model and intersection of elements. The size of the first element along Path 2 in Fig. 4.13 is 2 μm and the element size is then gradually increased. The first three nodes located at approximately 2, 4, and 6 μm can be seen as discontinuation spots in Fig. 4.13. From the last node forward, the field behavior

appears to be smoother. Therefore, the computational errors are expected in the first three elements.

According to the partial discharge measurements presented in Section 4.2 the critical field strength values are located at 40 – 120 μm away from the edge. Thus, the field strength was recorded at 40 μm away from the conductor edge. This value is much higher than the problematic distances seen in Fig. 4.13, whereupon errors caused by computational routines are not expected to have any effect. Nevertheless, the study is made in a comparative manner paying less attention to the absolute values.

4.3.4 Results

The results are presented with per unit values. The base value has been the field strength of the reference model, which is 12.37 kV/mm obtained with a 4 kV (RMS) voltage. This is almost four times the breakdown strength of air. Hence, the need for stress grading in a typical air-cooled machine is imminent. The reference model was calculated with variable voltages, but other models have been investigated with 4 kV (RMS) only.

No stress grading

The field strength with different line-to-line voltages is illustrated in Fig. 4.14. It can be seen in the figure that the old mica-asphalt insulation is not as prone to partial discharges as the modern insulation. The field strength at the given spot is 31% less than that with the modern insulation. By contrast, the future insulation is facing 44% higher local field strengths than the modern insulation. Therefore, the future trend of reducing the thickness of insulation requires additional evaluation on the partial discharge activity in the windings. Yet, the reduction of the thickness improves the heat transfer and allows to use larger conductors, because less space is occupied by the insulation. These both are significant improvements.

According to Fig. 4.14, the machine with 2 kV line-to-line voltage may face partial discharges. However, such a voltage level is generally considered as ”safe” in this respect. But it is worth mentioning that the machines of such voltage levels may well experience partial discharges, if the insulation thickness is reduced. The Fig. 4.14 only represents the linear behavior of the field with respect to the voltage, and it does not take the insulation thickness into account. It is, therefore, not very realistic with respect to motors working with a higher voltage.

Capacitive stress grading with termination layer

The field strength as a function of permittivity of the termination layer is illustrated in Fig. 4.15. Permittivity value 1 refers to air, 3.1 to epoxy resin, and 5 to the mainwall insulation,

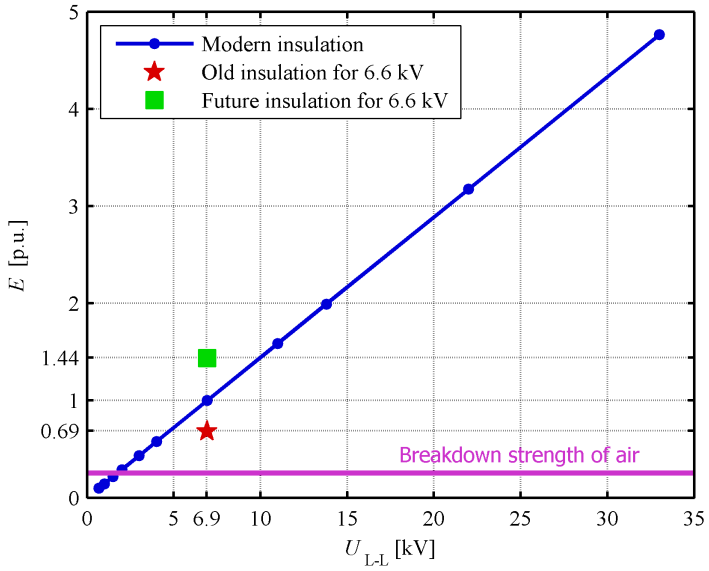

Fig. 4.14. Electrical field strength with different line-to-line voltages.

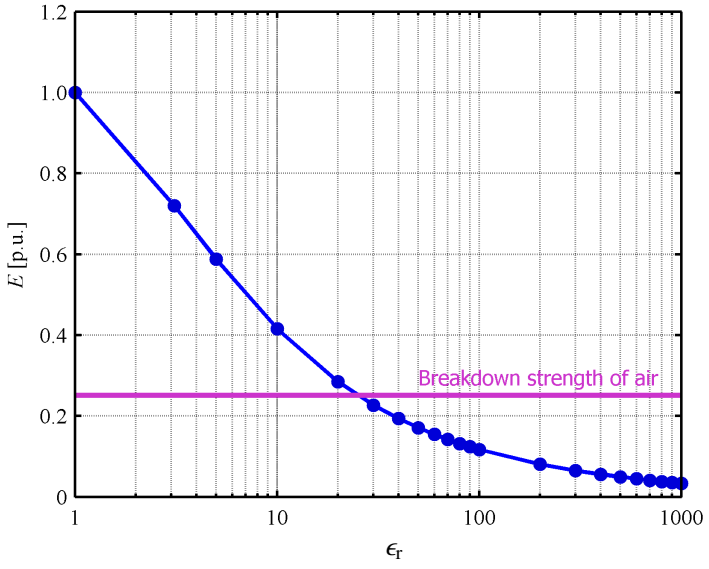

Fig. 4.15. Field strength as a function of permittivity of the termination layer. Permittivity of 1 refers to air, i.e. to the model with no termination.

respectively. Materials with a relative permittivity of more than 5 are considered here fictitious. Some of them (e.g. $\epsilon_r = 20$ and $\epsilon_r = 40$) are available for cable industry and electricity distribution purposes, but their use in electrical machine windings is not considered possible. The materials cannot be processed into thin and strong tape-like forms, which is required for electrical machine windings. The upper limit ($\epsilon_r = 1000$) of values matches that of barium titanate ($BaTiO_3$) ceramic, which is used in memory circuits in electronics.

It can be seen in Fig. 4.15 that the field strength curve crosses the breakdown strength of air at approximately $\epsilon_r = 25$. The claim by Rivenc and Lebey (1999) that the termination layer with a permittivity of 10 or less is not capable of adequate improvement in stress grading, is justified. Roberts (1995), advised the permittivity to be 30 or higher, which also seems reasonable. On a general level, from Fig. 4.15 it can be concluded that the stress grading with a termination layer is not applicable in the electrical machine windings, especially if harsh environments are present. The only materials that may be considered for termination are mainwall insulation ($\epsilon_r = 5$) and glass fiber impregnated with epoxy resin ($\epsilon_r = 3.1$). With a termination layer made of mainwall insulation, the field strength is reduced by more than 40%, but it is still above the breakdown strength of air.

Capacitive stress grading with a stress cone

The illustration of the behavior of a stress cone is presented in Fig. 4.16. The heights and angles are chosen so that they are possible to construct; obviously, this depends essentially

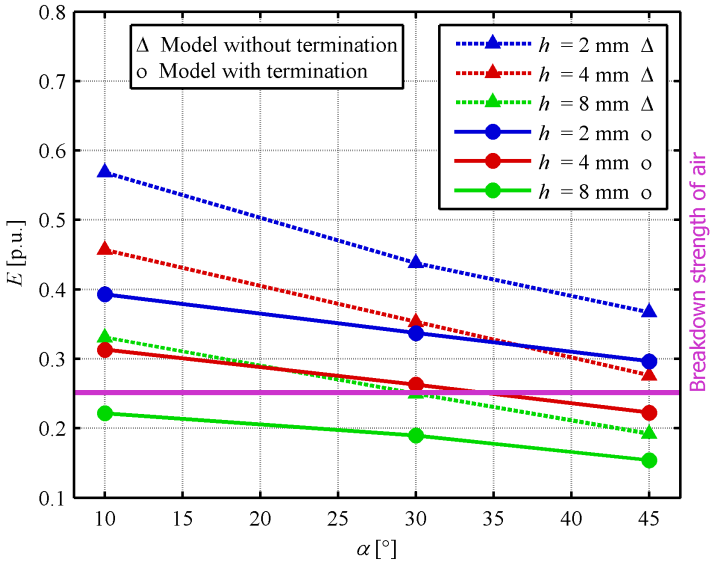

Fig. 4.16. Electrical field strength as a function of angle of the cone for various cone heights both with and without a termination layer.

on the electrical machine size and design. It is assumed that the space between the adjacent coils is 20 mm, half of which can be occupied by a single coil. Such a value may be too optimistic, but sometimes it may be desirable that the fundamental machine design takes special requirements into account.

It can be seen in Fig. 4.16 that the stress grading performance of the cone is better when its height is increased. This is rather obvious, because adding the height of the cone increases the insulation thickness. In addition, increasing the angle has a similar effect, because the end of the conductive layer is closer to the end plate and further away from the coil. Thus, the electric flux lines bend more smoothly. It can also be seen in Fig. 4.16 that adding a termination layer made of mainwall insulation on top of the cone provides additional stress grading performance, but its effect is not as significant as without the cone, Fig. 4.15. The stress cone, especially if reinforced with a termination layer, can provide efficient stress grading capability. However, such a method is not easy to implement in electrical machines.

Capacitive stress grading with a rounded conductive layer end

By installing a ring at the end of the conductive layer, notable reduction in the field strength can be achieved, as can be seen in Fig. 4.17. With the termination and 0.5 mm radius, the field strength can be reduced by over 70%, but it is still slightly above the breakdown strength of air. Such a method has not been used in practice and it may not even be feasible. Modifying the geometry is not a potential way to reduce the field strength in electrical machines. The space requirements are too strict for such methods.

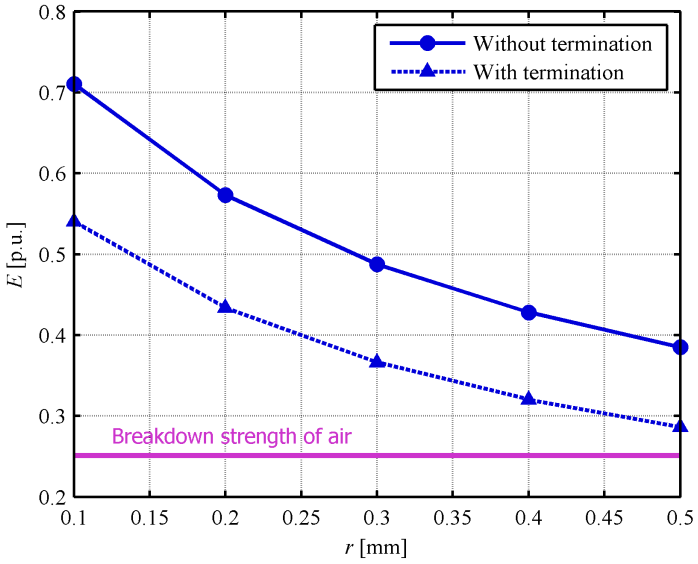

Fig. 4.17. Electrical field strength as a function of rounded end radius with and without termination.

Capacitive stress grading with conductive foils inside the mainwall insulation

The effect of the number of foils inside the mainwall insulation is illustrated in Fig. 4.18 and the effect of foil placement in Fig. 4.19. It can be seen in Fig. 4.18 that the foils can reduce the field strength by approximately 20%, if their number is three or more. Even though stated long time ago, the instruction by Laffoon and Calvert (1935) that the maximum number of foils is three, seems reasonable also from the performance point of view. According to Fig. 4.18, the field strength decreases by approximately 40%, if the termination with the mainwall insulation is used.

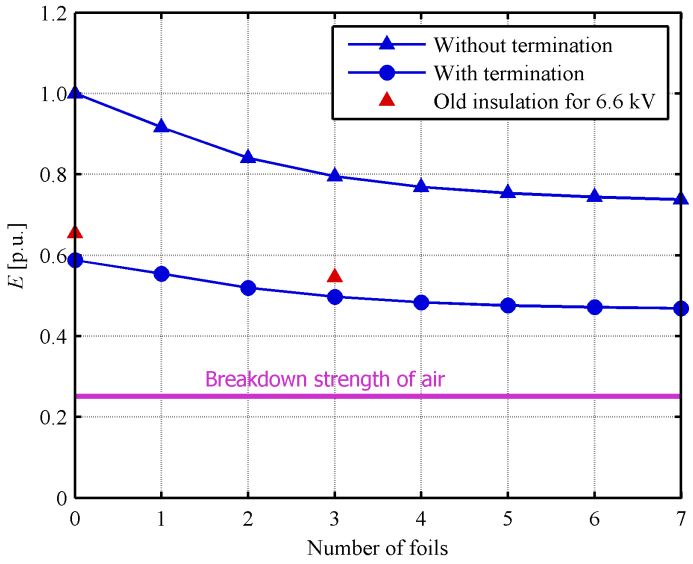

Fig. 4.18. Electrical field strength as a function of number of foils with and without termination.

The performance of this stress grading method depends on the positions of the foils, as can be seen in Fig. 4.19. The foils should be positioned close to the surface and also close to each other. The best performance is reached with foils so close to each other and to the surface that the construction is impossible to build. On the other hand, if the foils are placed more favorably from the manufacturing point of view, the field strength is actually increased. Therefore, the practical limitations in the use of foils are imminent, which was also mentioned by Roberts (1995). The foils do not provide significant reduction in field strength. Their use inside a modern mainwall insulation is not beneficial, because the insulation is so thin. The foils do not bring significant improvement in the old insulation either. Yet, they may have been considered as improvements in the early days, since there were not many alternatives available.

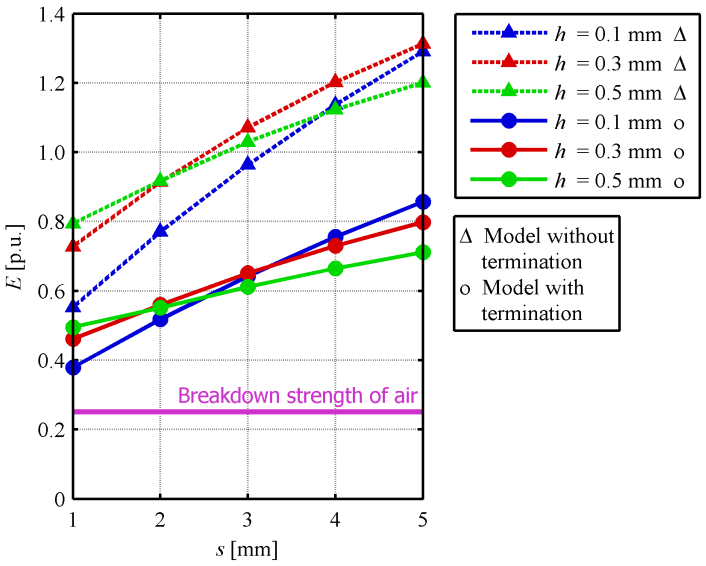

Fig. 4.19. Field strength depending on the placement of foils.

Resistive stress grading with high-resistance materials

The effect of the constant resistivity of stress grading layer on the field strength is illustrated in Fig. 4.20. It can be seen in the figure that the field strength is below the breakdown field strength of air, when the resistivity of the stress grading layer is between 0.015 – 4 MΩm. The low resistivity of stress grading layer causes a low field strength at the end of the conductive layer, but the field strength is very high at the end of the stress grading layer. Low resistivity does not reduce the potential and it just transfers the problematic spot to the end of the stress grading layer. From that point of view, it would be wise not to terminate the conductive layer at all, but to cover the whole end-winding with it. Such an insulation system would not have the problematic sharp edge. However, practice has shown that such an insulation system is not reliable and that the conductive layer should be terminated somehow (Stone et al., 2004). One of the reasons for poor reliability is the connection wires, which would also have to be covered with a conductive layer. Furthermore, there will inevitably be a sharp corner where a connection wire is extracted from the coil. In addition, the quality of the insulation is usually poorer in the end-winding region than in the slot portion of the coils. This is because of the manufacturing process, which includes bending of the coils and applying the mainwall insulation tape over the bent sections leading to flaws in the mainwall insulation as the tape gets tangled.

On the other hand, if the resistivity of the stress grading layer is very high, above 10 MΩm, the stress grading material begins to act like an insulation, and the stress grading method turns into a capacitive one. Above such a value, the resistivity is no more affecting and the performance of stress grading, which is already poor at this point, is dependent on its permittivity. The critical value of resistivity calculated from Eq. (4.8) with parameters given

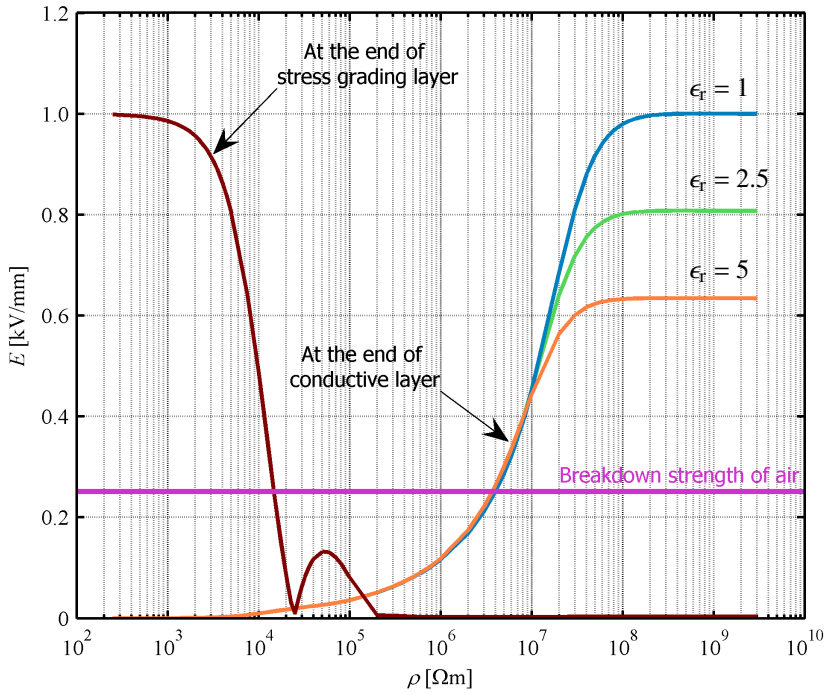

Fig. 4.20. Electrical field strength as a function of the resistivity of the stress grading layer at the ends of conductive and stress grading layers.

in Fig. 4.11 was 70 MΩm. The knee-points of the three curves recorded at the end of the conductive layer in Fig. 4.20 seem to lie in the vicinity of this critical value. Rivenc and Lebey (1999) claimed that the resistivity value 10 MΩm is too high and does not provide sufficient stress grading performance. They further instructed that the proper resistivity of the stress grading layer is approximately 0.1 MΩm. Based on Fig. 4.20, their both claims are justified. Materials to provide such resistivity exist, but their chemical resistance is poor, because they are constructed based on polyester materials. Thus, they are not suitable for harsh environments.

It is noteworthy in Fig. 4.20 that there is a hill in the field strength at the end of the stress grading layer between approximately 0.025 – 0.2 MΩm. This is related to the length of the stress grading layer. All the calculations were carried out using the same model, Fig. 4.12e, in which the length of the stress grading layer was 40 mm. The potential along the stress grading layer is illustrated in Fig. 4.21. It can be seen that there is an overshoot in potential before the steady value is reached. If the stress grading layer ends during the overshoot, there is a sudden voltage gradient and an unexpectedly high electrical field. This causes the hill in Fig. 4.20 with certain resistivity values.

The unexpectedly high field strength can be avoided by determining the length of the stress

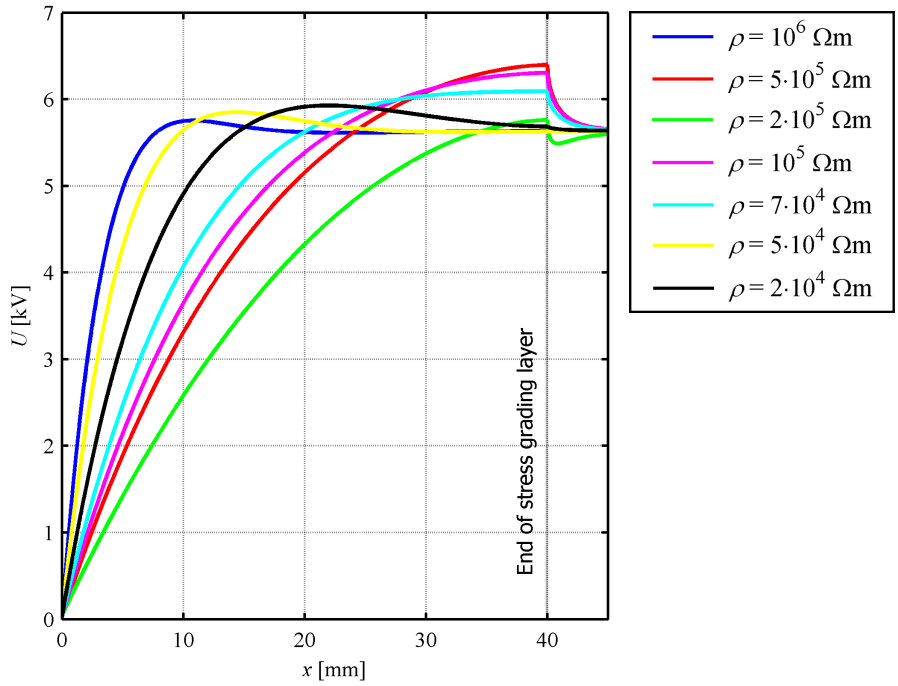

Fig. 4.21. Potential along the stress grading layer with different resistivities of the stress grading layer.

grading layer more carefully. In this study, the length of the stress grading layer was maximized with respect to the number of elements in the FEM model, and further, to the memory capability of the computer. Yet, the length was chosen wrongly, because the model gave erroneous results for the exact range of resistivity values, which are recommended for the implementation of the method. This was an unfortunate coincidence. However, in electrical motors it is easy to apply the stress grading layer, which is longer than 40 mm. Therefore, the hill in Fig. 4.20 occurs as such only in the theoretical study.

Resistive stress grading with nonlinear materials

The silicon carbide stress grading is illustrated in Fig. 4.22. The model is not optimized, which can be observed with the resistivity in Fig. 4.22. Yet, the field strength is everywhere beneath the breakdown strength of air. Consequently, the model was not optimized any further.

Rivenc and Lebey (1999) claimed that the performance of SiC stress grading is not dependent upon its nonlinear behavior, but because the level of resistivity is simply desirable. Based on the observation from Fig. 4.20 and Fig. 4.22 their claim seems justified. The highest field values, that is, the largest changes in potential, take place when the resistivity is in the same region than was recommended earlier for constant resistivity. However, the SiC

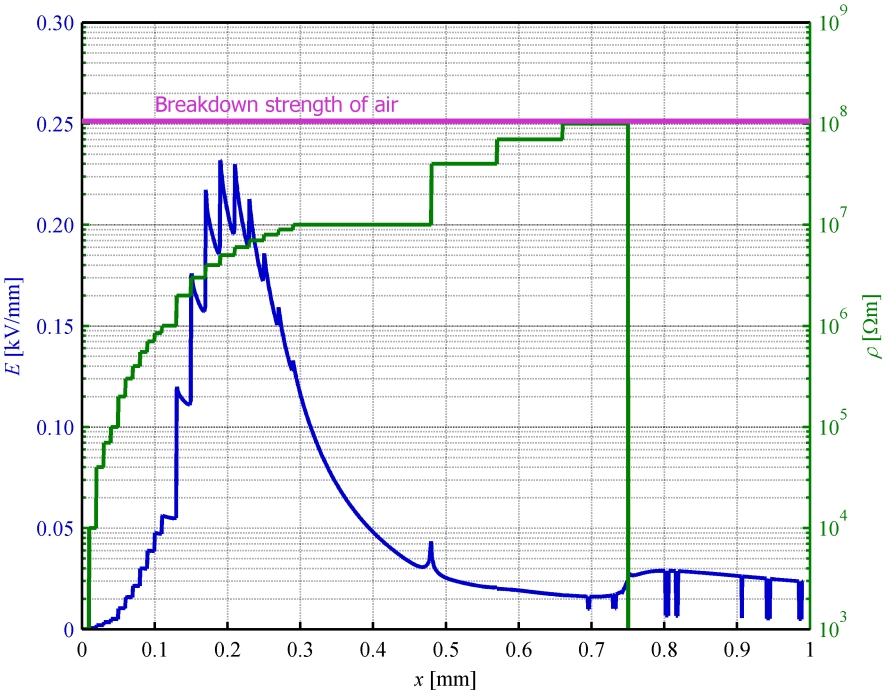

Fig. 4.22. Field strength as a function of distance along the silicon carbide stress grading. The resistivity of the material is also shown.

model implemented in this study may not be realistic. Nevertheless, adequate performance of the stress grading can be achieved with materials of constant resistivity and the nonlinear dependence is not necessary. Furthermore, materials providing nonlinear stress grading do not tolerate harsh environments.

4.3.5 Summary and discussion

The summary is presented in Fig. 4.23. It is possible to decrease the field strength value below the breakdown strength of air with three ways: resistive stress grading with a material of constant $\rho = 0.1$ MΩm, resistive stress grading with a nonlinear material (e.g. silicon carbide), and capacitive stress grading with a very high-permittivity material, $\epsilon_r > 25$. The last method cannot be applied to electrical machine windings.

Based on the theoretical study, resistive stress grading methods are more suitable for electrical machines than capacitive methods. It is therefore not surprising that electrical machines apply resistive methods, whereas cable industry may take capacitive ones into consideration. The resistive methods provide better performance without any considerations on the fundamental machine design. Termination with very high-permittivity materials can in theory provide

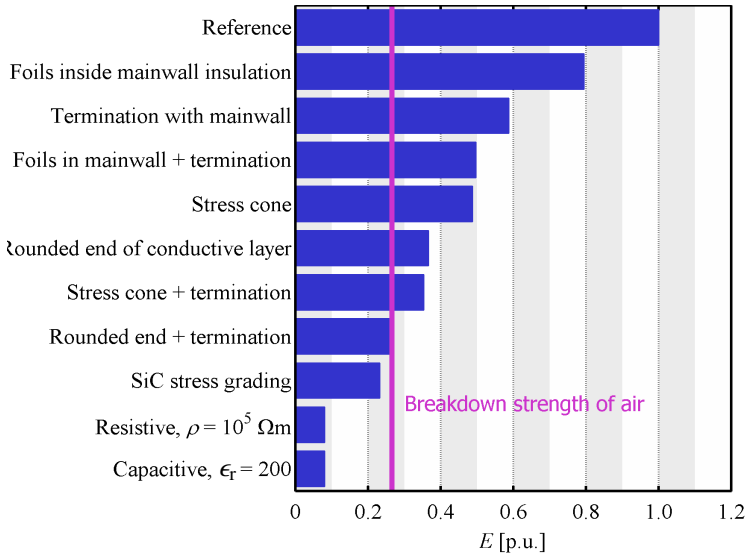

Fig. 4.23. Comparison of different stress grading methods. Field strength values are per unit values. The base value is the reference case, without any stress grading implemented.

equal stress grading performance, but such materials cannot be applied to electrical machine windings.

Capacitive stress grading with geometrical modifications, for instance a stress cone and a rounded conductive layer end, provide rather promising stress grading performance. However, they are difficult to apply to the winding, and the space between adjacent coils limits their performance. For true utilization of such methods, more space would have to be arranged between adjacent coils. The methods themselves can basically be applied with same materials as the insulation system, but their manufacturing is difficult. If there are two or more coils in one slot, which means that there are coils almost right next to each other in the slot exit region, it is virtually impossible to use any methods that notably increase the size of the insulation.

Terminating the conductive layer with a mainwall insulation can reduce the field strength by approximately 40%. The method can be applied with only little extra work and no additional materials. The reduction in field strength is distinctive with such a little effort. The performance of other capacitive methods is also significantly improved with an additional termination layer consisting of the mainwall insulation.

Different stress grading methods have been compared by measuring only a single value of electrical field strength, located at 40 µm away from the conductive layer. Based on this very value, it is not possible to determine whether there will or will not occur partial discharges. Partial discharge measurements presented in the previous section have, however, implied that this distance is relevant and high field strengths within that distance do not count.

According to Eq. (4.1), the field strength of the reference model would be lower than the breakdown strength of nitrogen at 5.10 bar. Based on measurements on partial discharges, this pressure was estimated to be in the region of 4 – 5 bar. Corresponding pressure for wet methane environment is 8.64 bar according to Eq. (4.4). The pressure limit of the model with termination with the mainwall insulation in nitrogen gas is 2.78 bar and in wet methane 4.86 bar.

Based on the measurements on breakdown strengths of gases and partial discharges presented in the previous sections and results shown here, it seems highly beneficial to pressurize the casing of an electrical machine. This has been proposed earlier by Terase et al. (1981), but they considered the cooling gas to be hydrogen. The insulation system would gain more efficiency and the choice of materials would be more flexible. With a 6.6 kV line-to-line voltage, the pressure of 3 bar is sufficient to prevent the partial discharge activity, if the conductive layer is terminated with a mainwall insulation. The thermal conductivity of the cooling air would also increase as a function of pressure, although according to Carroll et al. (1968) the thermal conductivity of air is increased only by 11% with the pressure increase of 100 bar. Therefore, the improvement in cooling capacity is negligible. Naturally, such a method would require plenty of additional equipment and increase the costs. Hence, regarding typical electrical machines, the idea was merely hypothetical.

Regrettably, taking the results and conclusions of Sections 4.1 and 4.2 into account, the validity of the whole study can be questioned. Because of the high pressure in the subsea compressor, even the reference case in Fig. 4.23 will not face problems. However, even though being not directly related to the subsea compressor, the study provides a method to investigate the stress grading and other dielectric systems. It provides information for other high-voltage motor applications for harsh environments, where commercial stress grading materials are not recommended to be used. Furthermore, the study provides a method to analyze the partial discharge risks in electrical motors operating at voltage levels between traditional low-voltage (690 V) and high-voltage (6.6 kV) classes. In the future, this is of interest for two reasons. Firstly, there is a desire to increase the operating voltage in certain types of electrical machines, particularly in wind generators. One of the initiatives towards this is the development of frequency converters capable of operation at higher voltages with the same switching speed and controllability. Secondly, there is a trend to reduce the thickness of the electrical machine mainwall insulation. These two future trends require a new analysis on the insulation system.

4.4 Conclusions

The measurements for breakdown strengths of nitrogen, methane, hydrocarbon gas mixture, and wet methane have been presented. The linear section of the Paschen curve has been defined for the gases. It has been found that the breakdown strength of nitrogen is higher than that of hydrocarbon gases, which all have relatively similar breakdown strength.

The measurements for partial discharges in the insulation have been performed at different

pressures with bar and cable samples. Both samples have been modeled with finite element methods and the model was compared with the measurements. A model was compiled for the FEM analysis of the dielectric system. The measurements indicate that the insulation faces a lot of partial discharges at atmospheric pressure, but the discharge activity is sensitive to pressure and begins to decrease instantly above atmospheric pressure. The insulation system of an electrical machine is not expected to face severe discharge activity, if the pressure is above the region of 4 – 5 bar. The analysis with FEM indicates that the length of a single discharge is 40 μm or more.

More extensive modeling for different methods of stress grading has also been carried out. The resistive methods are the most effective, but they usually require materials that do not tolerate harsh environments. The termination of the conductive layer end with a mainwall insulation tape reduces the field strength in the critical area by 40%.

The subsea compressor operates at pressure levels significantly higher than the region of 4 – 5 bar, where the discharges disappeared in the measurements. Therefore, the subsea compressor is not vulnerable to aging caused by partial discharges or surface tracking. Furthermore, there is no need to find alternative materials or methods to implement the stress grading in the end-winding region. The field does not need to be graded, if the pressure is above 4 bar. This is beneficial from the viewpoint of the subsea compressor manufacturer, because there is no method available for stress grading that tolerates the environment.

Chapter 5

Aging of insulating materials

The chapter presents the results obtained from different tests. The test matrix was shown in Fig. 3.2. This chapter refers to thermal, ambient, and mechanical stress factors in the figure. The first two sections primarily focus on comparative studies of different materials. They do not consider in detail the causes of aging. The third section aims to define the effects of different components in the wellstream gas mixture on the aging of insulating materials. The fourth section presents the effect of temperature on the aging. The fifth section discusses the diffusion phenomenon as a function of time. The sixth section focuses on the rapid decompression test.

The results obtained from the tests are presented in Sections 5.1 – 5.6. The discussion of the results in these sections rests on direct conclusions and references to the studies found in the literature. The detailed analysis on the test results and discussion on the physical phenomena are presented in Section 5.7. This section discusses all the results and its purpose is to create the main picture on the aging of insulating materials under hydrocarbon gas environment. The section also discusses the validity of the test matrix used.

5.1 Screening of epoxy resins

The test was carried out to compare different epoxy resins. Based on earlier studies with water, polyester and polyesterimide resins were not expected to be competitive (Sihvo et al., 2008). Thus, they were omitted. The materials used in the experimental test program are listed in Table 5.1. The test utilized wellstream gas mixture at 130 °C and 150 bar described in Section 3.5. The duration was 750 hours.

It has to be emphasized that the test procedure differed slightly from the other tests. Here, the samples were dried in an oven after the test. Some of the moisture they had absorbed was

thus removed. However, it was found out that the influence of drying was not very significant, because the hydrocarbon compounds are not removed that way. The depressurization of the chamber took place more rapidly than in other experiments. For these reasons, weight and volume increases during this very test have been smaller than during other experiments. The depressurization tends to remove the liquids that the material has absorbed from the material. This is seen as a reduction in weight, because the liquids are removed, but also as a reduction in volume, because the swelling effect is reversed. This is discussed in Section 5.7. For the analysis of the test environment (Section 5.3) and for screening of the mainwall insulation (Chapter 5.2) the test was repeated. However, the comparison of different materials is still valid, as they were all present in the very same exposure. The reader is advised not to compare the results presented in this chapter with the results of the following chapters.

Table 5.1. Materials used in the impregnating resin screening test. Curing times are approximations. They were not recorded. The first curing step with anhydride resins was final when the resin had turned into solid. This time was dependent on the amount of accelerator used. The unit pbw refers to parts by weight, not percentage. The resin mixtures based on bisphenol A included 100 pbw of epoxy component and 90 pbw of curing agent. The accelerator was portioned out accordingly.

Material	Description	Amount of accelerator [pbw]	Curing time and temperature
A	Epoxy novolac resin	single component	12 h at 165 °C
B	Bisphenol F epoxy resin	single component	12 h at 165 °C
C	Bisphenol A epoxy resin + BCl_3 + amine	0.2	12 h at 90 °C + 16 h at 140 °C
D2	Bisphenol A epoxy resin + BCl_3	0.2	12 h at 90 °C + 16 h at 140 °C
D4	”	0.4	11 h at 90 °C + 16 h at 140 °C
D6	”	0.6	10 h at 90 °C + 16 h at 140 °C
D8	”	0.8	9 h at 90 °C + 16 h at 140 °C
E	Bisphenol A epoxy resin + zinc naphthenate	12.1	12 h at 150 °C

5.1.1 Results

Relative weight and volume increases are illustrated in Fig. 5.1 for all materials investigated. The E-moduli before and after the exposure for each resin are illustrated in Fig. 5.2 and the relative changes in the tensile strength and the E-modulus are shown in Fig. 5.3.

Significantly higher increases in volume than in weight with materials B and E suggest that a large amount of molecules from the wellstream gas environment have penetrated into the specimens. When the test is stopped, the gas inside the specimens partly liquefies as the temperature is reduced from 130 °C to room temperature. This is seen as a weight increase.

It can be seen in Fig. 5.2 that materials D2, D4, D6, and D8 all have virtually identical E-modulus before and after the test. The amount of accelerator has no effect on it. However, it has some effect on the tensile strength as can be observed in Fig. 5.3. The amount of accelerator recommended by the manufacturer for material D is 0.4 pbw. The manufacturer

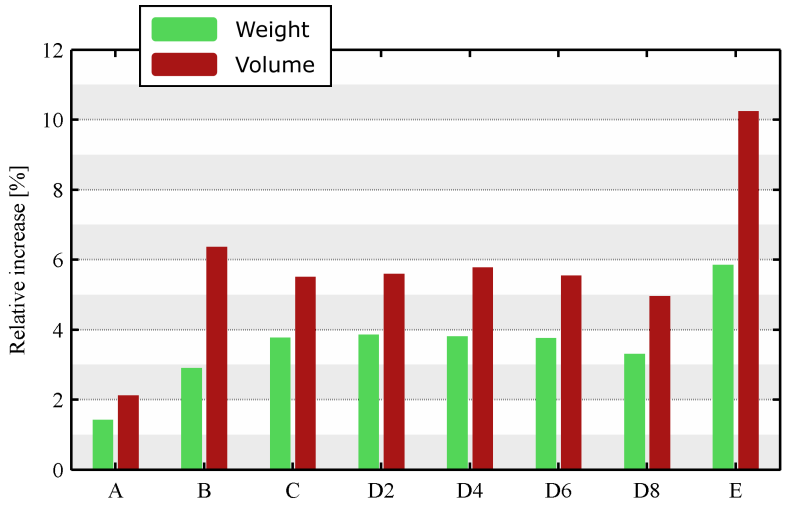

Fig. 5.1. Weight and volume increases during the exposure.

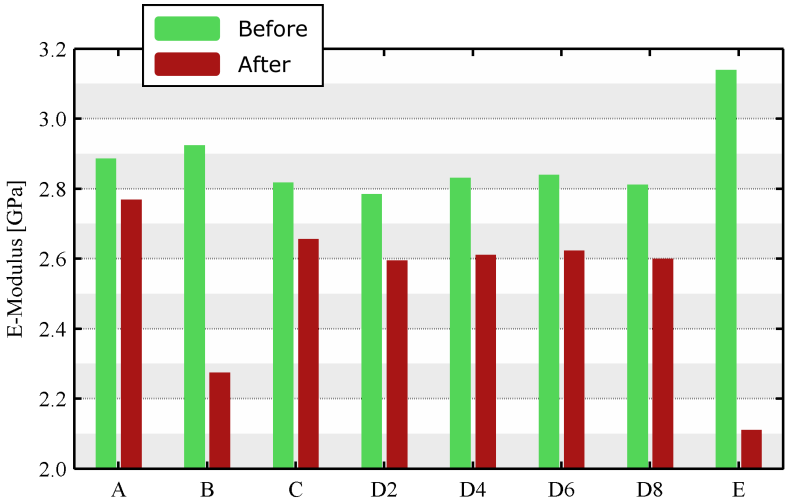

Fig. 5.2. E-Modulus before and after the test.

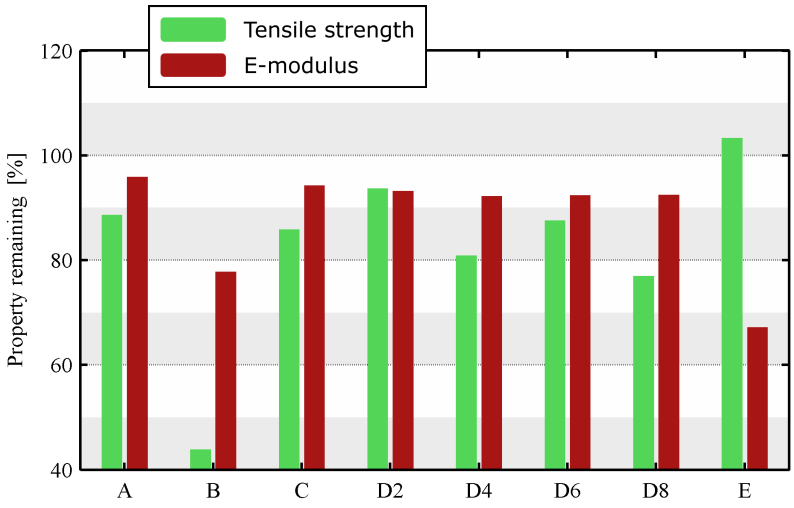

Fig. 5.3. Tensile strength and E-Modulus remaining after the exposure. The value of 100% refers to the reference sample for each material individually.

also instructed that in a harsh environment the amount should be increased in order to gain better chemical resistance. The study shows that this instruction cannot be fully justified for the wellstream gas environment applied in the experimental program. By contrast, the tensile strength is best retained, if the amount of accelerator is reduced to 0.2 pbw.

The relevance of the tensile strength values can be argued. The epoxy resin samples were all very brittle, especially material A. They broke down well below the ultimate tensile strength, which is the highest strength possible to achieve (see Fig. 3.14). The premature breaking point gives false information on strength, strain, and toughness. Breakdown has been due to small cracks near the stressed section and it does not correlate with the true mechanical properties of the material. Even with large sets of samples (up to 30) no single sample could have the tensile strength seen in Fig. 3.14. They all broke down too early. It is therefore not very informative to look at these quantities. Thus, with brittle materials, namely resins, the focus is to be turned to the E-modulus, as it is not affected by premature breakdown. The samples consisting of the whole mainwall insulation, on the other hand, did not generally experience premature breakdown, and their strength, strain, and toughness were valid.

It can be seen in Fig. 5.2 that material E (zinc naphthenate) had the highest E-modulus for non-aged specimens, but during the exposure it reduced more compared with the materials A – D. The material had become softer, but its tensile strength did not decrease. This conflict is due to the brittleness of the materials. The stress versus strain curve of the aged sample extended closer to the ultimate tensile strength before the sample broke down.

Correspondingly, bisphenol F epoxy resin (material B) is not capable to hold its properties very well. Bisphenol F resin after the exposure is illustrated in Fig. 5.4. It has obviously formed some kind of a crystal structure. Moreover, the samples of material B included large

blisters indicating that gas had penetrated into the resin. No such blisters were found in other materials.

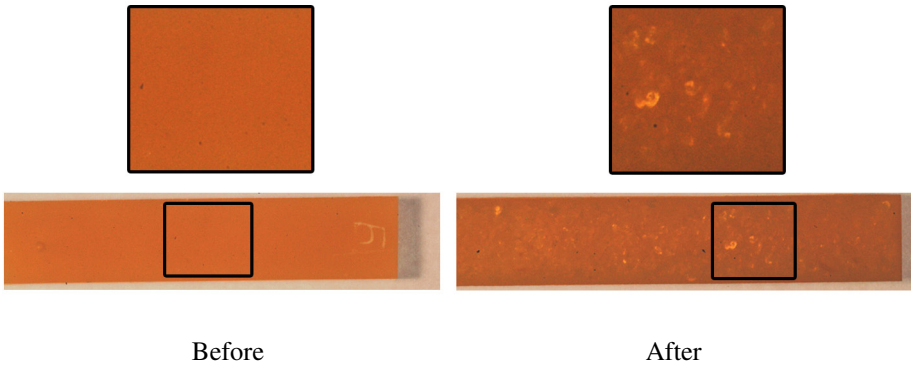

Fig. 5.4. Material B before and after the exposure. Crystals are visible in the aged sample. Furthermore, the aged sample included blisters, but they are not visible in the figure.

Glass transition temperatures of samples before and after the exposure are illustrated in Fig. 5.5. The glass transition temperature of material E was not measured. It is noteworthy in Fig. 5.5 that the glass transition temperature drops under the temperature of the aging test conditions for every material except D4. However, no significant improvement in the performance of material D4 compared with the others can be observed in Figs. 5.2 and 5.3. The glass transition temperature does not correlate with the E-modulus after chemical aging in the wellstream gas. It is also observed in Fig. 5.5 that material B has a glass transition temperature of 40% less compared with the other materials investigated. Furthermore, material B was the only material that had visible voids inside the epoxy after aging (Fig. 5.4). Based on this

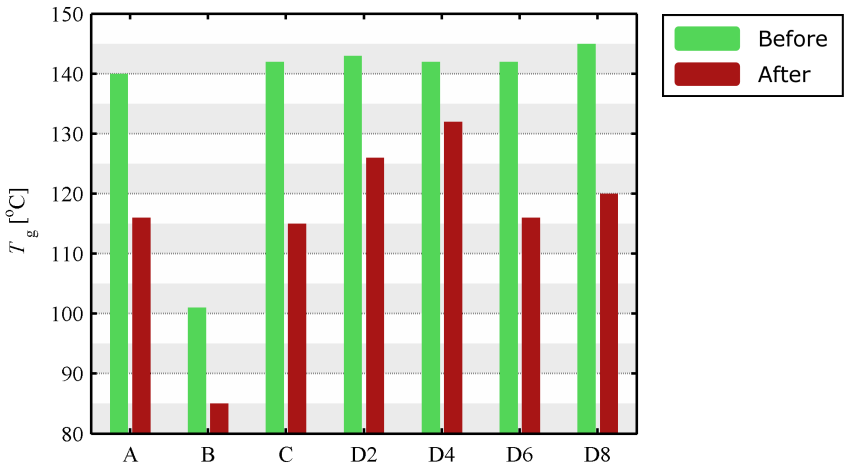

Fig. 5.5. Glass transition temperatures before and after the exposure. Material E is not included.

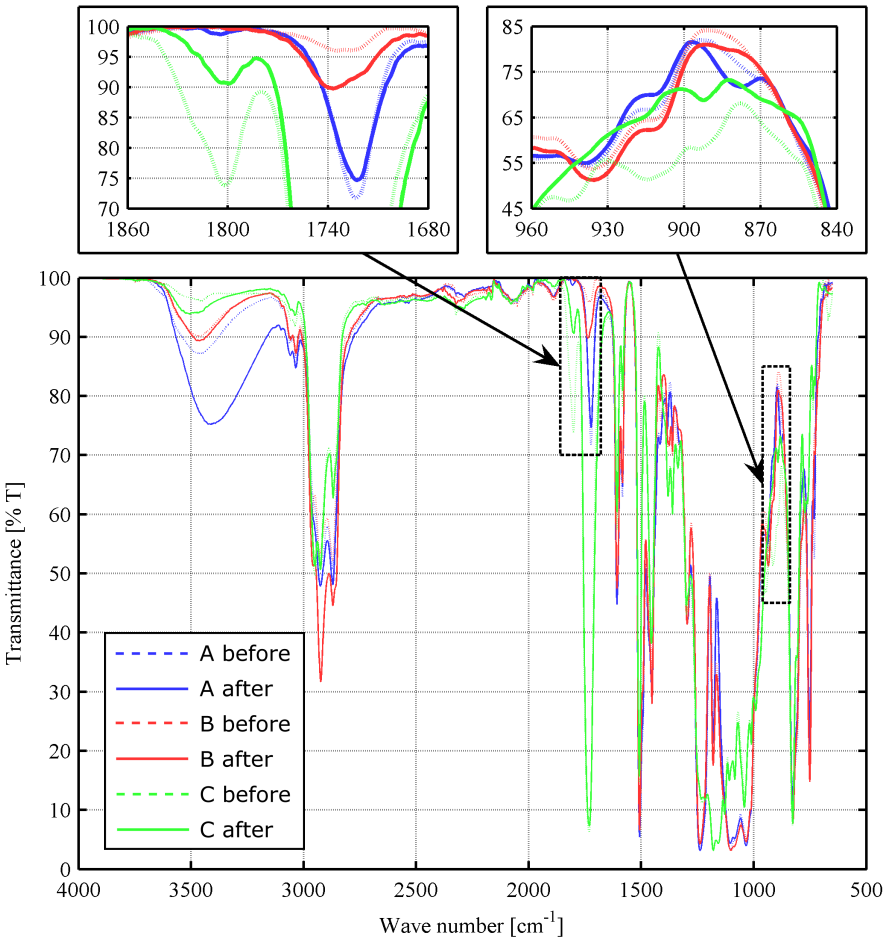

Fig. 5.6. Infrared spectra of materials A, B, and C before and after the exposure.

observation, it is indicated that the high-pressure wellstream gas is able to penetrate into the material to a larger extent as the material is exposed above its glass transition temperature.

Infrared spectra of materials A, B and C are illustrated in Fig. 5.6 and of materials D2, D4, D6, D8 and E in Fig. 5.7. A significant difference in the IR spectra can be observed in the region between 3700 and 3000 cm^{-1}. This is due to water inside the materials and has been reported by many researchers (Wu and Siesler, 2003; Fernández-García and Chiang, 2002; Liu et al., 2002; Musto et al., 2000).

The resin A does not suffer from changes in its chemical structure, as can be observed in Fig. 5.6. However, the change caused by water is larger in that material than with other materials, but such differences do not reflect chemical changes, because the water is only occupying the free volume. It can be observed in Fig. 5.6 that the peak of material C at 1801 cm^{-1} is

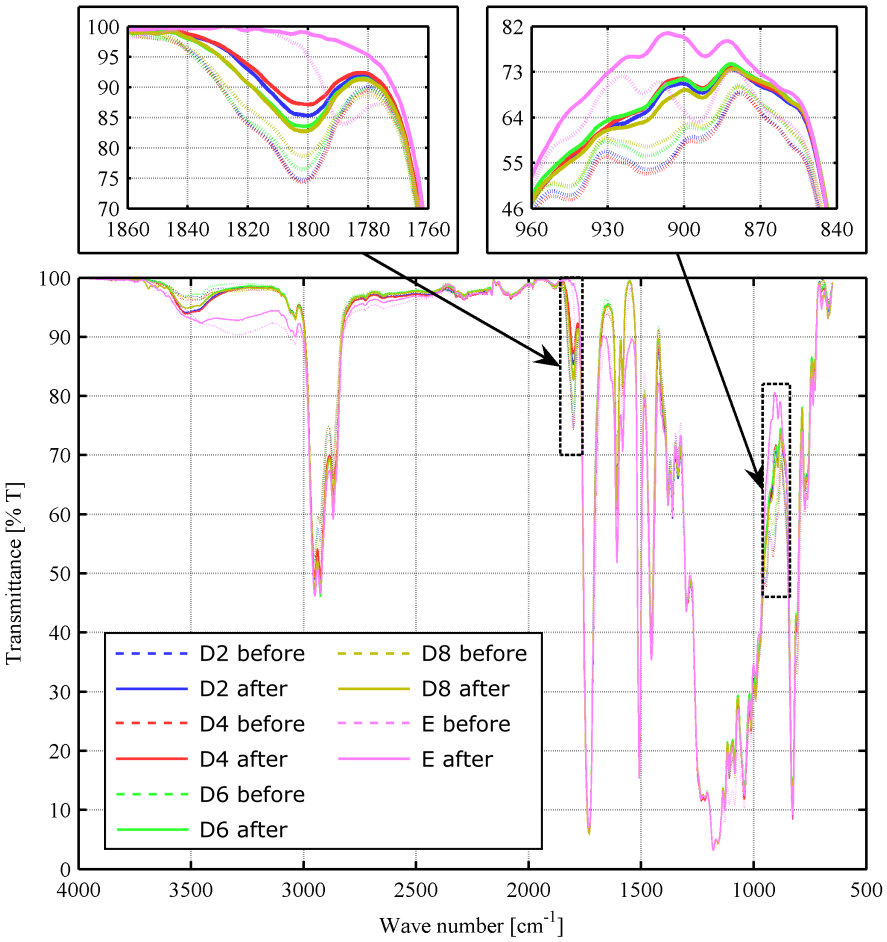

Fig. 5.7. Infrared spectra of materials D2, D4, D6, D8, and E before and after the exposure.

reduced during the exposure. Furthermore, material C experiences some changes within the range of 960 – 840 cm^{-1}. Both changes are of similar magnitude and refer to bonds that have disappeared or weakened during the exposure. The causes for anomalies are related to the basic functional groups (anhydride and epoxide) of the materials. Nevertheless, they are not discussed here any further, but the discussion is presented in Section 5.7. The same changes can also be observed with materials D2, D4, D6, and D8 in Fig. 5.7. This is not a surprise, since both resins are basically the same; they only have different accelerators.

However, it is interesting in Fig. 5.7 that the changes are of smallest magnitude with material D8, that is, with the material containing the largest amount of accelerator. Therefore, the results point to the suggestion given by the resin manufacturer that an increased amount of accelerator improves the chemical resistance. The material is more resistant to chemical changes that degrade it, but this was not supported by the mechanical properties, Figs. 5.3

and 5.2. It has to be emphasized that the changes observed are very small.

5.1.2 Summary and general discussion

Based on the experiment it is concluded that the epoxy novolac resin can hold its properties quite well. The wellstream gas obviously has some influence on it, but it is not critical. Similar performance can be achieved also with bisphenol A resin. By contrast, the study indicates that bisphenol F epoxy resin cannot tolerate the environment. Raw natural gas causes crystal structure to form and the mechanical properties are reduced significantly. One of the reasons for severe reduction in mechanical properties is that the material was exposed to a temperature higher than its glass transition temperature T_g. As such, this is not dangerous, because the thermal rating of material B, similarly as of all other materials, was well above its T_g. However, above T_g the wellstream gas is able to penetrate into the material more easily, because the material is flexible allowing the gas to reorganize its molecular structure.

The performance of bisphenol A epoxy resin is highly affected by its accelerator. Bisphenol A resin with zinc naphthenate accelerator is not able to hold its properties and it absorbs more gas mixture than other materials. The material also gets mechanically soft. The softening can be seen with other materials also, but not so significantly. Therefore, it is not considered as a competitive solution for a wellstream gas environment.

A resin with boron trichloride (BCl_3) accelerator is able to have chemical resistance fairly equal to that of epoxy novolac resins. The amount of BCl_3 accelerator was not seen to affect the E-modulus, but the infrared spectra indicated that the changes in the chemical structure reduced when the amount of BCl_3 accelerator was increased. However, the changes caused by the amount of BCl_3 accelerator were minor.

The test indicated a significant difference between the behavior of epoxy novolac resin and Bisphenol A epoxy resin, but the significance is related to the natural properties of the materials. Epoxy novolac resin is hard and brittle; it had a high E-modulus, but the material broke down well below its ultimate tensile strength. During the exposure to wellstream gas it absorbed only little gas and maintained its mechanical properties well. Bisphenol A epoxy resin, on the other hand, was of more flexible nature. During exposure to wellstream gas it expanded and gained more weight than the epoxy novolac resin.

Hence, the resins have notably different properties, but it is still difficult to say which performs better in the electrical machine. Therefore, both resins (materials A and C) are used in the more detailed investigations presented in the forthcoming sections.

The importance of experimental testing for environments such as the wellstream gas is imminent. Several large vendors of high-voltage electrical machine windings suggested to use material E in the insulation system. Obviously, they were wrong, but they all did emphasize that an extensive experimental test program was required to be sure of the suitability of the material.

5.2 Screening of mica tapes

The test was carried out to compare different mica tape structures on which the mainwall insulation is based. The tape structures used in the experimental test program are listed in Table 5.2. The tapes K, N, G1, and G2 are impregnated with bisphenol A epoxy resin using the VPI method. The impregnating resin was labeled C in the previous section, and it was also included as such, labeled as ”resin” in the test scheme. Material Z had the same tape structure as material G2 with the exception that the zinc naphthenate accelerator was included in the tape. The tape was impregnated with Bisphenol A epoxy resin without any accelerator. The insulation corresponds to a mica tape construction G2 impregnated with resin E described in Section 5.1. Tapes G2E and G2P have been manufactured by the insulation vendor. The tapes contain similar glass fabric as material G2, but the tape has been applied with a taping machine, not by hand. Material G2E was impregnated with resin C and material G2P with a polyesterimide resin. Material G2P is the most common insulation solution for a 6.6 kV electrical machine available today.

The test used artificial wellstream gas mixture at 130 °C and 150 bar. The duration was 750 hours. Unlike in the experiment presented in the previous section, the specimens were not dried after the exposures, and the depressurization was carried out at a slower rate leaving more gas trapped inside the materials. Therefore, the weight and volume of resin C are almost twice as high as the ones shown in Fig. 5.1. The resin for both experiments was manufactured in the exact same way. The difference emphasizes the role of the depressurization process after each test.

Table 5.2. Tape structures used in the test.

Label	Backing material	VPI / RR	Impregnating resin
K	Kapton® polyimide	VPI	Epoxy anhydride
N	Nomex® aramid paper	VPI	Epoxy anhydride
G1	Glass fabric	VPI	Epoxy anhydride
G2	Glass fabric	VPI	Epoxy anhydride
P	PET film	RR	Epoxy novolac
RR1	Glass fabric	RR	Epoxy novolac
RR2	Glass fabric	RR	Epoxy novolac
Z	Glass fabric	VPI	Epoxy anhydride with zinc naphthenate
G2E	Glass fabric	VPI	Epoxy anhydride
G2P	Glass fabric	VPI	Polyesterimide

Mainwall insulation samples from two different impregnation processes were tested: 1) fully impregnated and transparent samples and 2) samples not completely saturated with the resin. The purpose of this comparison is to emphasize the importance of the proper manufacturing procedure on the performance of the mainwall insulation. The level of cure was not measured. The determination of full and imperfect impregnation was carried out based on simple observations. It was seen during the cutting process of the test samples that the impregnation number 2 had not been good. Furthermore, the samples were not fully transparent, as they were with the impregnation 1. The fully saturated samples are transparent, because the resin, glass, and mica are all transparent and there is no air inside the insulation to diffract the light. The diffraction of light is determined by the speed of light in the medium (Young and Freedman, 2000), which in turn is proportional to the square root of the permittivity of the medium. The permittivities of the insulating materials are similar, but the permittivity of air is significantly lower, which causes the diffraction of light in the voids. The impregnation number 1 refers to a succesful impregnation process, even though it (and any industrial VPI process) is not absolutely perfect.

In the previous chapter it was pointed out that the mechanical parameters except E-modulus are not reliable because of the premature breaking points of brittle resins. With mica tapes, this statement is not valid, because the composite structure is not that brittle.

5.2.1 Fully impregnated mainwall insulation

Weight and volume increments during the test are shown in Fig. 5.8. Tensile strength retained during the test is illustrated in Fig. 5.9 and E-modulus and toughness in Fig. 5.10, respectively. In Fig. 5.11 the stress versus strain curves are shown. Materials G2E and

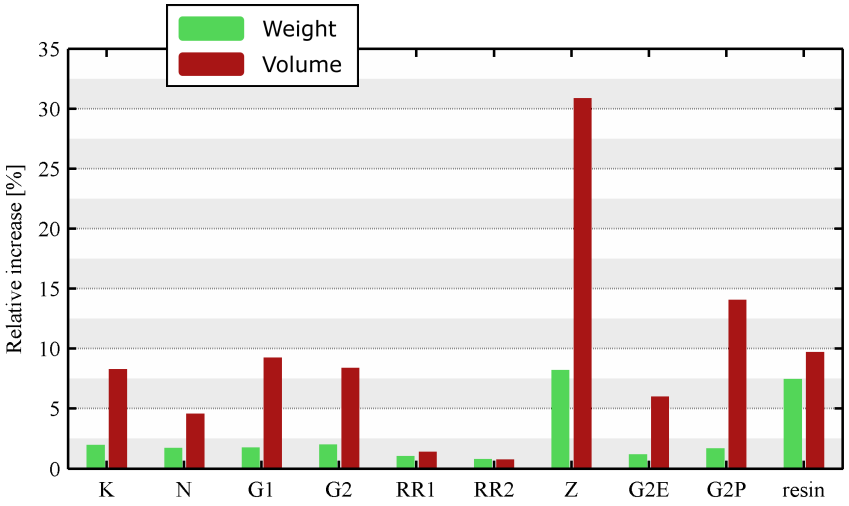

Fig. 5.8. Weight and volume increase of different mica tape samples.

G2P are not included in Fig. 5.11. They cannot be compared with other tapes, because they are manufactured with a different process and possess a higher quality than the hand-made samples.

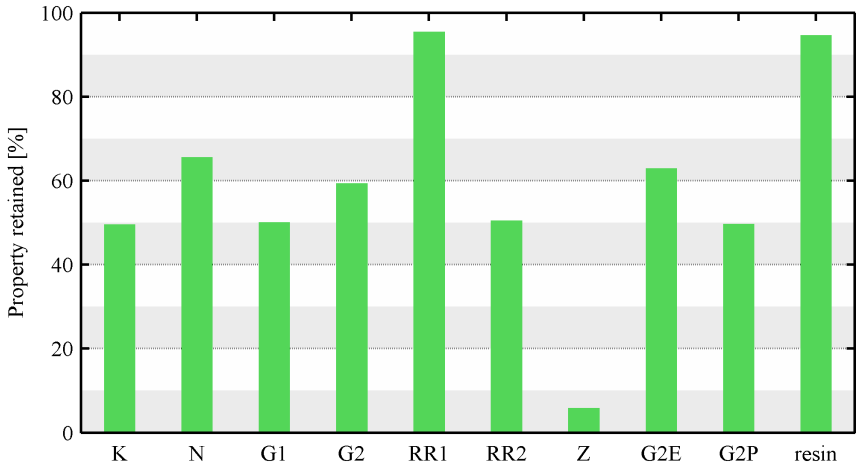

Fig. 5.9. Tensile strength remaining after the exposure to wellstream gas mixture.

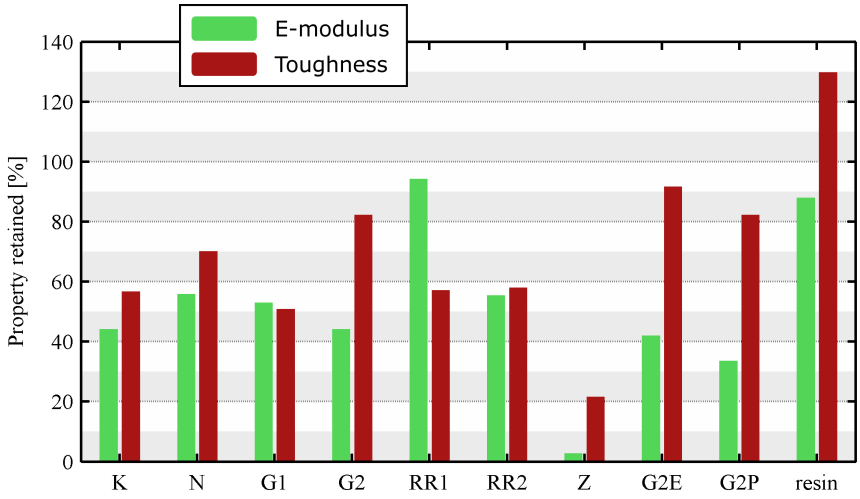

Fig. 5.10. E-modulus and toughness remaining after the exposure to wellstream gas mixture.

It is clear, based on Fig. 5.8, that RR tapes do not expand as much as VPI tapes and the resin, and furthermore, their weights do not increase as much. It is also evident that the insulation with zinc naphthenate (Z) has expanded over three times as much as the others. Furthermore, it has lost its strength and modulus almost completely, which can be seen in Figs. 5.9, 5.10, and 5.11. The insulation has absorbed a lot of liquids and become soft, and it clearly does not withstand the environment. It is also evident in Fig. 5.8 that the volume increase of material G2P has been notably higher than those of other VPI tapes.

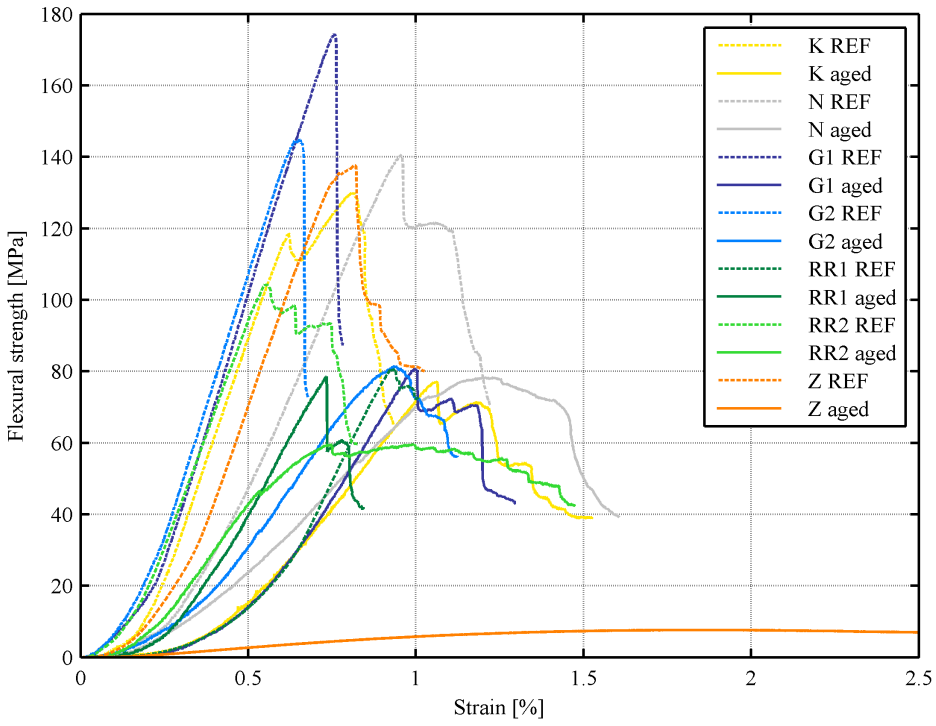

Fig. 5.11. Stress versus strain curves for mica tape samples.

The reference values for tensile strengths of mica tapes can be observed in Fig. 5.11. They differ slightly from the ones reported in (Emery and Smith, 2001) and (Emery and Williams, 2007), but they can be arranged in a similar order: tape with modified glass fabric (G1) is the strongest, Kapton® backing (K) comes next, and traditional woven glass-fabric-backed tape (G2) has the lowest tensile strength. Furthermore, Emery and Smith (2001) reported that the tape with zinc naphthenate is stronger than the Kapton®-backed tape. However, Emery and Smith (2001) and Emery and Williams (2007) used somewhat different manufacturing and testing methods and did not reveal their impregnating resins. Furthermore, they did not apply any aging to the samples and discussed only the reference samples.

The mechanical properties, namely tensile strength, of the reference samples depend somewhat on the tape structure, but as it can be observed in Fig. 5.11, the tensile strength after the test is virtually the same with materials K, N, G1, G2, and RR1. Excluding the last material, all the tapes have been impregnated with the ”resin” in a VPI process. Material Z contains similar glass fabric as material G2. The only difference of these two materials is the accelerator of the resin. As pointed out in the previous section, the resin containing zinc naphthenate does not withstand the environment. Its failure in the wellstream gas has been the reason for the failure of material Z in this experiment. Therefore, it can be stated that the strength after the exposure to wellstream gas environment is mainly provided by the resin and it is almost independent of the tape construction.

Based on the mechanical parameters and increases in weight and volume seen in Figs. 5.8 to 5.10, the RR tapes tolerate the environment better than the VPI tapes. They do not absorb as much gas and, presumably thus, retain their mechanical properties better. However, their mechanical properties have been initially lower. After the test, they have rather similar mechanical behavior as the VPI tapes, as can be seen in Fig. 5.11.

Resin rich tapes contain epoxy novolac resin, the resistance of which to wellstream gas mixture was discussed in the previous section. It was found that the epoxy novolac resin gained less weight and expanded less than the epoxy anhydride resin. Nevertheless, the difference in mechanical properties was marginal. The results presented in the previous section (Figs. 5.1 and 5.3) are therefore convergent with Figs. 5.8 to 5.10, although the epoxy novolac resin inside the RR tapes is not the very same as the material A in Section 5.1. Despite seemingly better performance of the RR tapes, it is not fully justified to favor them over the VPI tapes. All of the VPI tapes, except the one with zinc naphthenate (Z), were still in fair condition after the exposure. The changes in their parameters had not been critical.

The performance of material G2P has been slightly worse than that of the materials impregnated with epoxy resin, except material Z. According to Fig. 5.9, the tensile strength has decreased to half during the test, but accordingly, it has diminished also with materials K, G1, and RR2. But the E-modulus of G2P has dropped down to approximately one third, which is roughly 10% less than that of other VPI tapes, except material Z. The hyphothesis based on Sihvo et al. (2008) has obviously been too harsh, because the materials do tolerate the wellstream gas. Nevertheless, similar tape impregnated with epoxy resin using a BCl_3 accelerator is able to tolerate the environment better. The observation encourages to use epoxy resin over the common and cost-effective polyesterimide.

Material G2 before and after the test is illustrated in Fig. 5.12. Material P is not included in Figs. 5.8 to 5.10, because it was damaged very badly and no measurements were carried out. Material P was totally delaminated, which can be seen in Fig. 5.13.

It can be seen in Fig. 5.12 that the insulation has lost its transparency almost completely. It is virtually impossible to discern the logo in the right-hand figure, whereas it is clearly visible on the left. The lighting conditions have not been exactly the same, but the conclusion is still undeniable. No distinctive delamination was observed with a microscope on material G2. Transparency was weakened as a result of the diffusion of wellstream gas. The transparency of the samples was used as a sort of a quality indicator in the VPI process. A transparent build as seen on the left in Fig. 5.12 represents good impregnation.

The failure of material P is obvious in Fig. 5.13. The backing material has disappeared from the insulation causing total delamination. The insulation was based on resin rich technology and epoxy novolac resin, which means that neither the manufacturing process nor the impregnating resin has been the reason for its poor performance. PET film clearly reacts with the wellstream gas.

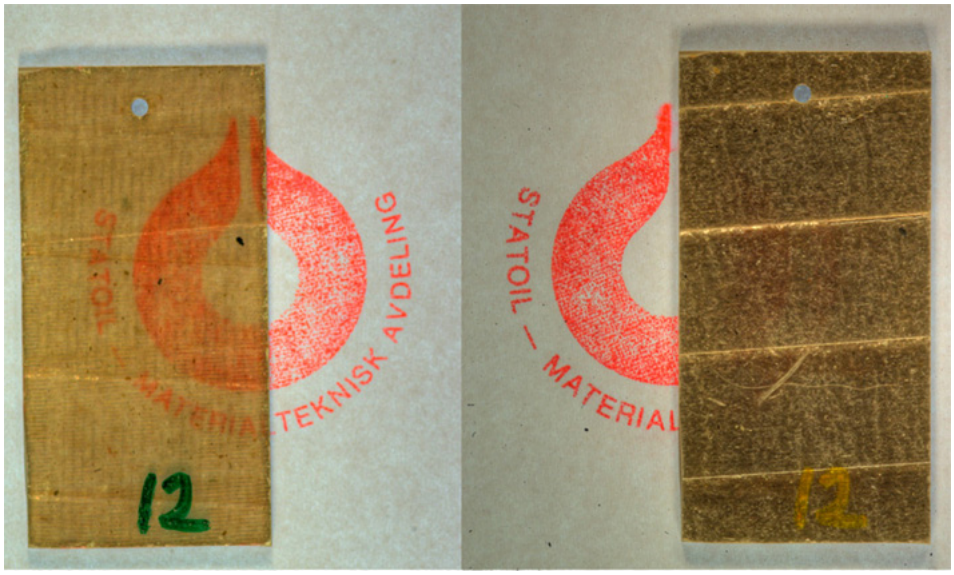

Fig. 5.12. Material G2 before (left) and after (right) the exposure.

Fig. 5.13. Material P after the exposure.

5.2.2 Imperfectly impregnated mainwall insulation

The effect of impregnation process quality on the weight and volume increase is illustrated in Fig. 5.14, on the tensile strength and elongation in Fig. 5.15, and on the E-modulus and toughness in Fig. 5.16, respectively.

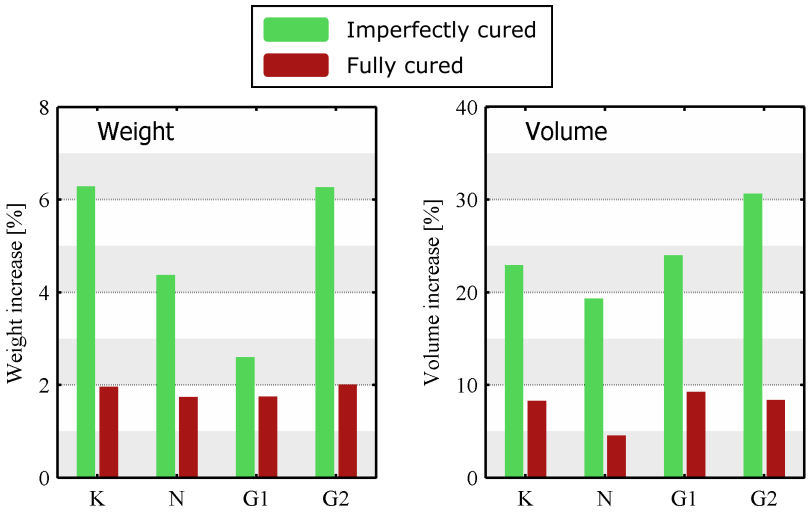

Fig. 5.14. Weight and volume increments in the VPI mica tapes of two different impregnation processes.

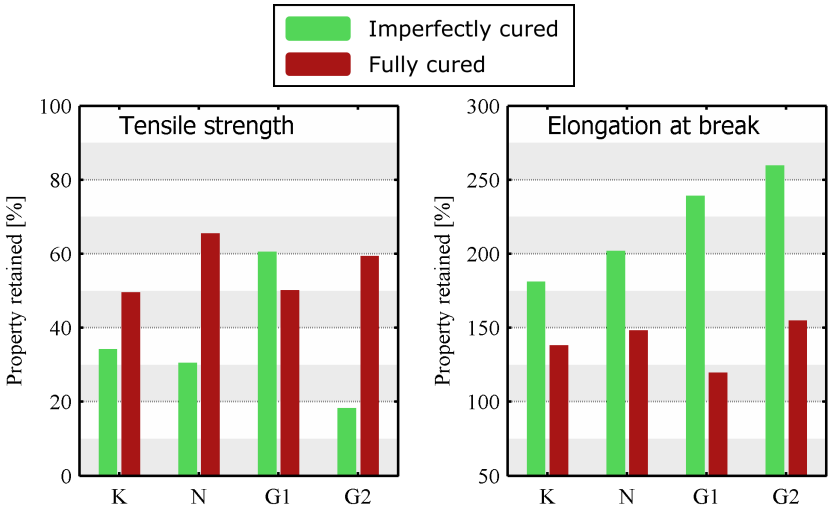

Fig. 5.15. Relative changes in tensile strength and elongation at break for the VPI mica tapes of two different impregnation processes.

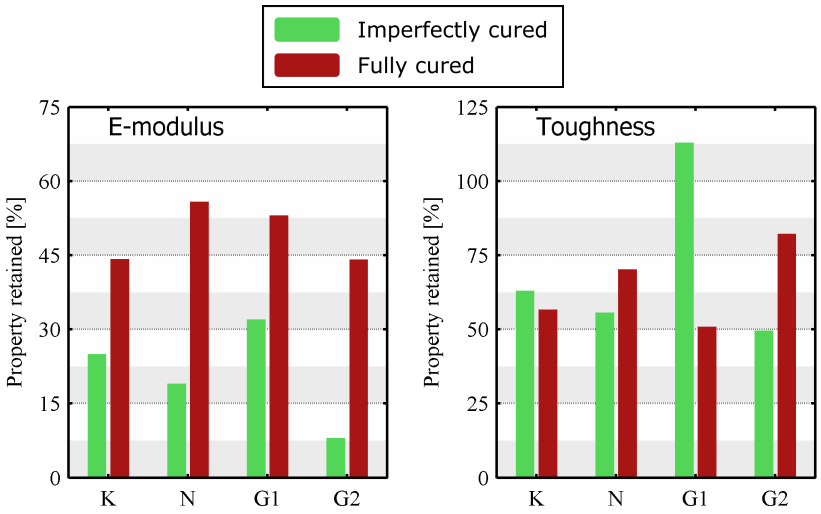

Fig. 5.16. Relative changes in E-modulus and toughness for the VPI mica tapes of two different impregnation processes.

It can be seen in Fig. 5.14 that increases in both weight and volume are significantly higher in imperfectly impregnated samples. Based on Fig. 5.15, fully cured samples generally have a higher strength, while imperfectly impregnated samples are more flexible. The significant decrease in the E-modulus in imperfectly impregnated samples can be observed in Fig. 5.16.

Figures 5.14, 5.15, and 5.16 indicate that the chemical aging has been more severe in the incompletely impregnated insulation systems. Insulation system G2 was impregnated poorly and it had lost its strength almost completely during the test. The mica tape and the VPI resin used in material G2 are able to tolerate the environment, as shown in the previous results (Fig. 5.9). The incomplete VPI process still seemed rather successful when evaluating the mechanical strength of unaged samples. The inadequacy of the VPI process quality has been emphasized in the chemical aging test.

5.2.3 Summary of the results

PET film has been identified to be sensitive to water-saturated hydrocarbon gas. It became partly dissolved at the investigated pressure and temperature of 150 bar and 130 °C. Mica tapes containing zinc naphthenate accelerator absorb much gas mixture, and thus, get mechanically soft. The insulation with zinc naphthenate is not capable of providing sufficient strength after the exposure to the wellstream gas.

Polyesterimide resin was capable of surviving in the environment, but it was not able to hold its properties as well as the corresponding tape impregnated with an epoxy resin. Furthermore, the volume increase in the material was high. The reasons for its poorer performance

were not analyzed in detail.

Glass fabric, Nomex® aramid fiber, and Kapton® polyimide film can provide sufficient resistance to the wellstream gas. If such materials are used in VPI mica tapes, the mechanical properties of the insulation are dependent upon the compatibility of the resin when exposed to a water-saturated hydrocarbon gas environment. The presented results indicate that the resin provides the strength of the insulation after chemical aging has been performed. The tested RR tapes contained epoxy novolac resin and retained their mechanical properties better than the VPI tapes impregnated with epoxy anhydride resin. The mechanical properties of VPI mica tapes in a pressurized water-saturated hydrocarbon gas environment are greatly dependent upon the impregnation process. If such tapes are not fully impregnated, they easily lose their strength.

The test procedure emphasizes the comparative nature of the examination. The properties of the samples after the test are generally worse than what was expected. The samples were relatively small and contained four cutting edges. It is inevitable that the samples delaminate slightly near the edges during the cutting process. Therefore, they are able to absorb more gas and deteriorate more regarding their mechanical properties. Aging to this extent is not expected with full-scale machine windings, which is discussed in more detail later in Section 5.7.

5.3 Wellstream gas content study

There are plenty of compressors similar to the one considered in this thesis, operating in dry hydrocarbon gas. Such compressors operate as parts of the natural gas supply network in Europe. They apply the same basic technological concept, which allows the gas to flow through the electrical motor. Therefore, it was hypothesized that dry hydrocarbon gas (sales gas) is not disastrous from the insulating materials' point of view. This was also verified by testing.

Furthermore, previous investigation (Sihvo et al., 2008) for insulating materials of a steam-filled turbo-generator showed that water is extremely aggressive to insulating materials, although the insulation systems considered were designed for low-voltage operation. It was observed that insulating materials partly dissolve into water. The earlier study served as a hypothesis that water as a part of a wellstream gas mixture will cause aging, even though the amount of water in the wellstream gas mixture is very low. In addition to the two hypotheses, the influence of hydrocarbon condensate was initially not known.

The test matrix is shown in Table 5.3. The results focus on ***Wellstream***, ***Cond***, ***HC + MW***, and ***Sales gas*** exposures. The liquid environments were used merely to give additional information on what happens to the materials and how to detect it.

Table 5.3. Test matrix for the wellstream gas content study.

Test label	Test fluids and gases	Temperature [°C]	Pressure [bar]	Time [h]
Wellstream	Dry HC gas + condensate + MEG/water	130	150	750
Cond	Dry HC gas + condensate	130	150	750
HC + MW	Dry HC gas + MEG/water	130	150	750
MW	Liquid MEG/water	130	1.4	168
MW II	Liquid MEG/water	130	6.9	168
FW gas	Dry HC gas + Fresh water	130	150	168
FW liquid	Liquid Fresh water	130	150	168
Sales gas	Dry HC gas	130	150	750

The problem was tackled with individual tests for the influences of the condensate and the mixture of MEG and water, respectively. The ***Cond*** experiment used a mixture containing dry hydrocarbon gas and hydrocarbon condensate of the exact same amounts that was used

in the ***Wellstream*** experiment, for instance in Sections 5.1 and 5.2. Correspondingly, the ***HC + MW*** mixture contained the mixture of water and MEG and no hydrocarbon condensate.

The purpose of experiments in liquid environments was to cause severe degradation to insulating materials and to detect which kinds of changes, particularly in the FTIR spectra, the test conditions cause. The hydrolysis reaction includes water molecules reacting with the insulating materials. Therefore, it causes changes in the chemical structure. The test was carried out with atmospheric pressure prior to heating and with an absolute pressure of 6 bar prior to heating. The actual pressures during the tests were not measured. The values in Table 5.2 are estimated pressures and obtained from the PVTSim simulation.

Correspondingly, a severe test was carried out with pressurized fresh water. The test itself was not essentially realistic from the perspective of the subsea natural gas compressor, since the composition of tap water does not correspond to the produced water from the well. The produced water contains ions and aggressive components, such as salts, which are at least to some extent also present in tap water. Nevertheless, fresh water is a good indicator on the insulation performance, because it rapidly causes severe damage. Furthermore, the test was to cause hydrolysis reaction, which could then be detected without the interference of MEG. The test was carried out in the same chamber as the tests with gas mixtures, Fig. 3.12. The chamber was half-filled with tap water. Half of the specimens were placed in the liquid phase, that is, below the surface, and half in the gaseous phase, i.e. above the surface. The chamber was then pressurized with dry hydrocarbon gas.

The materials used included two mica tape samples, VPI tape G2 and resin rich tape RR1 described earlier in Table 5.2, and two impregnating resins, epoxy anhydride resin C and epoxy novolac resin A described in Table 5.1. The resins are mentioned in the reverse alphabetical order to provide more informative presentation; resin C is included in tape G2, and tape RR1 contains impregnating resin similar to resin A.

5.3.1 Physical dimensions

Changes of weight and volume during the exposures are illustrated in Fig. 5.17 for the mainwall insulation and resin samples. Density changes during the exposures are illustrated in Fig. 5.18.

It is evident in Fig. 5.17 that both the weight and volume of the G2 mainwall insulation increase more in ***Wellstream*** and ***Cond*** exposures than in ***HC + MW*** exposure. A similar trend can be observed with resin C. The weight and volume increases of G2 in these three tests correlate with the weight and volume increases of resin C. This is a somewhat consistent outcome, because G2 mica tape is impregnated with resin C. However, a similar correlation cannot be found in either ***MW*** or ***MW2*** exposures. Tape G2 gains similar amount of weight as in the wellstream exposure, but the weight increase in resin C is much less than that.

Whereas G2 tape appears to be more vulnerable to heavy hydrocarbons than water, RR1 behaves in the exact opposite manner with respect to its weight. A comparable trend, but also

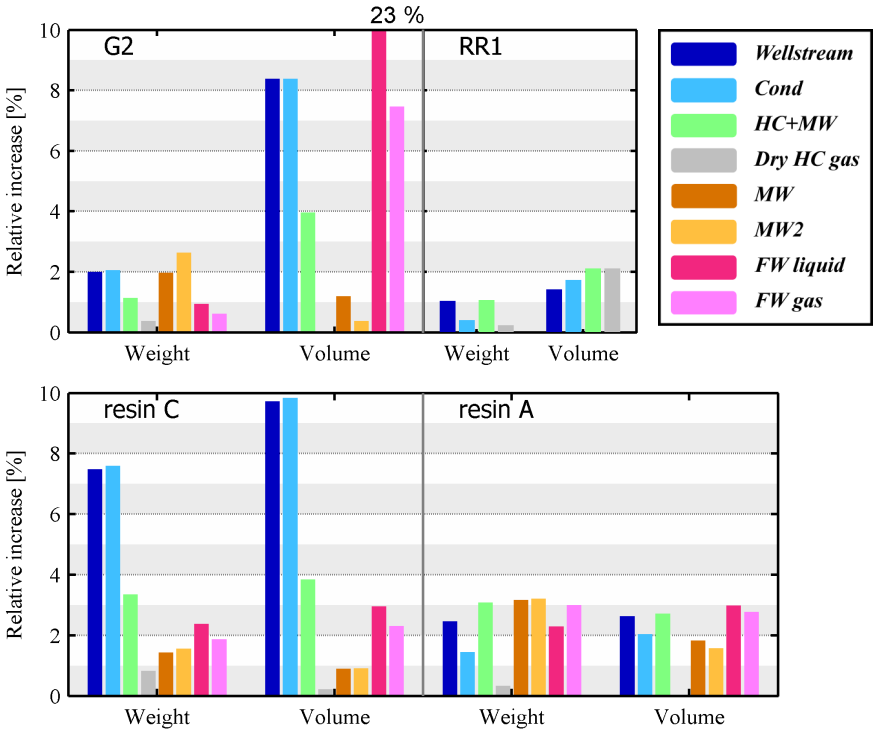

Fig. 5.17. Weight and volume increase of the mainwall insulation (top) and resin (bottom) samples during different exposures.

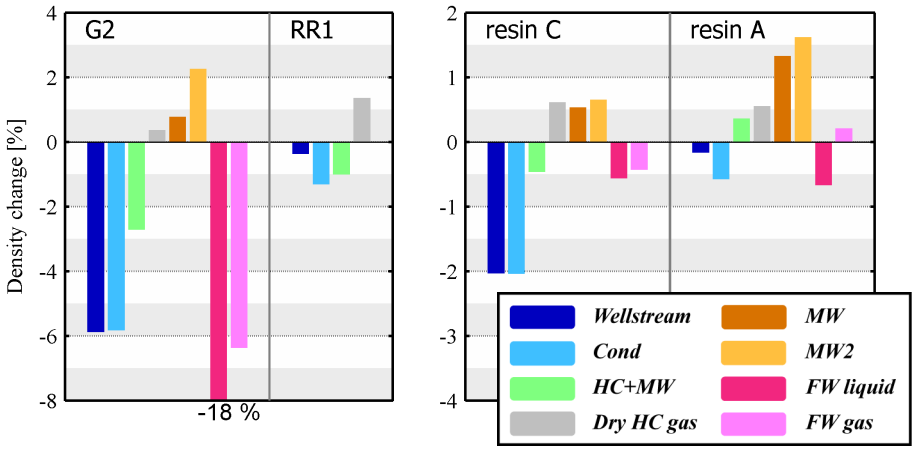

Fig. 5.18. Density changes of the mica tape and epoxy resin samples during different exposures.

applicable to volume, can be observed with resin A in Fig. 5.17. The impregnating resin in RR1 mica tapes is of similar chemistry, but not the very same as resin A.

The test indicates that the G2 mica tape structure is suffering from swelling during the exposure. With fresh water, the G2 material expanded approximately 23%. It is shown in the following subsection that the mechanical properties were also significantly changed during the exposure. However, the weight of the samples did not increase considerably during fresh water exposures. The changes in volume are therefore linked to delamination of tape layers.

It is worth noticing in Fig. 5.18 that hydrocarbon compounds cause a negative density change, whereas the mixture of MEG and water is producing a positive density change. Materials expand more because of the diffusion of hydrocarbons, and the hydrocarbon compounds get trapped inside the polymer matrix. They cannot depart the material during the depressurization. The diffusion is discussed further in Section 5.7.

5.3.2 Mechanical properties

Relative changes in tensile strength, elongation at break, E-modulus, and toughness of mica tape samples are illustrated in Fig. 5.19. The E-modulus of the resin samples is illustrated in Fig. 5.20. The stress versus strain curves for each material and exposure are depicted in Fig. 5.21. Absolute values of strength and elongation can be seen in the stress versus strain curves.

Dry hydrocarbon does not cause significant changes to any of the tested materials, as can be seen in Figs. 5.19 and 5.20. Based on Fig. 5.19, the changes in the tensile strength and E-modulus of RR1 mica tape have also been minor in ***Wellstream***, ***Cond***, and ***HC + MW*** exposures, during which the quantities of G2 mica tape have clearly reduced. Yet, after such exposures, the tensile strength of both mica tapes was approximately 80 MPa, which can be observed in the stress versus strain curves in Fig. 5.21. The G2 mainwall insulation was only initially much stronger.

It can be seen in Fig. 5.21b that the stress versus strain behavior of resin C is fairly similar in ***Wellstream*** and ***Cond*** exposures. These two curves also depart considerably from the reference curve. On the other hand, ***Sales gas*** exposure follows the reference curve rather closely, although the breaking point is found at a lower elongation and strength. The curve of ***HC + MW*** exposure sets roughly in the middle of the ***Wellstream*** and reference curves. Similar behavior can be seen with G2 mica tape in Fig. 5.21, but the ***HC + MW*** exposure has been almost as harsh as the ***Wellstream*** exposure. These observations are convergent with Figs. 5.19 and 5.20. It is concluded that the mechanical properties of the epoxy anhydride resin weaken during the exposure to the wellstream gas essentially because of the heavy hydrocarbon compounds in the gas mixture. The conclusion is supported by the weight and volume data in Fig. 5.17.

The results on tests with water are more difficult to interpret. It is evident in Figs. 5.20 and 5.21 that resin A suffered badly in the ***FW liquid*** experiment. The environment destroyed

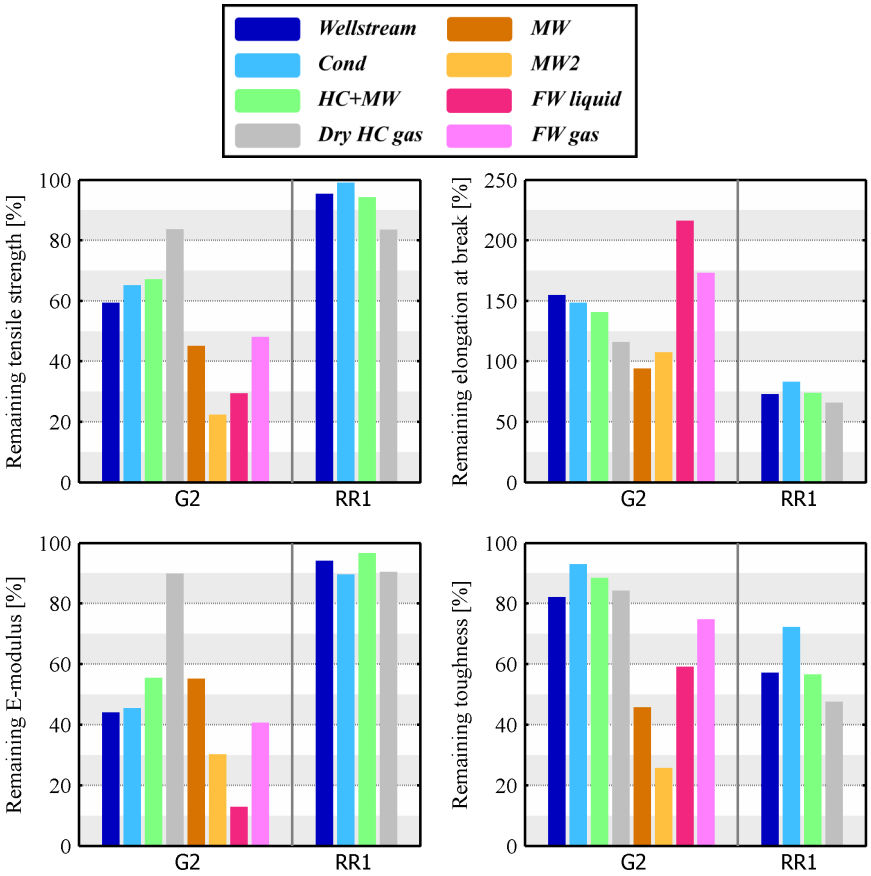

Fig. 5.19. Maintained properties of the mainwall insulation samples during different exposures.

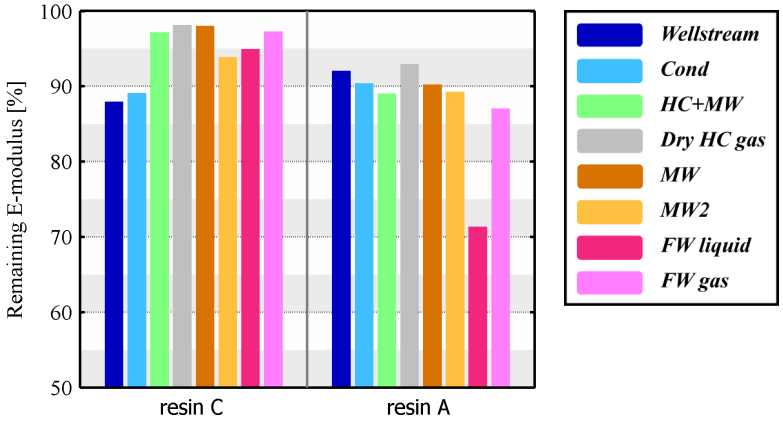

Fig. 5.20. E-modulus of the resin samples before and after the exposures to different environments.

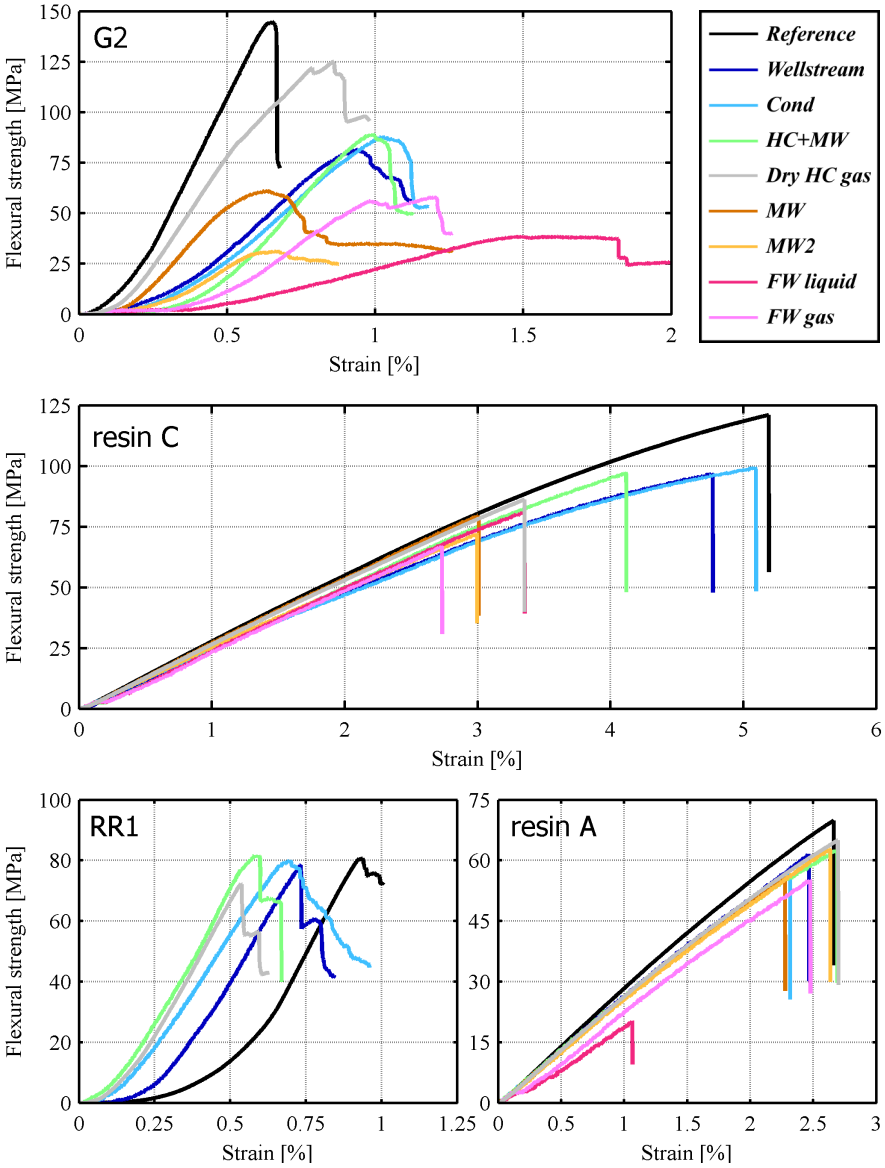

Fig. 5.21. Average stress versus strain curves for the mica tape samples and epoxy resins exposed in different environments.

the material almost completely and also changed the physical appearance, which indicated internal crystals similar as in Fig. 5.4. The E-modulus was reduced indicating mechanical softening.

In the exposures to liquid environments, resin C became more brittle. In Fig. 5.21 none of

the curves extend to the ultimate tensile strength, but still it can be seen that the curves for reference, ***Wellstream***, ***Cond***, and ***HC + MW*** all extend beyond the yielding point, that is, the point at which the curve begins to bend and the behavior becomes nonlinear. However, yielding point is not distinctly present with polymers, and it was therefore not defined. The deviation of samples from liquid environment exposures was relatively small. It was detected during measurements that the material had become more brittle. The E-modulus after ***MW*** exposure was almost that of the reference, Fig. 5.20. With resin C this observation is of importance, because ***Wellstream***, ***Cond***, and ***HC + MW*** exposures undeniably made the material softer.

5.3.3 Dielectric properties

The real parts ϵ' and imaginary parts ϵ" of complex permittivity as functions of frequency for the G2 mainwall insulation, resin C and resin A before and after ***Wellstream*** exposure are illustrated in Fig. 5.22 and Fig. 5.23. The ϵ' and ϵ" of the G2 mainwall insulation after different aging conditions are presented in Figs. 5.24 and 5.25, respectively. The curve fits have been derived according to Eqs. (2.25) and (2.26), respectively. The ϵ' and ϵ" before and after ***MW*** exposure for resin samples are illustrated in Figs. 5.26 and 5.27.

It can be seen in Fig. 5.22 that ϵ' of the resins has decreased during the ***Wellstream*** exposure. Diffusion studies by Pethrick et al. (1996) and Hong et al. (2009a) indicate that the ϵ'

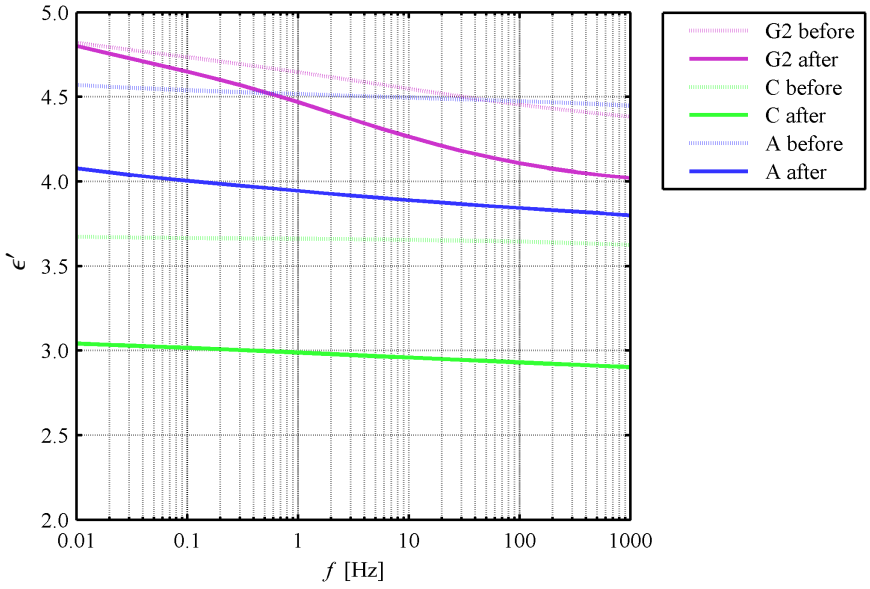

Fig. 5.22. Real part of complex permittivity before and after exposure to wellstream gas mixture. The conditions were 130 °C and 150 bar. The test duration was 750 h.

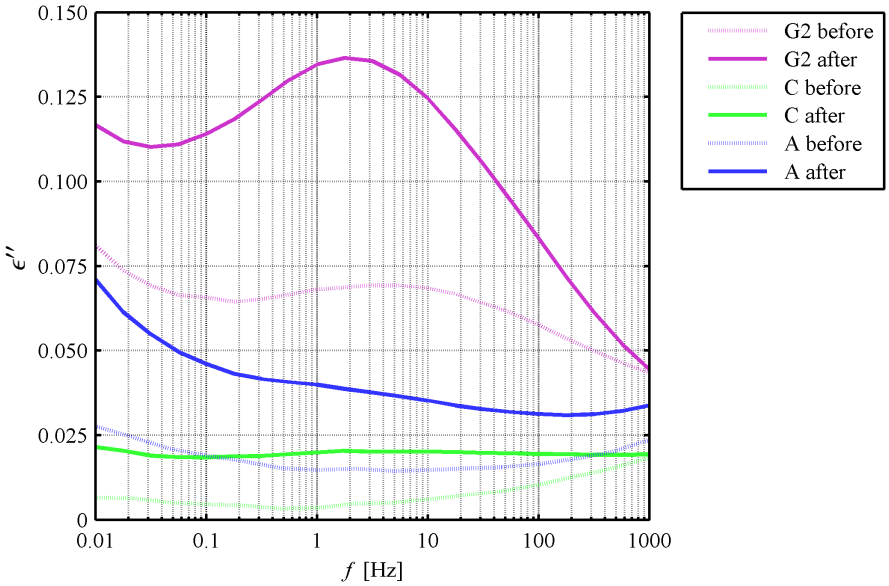

Fig. 5.23. Imaginary part of complex permittivity before and after exposure to wellstream gas mixture. The conditions were 130 °C and 150 bar. The test duration was 750 h.

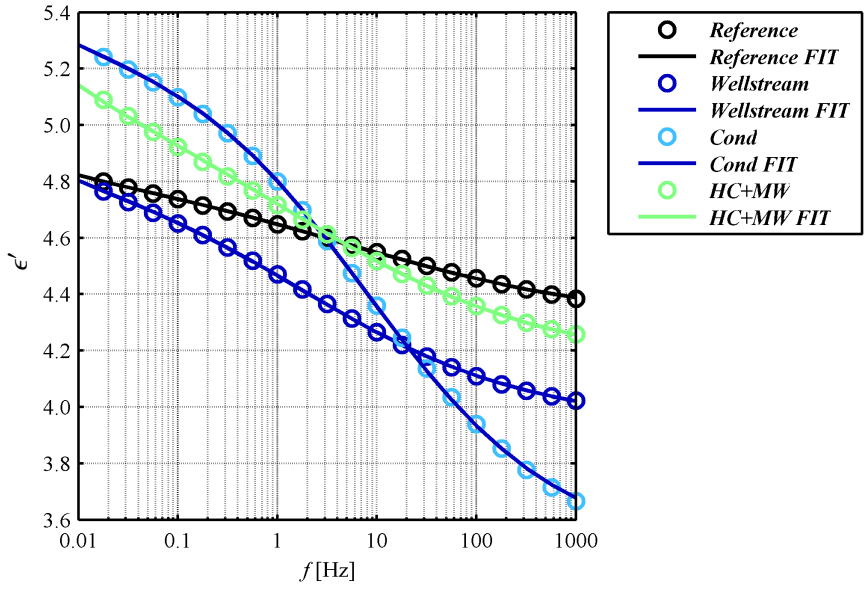

Fig. 5.24. Real part of complex permittivity of G2 mica tape before and after exposure to different environments. The conditions were 130 °C and 150 bar. The test duration was 750 h. The curve fits are defined to match Eq. (2.25).

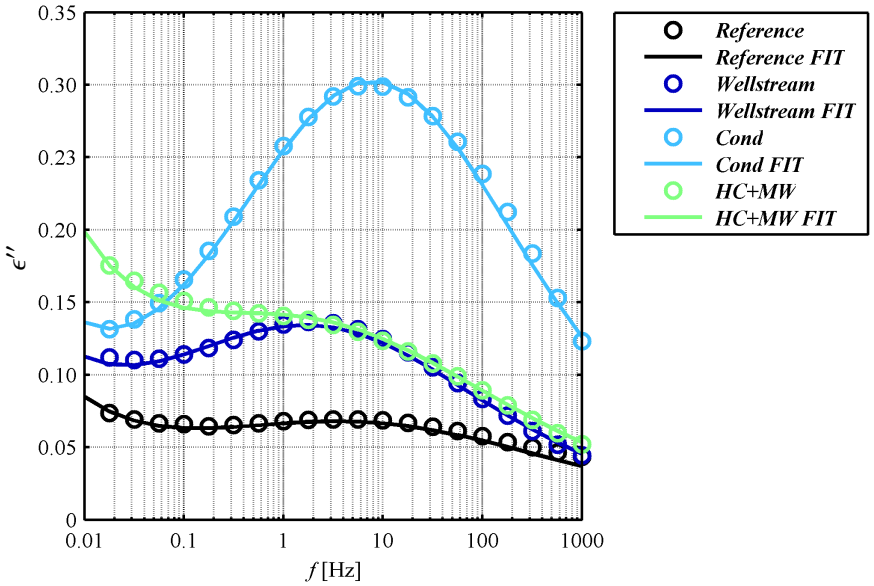

Fig. 5.25. Imaginary part of complex permittivity of G2 mica tape before and after exposure to different environments. The conditions were 130 °C and 150 bar. The test duration was 750 h. The curve fits are defined to match Eq. (2.26).

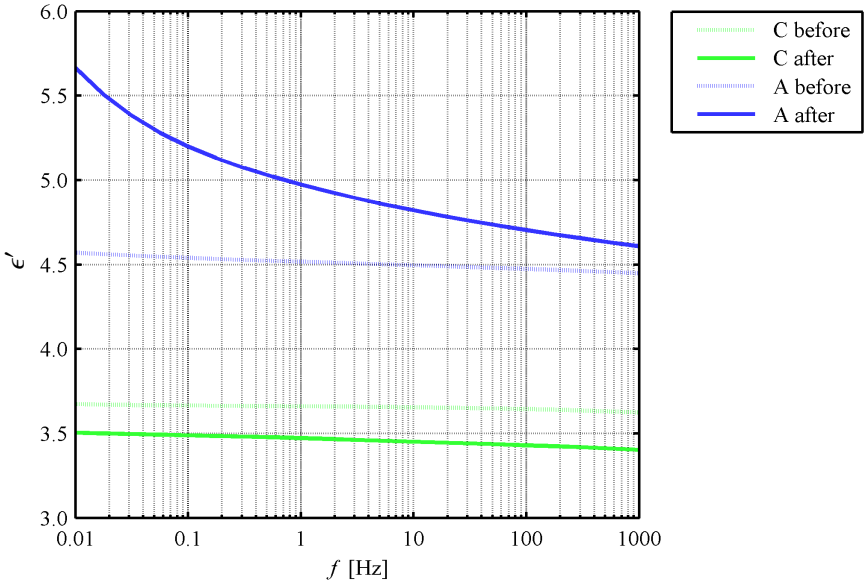

*Fig. 5.26. Real part of complex permittivity of the resins before and after **MW** exposure. The conditions were 130 °C and 1.4 bar. The test duration was 168 h.*

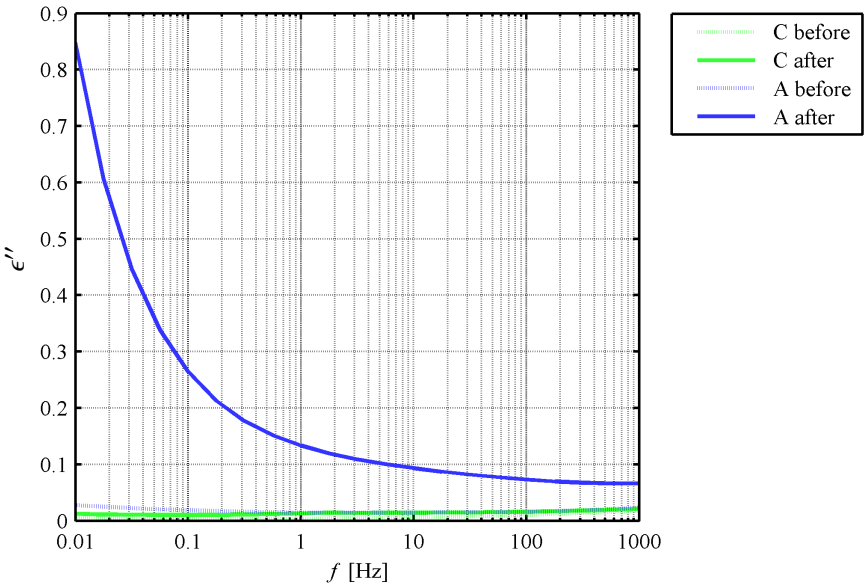

*Fig. 5.27. Imaginary part of complex permittivity of the resins before and after **MW** exposure. The conditions were 130 °C and 1.4 bar. The test duration was 168 h.*

increases as the amount of absorbed water increases. Water is a very polar molecule and its relative permittivity is 80.4 (Young and Freedman, 2000). Also Kärner and Ieda (1991) and Fukuda et al. (1997) reported similar behavior, but only with resins that contain fillers. They did not observe this with bulk resins. The observations reported are not convergent with Fig. 5.22. The reason for this is the complicated nature of the wellstream gas. It contains water, which has a high permittivity, but also heavy hydrocarbon compounds having low permittivity. The total permittivity is determined by the entire wellstream gas mixture, not only by water.

It can be observed in Fig. 5.23 that mica tape G2 experiences a distinctive polarization phenomenon, the peak of which occurs at approximately 2 Hz. A significant increase in ϵ" in the vicinity of 8 Hz can be seen after ***Cond*** exposure in Fig. 5.25. The loss peak can also be seen in the reference sample, but it is very flat. The peak is located at approximately 6 Hz. The polarization observed near 8 Hz with material G2 in Figs. 5.22 and 5.23 is apparently caused by the diffusion of heavy hydrocarbon compounds. As a result of the diffusion of water this peak has been shifted to a lower frequency, where it is seen after ***Wellstream*** exposure.

It can be seen in Fig. 5.23 that the ***HC + MW*** curve departs from the ***Wellstream*** curve in the low frequency region. This indicates that water can cause polarization at very low frequencies. This kind of behavior has been reported by Farahani et al. (2006), Pethrick et al. (1996), and Hong et al. (2009a). With resin A, the liquid MEG/water causes a distinctive polarization phenomenon at very low frequencies, which can be seen in Fig. 5.27. This can also be observed suggestively after the ***Wellstream*** exposure in Fig. 5.23. A similar effect

can be seen with material G2 after ***HC + MW*** exposure (Fig. 5.25), but it is not discernible with resin C.

It can be seen by comparing Figs. 5.22 – 5.27 with Fig. 2.7 that the dielectric relaxation does not obey the relaxation defined by Debye equations. Furthermore, no distinct relaxation is seen with the resins in the ***Wellstream*** exposure as the responses appear almost flat in Figs. 5.22. For neither of the resins, it is possible to define the parameters ϵ_s and ϵ_∞. The departure from the Debye model is obviously due to the complexity of the actual insulating materials, especially after the exposures. The diffusion case was approached by another method. The Debye model is defined for an ideal dielectric, and it explains the dielectric relaxation phenomenon for such a material. Practical measurements almost never completely follow the Debye model, because it is extremely difficult to manufacture a perfectly homogeneous polymer and connect it flawlessly to the measuring electrodes.

The parameters of the curve fits seen in Figs. 5.24 and 5.25 are listed in Table 5.4. The fit was quite good with all the aging conditions. It is worth noticing in Table 5.4 that the exponent $s \neq 1$, which indicates that the exponent s has to be taken into account. It was seen that the conductivity σ'' does not have a major influence on the permittivity ϵ' except with the ***HC + MW*** exposure. With other exposures and reference material, the conductivity was very small and its effect was discernible only at very small frequencies. The data without the conductivity proportion, that is, the base Cole-Cole relaxation, departed from the data only at two lowest frequency measurements. The effect of conductivity was negligible elsewhere. The conductivity σ' had a slightly higher influence on the dielectric losses. Its contribution to the results on the ***HC + MW*** exposure was significant. Basically, the difference between ***Wellstream*** and ***HC + MW*** curves is due to the conductivity σ', which has been provided by the diffusion of produced water, the conductivity of which is approximately 10 S/m. It is still interesting that the conductivity has not increased during the ***Wellstream*** exposure, because the produced water was present in such an experiment also. The effect of produced water on the conductivity of the whole insulation has been mostly canceled out by the heavy hydrocarbons, because the amount of heavy hydrocarbons in the gas mixture is significantly larger than the amount of water.

Table 5.4. Parameters for the curve fits in Figs. 5.24 and 5.25.

Test label	ϵ_s	ϵ_∞	α	s	σ'' [pS/m]	σ' [pS/m]	τ [μs]	f [Hz]
Reference	4.84	4.30	0.70	0.50	10	12.5	28.3	5.6
Wellstream	4.86	3.94	0.65	0.55	10	12.0	79.6	2.0
Cond	5.33	3.47	0.60	0.59	10	12.0	19.9	8.0
HC + MW	5.15	4.14	0.68	0.48	33	31.5	79.6	2.0

The reference sample of the mainwall insulation consists essentially of insulation and some voids, and its ϵ' and ϵ'' can be defined based on the reference curves in Figs. 5.22 and 5.23. During the exposure, the material experiences a volume increase and it also absorbs foreign

substances. Yet, everything the material contained initially is still inside the structure of the material. Hence, it is possible to model the sample after the exposure as two capacitors C_1 and C_2 connected in series as

$$C = \frac{C_1 C_2}{C_1 + C_2} \tag{5.1}$$

The capacitance C is now the capacitance observed with dielectric response measurements. Capacitor C_1 is the material as occurring in its original conditions, $\epsilon_r = \epsilon_1$, A, and d. The capacitor C_2 represents the diffused medium with $\epsilon_r = \epsilon_2$ is the permittivity of the diffused substance. The area A is not changed, but the distance between plates refers to the expanded section (volume increase) only. This is represented by volume fraction ϕ, which is the volume increase divided by the volume after the exposure. The capacitances C_1 and C_2 can be expressed as

$$C_1 = \epsilon_0 \epsilon_1 \frac{A}{d} = \epsilon_1 C_0 \tag{5.2}$$

$$C_2 = \epsilon_0 \epsilon_2 \frac{A}{d\phi} = \epsilon_2 \frac{1}{\phi} C_0 \tag{5.3}$$

Combining Eqs. (5.1), (5.2), and (5.3) yields

$$C = \frac{\epsilon_1 C_0 \epsilon_2 \frac{1}{\phi} C_0}{\epsilon_1 C_0 + \epsilon_2 \frac{1}{\phi} C_0} = \frac{\epsilon_1 \epsilon_2 \frac{1}{\phi} C_0}{\epsilon_1 + \epsilon_2 \frac{1}{\phi}} = C_0 \frac{\epsilon_1 \epsilon_2 \frac{1}{\phi}}{\frac{\phi \epsilon_1 + \epsilon_2}{\phi}} \tag{5.4}$$

On the other hand, the observed capacitance C can be expressed as

$$C = \epsilon' \epsilon_0 \frac{A}{d + d\phi} = \epsilon' C_0 \frac{1}{1 + \phi} \tag{5.5}$$

Combining Eqs. (5.4) and (5.5) and rearranging yields

$$\frac{\epsilon'}{1 + \phi} = \frac{\epsilon_1 \epsilon_2}{\phi \epsilon_1 + \epsilon_2} \tag{5.6}$$

and further to

$$\epsilon'(\phi \epsilon_1 + \epsilon_2) = (1 + \phi) \epsilon_1 \epsilon_2 \tag{5.7}$$

Regarding the ***Wellstream***, ***Cond***, and ***HC + MW*** exposures, where the permittivity has been reduced, the ϵ_2 can be solved by

$$\epsilon_2 = \frac{\phi\epsilon_1\epsilon'}{(1+\phi)\epsilon_1 - \epsilon'} \tag{5.8}$$

Permittivities of diffusing substances for the mainwall insulation in ***Wellstream***, ***Cond***, and ***HC + MW*** exposures calculated based on the volume increase, the volume fraction, and Eq. (5.8) are listed in Table 5.5.

Table 5.5. Permittivities of diffusing substances. Values of $\epsilon_1 = 4.48$ and ϵ' are obtained at 50 Hz frequency. ϵ_2 is calculated according to Eq. (5.8).

Test label	ΔV	ϕ	ϵ'	ϵ_2
Wellstream	0.0839	0.0774	4.14	2.09
Cond	0.0838	0.0773	4.03	1.75
HC + MW	0.0400	0.0381	4.39	2.87

Scaife (1972) measured the permittivities for n-alkanes from n-pentane (C_5H_{12} with all carbons in a single unbranched chain) to n-decane ($C_{10}H_{22}$). He reported the relative permittivity of n-pentane to be 1.841 at room temperature. The permittivity was increased along the molecular weight of n-alkanes, and the permittivity of n-decane was reported to be 1.989. Values of hydrocarbons lighter than pentane are difficult to determine, since the compounds are in a gaseous phase at room temperature. The value 1.75 in Table 5.5 for ***Cond*** mixture seems realistic with respect to the values reported by Scaife (1972). Higher ϵ' at ***Wellstream*** exposure is caused by the effect of water. The ϵ' at ***HC + MW*** exposure may be somewhat erroneous, because the diffusive compounds are mostly water. Water is able to fill the free volume between the polymer chains, which leads to changes in weight and dielectric properties, but not in volume, as the water is filling space that was initially empty. Therefore, ϵ_2 does no correlate with the volume increase. The ϵ_2 could not be determined for resins in the ***MW*** exposure.

5.3.4 FTIR spectroscopy

The FTIR spectra of resin C after testing in gas mixtures are illustrated in Fig. 5.28, and the spectra after the exposures to liquid conditions in Fig. 5.29. The FTIR spectra of resin A did not reveal any significant changes.

A significant difference in the spectra in the region of 3700 – 3000 cm^{-1} is observed in Figs. 5.28 and 5.29. This is due to water inside the materials and has been reported by many researchers, (Wu and Siesler, 2003; Fernández-García and Chiang, 2002; Liu et al., 2002;

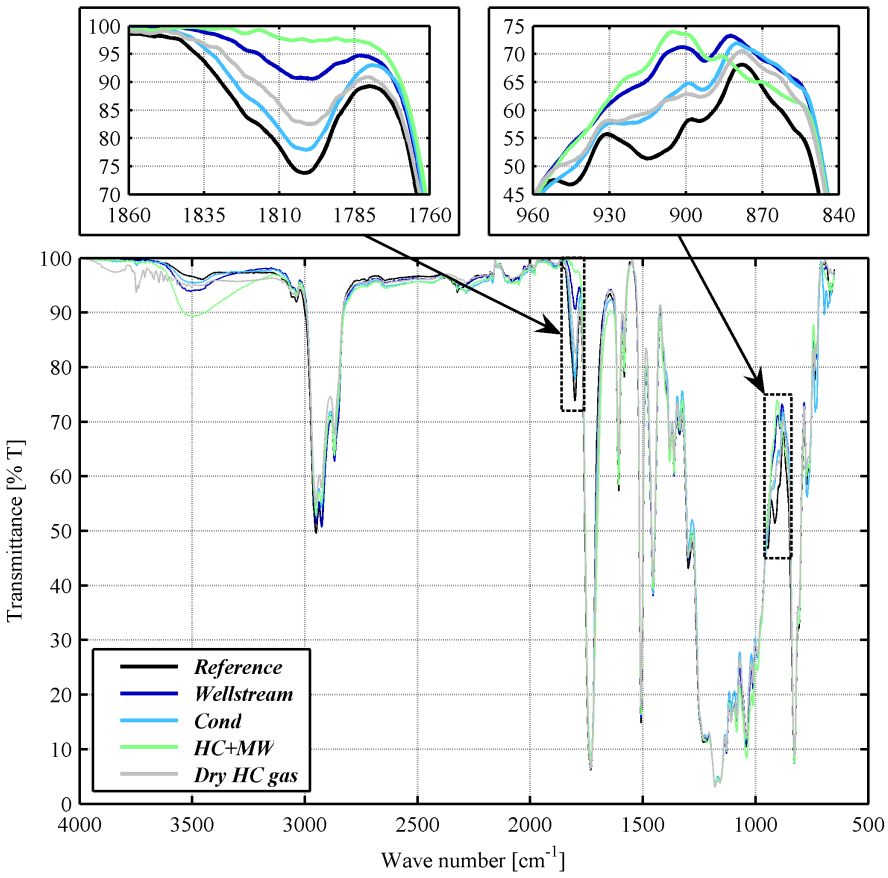

Fig. 5.28. FTIR spectra of resin C after exposures to various gas mixtures.

Musto et al., 2000). The water is trapped in the free volume of the polymer matrix and has not reacted with the material.

In Figs. 5.28 and 5.29, the IR spectra of resin C contain reduction of the peak at the wave number 1801 cm^{-1}. Furthermore, it includes changes in the region of 950 – 850 cm^{-1}. Both changes refer to bonds, the number of which has decreased during the exposure. It can be seen in the magnified section in Fig. 5.28 that the peak at approximately 1801 cm^{-1} disappears completely during the ***HC + MW*** exposure, but is only slightly reduced during the ***Cond*** and ***Sales gas*** exposures. This applies to the changes in the region between 950 – 850 cm^{-1} also. The transitions can be observed in Fig. 5.29 with all the liquid environments. Therefore, it is concluded that these changes have been caused by water. They are not affected by hydrocarbons or MEG.

The investigation of the peaks in the FTIR spectra is rather difficult. Depending on the material, the peaks can occur at slightly different wave numbers, and the information in the

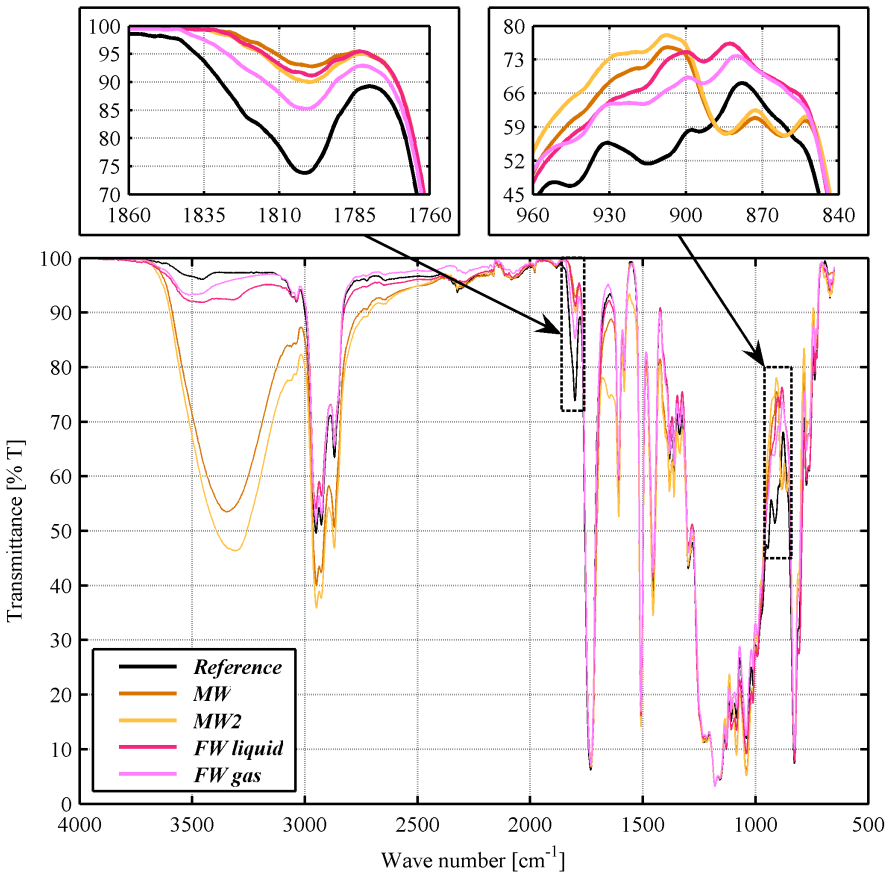

Fig. 5.29. FTIR spectra of resin C after exposures to liquid environments.

literature is not precise. Therefore, many peaks observed in the spectrum can have several possible causes. The peak observed at 1801 cm^{-1} in resin C is most likely linked to the anhydride crosslinking group, which links the molecular chains together. The changes in the region 950 – 850 cm^{-1} can refer to several bonds, but most likely they are attributed to an epoxide group. The reduction in this peak indicates that the remaining epoxide groups, which have not reacted in the curing process, have reacted with water. The considerations for these changes are presented in Section 5.7.

5.3.5 Glass transition temperature

Glass transition temperatures for epoxy resin samples are illustrated in Fig. 5.30. In the figure, it is evident that the dry hydrocarbon gas has virtually no effect on resin A, but has some effect on resin C. The glass transition temperature of both resins is heavily reduced

after the ***Wellstream*** exposure. The T_g of resin C has decreased more after the ***Cond*** than ***HC + MW*** exposure. By contrast, the T_g of resin A has decreased more during ***HC + MW*** than ***Cond*** exposure. These relations are in close agreement with the observations from the weight and volume data in Fig. 5.17. The former observation is also supported by the stress versus strain behavior in Fig. 5.21. Thus, regarding exposures to ***Wellstream***, ***Cond*** and ***HC + MW***, the data on glass transition temperature correlates with the data on weight, volume, and E-modulus.

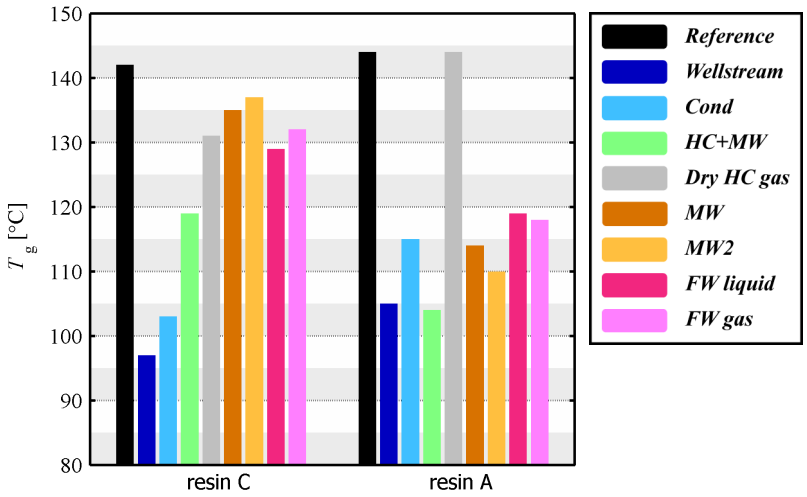

Fig. 5.30. Glass transition temperatures of epoxy resin samples before and after exposures to different environments.

The reduction of glass transition temperature caused by liquid environments (***MW***, ***MW2***, ***FW liquid***, and ***FW gas*** exposures) can be clearly seen with resin A, but not with resin C. The reduction of T_g in resin A is somewhat convergent with the weight increase seen in Fig. 5.17. The brittleness caused by water was not seen with resin A. In fact it had become soft during ***FW liquid*** and ***FW gas*** exposures, as can be seen in Fig. 5.21. Softening has also been indicated by the glass transition temperature.

Resin C, on the other hand, experienced softening in the ***Wellstream*** and ***Cond*** exposures. The material also experienced the most significant drops in T_g in the same exposures. Resin C became more brittle during ***MW***, ***MW2***, ***FW liquid***, and ***FW gas*** exposures, which indicate only little reduction in the glass transition temperature.

Many researchers have reported that T_g drops as a result of water absorption (Banks and Ellis, 1979; Nogueira et al., 2001; Xiao and Shanahan, 1998). Nogueira et al. (2001) used an epoxy novolac resin and reported softening because of water absorption. Their results are convergent with the results in Fig. 5.30 on resin A. Banks and Ellis (1979) and Xiao and Shanahan (1998) used bisphenol A epoxy resin, which corresponds to resin C.

Most likely, the glass transition temperatures measured on resin C after exposures to liquid environments have been too high. The water has partly evaporated during the heating of the sample. The evaporation could not be detected during the measurements. It did not produce any clearly discernible anomaly in the vicinity of the boiling point of water in the heat flow versus temperature curve. The first heating run, which has obviously caused most evaporation, contained also traces of the thermal history of the materials. To detect the glass transition temperature of an epoxy that has absorbed water, another test method should be used. Banks and Ellis (1979) used nuclear magnetic resonance study (NMR), and they sealed the samples tightly so that no water could escape from the sample. Xiao and Shanahan (1998) and Nogueira et al. (2001) used a dynamic mechanical analyzer (DMA).

5.3.6 Summary of the key results

Aging of mainwall insulation structures and epoxy impregnating resins caused by different components of the wellstream gas have been investigated, and the results have been presented in this section. Specimens have been exposed to different gas mixtures. The effects of heavy hydrocarbons and water on insulating materials have been distinguished.

Two different epoxy resins experience the wellstream gas in different ways. Bisphenol A epoxy anhydride resin is more vulnerable to heavy hydrocarbons, whereas epoxy novolac resin suffers more from water. Similar observations were made with mica tapes having similar impregnating resins. Epoxy resins experience some changes during the exposure to the wellstream gas. Epoxy novolac resin only absorbs water, and no distinct changes in its chemical structure can be detected. However, Bisphenol A epoxy resin suffers from slight chemical changes.

During the exposure to the wellstream gas, the bisphenol A epoxy resin is experiencing mechanical softening, which can be seen in the decrease in E-modulus, the increase in weight and volume, and the reduction in glass transition temperature. The chemical structure of the resin is not changed by heavy hydrocarbons, but it is slightly changed by water. Chemical changes were attributed to hydrolysis reactions in anhydride and epoxide groups. The discussion on the chemical changes is found in Section 5.7. The changes in the chemical structure do not cause the reduction in the mechanical properties, but it is caused by heavy hydrocarbons.

Epoxy novolac resin does not absorb much hydrocarbon compounds and does not experience significant mechanical softening when exposed to the wellstream gas. It does, however, experience softening caused by water. Furthermore, water causes polarization at low frequencies in the material. Some traces of the polarization phenomenon can be seen after exposure to the wellstream gas, but no softening.

Nevertheless, an order of preference cannot be defined between epoxy novolac resin and Bisphenol A epoxy anhydride resin based on their performance in the wellstream gas. Both resins experience aging, but it is of different nature and it is, above all, due to different substances in the gas mixture. Yet, the experiments gave indications that both resins could be

used in the subsea compressor.

The mainwall insulation behaves essentially similarly as the resin with which it is impregnated. The resin provides the strength, and the aging of resin results in the aging of the whole mainwall insulation. Therefore, a mainwall insulation impregnated with epoxy anhydride resin experiences mechanical softening similarly as the resin itself, and the mainwall insulation containing epoxy novolac resin is not significantly affected by the wellstream gas. Yet, the mainwall insulation experiences additional polarization effect, which was not seen with the resins. Furthermore, the composite mainwall insulation structure is more vulnerable to the environment than bulk epoxy resins. The changes in mechanical properties have been more distinctive. The last two observations indicate that the aging phenomenon is more complicated in a composite insulation structure. It is discussed more closely in Section 5.7.

5.4 Effect of the temperature study

The test matrix contained three tests at different temperatures, as listed in Table 5.6. The test environment was based on the ***Wellstream*** test (Table 5.3), which is now referred to as ***WS 130*** exposure according to the temperature. The accelerated conditions were then produced only by increasing the temperature. The materials used in the investigation include resins A and C described in Table 5.1 and the mainwall insulation structure G2 depicted in Table 5.2. The purpose of the test was simply to investigate the sensitivity the temperature has on the materials. It has to be emphasized that both overheated gas mixtures were at temperatures higher than the glass transition temperatures of the resins.

Table 5.6. Test matrix for the effects of the temperature study.

Test label	Test fluids and gases	Temperature [°C]	Pressure [bar]	Time [h]
WS 130	Wellstream gas	130	150	750
WS 150	Wellstream gas	150	150	750
WS 170	Wellstream gas	170	150	750

The conditions for increased temperatures differ from the ***WS 130*** conditions. According to the phase envelope illustrated earlier in Fig. 3.11, the mixture is not exactly at the dew point at 130 °C and 150 bar. Regarding to the pressure, there is a slight difference, but this has only a minimal influence on the test conditions, that is, the conditions virtually match the dew point. However, the gas mixture is very sensitive to the temperature. It can be seen in Fig. 3.11 that the hydrocarbon saturation line is located at a higher temperature than the water saturation line at 150 bar. Therefore, the gas is able to contain more liquids when the temperature is increased up to approximately 150 °C, when the mixture becomes saturated with respect of hydrocarbons also. The flash conditions of the test fluids are described in Table 5.7. The fractions are calculated with PVTSim software. Based on Table 5.7, the ***WS 150*** mixture is close to its hydrocarbon saturation state containing very little liquid components. The ***WS 170*** mixture is superheated with respect to both hydrocarbons and water.

Table 5.7. Mole percentages of the components and densities of the test fluids.

Test label	Mole % Vapor	Mole % Liquid	Mole % Aqueous	Density [g/cm^3]
WS 130	98.59	1.31	0.1	0.115
WS 150	99.93	0.07	0	0.107
WS 170	100	0	0	0.100

5.4.1 Physical dimensions

The weight and volume increases during the exposures to different temperatures are illustrated in Fig. 5.31 and the density changes in Fig. 5.32. According to Figs. 5.31 and 5.32, the resins gained more weight, they expanded more, and their density decreased more in the ***WS 150*** than in the ***WS 170*** exposure. The fact that the test conditions exceed the glass transition temperature of the resins is not visible in Fig. 5.31. The weight increase curves for the resins seem convergent. The largest increase in the ***WS 150*** is most likely related to the composition of the gas. In the ***WS 130*** exposure, the gas has not been fully saturated with respect to water and especially to hydrocarbons. In the ***WS 150*** exposure, the gas mixture has been water saturated and virtually also hydrocarbon saturated, which can be seen in the flash data in Table 5.7. In the ***WS 170*** exposure, the gas mixture has been superheated and fully in a gaseous phase. These differences mean that the gas mixture has contained the most heavy hydrocarbon compounds in the ***WS 150*** exposure. These compounds have condensed and trapped inside the polymer matrix as the temperature has been reduced. This is seen as the largest weight increase. By contrast, the gas mixture in ***WS 170*** has contained the least fractional amount of hydrocarbons and water, which can be seen in the lowest weight increase.

Mica tape G2, on the other hand, experiences further changes in weight, volume, and density in the ***WS 170*** exposure. This can be linked to delamination of the tape material. The

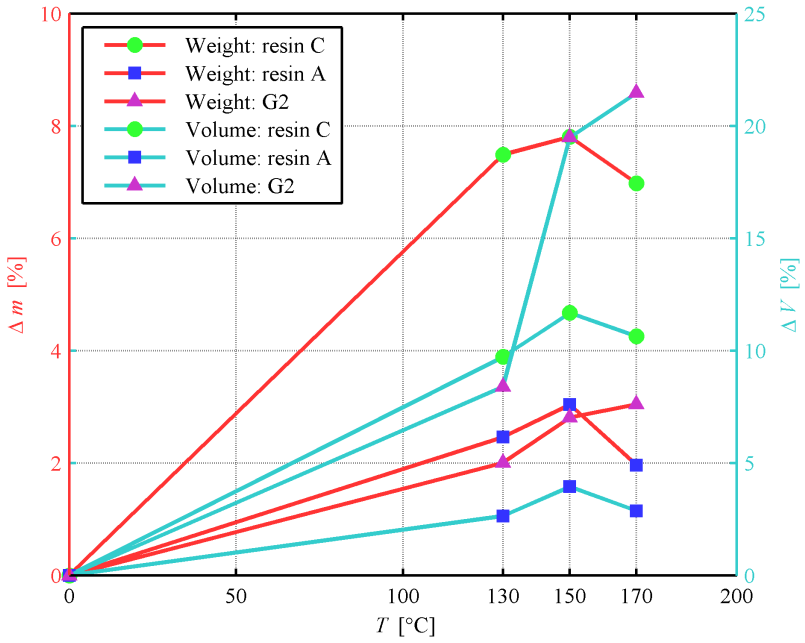

Fig. 5.31. Weight and volume increase of the resins and the mainwall insulation in exposures at different temperatures.

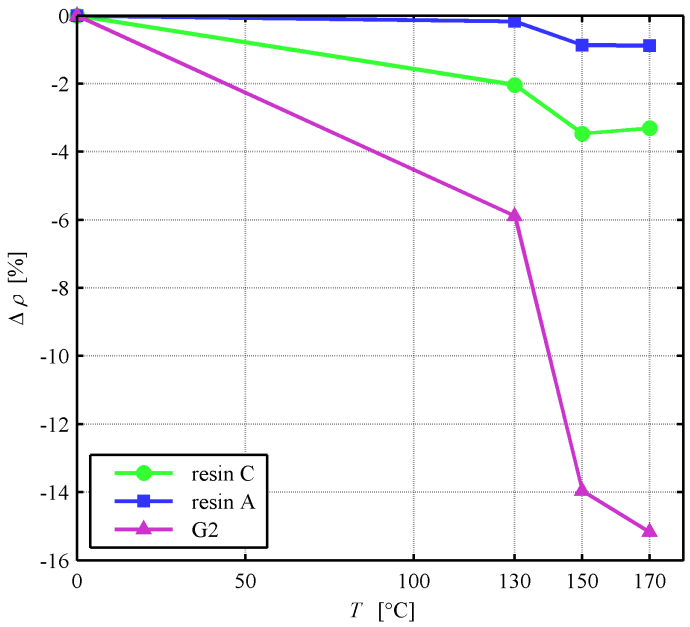

Fig. 5.32. Density change of the resins and the mainwall insulation in exposures at different temperatures.

temperature has assisted the delamination. The changes between the exposures are not likely to be linked to the depressurization. The ***WS 130*** exposure had been carried out two times both resulting in almost identical weight and volume changes. The test for longer duration also resulted in almost the same changes, as will be shown in the following section. Resin A has become darker during the exposures to higher temperatures. This can be seen in Fig. 5.33, in which the sample is illustrated. The discoloration also took place with this particular material when it was cured at a high temperature. The resin C did not change color during the exposures.

Fig. 5.33. Resin A after exposures at different temperatures.

5.4.2 Mechanical properties

The mechanical properties retained during the exposures for material G2 are illustrated in Fig. 5.34. The relative values of E-modulus of the resins are shown in Fig. 5.35. The stress versus strain curves for material G2 and resins are illustrated in Fig. 5.36.

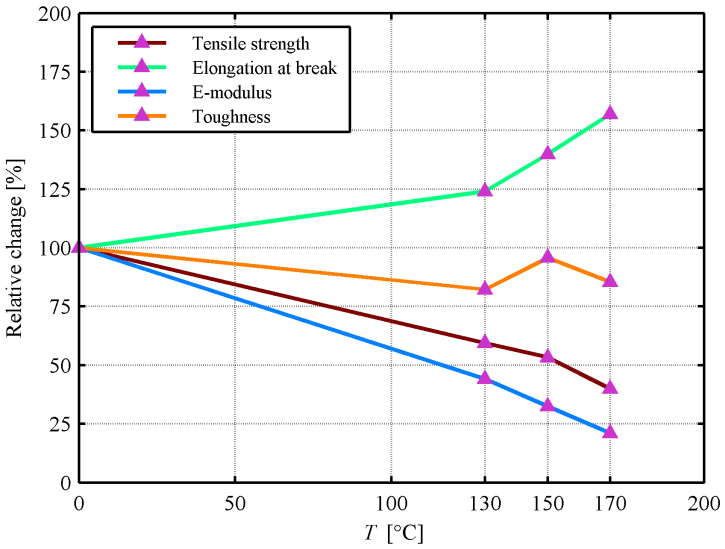

Fig. 5.34. Tensile strength, elongation at break, E-modulus, and toughness of G2 mica tape retained during the exposures at different temperatures.

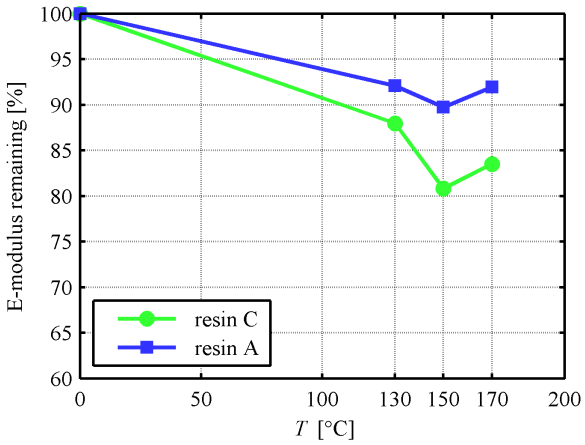

Fig. 5.35. E-modulus of the resins retained during the exposures at different temperatures.

It is noteworthy in Fig. 5.34 that the tensile strength and E-modulus of material G2 decrease almost linearly as the temperature is increased. By contrast, the elongation increases, but not

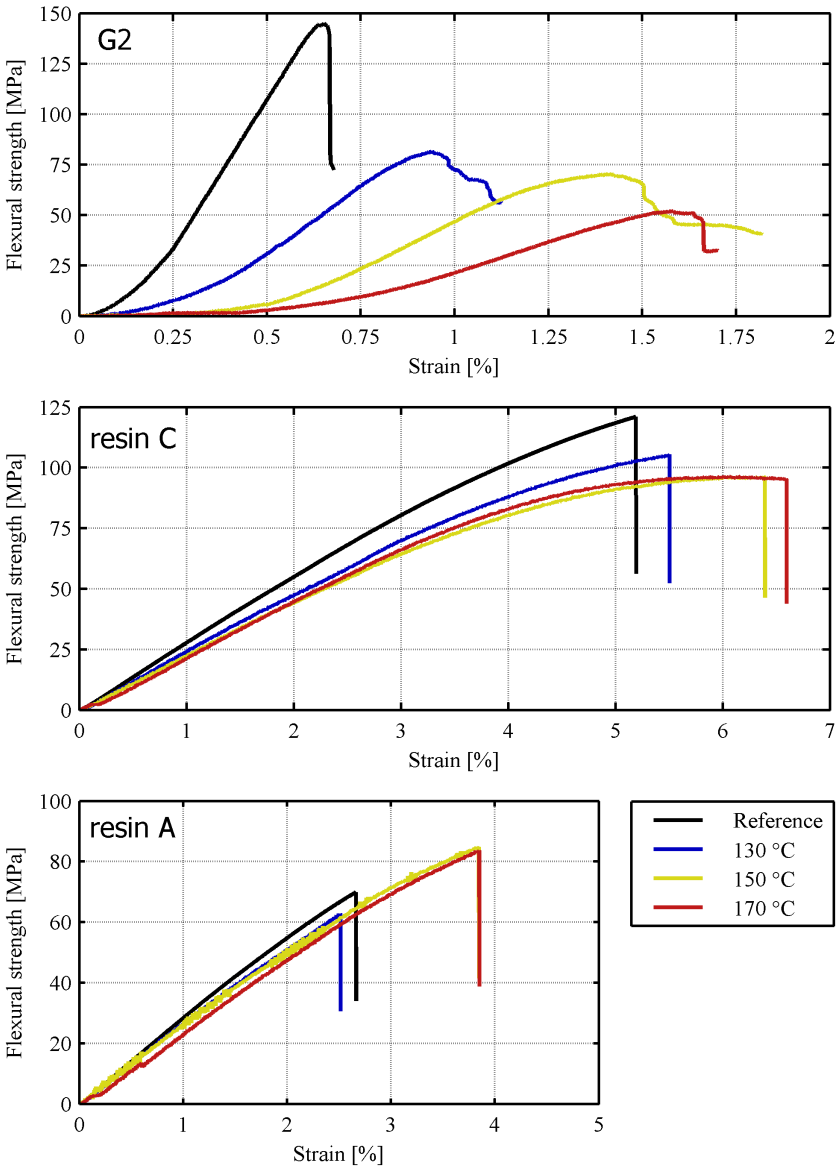

*Fig. 5.36. Stress versus strain curves before and after the exposures at different temperatures. The resin samples, excluding resin C in **WS 150** and **WS 170**, could not meet the ultimate tensile strength, because they are so brittle. Therefore, the comparison of resins focuses on the E-modulus.*

exactly linearly. The stress versus strain curve (Fig. 5.36) visualizes the increased softening of material G2. The E-moduli of the resins in Fig. 5.35 follow the same trends as their weights and volumes in Fig. 5.31 and densities in Fig. 5.32.

The stress versus strain curves of the resins in Fig. 5.36 are slightly misleading showing too much degradation for samples of the ***WS 170*** exposure. The bending head of the instrument was not tightly attached. This is seen as a short plateau in the initial sections of the curves for the ***WS 170*** exposure. This interference does not affect the E-modulus or the tensile strength. It only slightly increases the elongation at break, but this quantity was not analyzed. The interference is shifting the curves to larger elongation, which appears as if they have become softer. In reality, the resins had not become softer in the ***WS 170*** than in the ***WS 150*** exposure, which can be seen in the E-modulus in Fig. 5.35.

5.4.3 FTIR spectroscopy

The IR spectra of resin A did not reveal clear changes. The FTIR spectra of resin C before and after the exposures are illustrated in Fig. 5.37, and the areas of interest are magnified in Fig. 5.38. It can be seen in Fig. 5.37 that the changes observed with the ***WS 130*** exposure are more pronounced in the exposures at higher temperatures. Small departures from the reference curve can be seen at the wave numbers 1325 cm^{-1} and 1287 cm^{-1} after the ***WS 170*** exposure. The changes could not be unambiguously interpreted, but all the alternatives given by PerkinElmer and Hannah suggested that they are linked to changes in the aromatic rings.

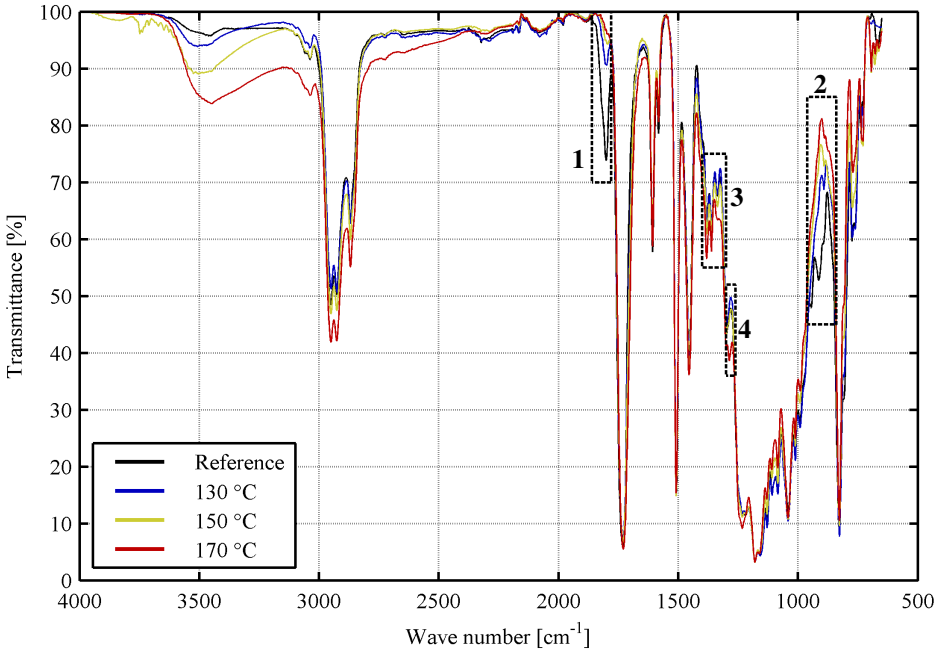

Fig. 5.37. IR spectra of resin C before and after the exposures. The numbered areas are magnified in Fig. 5.38.

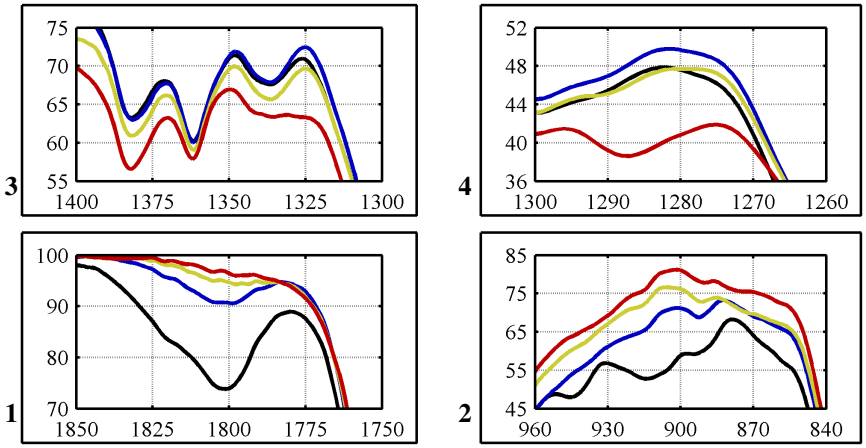

Fig. 5.38. Magnified regions of Fig. 5.37 with the same data and line colors.

5.4.4 Glass transition temperature

The glass transition temperatures of the resins before and after the exposures are illustrated in Fig. 5.39. It can be seen in Fig. 5.39 that T_g of resin A has been less after the ***WS 150*** exposure than after other exposures. This is convergent with the weights and volumes in Fig. 5.31.

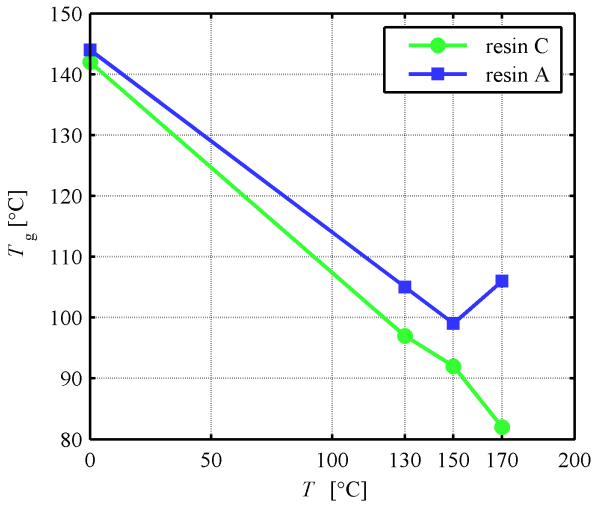

Fig. 5.39. Glass transition temperatures of the resins before and after the exposures.

However, the glass transition temperature of resin C appears to reduce linearly as a function of the exposure temperature. This is not supported by weight and volume, which means that the further reduction in T_g in the ***WS 170*** exposure is not caused by the absorption of

hydrocarbon compounds. It is more likely linked to the chemical changes observed. Yet, the reduction in glass transition temperature and the chemical changes possibly affecting it have not, at least significantly, influenced the E-modulus.

The measured value of T_g in the ***WS 170*** exposure appears to deviate from what was expected based on measurements on other quantities. Fundamentally, there are two possible reasons for this: an error in the measurement, and a physical phenomenon, which is merely not suggested by the other measured quantities. The erroneous measurement is supported, because the change in T_g was not seen as a change in weight increase. With all other exposures, these quantities were seen to correlate. However, the measurements were carried out by an automated scheme and repeated for two times, which minimizes the possibility of human error. The sample may have caused flaws, but such was not seen with other samples. Furthermore, the test procedure wipes out the thermal history of the sample. The traces caused by the cutting process or contamination are only visible in the first heating run, not in the succeeding ones.

The resin C was seen to absorb a lot of hydrocarbon compounds during the exposures. These compounds act as plasticizers inside the material and cause internal disorder, which is seen as a reduced E-modulus and glass transition temperature. The plasticizer can put the internal structure of the resin in a more severe disorder, if the temperature is increased. This is discussed in more detail in Section 5.7.

5.4.5 Summary

The wellstream gas mixtures at higher temperatures did not cause further degradation in the epoxy novolac resin. However, at higher temperatures, the epoxy anhydride resin did experience further reduction in the glass transition temperature. It also experienced new changes in its chemical structure while the changes observed also with other exposures were pronounced.

Mica tape impregnated with epoxy anhydride resin experienced more degradation when exposed to higher temperatures. The reduction in mechanical properties indicated a linear downward trend as a function of exposure temperature, which was supported also by the weight and volume data, although they did not have a linear trend. The impregnating resin of the G2 mainwall insulation had become more sensitive at higher temperatures, which has then weakened the composite insulation structure.

The experiments did not, however, give indications of the initial glass transition temperature of the resins. The hypothesis was that the materials would experience further degradation similar to that of material B described in Section 5.1. This, however, did not take place. The glass transition temperature of the resins decreases below the test conditions in any case as a result of the diffusion of the wellstream gas. This can be seen in the glass transition temperatures measured after the ***WS 130*** exposure, which are below the test temperature (130 °C), even though they were above that before the test. The properties of the mainwall insulation were seen to decrease almost linearly as a function of temperature and were not

dependent upon the initial glass transition temperature of the impregnating resin.

The conditions of the gas mixtures were different, which can also be seen in the results. In the ***WS 150*** exposure, the gas mixture was very close to the hydrocarbon saturation line. The gas mixture contained a larger fraction of heavy hydrocarbon compounds than the other mixtures. In ***WS 130*** such compounds had not all been evaporated and in ***WS 170*** they were all evaporated, but the mixture was superheated. Therefore, the resins experienced the largest absorbances in the ***WS 150*** exposure, which can also be seen in the largest mechanical softening, that is, the lowest E-modulus.

It is clear that the Arrhenius lifetime relation Eq. (2.2) does not hold. It has to be emphasized that the thermal classification is 180 for the resin C and 220 for the resin A, which are above the exposure conditions. However, the classification is defined for operation in dry conditions, and the wellstream gas environment is significantly harsher than that. Without the wellstream gas environment, the materials would not have experienced any aging within the given time. Yet, the resins were not particularly sensitive to the increase in temperature, and the aging phenomenon was more influenced by the content of the gas mixture, which was discussed in the previous section. Hence, the aging phenomenon is not plain thermal aging defined by the Arrhenius relation, but it is caused by the gas mixture penetrating into the materials.

The results of this study are of particular importance from the electrical machine point of view. The temperature in the winding is not (as it was in the experimental test program) a quantity defined by the surrounding conditions. The heat is generated by the windings of the machine itself and the temperature is adjusted by the surrounding conditions, which provide cooling. The temperature is defined essentially by the fundamental machine design, which determines the cooling arrangements, such as cooling ducts inside the stator stack. The experiments indicated that whether the operating temperature is below or above the initial glass transition temperature of the resin is strictly irrelevant, as the glass transition is ultimately defined by the diffusion of the gas.

5.5 Effect of exposure duration

The test matrix contained two exposures in the wellstream gas. The first exposure was the ***Wellstream*** exposure described in Table 5.3, which lasted for 750 hours. The second exposure was carried out in similar conditions, but for longer duration, 3726 hours. The exposures are labeled as ***WS 750*** and ***WS 3726*** in this section.

The IR spectra of resin A did not reveal any notable changes. The IR spectra of resin C after 3726 hours are not essentially different from those of after 750 hours. The changes observed after 750 hours were also present with no additional changes suggesting that the chemical changes have taken place within the first 750 h of aging. Therefore, no figures on FTIR spectra are presented in this section.

5.5.1 Physical dimensions

The weight and volume increases during the exposures to different temperatures are illustrated in Fig. 5.40 and the density changes in Fig. 5.41. It is evident in Figs. 5.40 and 5.41 that the weight, volume, and density of the resins are not significantly changed after 750 hours. This means that the diffusion of the wellstream gas into resins has met its saturation level. Furthermore, there appears to be a saturation level. The weight, volume, and den-

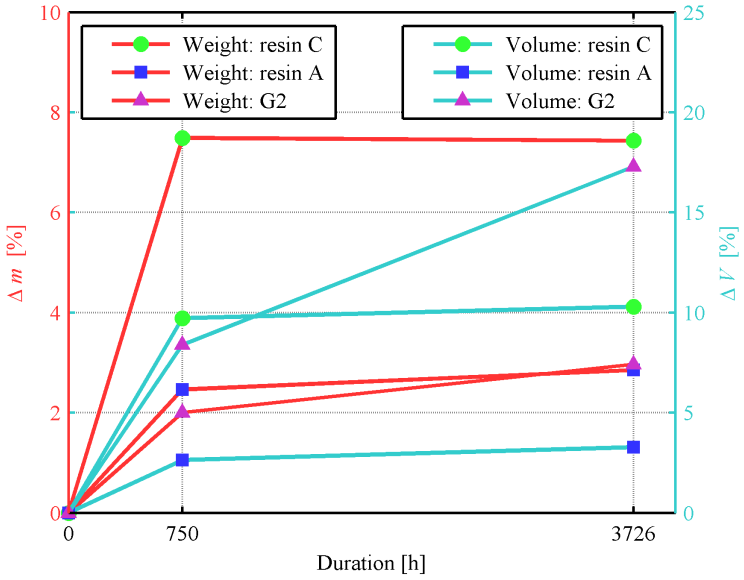

Fig. 5.40. Weight and volume increases of resins and the mainwall insulation as functions of time of exposure in the wellstream gas conditions.

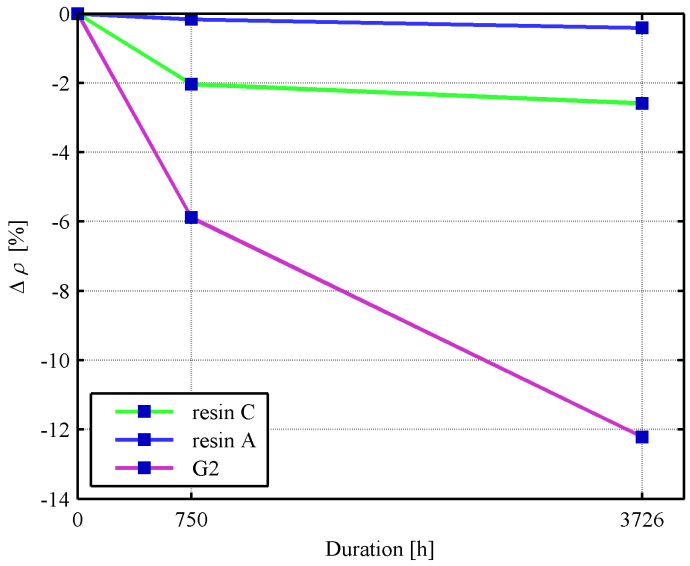

Fig. 5.41. Density changes of resins and the mainwall insulation as a function of time of exposure in the wellstream gas conditions.

sity changes of the mainwall insulation G2, on the other hand, experience further diffusion, which can be seen at 3726 hours. This suggests that there are two diffusion processes going on: diffusion into the epoxy resin and diffusion into the interfaces of epoxy and glass or mica.

Therefore, the diffusion of wellstream gas into resins follows the common trend of diffusion of water into plain epoxy resin, and the diffusion of wellstream gas into the mainwall insulation behaves like the diffusion of water into epoxy resin with fillers. Both diffusion cases were illustrated above in Fig. 2.6, which is based on the results by Fukuda et al. (1997), Fernández-García and Chiang (2002), and Maggana and Pissis (1999). In all the reports, the filler content in the resin was rather high. However, the results only suggest this. No undeniable conclusions can be drawn, because the number of data points is so low.

5.5.2 Mechanical properties

The mechanical properties retained during the exposures for material G2 are illustrated in Fig. 5.42. The relative values of the E-modulus of the resins are shown in Fig. 5.43. The stress versus strain curves for material G2 and resins are illustrated in Fig. 5.44.

It can be seen in Fig. 5.42 that the deterioration of material G2 has continued slightly after 750 hours. However, such a trend cannot be seen with the resins in Fig. 5.43. In fact, the E-modulus of resin A is higher after 3726 hours than after 750 hours. The material had become slightly more brittle. The mechanical properties are convergent with the weight increase.

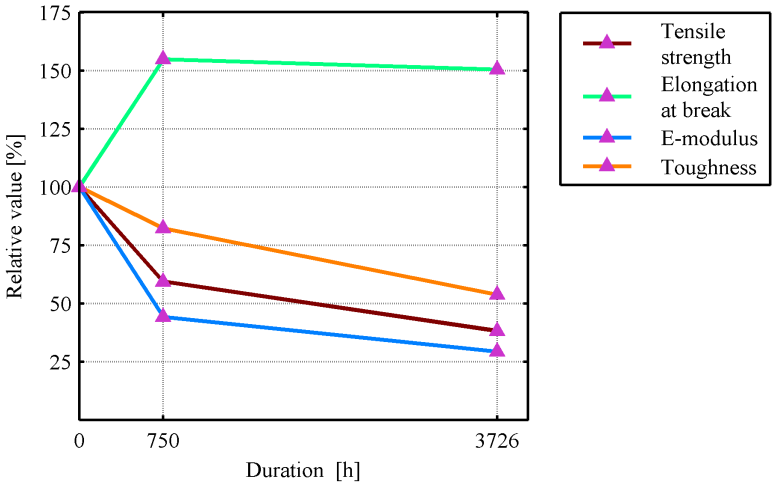

Fig. 5.42. Relative values of tensile strength, elongation at break, E-modulus, and toughness of G2 mica tape as functions of time of exposure in the wellstream gas conditions.

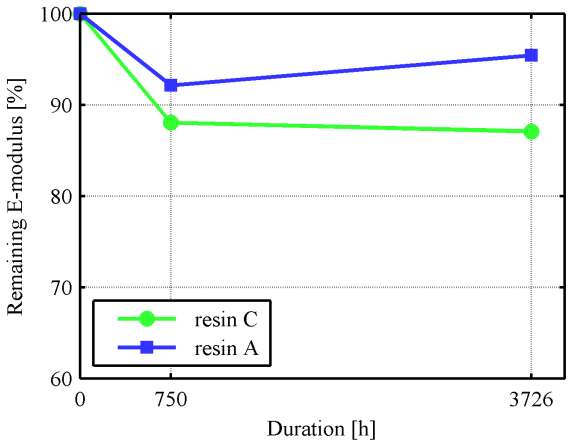

Fig. 5.43. Relative E-modulus of the resins as functions of time of exposure in the wellstream gas conditions.

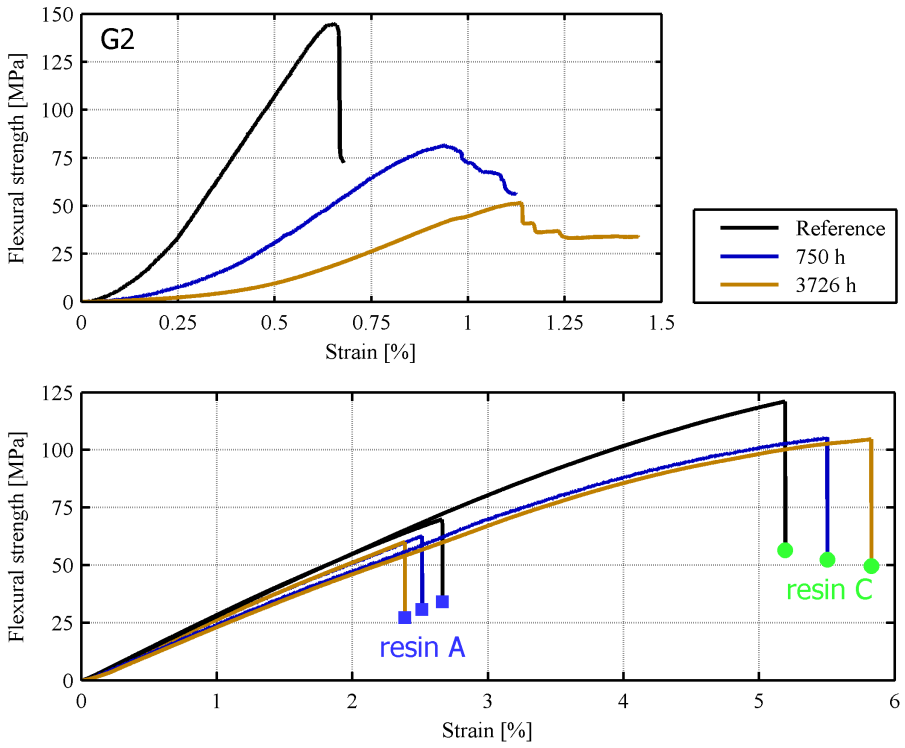

Fig. 5.44. Stress versus strain curves before and after the exposures to the wellstream gas conditions for different durations.

5.5.3 Dielectric properties

The real parts of the permittivity of the resins for different durations of aging are presented in Fig. 5.45 and the imaginary parts in Fig. 5.46, respectively. The dielectric response of the resins does not reveal any major changes, but small differences can be observed. The ϵ'' of resin A contains some polarization information in the low frequency range, which can be seen in Fig. 5.46. Interestingly, this effect has disappeared at 3726 hours. The ϵ' of resin A has decreased gradually as a function of time. The ϵ' of resin C has also decreased, but it is surprisingly slightly higher after 3726 hours than after 750 hours. The reduction in ϵ' is due to the absorption of wellstream gas, in particular heavy hydrocarbon compounds. The observations with the resins are, at least to some extent, affected by the sample quality. Furthermore, the differences are only minor.

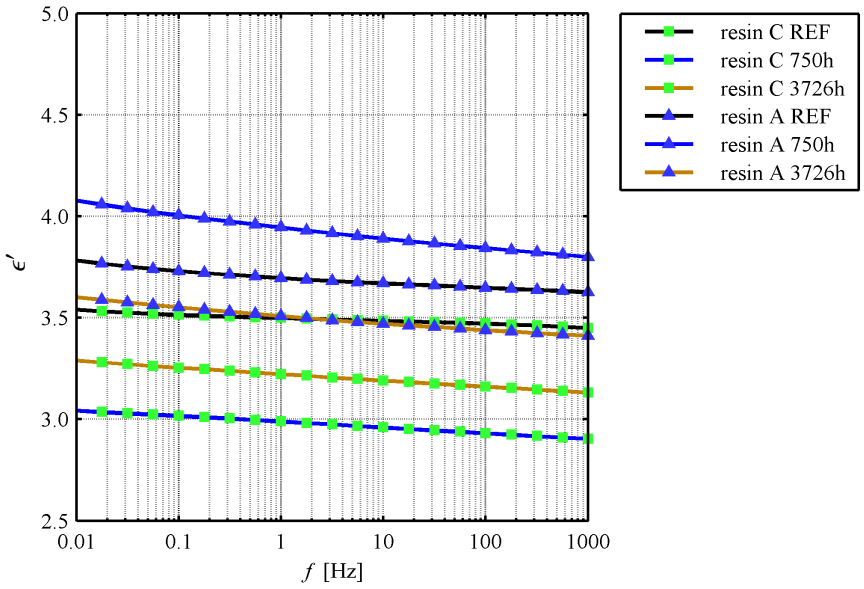

Fig. 5.45. Real part of the complex permittivity of the resins before and after exposures to wellstream gas mixture. The conditions were 130 °C and 150 bar.

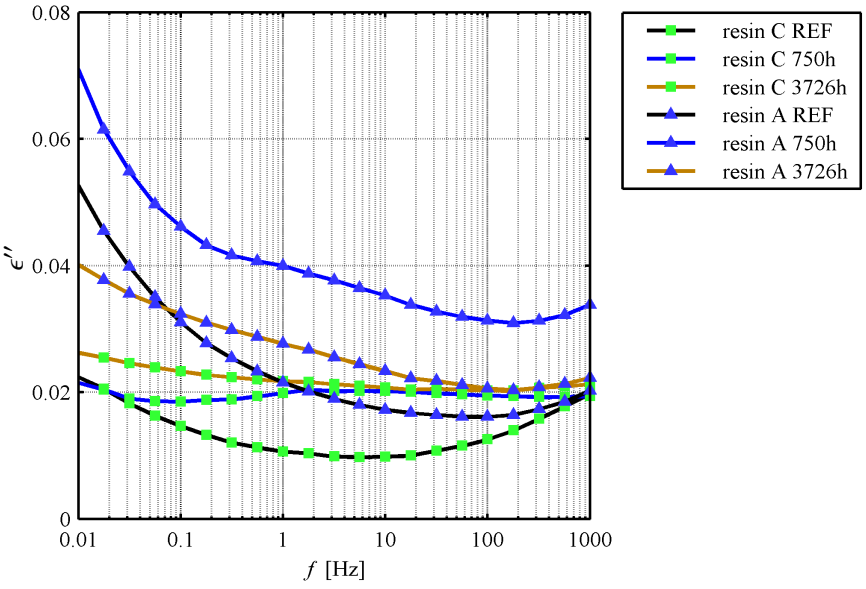

Fig. 5.46. Imaginary part of the complex permittivity of the resins before and after exposures to wellstream gas mixture. The conditions were 130 °C and 150 bar.

The real and imaginary parts of complex permittivity, ϵ' and ϵ'', as functions of frequency for G2 mica tape are illustrated in Fig. 5.47 and Fig. 5.48. Parameters for the curve fits are listed in Table 5.8.

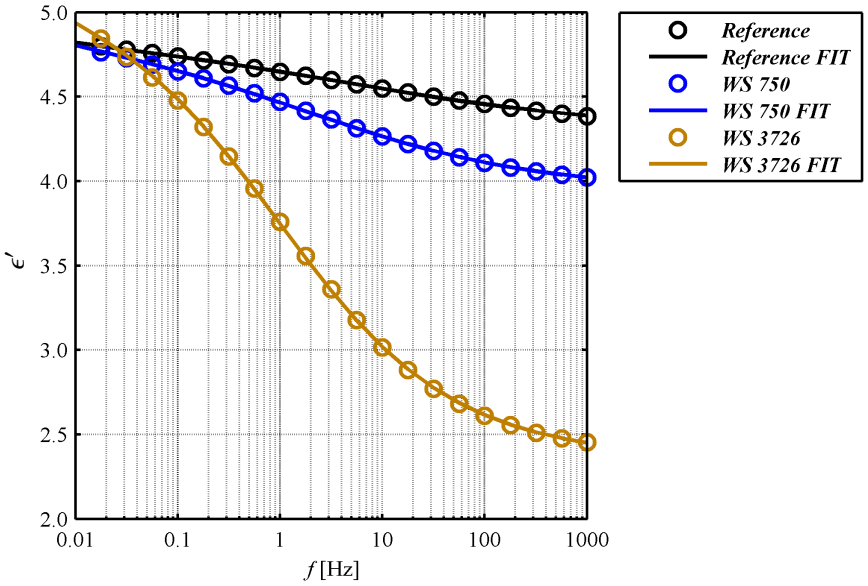

Fig. 5.47. Real part of the complex permittivity of G2 mica tape before and after exposures to wellstream gas mixture. The conditions were 130 °C and 150 bar. The curve fits are defined to match Eq. (2.25).

A distinct polarization phenomenon can be seen with material G2 both ϵ' in Fig. 5.47 and ϵ'' in Fig. 5.48. This phenomenon can be seen after 750 hours, but more strongly after 3726 hours. A similar effect was seen above in Fig. 5.25 and it was concluded to be linked to the hydrocarbon condensate. The polarization is attributed to diffusion, but also to the delamination. Because of the latter effect, Eq. (5.8) does not give accurate results for the case; the equation was only used in comparison of different environments, which did not cause significant delamination changes.

Table 5.8. Parameters for the curve fits in Figs. 5.47 and 5.48.

Test label	ϵ_s	ϵ_∞	α	s	σ'' [pS/m]	σ' [pS/m]	τ [μs]	f [Hz]
Reference	4.84	4.30	0.70	0.50	10	12.5	28.3	5.6
WS 750	4.86	3.94	0.65	0.55	10	12.0	79.6	2.0
WS 3726	5.13	2.36	0.55	0.62	10.5	19.5	159.2	1.0

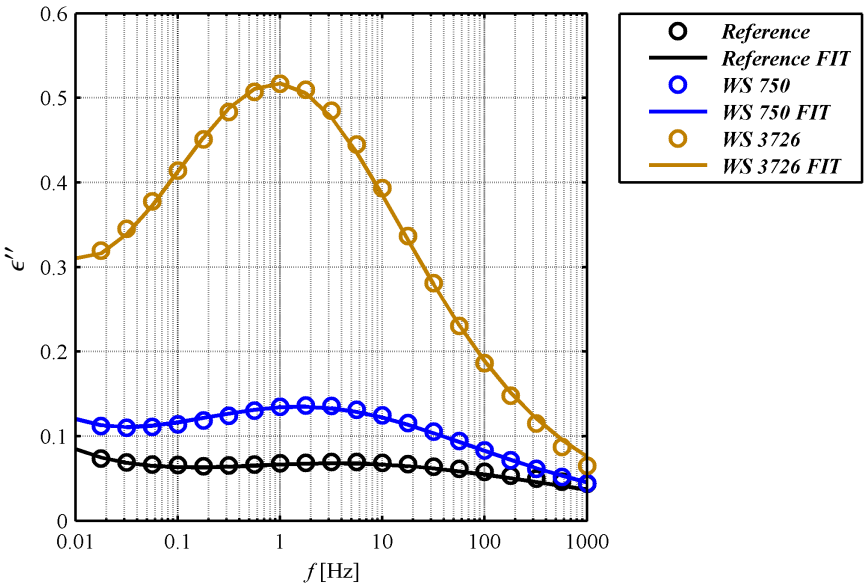

Fig. 5.48. Imaginary part of the complex permittivity of G2 mica tape before and after exposures to wellstream gas mixture. The conditions were 130 °C and 150 bar. The curve fits are defined to match Eq. (2.26).

It was concluded in Section 5.3 that the heavy hydrocarbons tend to shift the large loss peak towards higher frequencies. Based on Fig. 5.48 the peak appears to have been shifted towards lower frequencies. The loss peak generally appears similar to the one caused by hydrocarbon condensate (Fig. 5.25). This observation and the remark in Table 5.8 that the conductivity σ'' has increased point to the fact that water also contributes to the large dielectric loss indicated in Fig. 5.48. Furthermore, the influence of produced water has been emphasized in the long-term exposure, which can be seen in the increased conductivity of the material in Table 5.8.

The insulation resistance is illustrated in Fig. 5.49. During the exposure, the insulation resistance was decreased to a measurable level, where it initially was not, but it is still many decades above an acceptable level. Even though the dielectric losses have increased, the insulation resistance has not changed significantly. Furthermore, the standard deviation was high in all the measurements, which increases the uncertainty of the values presented in Fig. 5.49. The insulation resistance was very high, as a result of which the measured current was very low and easily interfered by the disturbances. The measurements on insulation resistance indicate far less deterioration than the measurements on mechanical properties or glass transition temperature. The breakdown strength was not determined, which prevents making any detailed conclusions on the deterioration of dielectric properties.

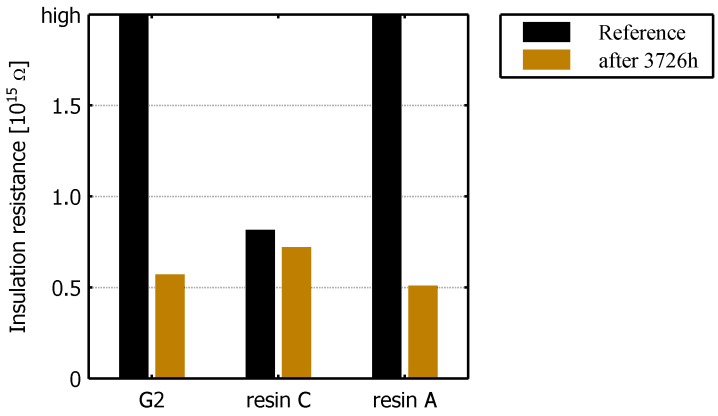

Fig. 5.49. Insulation resistance of the samples before and after ***WS 3726 exposure.***

5.5.4 Glass transition temperature

Glass transition temperatures of the resins after the exposures are illustrated in Fig. 5.50. It is surprising that T_g is higher after 3726 hours than after 750 hours. The measurements for T_g after 3726 hours were performed with a different instrument. The Perkin Elmer device described in Section 3.6.4 could not be used for this very set of samples and T_g had to be measured with a DSC instrument from another vendor (Netzsch). Therefore, also the sample holders were not exactly similar. The procedure used for the measurement was similar with the same heating rate. Yet, the values have obviously been higher than the ones measured after 750 hours. The difference, as it is in that direction, is not significant and the results can be concluded as with the weight and volume data: there has not been further aging after 750 hours.

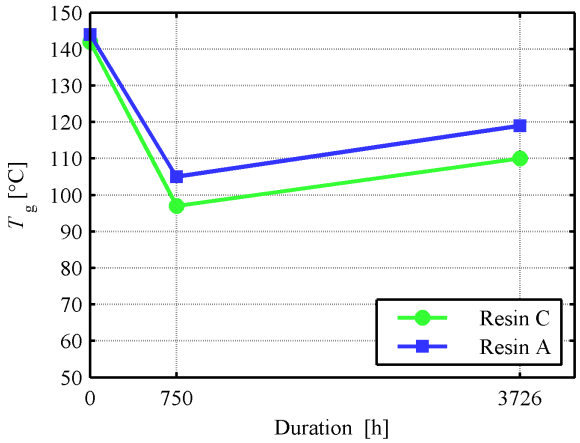

Fig. 5.50. Glass transition temperature of resin C and resin A after the exposures.

5.5.5 Summary and discussion

The results indicate that the resin samples do not experience further aging in the wellstream gas mixture after 750 hours. Their weight and volume do not virtually change. The mechanical properties of the resins are in close agreement with their weight and volume. This indicates that the aging of epoxies is related to the diffusion process and no additional phenomena are present.

On the other hand, mainwall insulation experiences further diffusion after 750 hours. This can be seen in the further, although not very significant, weight increase and in the reduction in mechanical properties. In addition, the polarization that the mainwall insulation experiences significant increase after 750 hours. This can be seen in the high dielectric loss peak at around 1 Hz in Fig. 5.48. The polarization can be linked to heavy hydrocarbon as concluded in Section 5.3, but the effect of produced water has been more distinct than in the exposure for 750 hours.

The purpose of this study was to analyze the diffusion as a function of time. Disappointingly, the test matrix was wrongly selected for such a purpose, since the knee-point of the weight increase curve (Fig. 5.40) has taken place before 750 hours, which was the first marker in the curve. Therefore, no information on the diffusion coefficient could be obtained. However, the long-term test revealed information on the properties of the materials after a long-time exposure. Regarding the subsea compressor, this is more informative. The compressor is designed to operate for years and its reliability is more dependent on the long-term behavior than on the performance during the first few weeks.

5.5.6 Inconsistency of the study

The inconsistency of the study lies in the initial experiments. As stated in Section 5.1, the depressurization rate was fast and the results shown in that section show much less weight increase and, correspondingly, much less mechanical softening than the results shown in Sections 5.3 and 5.4. The weight increase, remaining E-modulus, and glass transition temperature of such tests are illustrated in Figs. 5.51, 5.52, and 5.53, respectively. Tests for 1500 hours and 2000 hours had also been carried out with the same depressurization procedure as the first exposure for 750 hours described in Section 5.1.

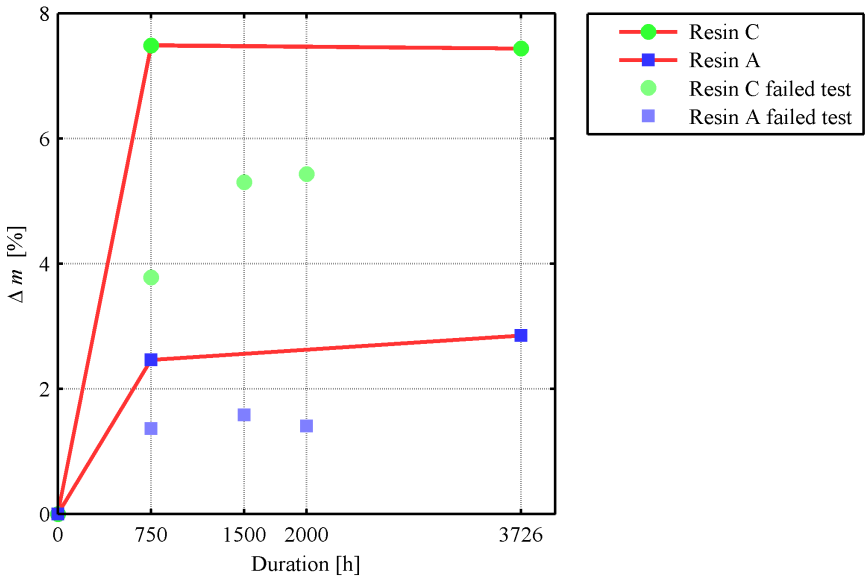

*Fig. 5.51. Weight increase of the resins in the tests of different durations. The markers connected with lines correspond to the data on **WS 750** and **WS 3726** exposures in Fig. 5.40. The data on failed tests are indicated with faded-out markers without line connection.*

The results of the failed experiments indicated that the knee-point of the diffusion curve was in the vicinity of 1600 – 1800 hours. This is best seen with resin C in Fig. 5.51. The fits for the other curves also suggested a knee-point in the vicinity, but it could only be detected by a curve fit, not by looking at individual markers. The curve fits are not shown as they were not very accurate. The knee-point was very difficult to determine, because the result did not have the expected trend. This had been caused by too rapid and too inaccurate depressurization procedure after each exposure. The weight increase of the resins in ***WS 750*** exposure is approximately two times the weight increase measured at the first exposure with too rapid a depressurization rate.

The diffusion process of the wellstream gas into insulating materials has not been investigated thoroughly enough. It is pointed out in Section 5.7 that the saturation value of the weight increase m_∞ is more important than the diffusion coefficient D. In other words, it is more important to detect the saturated state than the initial steps of the diffusion process.

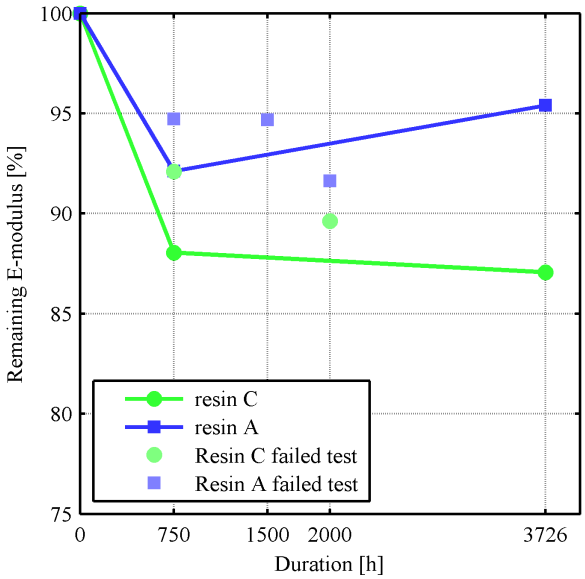

*Fig. 5.52. Remaining E-modulus after the exposure of different durations. The markers connected with lines correspond to the data on **WS 750** and **WS 3726** exposures in Fig. 5.43. The data on failed tests are indicated with faded-out markers without line connection. The E-modulus for resin C after 1500 h was not measured.*

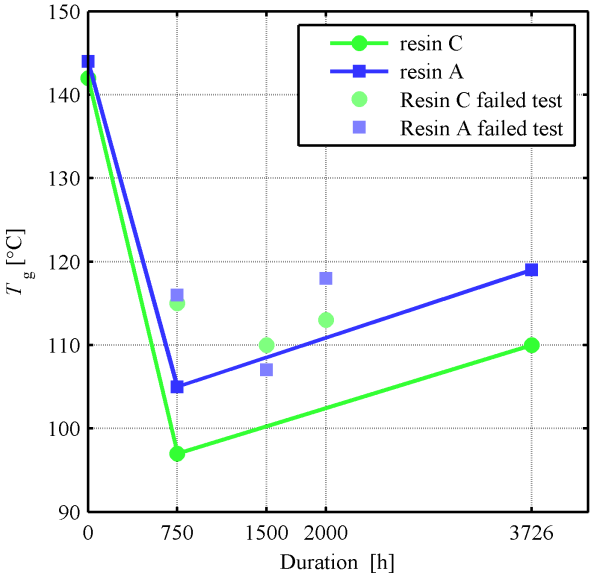

*Fig. 5.53. Glass transition temperature of resin C and resin A after the exposures. The markers connected with lines correspond to the data on **WS 750** and **WS 3726** exposures in Fig. 5.50. The data on failed tests are indicated with faded-out markers without line connection.*

5.6 Rapid decompression test

The test procedure is illustrated in Fig. 5.54. It contained ten decompressions in total, which were all performed at a high temperature. The depressurizations in the chemical aging tests were all done after the temperature had reduced. In that respect, this experiment is more stressing.

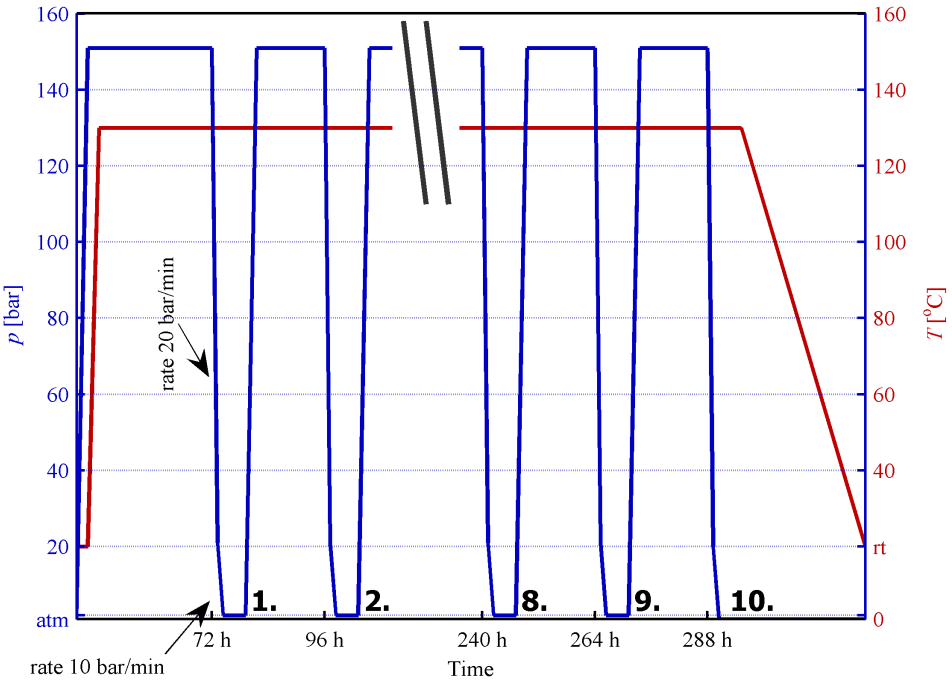

Fig. 5.54. Procedure of the rapid decompression test.

The samples for the test included the mainwall insulation G2 and resins C and A. Also complete bar samples were used in the tests. The bars were not tested with any diagnostic method. Their purpose was to see what the test environment causes for a complete bar, because the small cake samples of the mainwall insulation were seen to delaminate rather easily especially near the edges.

5.6.1 Physical appearance

The analysis is concentrated on the physical appearance and information on the previous tests. The diagnostic quantities were not measured, because the materials appeared to suffer so heavy damage. The material G2 after the test is illustrated in Fig. 5.55, resins C and A in Fig. 5.56, and the bar sample before and after the test in Fig. 5.57.

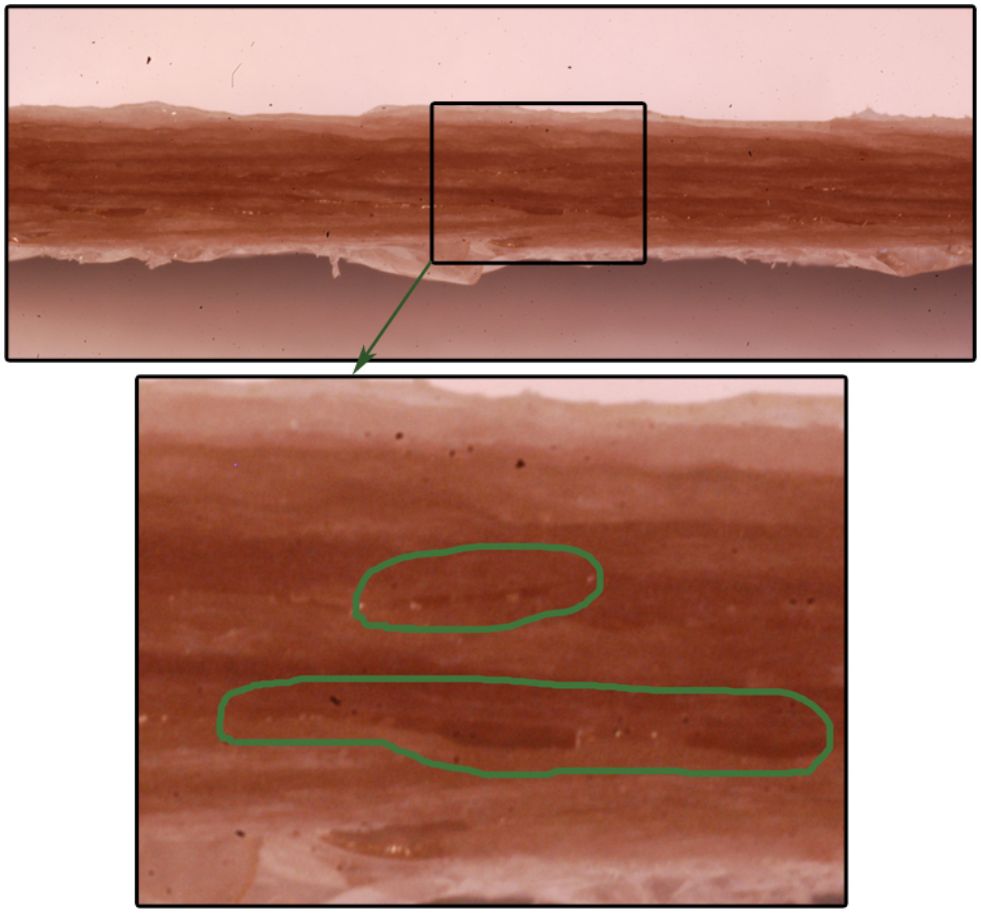

Fig. 5.55. Mainwall insulation samples after the rapid decompression test. The sample was submerged in water prior to photographing to emphasize the cracks. A few cracks are also highlighted.

The material G2 has suffered from distinct delamination, which can be seen in Fig. 5.55. The sample was destroyed almost completely. Delamination cracks were visible between almost every tape layer. Also the resins were heavily affected by the test. Both of them have suffered from internal changes, which can be seen in Fig. 5.56. These kinds of crystal structures were seen when the samples, which had absorbed wellstream gas, were heated above their glass transition temperature.

The severe damages observed in the mainwall insulation cakes and resins are not as such visible with the bar samples, but also the bar has suffered during the experiment. It can be seen in Fig. 5.57 that the color of the bar has changed. The copper is not shining through the insulation as it does in the reference sample. This indicates that the insulation has suffered from delamination as it is no longer transparent. The delamination can be seen in the end of the insulation in Fig. 5.57c. Yet, the insulation has still kept its form and the surface is

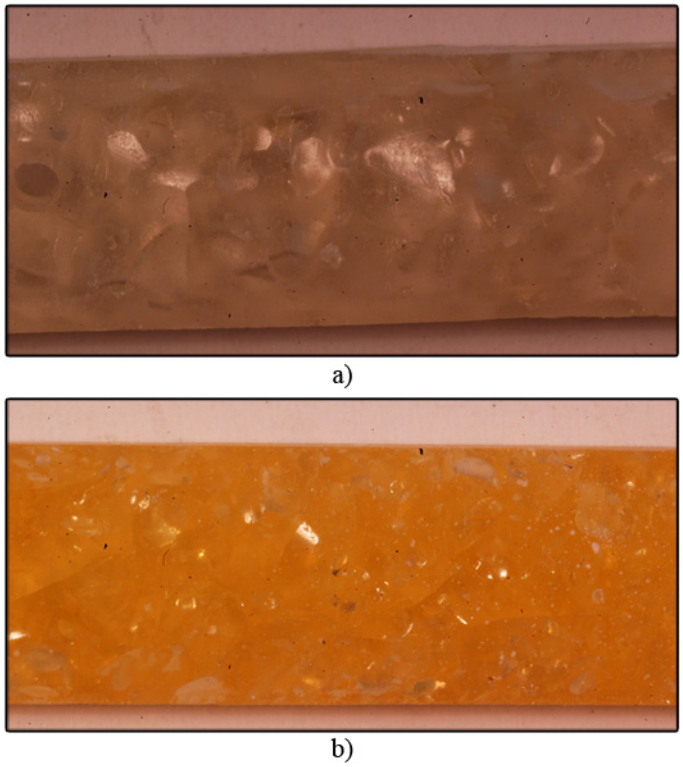

Fig. 5.56. Epoxy resin C (a) and A (b) after the rapid decompression test.

smooth. In similar experiments carried out earlier, the failure of insulation caused by rapid decompression was seen as blisters on the insulation surface; such were not found in the bar sample.

Internal cracks in the insulation caused by the pressure changes have been observed with high-voltage XLPE cables. This phenomenon, called environmental stress cracking, occurs in the insulation near the electrode in the presence of water. The oxygen is attached to the high-voltage electrode, and the remaining hydrogen diffuses into the insulating material. The diffused hydrogen becomes pressurized causing internal pressure changes in the material, which lead to the formation of cracks inside the insulation. Hvidsten et al. (2009) reported the cracks to be approximately 1 μm wide. Internal cracks of similar width (0.5 – 1 μm) were also found in resin A after the depressurization of the wellstream gas exposure, which is illustrated in Fig. 5.60 in the following section.

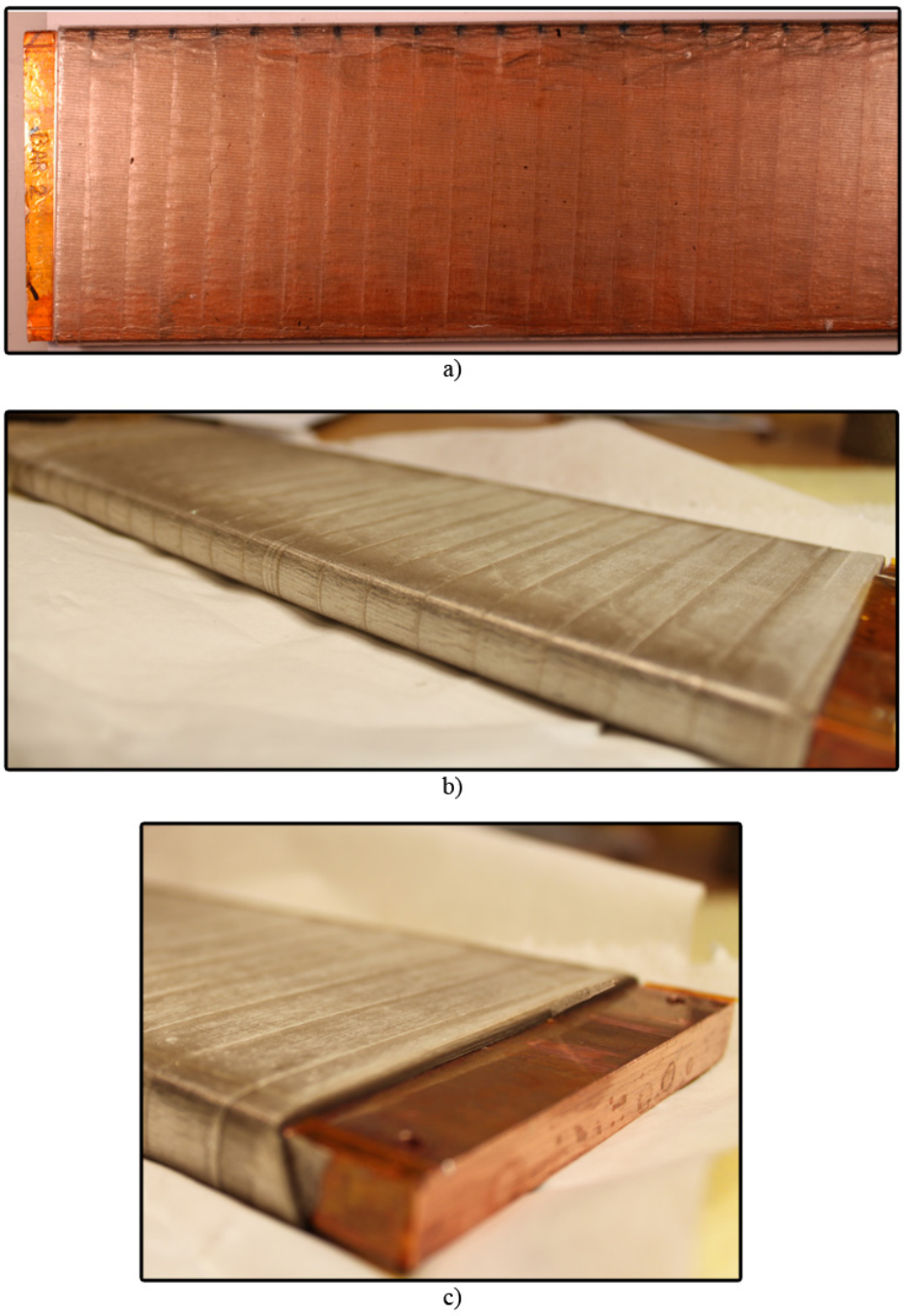

Fig. 5.57. Bar samples before (a) and after (b and c) the rapid decompression test.

5.6.2 Summary

The mainwall insulation cakes are seen to be badly damaged. This is related to their shape and size. Such samples are small and contain cutting edges, which are not present in the entire bar. During the diffusion process when the gas penetrates into the samples, it prefers the cutting edges over the smooth surface. Correspondingly, when the gas departs the material, it tends to flow through the cutting edges. This causes severe delamination. The diffusion and departure are discussed more closely in Section 5.7.

The results indicate that rapid decompression is a very harsh condition. The test procedure has probably been too severe for the materials. It has to be emphasized that all the depressurizations in this very test were carried out while the chamber was hot and the test specimens above the glass transition temperature of the resin. In the other tests, the chamber had been cooled before depressurization. Therefore, the pressure changes were not so severe for the other tests.

5.7 Aging of the insulation in the wellstream gas

So far, the preceding chapters have merely presented the observations made in the course of the study. The discussion on the results is presented here. The results are contemplated in new light with all performed tests taken into account. Furthermore, this section contains explanations on what has happened to the materials in the tests. The aging models presented in Section 2.5.1 have been discussed in the light of own results.

5.7.1 Physical integrity

The microscope image of the mainwall insulation G2 after the 750 h exposure to wellstream gas is illustrated in Fig. 5.58 and SEM images after the 3726 h exposure in Fig. 5.59, respectively. The SEM images of resin C are illustrated in Fig. 5.61 and of resin A in Fig. 5.60, respectively. The reference sample of resin C was not investigated with SEM.

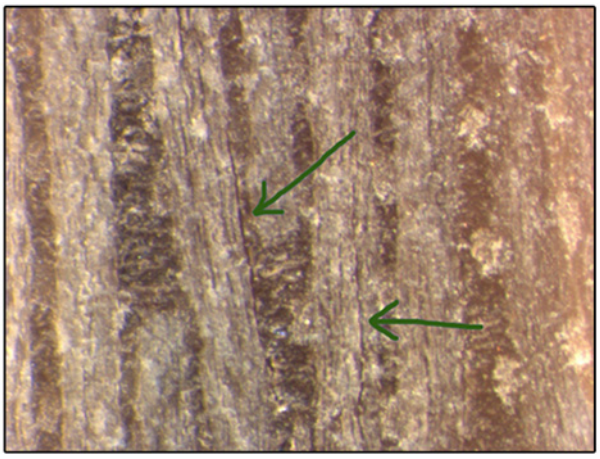

Fig. 5.58. Microscope image on the mainwall insulation G2 after 750 hours in the wellstream gas. The left arrow points to a crack between the mica layer and the epoxy layer. The right arrow indicates a crack within the mica layer.

It is evident in Fig. 5.58 that the mainwall insulation has experienced small cracks in parallel with the tape layers. The left arrow indicates a crack in the interface of the mica tape (lighter areas) and resin (darker sections). Interestingly, the right arrow points to the crack that has formed inside the mica tape between mica flakes. The SEM image, Fig. 5.59, illustrates the inner structure of the mainwall insulation with glass strains, mica flakes, and areas of epoxy resin clearly visible. The magnified section in the upper right corner illustrates the glass strains located perpendicular to the photographed plane. The blue arrows indicate gaps between the glass strains and the layer of epoxy resin. The resin has apparently detached from the glass strains. Correspondingly, the green arrow in the lower right image refers to the absence of epoxy binding on the glass strain. There seems to be no epoxy attached to the

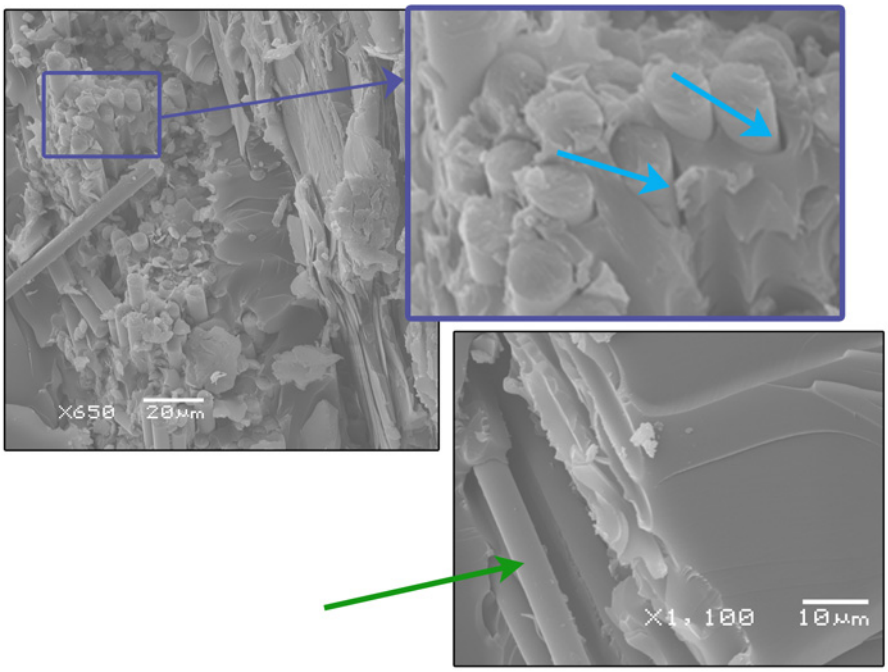

Fig. 5.59. SEM images on the mainwall insulation G2 after 3726 h in the wellstream gas. The blue arrows in the upper right corner point to gaps between epoxy and glass strains. The green arrow indicates that there is no epoxy attached to a glass strain.

strains in that area. The strains in the lower right corner are located in the opposite direction from the ones seen in the upper right corner. Prior to the SEM examination, the samples were broken into smaller pieces. Based on the images, the treatment has been rather violent, as the mica flakes were seen as disordered. The sample treatment may also have caused some detachment between the glass strains and epoxy. Nevertheless, during the SEM examination, the above conclusion was considered valid. Furthermore, it is supported by the lower right image in Fig. 5.59, in which the epoxy has disappeared from all around the glass strains; this cannot have been caused by external violence alone.

It has been reported that the composite insulation consisting of mica, glass, and epoxy is vulnerable in the interface of epoxy and glass. Jia et al. (2006) showed with SEM images that the epoxy detaches from the glass strands. Park (1987) reported that cracks in parallel with the tape direction are formed, when the insulation is stressed mechanically. The SEM images in Fig. 5.59 support the conclusion by Jia et al. (2006) that the delamination, as seen in Fig. 5.58, is caused by the reduced attachment between epoxy and glass.

It can be seen on the right in Fig. 5.60 that the structure of resin A (epoxy novolac resin) has suffered from internal cracks. The figure indicates that the exposure has caused irreversible changes. The resin structure was not perfect and contained some impurities, as seen on the left in Fig. 5.60, but the insulation built in an industrial process tends to include some impurities

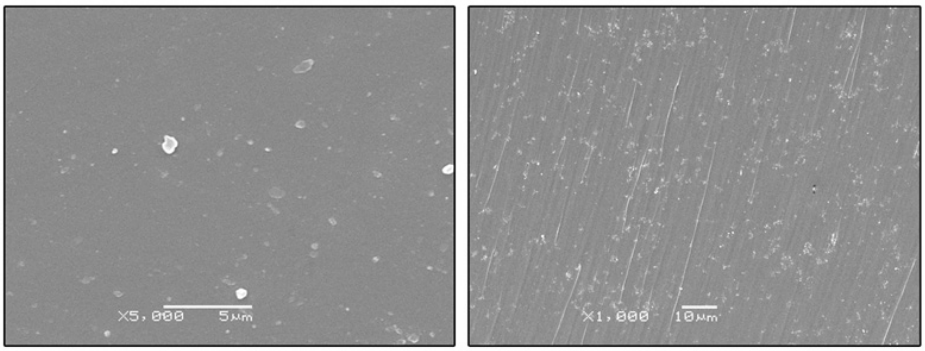

Fig. 5.60. Scanning electron microscope images on resin A before (left) and after (right) the exposure to the wellstream gas. The exposure duration was 3726 h. The cracks seen in the figure point to the nearest edge of the material.

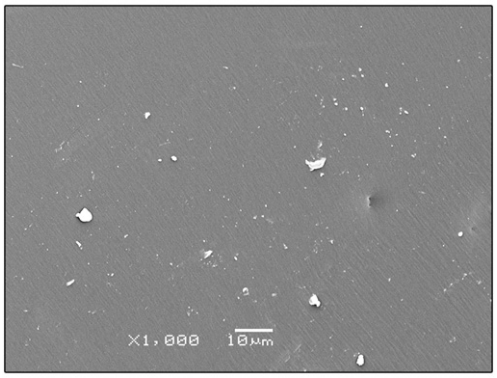

Fig. 5.61. Scanning electron microscope images on aged samples of resin C. Samples have been exposed to the wellstream gas for 3726 hours.

in any case. Only the samples built in the laboratory with extreme care and planning can be fully pure. The internal cracks cannot be seen in the resin C (bisphenol A anhydride resin) in Fig. 5.61, but impurities are present also in that one. Resin C absorbed more wellstream gas during the experiments, but it is a more flexible material. Hence, the SEM images support the conclusion that the impregnating resin C is more suitable than resin A. This conclusion could not have been made based on mechanical, or dielectric properties, glass transition temperature, or weight and volume data. On the contrary, such quantities rather favored resin A. Surprisingly, the internal cracks cannot be seen to affect the mechanical properties of the resin. Resin A was brittle after the exposures, but it was brittle also before them. The brittleness after the exposures may be linked to the internal cracks, without which the material could have appeared to have softened during the exposure, which was seen with resin C. Nevertheless, it has to be pointed out that the resin samples were tested as large samples, while they are designed to be impregnants of the whole mainwall insulation and to be applied only as thin layers. Therefore, it is not certain that such internal cracks are

present, when the resin is part of a complex insulation system. In addition, resin C suffered from internal cracks in the rapid decompression test.

The cracks formed inside resin A appear to be aligned. They may have been formed ultimately in the depressurization procedure, when some of the gas absorbed is forced out of the material. The cracks are formed in parallel with the direction in which the gas has flown. The molecular structure of resin A has been too stiff to reorganize itself when the gas has departed and left sections inside the polymer matrix empty. The polymer matrix has collapsed in these areas and the cracks have been formed. Alternatively, the cracks have formed when the gas has simply elbowed its way to the surface by cutting the bonds that stay in its way. The formation of cracks is illustrated later in Fig. 5.65. The structure of resin C, on the other hand, is more flexible and able to reorganize itself when the gas is leaving the insulation. Figure 5.60 indicates that also irreversible changes take place during the exposure to the wellstream gas, and the changes observed are not merely due to diffusion. Therefore, by the definition by IEC (2004), the phenomenon can be referred to as 'aging'.

5.7.2 Mechanical strength

Microscope images of the breaking points of the G2 mainwall insulation after the three-point bending tests are illustrated in Fig. 5.62. The figure illustrates the aging phenomena. It can be observed that the reference sample breaks so that some parts delaminate and the crack extends towards the surface. The aged sample experiences only delamination, which extends so far in horizontal direction that the overall strength of the sample is weakened. The aged sample does not experience a crack, which extends through the tape layers. The strength that keeps the adjacent tape layers together is much weaker than the strength of a single tape layer. With a reference sample, the strengths are theoretically equal.

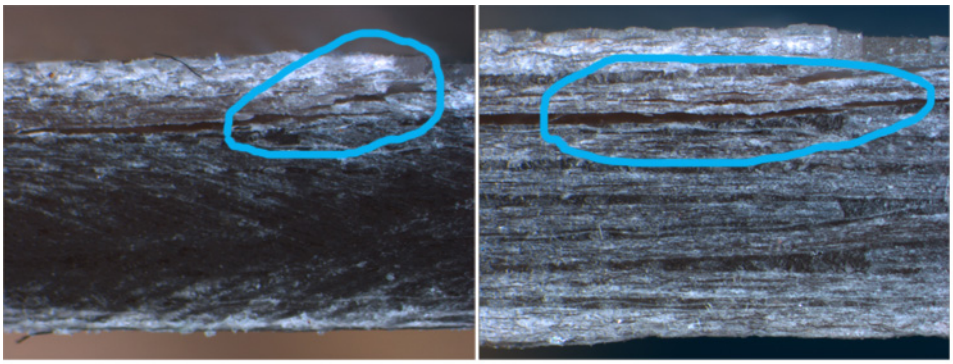

Fig. 5.62. Breaking point of material G2 after the three-point bending test. The reference sample on the left and the sample that has experienced wellstream gas exposure (750 hours) on the right.

Figure 5.62 supports the aging symptoms stated above and reported by Park (1987) and Jia et al. (2006). In the composite insulation structure, the attachment of epoxy to the glass

strands or mica flakes is weakened during the aging. The tape layers are separated from each other, and the mechanical strength of the composite insulation structure is thus reduced. The delamination of the insulation is even more severe, if the insulation is not thoroughly impregnated with the resin.

5.7.3 Dielectric properties

The dielectric properties of the mainwall insulation sample face slight changes during the exposure to wellstream gas. The dielectric constant of the insulation, that is, the real part of complex permittivity, reduces during the exposure. On the other hand, the dielectric losses increase. The changes are caused by the hydrocarbon compounds that the insulation absorbs. In the long-term exposure, the loss peak was notably increased, even though the other quantities remained almost at the same level as compared with the exposure for 750 hours. The insulation resistance did not significantly decrease in the long-term test.

The dielectric losses after 3726 hours of exposure were roughly 7.5 times the losses in the reference sample. The high-frequency permittivity ϵ_∞ has reduced by 46%. These quantities do not directly indicate a reduction in the dielectric strength, because the insulation resistance remained high. Rather, they indicate diffusion and delamination. Higher dielectric losses cause additional heat to generate and they can possibly increase the temperature of the insulation. However, it was pointed out in Section 5.4 that the insulation under the given conditions is not sensitive to small changes in temperature. Furthermore, partial discharge activity is not related to the dielectric losses, in other words, the increased losses do not increase the partial discharge magnitude. Therefore, the increased dielectric losses are not as severe a symptom as in a traditional industrial machine.

Regarding the wellstream gas environment, it is likely that the delamination of the tape layers takes place without an electrical breakdown. The delaminated mainwall insulation structure may still have fair dielectric strength, as all the layers of mica tape are still between the conductors. The delaminated sections are filled with pressurized gas, which does not enhance the progress of an electrical breakdown as fast as atmospheric air. Hence, the theory presented by Montsinger (1930) for mica-asphalt insulation that the mechanical strength is lost at first and the dielectric strength as its consequence, seems reasonable.

5.7.4 Chemical reactions in the epoxy anhydride resin

Changes in the chemical structure of bisphenol A epoxy anhydride resin were observed at 1801 cm^{-1} and in the range between 950 – 850 cm^{-1}. According to the reference material of the instrument (Hannah; PerkinElmer), the former change can be attributed to the carbonyl compound illustrated in Fig. 5.63. It can be seen in Fig. 2.4 that the anhydride component contains these carbonyl groups. It was concluded in Section 5.3 that these changes are caused by the produced water, not by hydrocarbons or MEG.

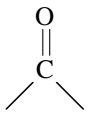

Fig. 5.63. Carbonyl compound attributed to the peak at 1801 cm^{-1} in the IR spectra.

During curing, the bisphenol A epoxy resin reacts with the anhydride curing agent so that a number of the epoxy groups react with the anhydride groups of the curing agent forming a complex chemical structure, as described above in Fig. 2.4. The epoxy chains are connected to each other by anhydride groups. When water is diffused into the material, it reacts with the anhydride groups by breaking the carbonyl compound seen in Fig. 5.63. The reaction causes new OH groups to form at both sides of the broken bond. The reaction is seen as a reduction of corresponding groups in the IR spectra, for instance in Fig. 5.28. The chemical reactions were seen to take place within the first 750 h of aging. This suggests that the anhydride groups attributed to the peak in the IR spectrum are the ones that have not reacted during the curing process. This is supported by the lack of correlation between the chemical changes and the mechanical properties. The reaction sites are located in the lone branches of the polymer chains, and the reactions do not involve the bond scission in the primary molecular chain. Therefore, the strength of the primary molecular structure is not affected.

The other reaction seen in the IR spectra of the bisphenol A epoxy resin, for instance in Fig. 5.28, takes place in the range between 950 – 850 cm^{-1}. The change is not as clear as the former, but it indicates the disappearance of the small peak observed at 915 cm^{-1} in the reference curve. This peak most likely points to the asymmetric stretching mode of the epoxy group. Such a peak takes place at different wave numbers depending on the epoxy structure (with many epoxies it is located at wave numbers smaller than 900 cm^{-1}). For the bisphenol A, the epoxy group has been reported to exist between 916 and 912 cm^{-1} (Cherdoud-Chihani et al., 2003; Sánchez-Soto et al., 2007; Denq et al., 1999; Kimura et al., 1998). These epoxy groups have not reacted in the curing process, but it does not mean that the curing has been incomplete. The reaction of these groups would have needed a larger amount of curing agent, which as such could have caused changes in the performance. The reaction of water and epoxy group includes the opening of the epoxide ring resulting in additional OH groups to form. The formation of new OH groups, both in this reaction and with the anhydride group, cannot be detected in the IR spectra, because the spectra already contain so many OH groups. Correspondingly with the reactions attributed to anhydride groups, these reactions were seen to occur within the first 750 h of aging and not to affect the mechanical properties. Thus, there is a certain amount of remaining epoxide groups, which can possibly react, and they all react within the first 750 h of aging. The reactions of epoxide and anhydride groups are not necessarily connected to each other. The amounts of data and experiments are too limited to fully determine this. The evolutions of the peaks are not fully comparable with respect to different gas mixtures in Figs. 5.28 and 5.29.

It is clear that chemical changes take place inside the bisphenol A epoxy resin. However, the only diagnostic method used in this doctoral thesis was the FTIR spectroscopy, which in many occasions is not the most informative one, and does not give clear information on which kinds

of reactions have taken place. Furthermore, it definitely does not give the reaction formulas. It only gives information on the chemical structure before and after changes have occurred. The explanations given above are only theories indicating that the reactions have probably taken place accordingly. A more thorough chemical analysis is needed to confirm them.

5.7.5 Diffusion

The aging of insulating materials is related to the diffusion of the gas mixture into the insulation. As the gas penetrates into the epoxy resin, the glass transition temperature reduces and the mechanical properties decrease. The resin becomes softer and more flexible. Therefore, the wellstream gas acts as a plasticizer inside the epoxy resin. Plasticizers are used in hard and brittle plastics, such as PVC (polyvinyl chloride), to increase their flexibility. They infiltrate into the polymer matrix, but do not chemically react with the polymer. When penetrating, the plasticizers force the polymer chains to move further away from each other creating more free volume between the chains. This is seen as a volume increase of the material.

The plasticizing effect of the wellstream gas is linked to heavy hydrocarbon compounds (hydrocarbon condensate). Water, on the other hand, is a small molecule and its diffusion is not causing so much internal disorder in the material. However, the nature of diffusion is dependent on the material. It was pointed out in Section 5.3 that the bisphenol A epoxy anhydride resin absorbs large amount of hydrocarbon condensate, whereas the epoxy novolac resin tends to absorb more water. The difference can be explained by the chemical compositions of the materials.

Epoxy novolac resin is hydrophilic containing relatively many OH groups. There are no OH groups present in the chemical structure, Fig. 2.3, but they are formed in the curing reaction. Its chemical structure, therefore, has similarities with the structure of water. The OH groups of these two molecules tend to interact, which is seen as high water absorption. By contrast, the chemical structure does not attract hydrocarbon molecules. Furthermore, the chemical structure of epoxy novolac resin is very dense. The structure contains many epoxy groups, and if they all react, the crosslink density is high, resulting in the brittle nature of the resin. A dense structure contains less free volume, which makes it more difficult for large molecules to diffuse into the polymer matrix. Therefore, the hydrocarbon compounds do not penetrate into the epoxy novolac resin as easily as they diffuse into the bisphenol A epoxy resin, the crosslink density of which is lower.

The diffusion of the wellstream gas into the epoxy anhydride resin occurs more easily than in the novolac resin. The chemical structure of the bisphenol A epoxy resin enables greater flexibility of the epoxy system. The epoxy groups are further away from each other than in the epoxy novolac resin, as was earlier mentioned with reference to Fig. 2.2 and Fig. 2.3, resulting in the crosslinking groups (anhydride groups) to exist further from each other. Such a structure has apparently more free volume inside the polymer matrix and it can also be more flexible. The applied force is allowed to bend the chains a little, because their support beams (crosslinking groups) are located further apart, and a force does not easily break bonds in the crosslinking groups, that is, cut the crosslinks. Hence, the wellstream gas can diffuse

more easily into the bisphenol A anhydride resin than into the epoxy novolac resin. The sparse chemical structure is also more easily reformed enabling a higher volume increase. On the other hand, the flexibility allows better resistance to internal cracks, when the gas diffused inside the polymer structure is departing. Yet, rapid decompression also causes internal cracks in the bisphenol A resin.

The diffusion process was not closely investigated. Because of the too long test durations, the diffusion coefficient was not determined. This is unfortunate and disappointing. However, the definition of such a quantity is not important with respect to the long-term performance of the insulation in wellstream gas, because it was stated in Section 5.5 that the diffusion does not progress further after 750 hours with epoxy resins. The epoxies meet the saturation of their absorbance. Therefore, the diffusion of wellstream gas into epoxy resins follows Fick's second law, Eq. (2.8). However, the diffusion into the mainwall insulation did not give clear information on saturation, as it seemed to have climbed after 750 hours. This supports the statement that the diffusion of wellstream gas into composite insulation does not follow Fick's second law. This has been reported by many authors (e.g. Fukuda et al., 1997; Fernández-García and Chiang, 2002; Maggana and Pissis, 1999), who have studied the diffusion of water into epoxy resins that contain fillers. It has been stated that such a diffusion process contains two separate diffusion processes, which both individually follow Fick's second law (Maggana and Pissis, 1999). This has also been reported for mainwall insulation (Hong et al., 2009a). Nevertheless, the diffusion coefficient will most likely be different in operating conditions, which involve less liquids in the gas, lower pressure, and lower temperature. However, information on the diffusion coefficient would probably have been fruitful.

The diffusion process as described here is practically almost irreversible. The changes observed in the chemical structure of the bisphenol A epoxy resin are minor and were not seen to have significant effects on the properties of the material. Therefore, the materials are expected to revert close to their initial behavior, when the hydrocarbons in them are removed. Hence, the phenomena observed would not resemble "aging" as described by IEC (2004), because the changes could be reversed.

However, it was seen that it is virtually impossible to remove the hydrocarbons from the materials without breaking them. It was seen that neither a vacuum treatment at room temperature nor heat treatment (close to T_g) at atmospheric pressure could remove them. With such methods, water could be removed. If heated above the T_g, the resins experienced internal cracks and bubbles as the hydrocarbons evaporated and the resins could not hold their structures. As seen in the results shown in the previous sections, the depressurization does not remove all the hydrocarbons, but causes internal cracks in the epoxy novolac resin as seen in Fig. 5.60. Also rapid decompression at the temperature above T_g causes internal cracks as shown in Section 5.6. It would have required careful treatment in laboratory conditions to remove the hydrocarbons from the material samples.

The diffusion process in general contains some irreversible features. Studies on the diffusion of water into epoxies by Xiao and Shanahan (1998) showed evidence on irreversible effects of the diffusion. They reported that a small amount of water may get permanently infiltrated

into the polymer structure of the resin and cause permanent reduction in the glass transition temperature of the epoxy. For the difficulties in the removal of the hydrocarbons mentioned above, such an effect was not investigated in this thesis.

The insulating materials experience the diffusion not as aging or degradation, but rather as a change into a different state. The hydrocarbons penetrate into the polymer matrix and force the molecular chains to set differently. The chains are reformed into a less energy efficient form, and there are internal tensions between the chains. Therefore, the external energy needed to cut the molecular chains is lower, which is seen as a reduced mechanical strength. If the hydrocarbons are gently removed from the polymer matrix, the chains reorganize back to their original places, and the initial properties of the material are restored. If the removal process is not gentle, the motion of hydrocarbon molecules may cut some of the polymer chains. This is illustrated in the following section.

5.7.6 Effect of pressure gradients

The pressure changes cause severe and irreversible deterioration as pointed out in Section 5.6. During the test conditions the specimens are partly filled with the gas. Furthermore, the resin is relatively soft, because it is above its glass transition temperature. When the pressure suddenly drops, the gas departs from the material. The volume of the material is suddenly decreased and the molecular chains are forced to move. When the gas has departed from the material, the glass transition temperature increases as the penetrating species no longer cause internal disorder in the molecular matrix. As the motion of the molecular chains ceases, the material turns into glass. If the molecular chains do not get reorganized before the material turns into glass, the structure will contain anomalies, which can be seen as crystallized structures in Fig. 5.56.

However, this kind of behavior can be assumed irreversible, because the materials should basically get organized again when the pressure is increased and a new amount of gas diffused. This means that before the depressurization runs, the materials are in equilibrium states. Certainly, such a glass transition effect is not expected to cause cracks inside the material. Therefore, another approach is needed. The materials are in equilibrium when the diffusion process has has been going on for a reasonable amount of time. At that point, the conditions can be illustrated as in Fig. 5.64. Even though it was not stated in Section 5.4, the diffusion of wellstream gas into mainwall insulation is expected to saturate completely. The depressurization is illustrated more closely in Fig. 5.65.

In equilibrium, the pressure p_1 of the gas inside the insulation is equal to the pressure p_2 of the surroundings. Accordingly, the chemical potential μ_1 inside the insulation is equal to the chemical potential μ_2 of the surroundings. During the depressurization, the pressure p_2 and the chemical potential μ_2 of the surroundings rapidly change, but the ones inside the insulation (p_1, μ_1) are not changed. Therefore, each gas particle inside the insulation are forced to flow out of the insulation. The force F_i appears towards the chemical bonds that lie in the way, as seen in Fig. 5.65a. The force F_i that causes a single gas particle to move can be expressed as

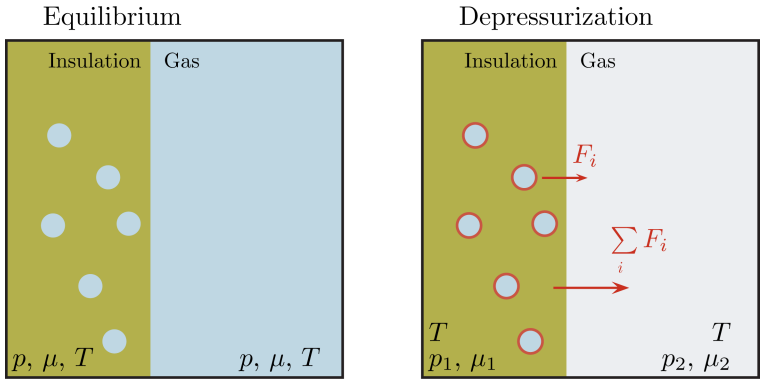

Fig. 5.64. Thermodynamic conditions of the gas and insulation in equilibrium and depressurization states.

$$F_i = (p_2 - p_1)A_i \tag{5.9}$$

The gas particle may go around the adjacent chemical bond (solid green in Fig. 5.65a), which stands on its way. Alternatively, the gas particle may go through by breaking the bond. Whichever way it proceeds, there is an area of low pressure p_3 behind it (white area in Fig. 5.65b). The molecular chains A and B on both sides of the gas particle in the equilibrium state are now forced by $F_{\text{chain, A}}$ and $F_{\text{chain, B}}$, respectively, to move back to their original places. These forces create stresses to the bonds marked with yellow in Fig. 5.65b. The departure of the gas may cause either the green or yellow bonds to break. In either case, the result is a crack, which extends straight towards the surface, as seen in Fig. 5.65c and in reality in Fig. 5.60.

The enthalpy, entropy, and Gibbs free energy of the wellstream gas mixture as functions of pressure are illustrated in Fig. 5.66. Enthalpy and entropy are defined by calculations on the flash conditions of the gas mixture with PVTSim software. The Gibbs free energy is calculated according to Eq. (2.7).

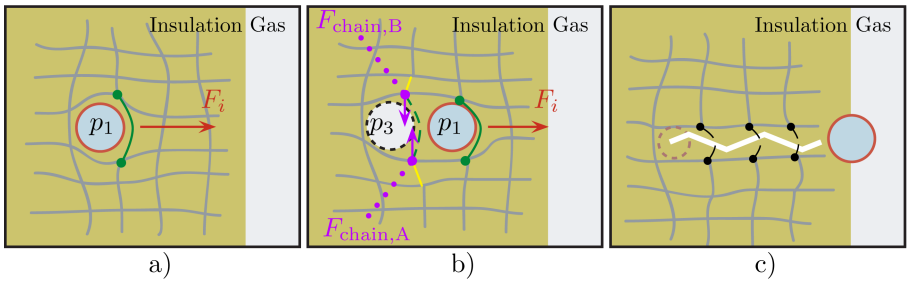

Fig. 5.65. Departure of the diffused gas from the insulation as seen at the molecular level. The grey network indicates the molecular structure.

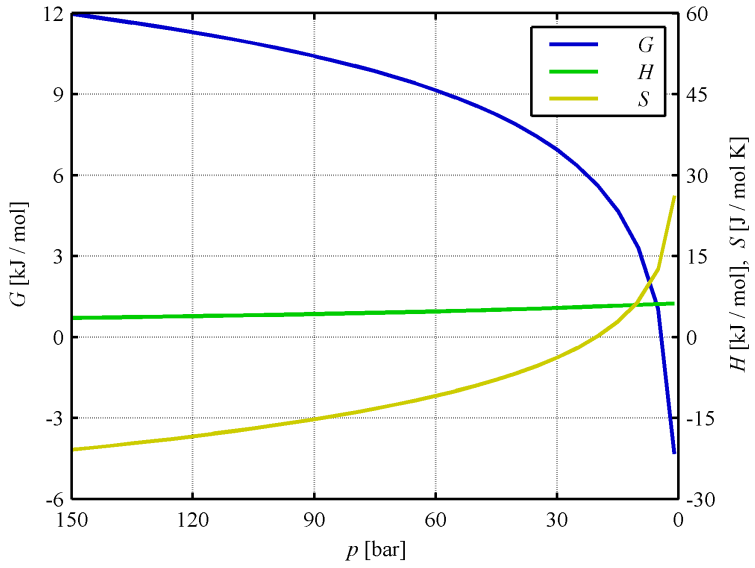

Fig. 5.66. Gibbs free energy G, enthalpy H, and entropy S as functions of pressure. The temperature is 130 °C.

The change in the Gibbs free energy is most rapid in the pressure range close to atmospheric pressure. The Gibbs free energy is the sum of the particles in the thermodynamic system multiplied by their chemical potentials:

$$G = \sum_i \mu_i N_i \tag{5.10}$$

The change in the Gibbs free energy is related to the change in chemical potentials, which in the equilibrium state are same both inside and outside of the insulation. The amount of Gibbs free energy per a single pressure step is at highest near the atmospheric pressure. This is related to the volume of the gas. Under high pressure, the gas is compressed and its volume hardly changes as a result of small pressure gradients. Near atmospheric pressure, the gas is less compressed and allowed to expand or contract as a result of pressure gradients. Therefore, the volume of the insulation is virtually constant during the pressure gradients at high pressure, but it changes accordingly under the pressure gradients near atmospheric pressure. The change in volume creates additional forces inside the molecular structure. Thus, the reason for bond scission and formation of internal cracks is not only the force in Eq. (5.9), but the combination of that and other forces including the ones created by the expansions of the gas and the insulation. In other words, the case is too complicated to be approached in this way. Equation (5.9) is not valid, because it gives the highest force at high pressure. The volume change is included in the Gibbs free energy in Fig. 5.66. Therefore, the depressurization has the most severe influence near the atmospheric pressure.

5.7.7 Lifetime of insulation

The tensile strength and the E-modulus as functions of weight increase for the G2 mainwall insulation are illustrated in Fig. 5.67. The E-modulus and glass transition temperature of the resins as functions of weight increase are illustrated in Fig. 5.68. Curve fits are made based on the exposures to the environments that contain hydrocarbons: ***Wellstream*** for various durations and temperatures, ***Cond***, and ***Sales gas***. ***HC + MW*** exposure was not included in the curve fits, because it did not follow the trend with the G2 mainwall insulation. Such an environment had an effect more similar to that of liquid environments. Nevertheless, all the test environments are illustrated in the figures mentioned above. The ***Wellstream*** exposures for 1500 h and 2000 h, which contained only resin samples, were considered as failed experiments in Section 5.5. They involved similar, too fast depressurization as the experiment described in Section 5.1, which is labeled as ***WS 750h*** in Fig. 5.68. Therefore, the results were not comparable with the other exposures in the methods used in the preceding sections. Nevertheless, with a few exceptions, the test results follow the trend, if the properties are discussed as functions of weight increase, as can be seen in Fig. 5.68.

Curve fits have not been made for resin A, because the data was too widely scattered. The curve fit of the glass transition temperature for resin C does not take the ***WS 170*** and ***WS 3726*** exposures into account. It was stated in Section 5.4 that the ***WS 170*** exposure further reduced the glass transition temperature. The reason for the reduction could not be fully clarified.

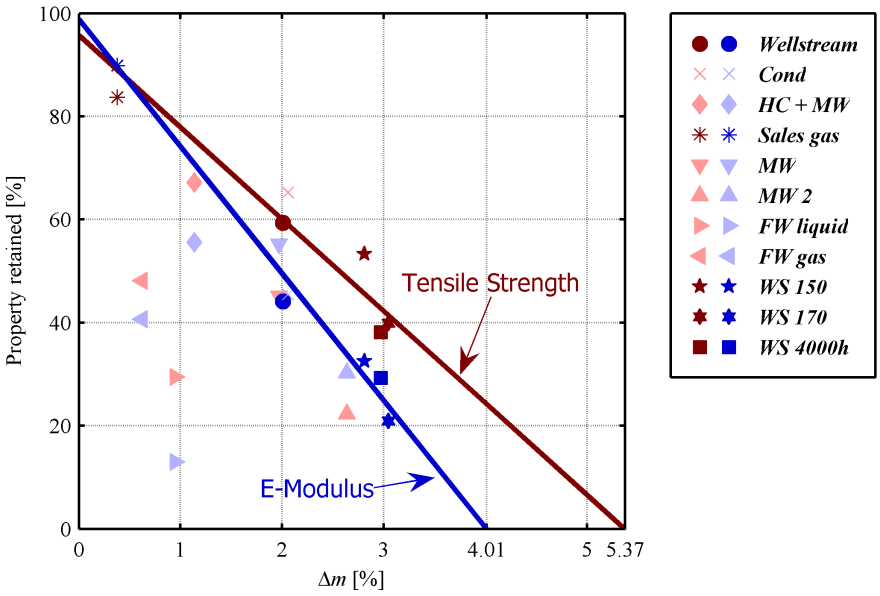

*Fig. 5.67. Tensile strength (left) and E-modulus (right) of the G2 mainwall insulation as functions of weight increase. Curve fits are drawn based on the data from the **Wellstream** (750 h and 3726 h, and also at 150 °C and 170 °C), **Cond**, and **Sales gas** exposures.*

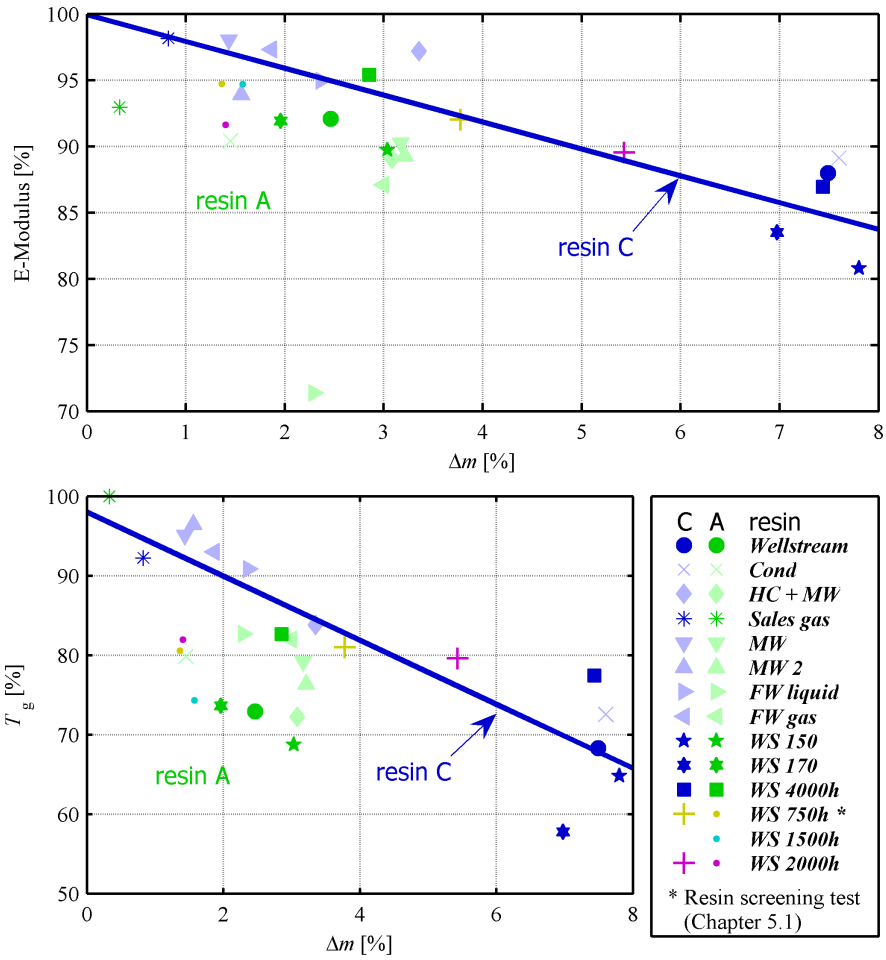

Fig. 5.68. E-modulus (top) and glass transition temperature (bottom) of resin C and resin A (right) as functions of weight increase.

With the ***WS 3726*** exposure, the glass transition temperatures shown in Section 5.5 appeared higher than expected because of the different measuring scheme and equipment. It can be seen in Fig. 5.68 that these two markers depart considerably from the trend line. Actually, they depart in different directions, whereupon their inclusions would not have significantly affected to the curve fit. Interestingly, the experiments considered earlier as failed appear to follow the general trend in Fig. 5.68. The amount of liquids in the samples did not correlate with the test duration, but it correlates with the properties of the materials.

According to Fig. 5.67, the properties of the mainwall insulation G2 appear to be dependent on the amount of the wellstream gas they have absorbed. With resins, the relationship is not that clear (Fig. 5.68). The curve fitting equations are written as

$$\text{G2, Tensile strength :} \quad \sigma_\text{f} = -17.8\Delta m + 95.7 \tag{5.11}$$

$$\text{G2, E-modulus :} \quad U_\text{E} = -24.7\Delta m + 98.8 \tag{5.12}$$

$$\text{resin C, E-modulus :} \quad U_\text{E} = -2.03\Delta m + 99.9 \tag{5.13}$$

$$\text{resin C, Glass transition temperature :} \quad T_\text{g} = -4.03\Delta m + 98.0 \tag{5.14}$$

where the quantities σ_f, U_E, and T_g are expressed as percentages of the initial property. By extending the trend line of the G2 mainwall insulation, it can be seen that the E-modulus is completely lost when the weight increase is 4%, and the tensile strength, when the weight increase is 5.37%. Therefore, the insulation has to break down at 4% at the latest. Such an estimate cannot be defined for the plain epoxy resins. Their data are too widely scattered for that. Furthermore, the weight incease required to cause the E-modulus of resin C to reduce to zero is over 49%, which is far from reach. Nevertheless, it is not realistic to use the value of 0% of the property remaining as an end-point criterion. The insulation must break down some time before its strength is reduced to zero.

The properties of the G2 mainwall insulation appear to be linearly dependent on the weight increase. Thus, also the lifetime is linearly dependent on the weight increase, which appears to be dependent on the time of exposure in the given environment, but not linearly. It was concluded in Section 5.5 that the weight increase is likely to follow the curve defined for resins with fillers, as illustrated in Fig. 2.6. The weight increase as a function of time is illustrated in Fig. 5.69 with the curve fit according to Eq. (2.10). The curve fitting estimates that the curve will be saturated at approximately $\Delta m = 3.06\%$ and the diffusion coefficient is $4.11 \cdot 10^{-4}$ mm^2/h.

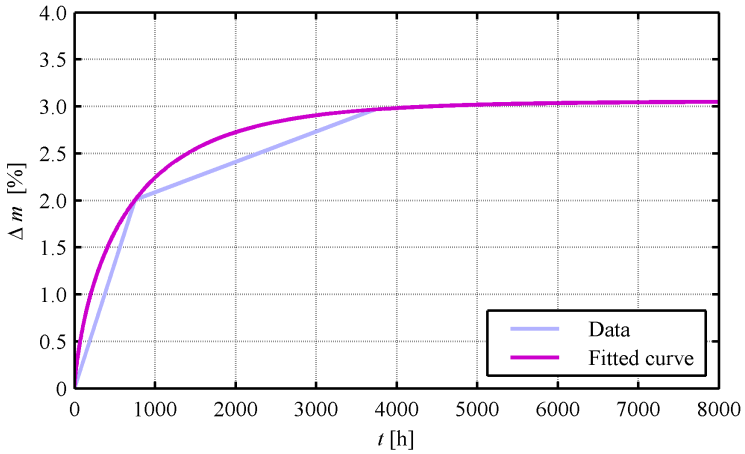

Fig. 5.69. Weight increase of G2 mainwall insulation as a function of time. The curve fit is defined according to Eq. (2.10).

The curve fitting suggests that there is only little additional diffusion after the long-term test duration (3726 h). The tensile strength of G2 mainwall insulation in saturated conditions is

according to Eq. (5.11) 41.1% of the original, and the E-modulus according to Eq. (5.12) 23.4%, respectively. Based on the fit in Fig. 5.69, it takes approximately 7000 h (approx. 292 days) to reach these values. A common determination for the end-point is that the mechanical strength is reduced by 50% (Stone et al., 2004). According to Eq. (5.11), this is met at 2.56% weight increase. The time required for this can be calculated from Eq. (2.10) as

$$t = \frac{d^2}{D}\left(\frac{1}{7.3}\right)^{4/3}\left|\ln\left(1-\frac{m_t}{m_\infty}\right)\right|^{4/3} \tag{5.15}$$

With corresponding parameters, the time for 2.56% of weight increase is 1534 h. This would be the lifetime estimate for such conditions. It cannot, however, represent the lifetime of the insulation in the windings of an actual electrical machine. The small cakes used in the aging experiments are more vulnerable to delamination during the depressurization of the test, which was pointed out in Section 5.6. Furthermore, the conditions inside the natural gas compressor are less harsh, with less heavy hydrocarbon compounds and water in the gas. Thus, the diffusion in such conditions is espected to be significantly smaller. The diffusion is related to the composition of the gas, as was concluded in Section 5.3. The parameters given above represent the accelerated conditions. Considering the thermodynamic states of the accelerated conditions and the real conditions, particularly the dew point and temperature, it is likely that the saturation value of weight increase m_∞ is below the end-of-life value, 2.56% in the subsea compressor. However, to properly determine the lifetime estimate, the diffusion parameters have to be determined for real conditions, and this has to be done with more markers than in Fig. 5.69. The above-mentioned estimates for D and m_∞ are not accurate, because the curve fit is determined based on only three points in the curve, and one of the points is zero.

The general lifetime equation can be defined based on Eqs. (5.11) and (5.15). The former equation describes only the curve fit in Fig. 5.67. It can be generalized by changing the percentages into real values and by denoting the slope as a constant A. This yields:

$$\frac{\sigma_\mathrm{f}(m_\mathrm{t})}{\sigma_\mathrm{f}(0)} = -Am_\mathrm{t} + 1 \tag{5.16}$$

If the end-point criterion is considered as half of the initial strength as above, the left-hand side of Eq. (5.16) becomes 1/2. Therefore, by substituting that and Eq. (2.10) to m_t, becomes:

$$\frac{1}{2} = Am_\mathrm{t} = Am_\infty\left[1-\exp\left\{-7.3\left(\frac{Dt}{d^2}\right)^{0.75}\right\}\right] \tag{5.17}$$

Now, time t is the lifetime L and it can be solved as:

$$L = \frac{d^2}{D}\left(\frac{1}{7.3}\right)^{4/3}\left|\ln\left(1-\frac{1}{2Am_\infty}\right)\right|^{4/3} \tag{5.18}$$

The lifetime is determined based on the diffusion process. It is not, in this case, dependent on temperature, which was not seen to affect the saturation value m_∞. However, the temperature may have an influence on the diffusion coefficient D and thus on the weight increase at a certain time m_t. Yet, it is not reasonable to formulate the lifetime equation, Eq. (5.18), as such was formulated by Montanari and Mazzanti (1994) in Eq. (2.4) and by Crine (1991) in Eq. (2.6) by including the term $h/k\Theta$ and thermodynamic potentials. The test program carried out did not provide enough information for that. It has to be emphasized that Eq. (5.18) is empirical and does not work with common thermal or electrical aging experiments. It can potentially work when diffusion is the dominating aging process.

Based on this rough approximation, the insulation system G2 is expected to withstand the conditions in long-term operation. The diffusion phenomenon, which is considered the dominating aging effect, does not cause too much reduction in strength during steady-state operation. Still, the lifetime estimate given here is merely a detail. The true value of the chemical aging test procedure lies in the observations on the material properties, how they behave, and how they are dependent upon the weight increase caused by the diffusion process.

The diffusion reduces the strength of the material, as has been stated. It also reduces the materials' ability to tolerate additional stresses caused by for instance depressurization. The failure of insulation as a result of these processes can be illustrated as in Fig. 5.70, which is based on Fig. 2.5. Even though the empirical lifetime equation, Eq. (5.18), is not capable of defining the potential wells, they can be discussed macroscopically. The potential well approach states that the diffusion process provides a certain energy, which participates in the breakdown process. The lifetime equation (5.18) is assuming that all the energy needed to reduce the mechanical strength by 50% is provided by diffusion, which practically was the case in the chemical aging tests carried out. The reduction of mechanical strength by 50% is now illustrating the aging needed to make the insulation so weak that a sudden pressure change can break it.

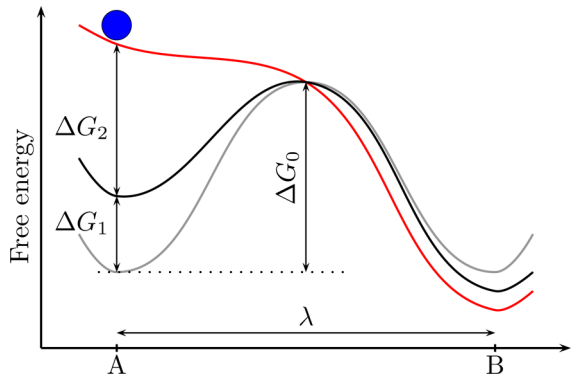

Fig. 5.70. Potential wells, original (A) and failure (B). The grey curve represents new insulation, the black curve the insulation after diffusion process, and the red curve the insulation after a sudden and high pressure change. The thermodynamic state of the insulation is represented by the blue ball.

The diffusion process is associated with the Gibbs free energy ΔG_1, which reduces the

strength of the insulation. During a rapid pressure drop, the Gibbs free energy of the surrounding gas suddenly reduces according to Fig. 5.66, while the Gibbs free energy of the gas inside the insulation remains unchanged. Hence, there is "available" Gibbs free energy ΔG_2 released for mechanical work. The work is done for lifting the potential in the well A. If the pressure gradient is high, the Gibbs free energy of the well A, that is, the sum $\Delta G_1 + \Delta G_2$ exceeds the energy barrier ΔG_0. As a consequence, the ball representing the state of the material can roll downhill towards the well B. The state of the insulation is then changed from "original" to "failure," which is seen as the breakdown of the insulation. The diffusion process provides the first steps towards the peak of the energy barrier, which is ultimately reached with the aid of some additional stress, such as rapid pressure changes. The diffusion process extends towards an equilibrium, which is indicated by the weight increase at saturation m_∞. When this is reached, the weight increase is not likely to change. Therefore, in steady state conditions the Gibbs free energy of the diffusion ΔG_1 in Fig. 5.70 remains constant.

The diffusion of the wellstream gas into insulation is practically an irreversible phenomenon, the reversion of which causes irreversible changes in the materials. This would justify the use of the term 'aging' as described by IEC (2004). However, it is really difficult to quantify the term 'aging'. Regarding the application and operating conditions, the diffusion is about a permanent change of state in the materials, because the hydrocarbons cannot be removed under service conditions. On the other hand, the diffusion process is stopped when the polymer has saturated with the penetrant. At this point, it cannot absorb any more penetrant. Correspondingly, aging in the insulation stops in saturated conditions, when the equilibrium has been reached. However, the equilibrium in this case refers to a constant current through the insulation, at which point the layer of insulation has turned into a layer of conductive material. The general forms of aging, such as tree growth caused by partial discharges or deterioration caused by chemical reactions under high temperature, extend towards the failure state. The diffusion process, on the other hand, does not really intend to break the insulation, but only to make it weaker. After the diffusion process and the change of state, the material can tolerate significantly less of typical forms of aging as can be seen in Fig. 5.70. Therefore, it is practical in this case to discuss the diffusion process as one form of aging.

5.7.8 Validity of the aging test matrix

The test matrix was illustrated in Fig. 3.2. The tests carried out have provided information on the aging of the insulating materials and also provided a rough lifetime estimate and information on the aging phenomena. Yet, improvements could be made.

For material comparison, the test matrix was chosen appropriately. The exposures in the wellstream gas mixture for 750 h caused clearly observable degradation of the materials. Insulation systems can be compared with such a test, because the failed materials and systems can be detected. The depressurization was too rapid at the resin screening test, but it did not interfere the material comparison. It was observed that it is fundamental to a material comparison to test all the materials in the same exposure. Also the tests for the wellstream gas content study formed a logical set and provided information on different parameters. However, dielectric response measurements were not carried out for all the samples and all

the tests, which caused some gaps in the overall knowledge. Such measurements would have provided more information on the effects of water and hydrocarbons on the dielectric properties.

The exposures at higher temperatures caused unexpected results. It was seen that the aging was determined by the thermodynamic state of the gas, and the temperature itself appeared not to be significant. The Arrhenius relationship did not hold. Based on the test, the hypothesis could be rejected and replaced with a new theory.

The tests performed to discern the diffusion curve failed, because the first tests were carried out with too rapid depressurization after the test. The durations of the further tests were dictated by the first test leading to a wrong test matrix. Furthermore, the depressurization process was too rapid also in the other experiments. Three experiments were performed with the wrong test procedure, and they did not provide information on the diffusion process. However, the results on such tests were valid when the degradation was recorded as a function of weight increase. The repeated test for 750 h and a long-term test for 3726 h provided good markers in the diffusion curve, and the latter exposure gave information on the long-term behavior. However, these two tests were inadequate to obtain the diffusion parameters. Additional experiments for 250 h, 500 h, and 1500 h could have provided the missing information.

Another weak point was the rapid decompression test. The results indicated that the test had been too harsh as the damage in the small samples was almost total. However, the entire bar sample did not break down as badly, which highlighted the difference between the actual insulation system and the test pieces. The only way to carry out the test was to insert all the liquid components into the chamber at once. Adding them in between the depressurizations would have required an additional day each time for the chamber to cool down. The test results suggest that the test should have been carried out with a drier gas mixture and by cooling down the pressure vessel after each depressurization. It has to be emphasized that the depressurizations that the materials experienced were not too frequent, but too harsh. The subsea compressor is expected to face more depressurizations during its lifetime than the samples did in the test.

The mainwall insulation test samples were seen to break down more easily than the actual insulation. It would have been more informative to expose the entire bars and cut them into small cakes after the test. Then, the mechanical properties would have correlated better with the acutal samples. However, the pressure vessels were too small for these kinds of test samples. Yet, an additional test should have been carried out with the bar samples and the type of samples used to find the difference between the samples. Furthermore, the number of test samples should have been higher to carry out backup measurements. This way, the diagnoses the results of which were interfered by the measuring setup, such as in Fig. 5.36, could have been adjusted accordingly. In addition, the test matrix lacks an actual bond between the accelerated tests and the real operating conditions. However, the tests indicate that such a bridge can be built by measuring the weight increase of the insulation in operating conditions. The tests indicate that the decrease in strength can be determined based on the weight increase.

Chapter 6

Conclusions

The effects of partial discharges on the insulation system in a pressurized subsea natural gas compressor were investigated. The breakdown strengths for the hydrocarbon gases were compared with nitrogen. The magnitude of partial discharges was measured as a function of voltage, and a pressure limit above which the discharges are no longer active was determined. A theoretical 2D FEM model was built to match the measurements.

An experimental chemical aging test program was carried out. The insulating materials and their suitability were investigated by a comparative test in raw natural gas. The individual effects of the components in the raw natural gas were studied by tests in modified gas mixtures that emphasize the effect of a given component. The effect of temperature on aging was investigated by three tests with similar gas mixtures in different temperatures. The long-term effect of raw natural gas on the insulation was examined by a test, which lasted for almost six months. The effect of rapid pressure changes was studied with a test including several decompression steps. Finally, the observations from all chemical aging tests were combined in an explanation on what has happened to the insulation and why.

Hydrocarbon gases have lower breakdown strengths than nitrogen. The difference is not significant, but has nevertheless to be taken into account. The effect of moisture on the breakdown strength of methane was only marginal. The use of nitrogen gas instead of hydrocarbon gases in an analysis of discharge-related measurements, in particular partial discharges in electrical machine windings, is justifiable when the difference in breakdown strength is taken into account in the analysis.

Surface discharges on the electrical machine windings reduce significantly when the pressure is increased. Above the pressure of 4 – 5 bar, the discharges virtually disappear. From the perspective of a subsea natural gas compressor, the role of partial discharges can be considered negligible in the operating pressure. The existence of partial discharges is related to the local electrical field strength. It was shown with a theoretical model that there is a region of high field strength (higher than the breakdown strength of the gas) even when no discharges can

be seen. This means that a single discharge must have a physical observable length. It was approximated to be 40 μm. The approximation was based on the breakdown field strength at a 1 mm gap distance. If the region of high field strength is too small to include a discharge of such a distance, no discharges can take place.

Theoretical examination on the methods to reduce the local field strength in the critical areas in the end-windings of an electrical machine reveals some ways to achieve major reductions in the local field strength. However, these methods would require materials that cannot tolerate raw natural gas or methods that cannot be applied to the windings of electrical machines because of the limited space between the coils. The only way is to use a mainwall insulation to terminate the conductive layer on the coil. Such a method can reduce the field strength by 40%, but still, the field strength is above the breakdown strength of the gas.

The chemical aging tests indicate that PET films cannot withstand raw natural gas. Other backing materials of a mica tape (Kapton® polyimide film, Nomex® aramid paper, and glass) can be used. With such backing materials, the performance is essentially determined by the impregnating resin. The epoxy novolac resin and bisphenol A epoxy anhydride resin can withstand the environment, when they are cured with a boron trichloride accelerator. A zinc naphthenate accelerator cannot provide sufficient chemical resistance and it was found to react with the gas. The VPI manufacturing process has to be completed carefully to ensure perfect impregnation. If the insulation is not fully impregnated, the aging effect is more severe.

The epoxy resins experience the raw natural gas rather differently. The epoxy novolac resin does not absorb much hydrocarbons, and its weight does not increase as much as that of the bisphenol A epoxy resin. The high crosslink density of the epoxy novolac resin prevents large molecules from penetrating, but it also lacks flexibility during sudden pressure changes. On the other hand, the epoxy novolac resin absorbs water more easily than the bisphenol A epoxy resin. No changes were observed in the chemical structure of the epoxy novolac resin.

The heavy hydrocarbons cause the bisphenol A epoxy resin to gain relatively much weight. The resin also absorbs a small amount of water, which causes small chemical changes in the structure of the resin. These changes are attributed to the reactions between the anhydride crosslinking groups and epoxy groups, but they do not have a distinct influence on the properties of the resin. The mechanical and dielectric properties and the glass transition temperature of the resin are reduced as a result of the diffusion of raw natural gas. The gas acts as a plasticizer inside the bisphenol A epoxy resin.

The mechanical properties of the mainwall insulation system consisting of mica, glass, and epoxy resin are closely dependent on the amount of raw natural gas absorbed. The aging of an insulation under such conditions is clearly discernible, but the only factor clearly dominating is the diffusion process. Based on the behavior of the tensile strength of the insulation as a function of weight increase, a lifetime equation has been derived. A lifetime estimate for the accelerated test conditions was calculated assuming that the end-point takes place when the strength has decreased by 50%. Yet, the lifetime estimate does not represent the operating conditions, because it was determined for accelerated conditions only. In order to find the

correlation with accelerated tests and operating conditions, further investigation is needed for the definition of the diffusion parameters in normal operating conditions, particularly the weight increase at saturation.

Both resins and the entire insulation system are vulnerable to sudden pressure changes. When the pressure suddenly drops, the gas diffused inside the insulation is forced to flow out. The departure of the gas cause internal cracks in the insulation. There are cracks in the bulk epoxy and detachment of epoxy from glass strains in the entire insulation system. The latter effect leads to the delamination of the mainwall insulation, and further, to a lower mechanical strength and higher dielectric losses. The diffusion process softens the insulation, but sudden pressure changes can ultimately cause it to crack.

The effect of voltage on the diffusion was not investigated. This study would have required complicated experiments and it was not included in this dissertation. This, however, is an obvious topic for future research. The electrical field in an electrical machine is not very high and effects of very high fields, such as space charges, are not present. Therefore, it is not expected that the voltage would have a significant effect on the aging. Yet, the aging process is related to the motion of substances inside the molecular structure of insulating materials. An external electrical field can accelerate certain chemical reactions. Thus, it is not fully justified to exclude its influence without thorough testing and discussion.

References

Alger, P.L. (1928). "Discussion on "Improvements in Insulation for High-Voltage A-C Generators" by C. F. Hill." *Transactions on AIEE*, 47(3), p. 852.

Andersen, O.W. (1977). "Finite Element Solution of Complex Potential Electric Fields." *IEEE Transactions on Power Apparatus and Systems*, 96(4), pp. 1156 – 1161.

Andersson, A.R. and Örbeck, T. (1967). "Evaluation of a New Development in HV Insulation for Large Machines." *IEEE Transactions on Power Apparatus and Systems*, 86(2), pp. 224 – 230.

ASTM (2004). *ASTM D150 - 98: Standard Test Methods for AC Loss Characteristics and Permittivity (Dielectric Constant) of Solid Electrical Insulation*. West Conshohocken, PA, USA: ASTM International.

Banks, L. and Ellis, B. (1979). "The Glass Transition Temperature of an Epoxy Resin and the Effect of Absorbed Water." *Polymer Bulletin*, 1(6), pp. 377 – 382.

Blythe, T. and Bloor, D. (2005). *Electrical Properties of Polymers*, 2nd edition. Cambridge, UK: Cambridge University Press.

Brenne, L., Bjørge, T., Bakken, L.E., and Hundseid, Ø. (2008). "Prospects for Sub Sea Wet Gas Compression." In *Proceedings of ASME Turbo Expo 2008: Power for Land, Sea and Air*.

Brütsch, R., Allison, J.A., Scollay, R., and Wolf, F. (1999). "New Trends in the Insulation Technology of Rotating High Voltage Machines." In *Proceedings of Electrical Insulation Conference and Electrical Manufacturing and Coil Winding Conference*.

Calvert, J.F. (1931). "Forces in turbine generator stator windings." *Transactions on AIEE*, 50(1), pp. 178 – 194.

Carroll, D.L., Lo, H., and Stiel, L.I. (1968). "Thermal Conductivity of Gaseous Air at Moderate and High Pressures." *Journal of Chemical Engineering Data*, 13(1), pp. 53 – 57.

Cherdoud-Chihani, A., Mouzali, M., and Abedie, M.J.M. (2003). "Study of Crosslinking Acid Copolymer/DGEBA Systems by FTIR." *Journal of Applied Polymer Science*, 87(13), pp. 2033 – 2051.

Cole, K.S. and Cole, R.H. (1941). "Dispersion and Absorption in Dielectrics I: Alternating Current Characteristics." *Journal of Chemical Physics*, 9, pp. 341 – 351.

Crank, J. (1975). *The Mathematics of Diffusion*, 2nd edition. Oxford, UK: Oxford University Press.

Crine, J.P. (1991). "The Compensation Law Revisited: Application to Dielectric Aging." *IEEE Transactions on Electrical Insulation*, 26(4), pp. 811 – 818.

Dakin, T.W. (1948). "Electrical Insulation Deterioration Treated as a Chemical Rate Phenomenon." *Transactions on AIEE*, 67, pp. 113 – 122.

David, E., Lamarre, L., and Nguyen, D.N. (2004). "Low-Frequency Dielectric Response of Asphalt Bonded Insulation." In *Proceedings of IEEE International Conference on Solid Dielectrics, ICSD 2004*.

Debye, P. (1929). *Polar Molecules*. Chemical Catalog Company, reprinted in USA by Dover Publications Inc.

Denq, B.L. et al. (1999). "The Curing Reaction and Physical Properties of DGEBA/DETA Epoxy Resin Blended with Propyl Ester Phosphazene." *Journal of Applied Polymer Science*, 74(1), pp. 229 – 237.

EIA (1999). *Natural Gas 1998: Issues and Trends*. Washington, DC, USA: U. S. Energy Information Administration.

Emery, F.T. (2005). "Partial Discharge, Dissipation Factor, and Corona Aspects for High Voltage Electric Generator Stator Bars and Windings." *IEEE Transactions on Dielectrics and Electrical Insulation*, 12(2), pp. 347 – 361.

Emery, F.T. and Smith, J.D.B. (2001). "Next Generation Insulation of High Operating Stress." In *Proceedings of Electrical Insulation Conference and Electrical Manufacturing and Coil Winding Conference*.

Emery, F.T. and Williams, M. (2007). "Application of Flat Glass Backed Mica Paper Tape to VPI'ed High Voltage Stator Coils." In *Proceedings of Electrical Insulation Conference and Electrical Manufacturing Expo*, pp. 21 – 25.

Espino-Cortez, F.P., Cherney, E.A., and Jayaram, S. (2005). "Effectiveness of Stress Grading Coatings on Form Wound Stator Coil Groundwall Insulation under Fast Rise Time Pulse Voltages." *IEEE Transactions on Energy Conversion*, 20(4), pp. 844 – 851.

Evershed, S. (1913). "The Characteristics of Insulation Resistance." *Journal of IEE*, 52(224), pp. 51 – 73.

Farahani, M., Borsi, H., and Gockenbach, E. (2006). "Dielectric Response Studies on Insulating System of High Voltage Rotating Machines." *IEEE Transactions on Dielectrics and Electrical Insulation*, 13(1), pp. 383 – 393.

Fargione, J. et al. (2008). "Land Clearing and the Biofuel Carbon Debt." *SCIENCE*, 319, pp. 1235 – 1238.

Fernández-García, M. and Chiang, M.Y.M. (2002). "Effect of Hygrothermal Aging History on Sorption Process, Swelling and Glass Transition Temperature in a Particle-Filled Epoxy-Based Adhesive." *Journal of Applied Polymer Science*, 84(8), pp. 1581 – 1591.

Fick, A. (1855). "On liquid diffusion." *Philosophical Magazine Series 4*, 10(63), pp. 30 – 39.

Fleming, A.P.M. and Johnson, R. (1913). *Insulation and Design of Electrical Windings*. London, UK: Longmans, Green & Co.

Flight, W.S. (1923). *Electrical Insulation and Design of Electrical Windings*. Bath, UK: Sir Isaac Pitman & Sons, ltd.

Flynn, E.J., Kilbourne, C.E., and Richardson, C.D. (1958). "An Advanced Concept for Turbine-Generator Stator-Winding Insulation." *IEEE Transactions on Power Apparatus And Systems*, 77(3), pp. 358 – 365.

Foster, W.J. and Glass, A.E. (1924). "The 65000 kVA Generator of the Niagara Falls Power Company." *Transactions on AIEE*, 43, pp. 678–685.

Fukuda, A., Mitsui, H., Inoue, Y., and Goto, K. (1997). "The Influence of Water Absorption on Dielectric Properties of Cycloaliphatic Epoxy Resin." In *Proceedings of International Conference on Properties and Applications of Dielectric Materials, ICPADM 1997*, pp. 58 – 61.

Grubelnik, W., Roberts, J., Koerbler, B., and Marek, P. (2005). "A New Approach in insulation Systems for Rotating Machines." In *Proceedings of Electrical Insulation Conference and Electrical Manufacturing and Coil Winding Conference*.

Hannah, R. (n.d.). *Theory and Practice of Spectral Interpretation*. Perkin-Elmer Corporation. (Reference material for FTIR spectroscopy).

Hill, C.F. (1928). "Improvements in Insulation for High-Voltage AC Generators." *Transactions on AIEE*, 47(3), pp. 845 – 852.

Hong, T.P., Gonon, G., and Lesaint, O. (2009a). "Water Absorption in a Glass-mica-epoxy Composite I: Influence of Electrical Properties." *IEEE Transactions on Dielectrics and Electrical Insulation*, 16(1), pp. 1 – 10.

Hong, T.P., Gonon, G., and Lesaint, O. (2009b). "Water Absorption in a Glass-mica-epoxy Composite II: Field Distribution and Diagnostic in a Stator Bar Geometry." *IEEE Transactions on Dielectrics and Electrical Insulation*, 16(1), pp. 11 – 16.

Hvidsten, S., Kvande, S., Ryen, A., and B., L.P. (2009). "Severe Degradation of the Conductor Screen of Service and Laboratory Aged Medium Voltage XLPE Insulate Cables." *IEEE Transactions on Dielectrics and Electrical Insulation*, 16(1), pp. 155 – 161.

IEA (2009). *Key World Energy Statistics 2009*. Paris, France: International Energy Agency.

IEC (1969). *IEC 60250: Recommended methods for the determination of the permittivity and dielectric dissipation factor of electrical insulating materials at power, audio and radio frequencies including metre wavelengths*. Geneva, Switzerland: International Electrotechnical Comission.

IEC (2000). *IEC 60270: High voltage test techniques: Partial discharge measurements*, 3rd edition. Geneva, Switzerland: International Electrotechnical Comission.

IEC (2004). *IEC 60505: Evaluation and qualification of electrical insulation systems*, 3rd edition. Geneva, Switzerland: International Electrotechnical Comission.

IEEE (2006). *IEEE Std 43-2000: Recommended Practice for Testing Insulation Resistance of Rotating Machinery*, r2006 edition. New York, NY, USA: Institution of Electrical and Electronics Engineers, Inc.

IEEE (2007). *IEEE Std 434-2006: IEEE Guide for functional evaluation of insulation systems for AC electric machines rated 2300 V and above*. New York, NY, USA: Institution of Electrical and Electronics Engineers, Inc.

ISO (2001). *ISO 178:2001(E), Plastics: Determination of flexural properties*, 4th edition. Geneva, Switzerland: International Organization for Standardization.

ISO (2008). *ISO 62:2008(E), Plastics: Determination of water absorption*, 3rd edition. Geneva, Switzerland: International Organization for Standardization.

Jacobs, P.M. and Jones, F.R. (1989). "Diffusion of moisture into two-phase polymers." *Journal of Materials Science*, 24, pp. 2331 – 2336.

Jia, Z., Hao, Y., and Xie, H. (2006). "The Degradation Assessment of Epoxy/Mica Insulation under Multi-stresses Aging." *IEEE Transactions on Dielectrics and Electrical Insulation*, 13(1), pp. 415 – 422.

Johnson, J.D. (1998). *Classical Electrodynamics*, 3rd edition. Hoboken, NJ, USA: John Wiley & Sons.

Jonscher, A.K. (1983). *Dielectric Relaxation in Solids*. London, UK: Chelsea Dielectrics Press.

Kadotani, K., Sato, T., and Kako, Y. (1980). "Study on Corona Suppression for Fusion Reactor Coils." *IEEE Transactions on Electrical Insulation*, 15(4), pp. 322 – 330.

Kelen, A. and Virsberg, L.G. (1964). "Discharge Suppression on Surfaces of High-Voltage Insulation." *Elteknik*, 4, pp. 59 – 65.

Kimura, H. et al. (1998). "Epoxy Resin Cured by Bisphenol A Based Benzoxazine." *Journal of Applied Polymer Science*, 68(12), pp. 1903 – 1910.

Kimura, K. and Hirabayashi, S. (1985). "Improved Potential Grading Methods with Silicon Carbide Paints for High Voltage Coils." *IEEE Transactions on Electrical Insulation*, 20(3), pp. 511 – 517.

Kärner, H.C. and Ieda, M. (1991). "Technical Aspects of Interfacial Phenomena in Solid Insulating Systems." In *Proceedings of International Conference on Properties and Applications of Dielectric Materials, ICPADM 1991*, pp. 592 – 597.

Kuffel, E., Zaengl, W.S., and Kuffel, J. (2000). *High Voltage Engineering*, 2nd edition. Hoboken, NJ, USA: Butterworth & Heinemann.

Kumazawa, T., Oishi, M., and Todoki, M. (1994). "High Humidity Deterioration and Internal Structure Change of Epoxy Resin for Electrical Insulation." *IEEE Transactions on Dielectrics and Electrical Insulation*, 1(1), pp. 133 – 138.

Laffoon, C.M. (1930). "Increased Voltages for Synchronous Machines." *Transactions on AIEE*, 49, pp. 213 – 221.

Laffoon, C.M. and Calvert, J.F. (1935). "Insulation for High Voltage Alternators." *Transactions on AIEE*, 54(6), pp. 624 – 630.

Laffoon, C.M., Hill, C.F., Moses, G.L., and Berberich, L.J. (1951). "A New High-Voltage Insulation for Turbine-Generator Stator Windings." *Transactions on AIEE*, 70(1), pp. 721 – 726.

Lamme, B.G. (1913). "High-Speed Turbo-Alternators - Design and Limitations." *Transactions on AIEE*, 32(1), pp. 1 – 37.

Lecarpentier, A., ed., (2009). *Natural Gas in the World - 2009 Edition*. Rueil Malmaison, France: CEDIGAZ.

Lewis, T.J. (2001). "Ageing - a Perspective." *Electrical Insulation Magazine*, 17(4), pp. 6 – 16.

Linhjell, D., Lundegaard, L., and Gäfvert, U. (2007). "Dielectric Response of Minearl Oil Impregnated Cellulose and the Impact of Aging." *IEEE Transactions on Dielectrics and Electrical Insulation*, 14(1), pp. 156 – 169.

Liu, M. et al. (2002). "Two-Dimensional (2D) ATR-FTIR Spectroscopic Study on Water Diffusion in Cured Epoxy Resins." *Macromolecules*, 35, pp. 5500 – 5507.

Maggana, C. and Pissis, P. (1999). "Water Sorption and Diffusion Studies in an Epoxy Resin System." *Journal of Polymer Science: Part B: Polymer Physics*, 37, pp. 1165 – 1182.

Makuc, D., Ikanovic, J., and Lenasi, K. (2005). *Electrical Field Analysis of the Insulation Structure of Power Transformer*, pp. 155 – 160. Springer Neatherlands. ISBN 978-1-4020-3168-7.

Manni, V.E. and Schneider, W. (1960). "An Improved Method for Corona Suppression for High Voltage Rotating Machines." *IEEE Transactions on Power Apparatus and Systems*, 79(3), pp. 49 – 52.

MATLAB (2005). *Help files for MATLAB® 7.1*. The MathWorks Inc.

Maxwell, J.C. (1892). *A treatise on electricity and magnetism, Vol. 1*, 3rd edition. London, UK: Oxford University Press.

McCarty, R.A. and Hart, E.U. (1922). "Design of 45000 kVA Generators, Queenston Plant." *Transactions on AIEE*, 41(3), pp. 496 – 499.

McNaughton, H.S. (1993). "Comparative Performance of Woven Glass and Polyester Film Backed Micaceous Tapes for the Insulation of High Voltage A.C. Stator Windings of Rotating Electrical Machines." In *Proceedings of Electrical Electronics Insulation Conference, EEIC/ICWA Exposition*, pp. 545 – 551.

Meek, J.M. and Craggs, J.D. (1953). *Electrical Breakdown of Gases*. London, UK: Oxford University Press.

Melillo, J.M. et al. (2009). "Indirect Emissions from Biofuels: How Important?" *SCIENCE*, 326, pp. 1397 – 1399.

Miner, D.F. (1941). *Insulation of Electrical Apparatus*. York, PA, USA: McGraw-Hill Book Company Inc.

Mitsui, H. and Inoue, Y. (1977). "Statistical analysis on the electrical failure properties of the form-wound epoxy micaceous insulation systems for rotating machines." *IEEE Transactions on Electrical Insulation*, 12(3), pp. 237 – 248.

Montanari, G.C. and Mazzanti, G. (1994). "From Thermodynamic to Phenomenological Multi-Stress Models for Insulating Materials without or with Evidence of Threshold." *Journal of Physics D: Applied Physics*, 27, pp. 1691 – 1702.

Montsinger, V.M. (1930). "Loading Transformers by Temperature." *Transactions on AIEE*, 49(2), pp. 776 – 790.

Moses, G.L. (1951). "Alternating and Direct Voltage Endurance Studies on Mica Insulation for Electric Machinery." *Transactions on AIEE*, 70, pp. 763 – 769.

Mårtensson, E. (2003). *Modelling electrical properties of composite materials*. Ph.D. thesis. Kungliga Tekniska Högskolan, Stockholm, Sweden. ISSN 1650-674-X, 88 p.

Musto, P., Ragosta, G., and Mascia, L. (2000). "Vibrational Spectroscopy for the Dual Nature of Water Sorbed into Epoxy Resins." *Chemistry of Materials*, 12(5), pp. 1331 – 1341.

Nelson, P.N. and Hervig, H.C. (1984). "High Dielectric Constant Materials for Primary Voltage Cable Terminations." *IEEE Transactions on Power Apparatus and Systems*, 103(11), pp. 3211 – 3216.

Nelson, P.R., Coffin, M., and Copeland, K.A.F. (2003). *Introductory Statistics*. San Diego, CA, USA: Elsevier Science.

Nestli, T.F. et al. (2003). "Powering Troll with New Technology." *ABB Review*, (2), pp. 15 – 19.

Newbury, F.D. (1915). "Experimental Data Concerning the Safe Operating Temperature for Mica Armature-Coil Insulation." *Transactions on AIEE*, 34(2), pp. 2747 – 2764.

Nikolajevic, S.V., Pekaric-Nad, N.M., and Dimitrijevic, R.M. (1998). "A New Concept in Contruction of Cable Terminations for Medium Voltages." *IEEE Transactions on Power Delivery*, 13(3), pp. 712 – 717.

Nogueira, P. et al. (2001). "Effect of Water Sorption on the Structure and Mechanical Porperties of an Epoxy Resin System." *Journal of Applied Polymer Science*, 80(1), pp. 71 – 80.

Paloniemi, P. (1982). "Multi-stress endurance tests on high-voltage motor insulations, with equal acceleration of each stress." *IEEE Transactions on Electrical Insulation*, 17(3), pp. 253 – 261.

Park, C.H. (1987). "A Study of the Dielectric and Mechanical Property Interactions of Glass-Cloth/Epoxy Composites." *IEEE Transactions on Electrical Insulation*, 22(4), pp. 389 – 395.

Parsons, C. and Rosen, J. (1929). "Direct Generation of Alternating Current at High Voltages." *Journal of the IEE*, 67, pp. 1065 – 1080.

Paschen, F. (1889). "Über die zum Funkenübergang in Luft, Wasserstoff und Kohlensäure bei verschiedenen Drucken erforderliche Potentialdifferenz." *Annalen der Physik*, 273(5), pp. 69 – 96.

PerkinElmer (n.d.). *Spectrum Search Plus, spectrum library*. PerkinElmer Corporation. (Analysis software for FTIR spectra).

Pethrick, R.A. et al. (1996). "Effect of Cure Temperature on the Structure and Water Absorption of Epoxy/Amine Thermosets." *Polymer International*, 39(4), pp. 275 – 288.

Petrie, E.M. (2006). *Epoxy Adhesive Formulations*. Hoboken, NJ, USA: McGraw-Hill.

Pyrhönen, J., Nerg, J., Kurronen, P., and Lauber, U. (2010). "High-Speed High-Output Solid-Rotor Induction-Motor Technology for Gas Compression." *IEEE Transations on Industrial Electronics*, 57(1), pp. 272 – 280.

Råde, B. and Westergren, L. (1998). *Mathematics handbook for science and engineering*, 4$^{\text{th}}$ edition. Lund, Sweden: Studentlitteratur.

Rivenc, J.P., Bidan, P., and Lebey, T. (1998). "Stress Grading Materials: a Discussion on Lumped Circuits Validity." In *Proceedings of IEEE International Conference on Conduction and Breakdown in Solid Dielectrics*.

Rivenc, J.P. and Lebey, T. (1999). "An Overview of Electrical Properties for Stress Grading Optimization." *IEEE Transactions on Dielectrics and Electrical Insulation*, 6(3), pp. 309 – 318.

Roberts, A. (1995). "Stress Grading for High Voltage Motor and Generator Coils." *Electrical Insulation Magazine*, 11(4), pp. 26 – 31.

Scaife, W.S. (1972). "The relative permittivity of the n alkanes from n pentane to n decane as a function of pressure and temperature." *Journal of Physics A: General Physics*, 5, pp. 897 – 903.

Searchinger, T. et al. (2008). "Use of U.S. Croplands for Biofuels Increases Greenhouse Gases Through Emissions from Land-Use Change." *SCIENCE*, 319, pp. 1238 – 1240.

Sharifi, E., Jayaram, S., and Cherney, E.A. (2008). "Capacitive Grading of 13.8 kV Form-Wound Motor Coil Ends for Pulse Width Modulated Drive Operation." In *Proceedings of IEEE International Symposium on Electrical Insulation*, pp. 632 – 635.

Short, H.D. (1949). "A Theoretical and Practical Approach to the Design of High Voltage Cable Joints." *Transactions on AIEE*, 68(2), pp. 1275 – 1283.

Sihvo, V., Nerg, J., and Pyrhönen, J. (2007). "Insulation System and Thermal Design of a Hermetically Sealed Turbo-Generator Operating in a Small-Power CHP Plant." In *Proceedings of IEEE International Conference on Clean Electrical Power, ICCEP 2007*, pp. 45 – 50.

Sihvo, V., Nerg, J., and Pyrhönen, J. (2008). "Design and testing of a steam-resistant insulation system for the stator of a low-voltage turbo-generator taking thermal aspects into account." *WSEAS Transactions on Power Systems*, 3(9), pp. 587 – 597.

Simoni, L. (1973). "A New Approach to the Voltage-Endurance Test on Electrical Insulation." *IEEE Transactions on Electrical Insulation*, 8(3), pp. 76 – 86.

Sánchez-Soto, M. et al. (2007). "Curing FTIR study and mechanical characterization of glass bead filled trifunctional epoxy composites." *Composites Science and Technology*, 67(9), pp. 1974 – 1985.

Solymar, L. and Walsh, D. (2004). *Electrical Properties of Materials*, 7th edition. Ofxord, UK: Oxford University Press.

Sperling, L.H. (2006). *Introduction to physical polymer science*, 4th edition. Hoboken, NJ, USA: John Wiley & Sons, Inc.

Steinmetz, C.P. and Lamme, B.G. (1913). "Temperature and Electrical Insulation." *Transactions on AIEE*, 32(1), pp. 79 – 89.

Stone, G. and Lawless, J.F. (1979). "The Application of Weibull Statistics to Insulation Aging Tests." *IEEE Transactions on Electrical Insulation*, 14(5), pp. 233 – 239.

Stone, G.C., Boulter, E.A., Culbert, I., and Dhirani, H. (2004). *Electrical Insulation for Rotating Machines*. Hoboken, NJ, USA: John Wiley & Sons, Inc.

Tari, M. et al. (2002). "Impacts on Turbine Generators Design by the Application of Increased Thermal Conducting Stator Insulation." *CIGRE Paper 11-105*.

Terase, H. et al. (1981). "Proposal of GF (Gas Filled) Insulation for Rotating Machines." *IEEE Transactions on Power Apparatus and Systems*, 100(6), pp. 2955 – 2962.

Thienpont, J. and Sie, T.H. (1964). "Suppression of surface discharges in the stator windings of high voltage machines." *CIGRE Paper 122*, pp. 1 – 25.

Thongbai, P., Tangwancharoen, S., Yanwong, T., and Maensiri, S. (2008). "Dielectric relaxation and dielectric response mechanism in (Li, Ti)-doed NiO ceramics." *Journal of Physics: Condensed Matter*, 20(39), pp. 1 – 11.

Thorsen, O.V. and Dalva, M. (1995). "A Survey of Faults in Induction Motors in Offshore Oil Industry, Petrochemical Industry, Gas Terminals, and Oil Refineries." *IEEE Transactions on Industry Applications*, 31(5), pp. 1186 – 1196.

Timperley, J.E. and Michalek, J.R. (1994). "Estimating the Remaining Service Life for Asphalt-Mica Stator Insulation." *IEEE Transactions on Energy Conversion*, 9(4), pp. 686 – 693.

Townsend, J.S. (1915). *Electricity in gases*. Oxford University Press.

Wagner, K.W. (1914). "Erklärung der dielektrischen Nachwirkungsvorgänge auf Grund Maxwellscher Vorstellungen." *Archiv für Electroteknik*, 2(9), pp. 371 – 387. (in German).

Wheeler, J.C.G., Gully, A.M., Baker, A.E., and Perrot, F.A. (2007). "Novel Stress Grading Systems for Converter-Fed Motors." *Electrical Insulation Magazine*, 23(1), pp. 29 – 35.

Wichmann, A. (1972). "Reliability and Testing of High-Voltage Stator Insulation for Large Rotating Machines." *IEEE Transactions on Power Apparatus and Systems*, 91(5), pp. 2230 – 2236.

Wichmann, A. (1983). "Two Decades of Experience and Progress in Epoxy Mica Insulation Systems for Large Rotating Machines." *IEEE Transactions on Power Apparatus and Systems*, 102(1), pp. 74 – 82.

Wu, P. and Siesler, H.W. (2003). "Water Diffusion into Epoxy Resin: A 2D Correlation ATR-FTIR Investigation." *Chemical Physical Letters*, 374(1-2), pp. 74 – 78.

Xiao, G.Z. and Shanahan, M.E.R. (1998). "Irreversible Effects of Hygrothermal Aging on DGEBA/DDA Epoxy Resin." *Journal of Applied Polymer Science*, 69(2), pp. 363 – 369.

Young, H.D. and Freedman, R.A. (2000). *University Physics*, 10^{th} edition. Addison-Wesley.

Zhurkov, S.N. (1984). "Kinetic Concept of the Strength of Solids." *International Journal of Fracture*, 26, pp. 295 – 307.

Appendix A

Derivations for the real and imaginary parts of the dielectric response function

Equation (2.24) can be divided into real and imaginary parts. First, the imaginary unit i is taken out from the exponential part according to de Moivre's formula (Råde and Westergren, 1998)

$$(\cos\theta + i\sin\theta)^n = \cos(n\theta) + i\sin(n\theta) \tag{A.1}$$

For that purpose, Eq. (2.24) must be rearranged to the form in which de Moivre's formula can be used. The corresponding part of the equation can be written as

$$\frac{\epsilon_s - \epsilon_\infty}{1 + (i\omega\tau)^{1-\alpha}} = \frac{\epsilon_s - \epsilon_\infty}{1 + (\omega\tau)^{1-\alpha} i i^{-\alpha}} = \frac{\epsilon_s - \epsilon_\infty}{1 + i(\omega\tau)^{1-\alpha}(\cos\frac{\pi}{2} + i\sin\frac{\pi}{2})^{-\alpha}} \tag{A.2}$$

Applying de Moivre's formula (Eq. (A.1)) yields

$$\frac{\epsilon_s - \epsilon_\infty}{1 + (i\omega\tau)^{1-\alpha}} = \frac{\epsilon_s - \epsilon_\infty}{1 + i(\omega\tau)^{1-\alpha}\left(\cos\left(-\alpha\frac{\pi}{2}\right) + i\sin\left(-\alpha\frac{\pi}{2}\right)\right)} \tag{A.3}$$

Substituting negative angles and uniting the imaginary units produces

$$\frac{\epsilon_s - \epsilon_\infty}{1 + (i\omega\tau)^{1-\alpha}} = \frac{\epsilon_s - \epsilon_\infty}{1 + (\omega\tau)^{1-\alpha}\left(\sin\left(\alpha\frac{\pi}{2}\right) + i\cos\left(\alpha\frac{\pi}{2}\right)\right)} \tag{A.4}$$

Multiplication by the complex conjugate of the denumerator yields

$$\frac{\epsilon_s - \epsilon_\infty}{1 + (i\omega\tau)^{1-\alpha}} = (\epsilon_s - \epsilon_\infty)\frac{1 + (\omega\tau)^{1-\alpha}\left(\sin\left(\alpha\frac{\pi}{2}\right) - i\cos\left(\alpha\frac{\pi}{2}\right)\right)}{1 + 2(\omega\tau)^{1-\alpha}\sin\left(\alpha\frac{\pi}{2}\right) + (\omega\tau)^{2-2\alpha}} \tag{A.5}$$

Equation (A.5) is similar to (2.12). Hence, taking also the conductivity terms into account, the modified Cole-Cole equation can be divided into real and imaginary parts as:

$$\epsilon(\omega)' = \epsilon_\infty + (\epsilon_s - \epsilon_\infty)\frac{1 + (\omega\tau)^{1-\alpha}\sin\left(\alpha\frac{\pi}{2}\right)}{1 + 2(\omega\tau)^{1-\alpha}\sin\left(\alpha\frac{\pi}{2}\right) + (\omega\tau)^{2-2\alpha}} + \frac{\sigma''}{\epsilon_0\omega^s} \tag{A.6}$$

$$\epsilon(\omega)'' = (\epsilon_s - \epsilon_\infty)\frac{(\omega\tau)^{1-\alpha}\cos\left(\alpha\frac{\pi}{2}\right)}{1 + 2(\omega\tau)^{1-\alpha}\sin\left(\alpha\frac{\pi}{2}\right) + (\omega\tau)^{2-2\alpha}} + \frac{\sigma'}{\epsilon_0\omega^s} \tag{A.7}$$

Appendix B

Step-by-step procedure for vacuum pressure impregnation

The procedure for VPI impregnation with resin C was carried out as follows. Temperatures and pressures are indicated by **bold** and durations of each step by *italic* letters.

1. Preparations
   - Manufacturing of the insulation on the bars and installing them into the dummy stator
   - Mixing of the resin
   - Pre-heating of the dummy stator, **80 °C**
   - Cleaning of the VPI chamber and equipment
2. Inserting the dummy stator into the VPI chamber
3. Flushing the VPI chamber with nitrogen gas (5 bar) for three times to remove moisture
4. Heating of the VPI chamber and applying the vacuum, **70 °C, 5 mbar**, *over night*
5. Pre-heating of the resin, **60 °C**
6. Inserting the resin into the chamber, **70 °C, 5 mbar**, *2 h*
7. Increasing the pressure in steps, **70 °C**
   I. Slowly from vacuum to atmospheric allowing some relaxation time at atmospheric, *10 min*
   II. Quite slowly to 5 bar allowing some relaxation time at 2 bar, 3 bar, 4 bar, and 5 bar, *40 min altogether*
   III. At an increasing rate to 100 bar allowing some relaxation time at 10 bar, 20 bar, 40 bar, and 80 bar, *40 min altogether*
8. Maintaining the high pressure until 6 h has passed from inserting the resin, **70 °C, 100 bar**, *2 h 30 min*
9. Switching off the chamber heating and allowing the chamber to cool, **70 – 40 °C, 100**

bar, *several hours*

10. Decreasing the pressure level at approximately 5 bar/min, **<40 °C, 5 bar**, *20 min*
11. Pumping the resin out from the chamber, **<40 °C, <5 bar**, *15 min*
12. Slowly decreasing the pressure to atmospheric, **<40 °C, 1 bar**, *10 min*
13. Opening of the chamber and removal of the dummy stator
14. Dummy stator put into the oven for the curing process
    I. **90 °C**, *12 h*
    II. **140 °C**, *16 h*
15. Cleaning of the VPI chamber and equipment

Appendix C

Procedure for aging experiments using wellstream gas

The aging experiments with hydrocarbon gases were carried out according to the following procedure. It was used with the wellstream gas mixture.

1. Preparations
    - Calculation on the amounts of liquid components and stabilization pressure
    - Manufacturing of the test specimens
    - Cleaning of the chamber
2. Inserting the test specimens and liquid components into the chamber
3. Flushing the VPI chamber with nitrogen gas (5 bar) for three times to remove moisture, checking for leakages
4. Increasing the pressure gradually to the stabilization pressure (approximately 90 bar)
5. Leakage inspection
6. Heating the chamber to 130 °C
7. Adjusting the pressure to 150 bar
8. Time recording started
9. Maintaining the conditions for the entire duration of the test
10. Time recording stopped
11. Switching off the heat and allowing the chamber to cool
12. Depressurization carried out manually by clicking the valve on and off and allowing some relaxation time after each valve opening, the average depressurization rates being roughly as follows:
    I. 20 bar/min at pressures above 20 bar
    II. Gradually decreasing the depressurization rate
    III. approx. 3 bar/min below 3 bar

13. Opening of the chamber and removal of the test specimens
14. Removal of flammable liquid components from the chamber, cleaning of the equipment
15. Allowing the test specimens to relax for a few hours and let the surface moisture to evaporate
16. Diagnostic tests

Appendix D

Use of statistical distributions to interpret the aging data

The density functions and estimates for normal, lognormal, and Weibull distributions, respectively, can be written as (MATLAB, 2005)

$$F_{\text{norm}}(y) = \frac{1}{\sqrt{2\pi\sigma^2}} \exp\left\{-\frac{1}{2}\frac{(y-\mu)^2}{\sigma^2}\right\} \qquad \text{for} \quad -\infty < y < \infty \tag{D.1}$$

$$F_{\text{logn}}(y) = \frac{1}{\sqrt{2\pi\sigma^2 y}} \exp\left\{-\frac{1}{2}\frac{(\ln y-\mu)^2}{\sigma^2}\right\} \qquad \text{for} \quad y > 0 \tag{D.2}$$

$$F_{\text{wbl}}(y) = \frac{\alpha}{\beta}\left(\frac{y}{\beta}\right)^{\alpha-1} \exp\left\{-\left(\frac{y}{\beta}\right)^{\alpha}\right\} \qquad \text{for} \quad y => 0 \tag{D.3}$$

$$\hat{\mu}_{\text{norm}} = \frac{1}{N}\sum_{i=1}^{N} y_i \tag{D.4}$$

$$\hat{\mu}_{\text{logn}} = \frac{1}{N}\sum_{i=1}^{N} \ln y_i \tag{D.5}$$

$$\hat{\mu}_{\text{wbl}} = \beta\Gamma\left(1+\frac{1}{\alpha}\right) \tag{D.6}$$

where Γ is the Gamma function. The statistical data on resin C from the wellstream gas exposure are presented in Table D.1, and the data on resin A in Table D.2, respectively. Both data sets are obtained from the screening test discussed in Section 5.1.

Table D.1. Statistical parameters of the E-modulus data of resin C before and after exposure to wellstream gas. The data set is taken from the experiments discussed in Section 5.1.

Distribution	Reference data		Aged data		Remaining E-modulus [%]
Normal distribution	Estimate Variance	2819.53 998.37	Estimate Variance	2657.77 3693.52	94.263
Lognormal distribution	Estimate Variance	2819.54 997.00	Estimate Variance	2657.81 3715.23	94.264
Weibull distribution	Estimate Variance α β	2817.51 1514.00 2834.94 92.15	Estimate Variance α β	2656.58 4407.26 2686.20 50.61	94.288
Number of samples	19		22		

Table D.2. Statistical parameters of the E-modulus data of resin A before and after exposure to wellstream gas. The data set is taken from the experiments discussed in Section 5.1.

Distribution	Reference data		Aged data		Remaining E-modulus [%]
Normal distribution	Estimate Variance	2869.58 379.21	Estimate Variance	2745.61 2776.91	95.680
Lognormal distribution	Estimate Variance	2869.58 378.75	Estimate Variance	2745.63 2803.90	95.681
Weibull distribution	Estimate Variance α β	2868.69 549.87 2879.21 156.18	Estimate Variance α β	2744.57 3261.40 2770.00 60.92	95.673
Number of samples	26		28		

It can be seen in the tables that the differences between the distributions are negligibly small. Only the Weibull distribution has a higher variance. The function of the Weibull distribution for interpreting the weakest link -data can be seen in Fig. D.1, where the probability plot of resin A after the exposure to the wellstream gas is illustrated. The Weibull distribution appears to give a slightly poorer fit than the normal and the lognormal distributions in the

middle section, where most of the markers are located, but it best follows the markers located at each end. The variance of the Weibull distribution is higher, but it can best predict the markers that deviate from the main group. Therefore, the E-modulus data was treated with the Weibull distribution for all samples, both references and aged samples. Nevertheless, the differences between the distributions were negligibly small.

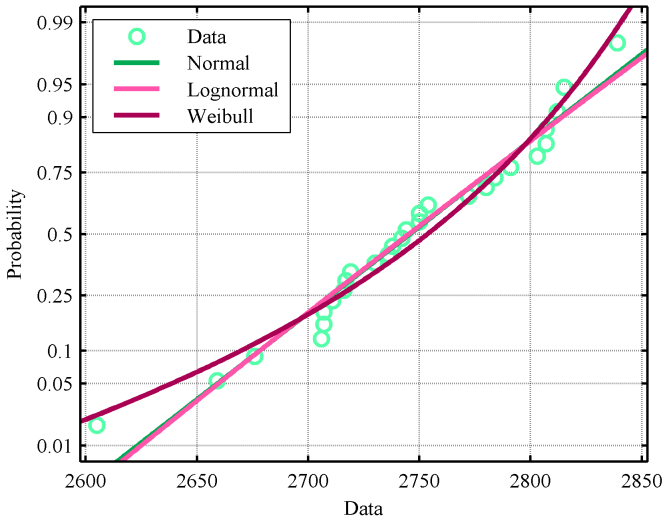

Fig. D.1. Probability plot of the E-modulus of resin A after the exposure to the wellstream gas and fits according to normal, lognormal, and Weibull distributions. The data are illustrated with circles, each of which having the same probability. The curve is scaled according to the normal distribution, i.e. the normal distribution is shown as a straight line.

ACTA UNIVERSITATIS LAPPEENRANTAENSIS

367. JALKALA, ANNE. Customer reference marketing in a business-to-business context. 2009. Diss.

368. HANNOLA, LEA. Challenges and means for the front end activities of software development. 2009. Diss.

369. PÄTÄRI, SATU. On value creation at an industrial intersection – Bioenergy in the forest and energy sectors. 2009. Diss.

370. HENTTONEN, KAISA. The effects of social networks on work-team effectiveness. 2009. Diss.

371. LASSILA, JUKKA. Strategic development of electricity distribution networks – Concept and methods. 2009. Diss.

372. PAAKKUNAINEN, MAARET. Sampling in chemical analysis. 2009. Diss.

373. LISUNOV, KONSTANTIN. Magnetic and transport properties of II-V diluted magnetic semiconductors doped with manganese and nickel. 2009. Diss.

374. JUSSILA, HANNE. Concentrated winding multiphase permanent magnet machine design and electromagnetic properties – Case axial flux machine. 2009. Diss.

375. AUVINEN, HARRI. Inversion and assimilation methods with applications in geophysical remote sensing. 2009. Diss.

376. KINDSIGO, MERIT. Wet oxidation of recalcitrant lignin waters: Experimental and kinetic studies. 2009. Diss.

377. PESSI, PEKKA. Novel robot solutions for carrying out field joint welding and machining in the assembly of the vacuum vessel of ITER. 2009. Diss.

378. STRÖM, JUHA-PEKKA. Active*du*/d*t* filtering for variable-speed AC drives. 2009. Diss.

379. NURMI, SIMO A. Computational and experimental investigation of the grooved roll in paper machine environment. 2009. Diss.

380. HÄKKINEN, ANTTI. The influence of crystallization conditions on the filtration characteristics of sulphathiazole suspensions. 2009. Diss.

381. SYRJÄ, PASI. Pienten osakeyhtiöiden verosuunnittelu – empiirinen tutkimus. 2010. Diss.

382. KERKKÄNEN, ANNASTIINA. Improving demand forecasting practices in the industrial context. 2010. Diss.

383. TAHVANAINEN, KAISA. Managing regulatory risks when outsourcing network-related services in the electricity distribution sector. 2010. Diss.

384. RITALA, PAAVO. Coopetitive advantage – How firms create and appropriate value by collaborating with their competitors. 2010. Diss.

385. RAUVANTO, IRINA. The intrinsic mechanisms of softwood fiber damage in brown stock fiber line unit operations. 2010. Diss.

386. NAUMANEN, VILLE. Multilevel converter modulation: implementation and analysis. 2010. Diss.

387. IKÄVALKO, MARKKU. Contextuality in SME ownership – Studies on owner-managers´ ownership behavior. 2010. Diss.

388. SALOJÄRVI, HANNA. Customer knowledge processing in key account management. 2010. Diss.

389. ITKONEN, TONI. Parallel-operating three-phase voltage source inverters – Circulating current modeling, analysis and mitigation. 2010. Diss.

390. EEROLA, TUOMAS. Computational visual quality of digitally printed images. 2010. Diss.

391. TIAINEN, RISTO. Utilization of a time domain simulator in the technical and economic analysis of a wind turbine electric drive train. 2010. Diss.

392. GRÖNMAN AKI. Numerical modelling of small supersonic axial flow turbines. 2010. Diss.

393. KÄHKÖNEN, ANNI-KAISA. The role of power relations in strategic supply management – A value net approach. 2010. Diss.

394. VIROLAINEN, ILKKA. Johdon coaching: Rajanvetoja, taustateorioita ja prosesseja. 2010. Diss.

395. HONG, JIANZHONG. Cultural aspects of university-industry knowledge interaction. 2010. Diss.

396. AARNIOVUORI, LASSI. Induction motor drive energy efficiency – Simulation and analysis. 2010. Diss.

397. SALMINEN, KRISTIAN. The effects of some furnish and paper structure related factors on wet web tensile and relaxation characteristics. 2010. Diss.

398. WANDERA, CATHERINE. Performance of high power fiber laser cutting of thick-section steel and medium-section aluminium. 2010. Diss.

399. ALATALO, HANNU. Supersaturation-controlled crystallization. 2010. Diss.

400. RUNGI, MAIT. Management of interdependency in project portfolio management. 2010. Diss.

401. PITKÄNEN, HEIKKI. First principles modeling of metallic alloys and alloy surfaces. 2010. Diss.

402. VAHTERISTO, KARI. Kinetic modeling of mechanisms of industrially important organic reactions in gas and liquid phase. 2010. Diss.

403. LAAKKONEN, TOMMI. Distributed control architecture of power electronics building-block-based frequency converters. 2010. Diss.

404. PELTONIEMI, PASI. Phase voltage control and filtering in a converter-fed single-phase customer-end system of the LVDC distribution network. 2010. Diss.

405. TANSKANEN, ANNA. Analysis of electricity distribution network operation business models and capitalization of control room functions with DMS. 2010. Diss.

406. PIIRAINEN, KALLE A. IDEAS for strategic technology management: Design of an electronically mediated scenario process. 2010. Diss.

407. JOKINEN, MARKKU. Centralized motion control of a linear tooth belt drive: Analysis of the performance and limitations. 2010. Diss.

408. KÄMÄRI, VESA. Kumppanuusohjelman strateginen johtaminen – Monitapaustutkimus puolustushallinnossa. 2010. Diss.

409. KARJALAINEN, AHTI. Online ultrasound measurements of membrane compaction. 2010. Diss.

410. LOHTANDER, MIKA. On the development of object functions and restrictions for shapes made with a turret punch press. 2010. Diss.